United Arab Emirates University
Scholarworks@UAEU

Theses | Electronic Theses and Dissertations

11-2010

Fracture behavior of cracked full scale steel pipes used for gas and petroleum industries

Jaafer Altarawneh

Follow this and additional works at: https://scholarworks.uaeu.ac.ae/all_theses

Part of the Mechanical Engineering Commons

Recommended Citation

Altarawneh, Jaafer, "Fracture behavior of cracked full scale steel pipes used for gas and petroleum industries" (2010). *Theses*. 368.
https://scholarworks.uaeu.ac.ae/all_theses/368

This Thesis is brought to you for free and open access by the Electronic Theses and Dissertations at Scholarworks@UAEU. It has been accepted for inclusion in Theses by an authorized administrator of Scholarworks@UAEU. For more information, please contact fadl.musa@uaeu.ac.ae.

United Arab Emirates University

Deanship of Graduate Studies

FRACTURE BEHAVIOUR OF CRACKED FULL SCALE STEEL PIPES USED FOR GAS AND PETROLEUM INDUSTRIES

By

Jaafer Altarawneh

Thesis submitted to the Deanship of Graduate Studies at the United Arab Emirates University in partial fulfillment of the requirements for the degree of Master of Science in Mechanical Engineering

Supervised By

Dr. Abdel – Hamid I. Mourad

Mechanical Engineering Department

U. A. E University

November, 2010

Al Ain, UAE

ES/F11

United Arab Emirates University
Faculty of Engineering, Graduate Studies
M.S.c. Program in Mechanical Engineering

THESIS EXAMINATION REPORT

Student ID 200850041

Student Name : Jaafer Yusuf altarawneh

Title of the Thesis Fracture behavior of cracked full scale steel pipes used for gas and petroleum industries

The Thesis Examination as A Partial Fulfillment of M Sc. Degree in Mechanical Engineering Was conducted on 10/11/2010 Based on Examining the Thesis and the Students Presentation and the Subsequent Discussion, The Committee Recommends:

- ☐ Thesis is Satisfactory as is.
- ☑ Thesis is Satisfactory After Minor Modifications.
- ☐ Thesis should be Re-Evaluated After Major Modifications
- ☐ Thesis is Rejected

Examining Committee Members:

Thesis Supervisor: Name: Dr. Abdel-Hamid I. Mourad Signature: ..... Date: 10/11/2010

Member: Name: Dr. Abdennour C. Seibi Signature: ..... Date 10/11/2010

Member: Name: Dr. Khaled El-Sawy Signature: ..... Date 10/11/2010

Member: Name: Prof. Aly Al-Domiaty Signature: ..... Date 10/11/2010

Approval of Program Coordinator:

Dr. Mohamed Younes ..... Date: 10/11/2010

APPROVAL:

Associate Dean for Research and Graduate Studies ..... Date : 1/12/2010

U.A.E UNIVERSITY

جامعة الإمارات العربية المتحدة
عمادة المكتبات الجامعية
UNIVERSITY LIBRARIES DEANSHIP
U.A.E. UNIVERSITY
UAEU LIBRARIES
1000474836
مكتبات الطالبات بالمقام
MAQAM LIBRARIES

ACKNOWLEDGEMENTS

First of all thanks to God, the Lord of worlds, for offering me the means of everything in my life including and not limited to completing this work. I would like to acknowledge my family for their emotional stand. I will always be grateful for their love and support. My mother and my wife are one of the true driving forces behind me who truly understand and inspired me to achieve my inspirations.

I would like to express my gratitude to Dr. Abdel-Hamid Mourad under whose guidance this investigation was conducted, for his patient guidance and criticism throughout the investigation, for all the valuable ideas and suggestions, and for our conversations on science and others, often until late in the evening, and which I enjoyed much. It was privileged to work under Dr. Abdel-Hamid Mourad who influenced this work in many ways, his patient and sincere efforts during the whole work will stick in mind.

I would also like to acknowledge National Petroleum Construction Company / Abu Dhabi for providing the material that has been used in this work. Further thanks go to the members of the Department who were involved in my work, special thanks to professor Ali al-domiaty for his prominent contribution and assistant during the work, also to engineer Abdulsattar NourAldain for his help in the laboratory and to Eng. Ammar Alomari for his help in finite element modeling; also l would not forget CLU staff for their kind assistance to conduct SEM.

ABSTRACT

The fracture toughness of pipeline steel grade X65 was investigated utilizing linear elastic fracture mechanics analysis, K_{IC} testing according to non standards techniques, as well as the elastic-plastic fracture mechanics analysis (J-Integral and crack opening displacement COD methods). The fracture toughness tests were conducted at full scale pipe used for gas and oil industry, circumferential surface crack were introduced to nine pipe specimens with different depths, crack/notch depths were selected to cover wide range of remaining material of the original pipe thickness, the original pipe thickness remain unchanged, a special fixture was manufactured to perform the experimental works, plane strain condition was confirmed by using plug insert inside the pipe specimen under the introduced circumferential surface crack.

While for elastic-plastic fracture analysis a circumferential through-wall-cracked (TWC) pipes subjected to pure bending experiments were conducted on four pipe specimens, pipe thickness was reduced to 5mm to meet the capacity of MTS machine used to perform the experimental works, in this analysis different parameters were measured.

Tensile properties of the x-65 steel as well the chemical composition were measured and compared with that provided at inspection certificate and API standards, the results from experimental work were very close.

Beside experimental work finite element method were used for analysis. Finite element modeling was used for comparison with experimental results. ABAQUS is used for FEM calculations for stresses distribution along the crack area, the simulation results were observed to have a good agreement with the experimental results

TABLE OF CONTENETS

List of Figures

List of Tables

List of Tables

Chapter 1

Introduction

1.1 Motivation

In order to analyze the elastic-plastic fracture behavior of a structure such as a pipeline system, the material fracture resistance should first be determined. Standard specimens are used to determine the fracture resistance of the material. It is worth noting here that, such resistance is very conservative in evaluating the integrity of a structure. Also the fracture resistance of the material is highly affected/ altered by the specimen geometry and dimensions due to the constraint effect. Therefore, the fracture behavior of the full scale pipes represents a crucial point for evaluating the integrity of the piping system. In the present study, fracture behavior of steel pipe with short/fine circumferential through-wall crack or surface crack under bending will be investigated.

1.2 Aims and Objectives

The main objective of this work is to study the fracture behavior of real pipes/full scale pipes that are used in the gas, oil, water transmission applications in the United Arab Emirates. It is well known that the X65 steel is one of the most used materials in such applications. Therefore this material is selected for the present research. The comparison between the material resistance obtained from the lab size specimens and the full scale pipe will be conducted to determine the margin of conservativeness. The analytical models available in the literature will be used to predict the J values and compare it with experimentally determined ones. An external circumferential crack with initial finite length is introduced to the pipe which may simulate the corrosion cracks, material defects, manufacturing defects, etc. Recent analytical and experimental studies on Elastic-Plastic Fracture Mechanics (EPFM) indicate that the energy release rate (also known as the J-Integral) and crack-tip opening displacement (CTOD) are most viable fracture parameters for characterizing initiation of crack growth, stable crack growth, and subsequent instability in ductile materials . The method introduced by S. Rahman [71] was used to predict the energy release rate of circumferentially cracked pipe with an

internal, constant depth, finite length surface crack under pure bending load. In this study the J values obtained from the experimental load-point load displacement data are used to investigate the fracture behavior of the material.

1.3 Outline of the dissertation

The dissertation is divided into six chapters, in chapter one, the present chapter, the motivation of study, aims and objectives and outline of dissertation are presented. the relevant literature on the linear elastic fracture mechanics (LEFM) and elastic plastic fracture mechanics (EPFM) are reviewed in chapter two. Commonly used procedures to estimate the fracture toughness for different shapes were also described in chapter 2. Chapter 2 gives a literature review on Standard fracture toughness, Fracture toughness from notched bars/rods, Fracture toughness from notched tubes and STable crack growth through pipe were presented in details.

In chapter three the experimental procedures (material, mechanical and chemical properties) were discussed. In chapter four and five the experimental procedures (Specimen preparation, Test procedure, Results and discussion) for fracture and fracture toughness tests respectively were discussed. Chapter six discusses the finite element analysis, modeling, boundary conditions, and the obtained results. Chapter seven presents a discussion of the results, general conclusion and suggestion for future study.

Chapter 2

LITERATURE REVIEW

2.1 Introduction

Several structural failures can be associated with the fracture of one or more of the materials making that structure. Several examples of such failures took place , one of these failures happened at gulf of Mexico 2010 when a massive oil leakage came out from British Petroleum oil well under Atlantic ocean deep water because of pipe fracture. When such events occur ,they are mostly unexpected, sudden, and unfortunate, and it is natural for us to focus attention on minimizing the undesired consequences when designing and analyzing modern today structures. The study of crack behavior, prevention and analysis of fracture of materials is known as fracture mechanics.

The concept of fracture is old. Example of best engineering mechanics can be seen in the structures commissioned by the Pharaohs of Egypt and the Caesars of Rome which are still standing as a testimony to the ability of early architects and engineers. Advances in fracture mechanics came into account since World War II and the field known as fracture mechanics was born in Naval Research Laboratory in Washington D.C.while investigating the reasons for the failure of Liberty Ship during war as reported in [1]. The contribution of researchers Inglis, Griffith, Irwin, Wells, Dugdale and Barenblatt helped very much to understand the concepts of the Fracture Mechanics Theories and put base for further work in Fracture Mechanics of different materials.

The Fracture Mechanic theories made easiness and competence in designing, product development and used in different application ranging from Dams, Welding and joints, Gas Pipe, Polymers, Composite and Laminates etc [2].

However, when solids contain flaws or cracks, the field Equations is not completely defined by the theory of elasticity since it does not consider the stress singularity phenomenon near the crack tip. It only provides the means to predict general yielding as a failure criterion .Despite the usefulness of predicting yielding, it is necessary to use the principles of fracture mechanics to predict fracture of solid components containing cracks

So, fracture mechanics is the study of mechanical behavior of cracked materials subjected to an applied load. Fracture mechanics deals with the irreversible process of rupture due to nucleation and growth of cracks. The formation of cracks may be a complex fracture process, which strongly depends on the microstructure of a particular crystalline or amorphous solid, applied loading, and environment. The microstructure plays a very important role in a fracture process due to dislocation motion, precipitates, inclusions, grain size, and type of phases making up the microstructure. All these micro structural features are imperfections and can act as fracture nuclei under unfavorable conditions. For instance, Brittle Fracture is a law-energy process (law energy dissipation), which may lead to catastrophic failure without warning since the crack velocity is normally high. On the other hand, Ductile Fracture is a high-energy process in which a large amount of energy dissipation is associated with a large plastic deformation before crack instability occurs. Consequently, slaw crack growth occurs due to strain hardening at the crack tip region.

2.2 Historical Review on Fracture Mechanics

By the end of the 19th century, the influence of crack on the structural strength was widely appreciated, but its nature and influence was still unknown. In 1913, Inglis published the first significant work in the development of fracture mechanics. [3] The work was an analytical formulation of stresses in a plate in the vicinity of a two dimensional elliptical hole. The plate was pulled at both ends perpendicular to the ellipse as shown in Figure 2.1. Inglis observed that the corner of the ellipse (point A) was feeling the most pressure and as the ellipse gets longer and thinner the stresses at (point A) become larger. He examined local stresses at the tip of the ellipse and estimated that the stress intensity factor (SIF) k which has a great significance in measuring the intensity of stress and strain at crack tip was approximately

$$k = 2\sqrt{\frac{a}{\rho}} \quad or \quad k = 2\left(\frac{a}{b}\right) \qquad (2.1)$$

where a and b are the semi major and semi minor axes respectively and ρ is the radius at the tip of the ellipse. Inglis evaluated various hole geometries and realized that it was not really the shape of the hole that mattered but it was the length of hole perpendicular to the load and the curvature at the end of the hole that mattered in cracking. He also noticed that pulling in a direction parallel to the hole did not produce a great effect.

The basic ideas leading to the start of modern fracture mechanics can be attributed to a theory of fracture strength of glass, which was published by A.A. Griffith in 1920 [4] Using Inglis' work as a foundation, Griffith proposed an energy balance approach to study the fracture phenomenon in cracked bodies.

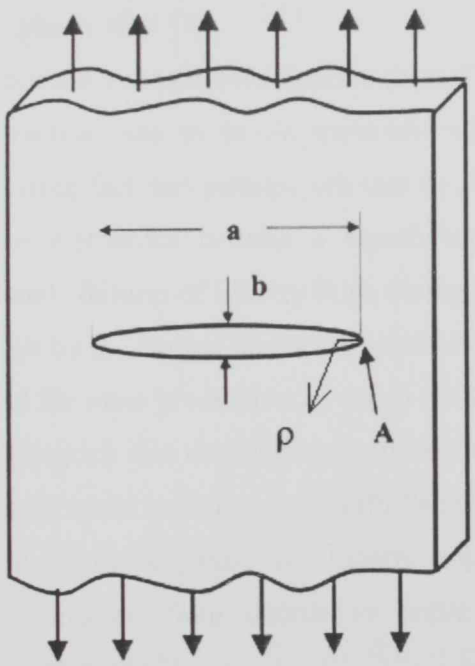

Figure 2.1 Inglis problem 1913; Elliptical hole in a flat plate.

A great contribution to the ideas about breaking strength of materials emerged when Griffith suggested that the weakening of material by a crack could be treated as an equilibrium problem. He proposed that the reduction in strain energy of a body when the

crack propagates could be equated to the increase in surface energy due to the increase in the surface area. The Griffith theory assumed that the fracture strength was limited by the existence of initial cracks and those brittle materials contain elliptical micro cracks, which introduce high stress concentrations near their tips. He developed a relationship between crack length a, surface energy connected with traction-free crack surfaces 2γ and applied stress, which is given by

$$\sigma^2 = \frac{2\gamma E}{\pi a} \qquad (2.2)$$

Plasticity effects in metals limited the theorem and it was not until Irwin's work in 1948, that a modification was made to Griffith's model to make it applicable to metals. Irwin's first major contribution was to extend the Griffith approach to metals by including the energy dissipated by local plastic flaw [5].

Orowan independently proposed a similar modification [6] to Griffith's theory in 1949. Orowan limited practical use to brittle materials while Irwin made no such restrictions. It is an interesting fact and perhaps relevant to point out that the scientific curiosity towards fracture mechanics became a significantly important engineering discipline after the unfortunate failures of Liberty ships during World War II.

The Liberty ships were built by the United States to support Britain's war effort and used a new construction method for mass production in which the hull was welded instead of riveted. The Liberty ship program was an astounding success until 1943, when a Liberty ship broke completely in two while sailing in the North Pacific. Later, hundreds of other vessels sustained fractures. An investigation into Liberty ship failures pointed out poor toughness of steel and transition from ductile to brittle behavior at the service temperatures that ships experienced [7].

It was noticed that the fractures initiated at the square hatched corners on the deck where there was a local stress concentration and the sharp corners acted like starter cracks. Research into this problem was led by George Rankine Irwin at the Naval Research Laboratory in Washington, DC. It was the research during this period that resulted in the development and definition of what we now refer to as linear-elastic fracture mechanics

(LEFM). A major breakthrough occurred in the early 1950s when Irwin and Kies [8, 9] and Irwin [10] provided the extension of Griffith theory for an arbitrary crack and proposed the criteria for the growth of this crack. The criterion was that the strain energy release rate (G) must be larger than the critical work (G_C), which is required to create a new unit crack area. Irwin also related strain energy release rate to the stress field at the crack tip using Westergaard's work. Westergaard had developed a semi-inverse technique for analyzing stresses and displacements ahead of a crack tip. Using Westergaards' method, Irwin showed that the stress field in the area of the crack tip is completely determined by a quantity k called the stress intensity factor. Using the method of virtual work and referring to Figure 2.3 Irwin presented a relationship between the energy release rate and the stress intensity factor as

$$\sigma_{ij} = \frac{k f_{ij(\theta)}}{\sqrt{2\pi r}} \qquad (2.3)$$

$$k^2 = EG \qquad (2.4)$$

Where E is Young's modulus and G is the strain energy release rate.

Other serious failures that were experienced during that period were those of the de Havilland "Comet" commercial aircraft. The Comet was first manufactured in 1952, and was the first two-jet-engine aircraft to fly at 40,000 ft with a pressurized cabin. After about a year in service, three aircraft failed, resulting in the tragic loss of several lives. In 1955, Wells [11] used fracture mechanics to show that the fuselage failures in several Comet jet aircraft resulted from fatigue cracks reaching a critical size. These cracks were initiated at windows and were caused by insufficient local reinforcement in combination with square corners, which produced higher stress concentrations. It was noticed that the fracture of welded Liberty ships, the pressurized cabin fractures of de Havilland Comet jet airplanes, bursts of several large petroleum storage tanks, and several other unpredicted failures, all seemed understandable in terms of the new fracture strength points of view. The evaluation method was straightforward, a value of G_C was established from laboratory tests on pre cracked specimens and the value of the driving force G that

tended to extend the starting crack was computed using appropriate stress analysis methods. The comparison showed that the fracture toughness had not been large enough to prevent crack propagation in the failure cases mentioned above.

In 1957, Williams [12] developed an infinite series that defined stress around a crack for any geometry. The use of the optical method "photo elasticity" to examine the stress fields around the tip of a running crack was published by Wells and Post in 1958, [13] and Irwin [14] observed that the photo elastic fringes not only formed closed loops at the crack tip as predicted by singular stress field Equations but also showed a tilt as a result of the near specimen boundaries. In 1960, a significant contribution to the development of LEFM was put forth when Paris and his coworkers advanced an idea to apply fracture mechanics principles to fatigue crack growth. Although they provided convincing experimental and theoretical arguments for their approach, the initial resistance to their work was intense and they could not find a peer-reviewed technical journal to publish their manuscript. They finally opted to publish their work in a University of Washington periodical entitled The Trend in Engineering [15].

Linear elastic fracture mechanics is not valid when significant plastic deformation precedes failure. Although earlier theoretical developments were aimed at understanding brittle crack behavior, it became apparent from experiments that except for a few, most materials are ductile and therefore linear elastic analysis should be modified accordingly. Dugdale [16] in 1960 and Barenbelt [17] in 1962 made the first attempts to include cohesive forces in the crack tip region by developing an elaborate model within the limits of elasticity. Later, in 1968, Rice conducted a simplified analysis of complete plastic zone formation, approximated by a circular region ahead of the crack tip [18, 19]. The results derived from the energy–momentum tensor concept and applied to elastic cracks were extended to include plastic cracks by defining a path-independent integral termed the J integral. The plastic zone size and the crack opening displacement were found to correlate with the elastic stress intensity factor criterion. The successful experiments in 1971 by Begley and Landes [20] who were the research engineers at Westinghouse, led to the publication of a standard procedure for J testing of metals in 1981[21]. In 1976, Sih [22] introduced the strain–energy density concept, which was a departure from classical fracture mechanics. He was able to characterize mixed-mode extension problems with

this method, which also provided the direction of the crack propagation in addition to the amplitude of the stress field.

Contemporary research and development in fracture mechanics focuses on several interesting areas, such as dynamic fracture mechanics, interface fracture mechanics, shear ruptures in earthquakes, stress corrosion cracking, environmental effects on fatigue crack propagation, fracture of novel materials such as Nano composites and graded materials. Extremely powerful numerical codes that are able to investigate fracture due to separation of atoms are being developed.

Also, experimental techniques have progressed enough to investigate fracture in materials at nanometer length scales and nanosecond time resolution. However, experimental techniques that could provide spatial and temporal resolution simultaneously at the Nano level are still not available. At this point it is pertinent to point out that in the present age of unprecedented technological growth, we are inclined to believe that technology and knowledge are accelerating in an exponential fashion. However, we must recognize that we are observing an exceedingly tiny period of human development on a historic time scale. Although the field of fracture mechanics has matured in recent years, there will be a lot more to learn in the future.

2.3 Linear Elastic Fracture Mechanics (LEFM)

Fracture mechanics is based on the assumption that all engineering materials contain cracks from which failure starts. The estimation of the remaining life of machine or structural components requires knowledge of the redistribution of stresses caused by the introduction of cracks in conjunction with a crack growth condition. Cracks lead to high stresses near the crack tip; this point should receive particular attention since it is here that further crack growth takes place. Loading of a cracked body is usually accompanied by inelastic deformation and other nonlinear effects near the crack tip, except for ideally brittle materials. There are, however, situations where the extent of inelastic deformation and the nonlinear effects are very small compared to the crack size and any other characteristic length of the body. In such cases the linear theory is adequate to address the problem of stress distribution in the cracked body.

Solid bodies containing cracks can be characterized by defining a state of stress near a crack tip and the energy balance coupled with fracture. Introducing the Westergaard's complex function and will allaw the development a significant stress analysis at the crack tip. These particular functions can be found elsewhere [23]. For instance, Irwin [24] treated the singular stress field by introducing a quantity known as the stress intensity factor, which is used as the controlling parameter for evaluating the critical state of a crack.

The field Equations are assumed to be within a small plastic zone ahead of the crack tip. If this plastic zone is sufficiently small, the small-scale yielding approach is used for characterizing brittle solids and for determining the stress and strain fields when the size of the plastic zone is sufficiently smaller than the crack length; than is $r << a$, In contrast, a large-scale yielding is for ductile solids, in which $r \geq a$. Most static failure theories assume that the solid material to be analyzed is perfectly homogeneous, isotropic and free of stress risers or defects, such as voids, cracks, inclusions and mechanical discontinuities (indentations, scratches or gouges). Actually, fracture mechanics considers structural components having small flaws or cracks which are introduced during solidification, quenching, welding, machining or handling process. However, cracks that develop in service are difficult to predict and account for preventing crack growth.

A crack in a body may be subjected to three different types of loading, which involve displacements of the crack surfaces. The mechanical behavior of a solid containing a crack of a specific geometry and size can be predicted by evaluating the stress intensity factors (K_I, K_{II} and K_{III}) shown in Figure 2.2 and Figure 2.3.

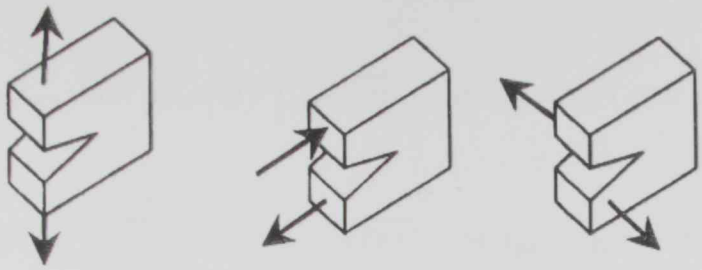

Mode I (Opening) Mode II (Sliding) Mode III (Tearing)

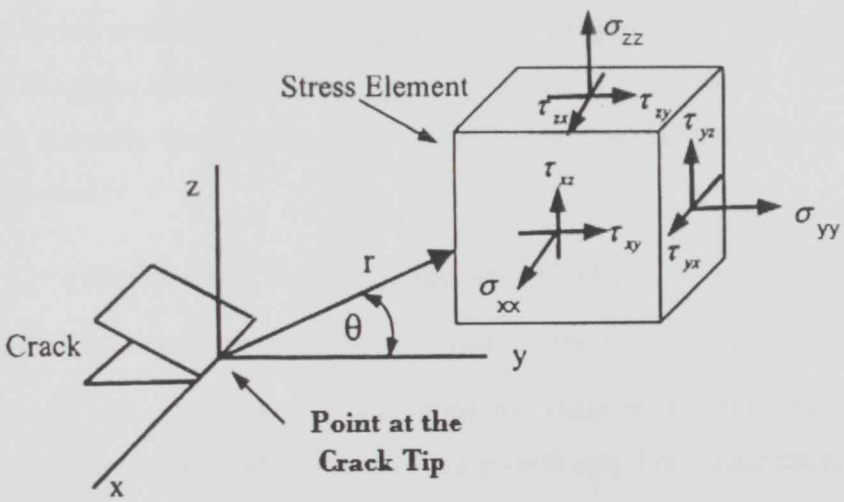

Figure 2.3 stress component ahead of crack tip and coordinate system

If crack growth occurs along the crack plane perpendicular to the direction of the applied external loading mode, then the stress intensity factors are defined according to the American Society for Testing Materials (ASTM) E1820 Standard Test Method as

For mode I

$$K_I = \lim_{r\to 0}(\sigma_{yy}\sqrt{2\pi r})\, f_I(\theta) = \sigma_{yy}\sqrt{2\pi r} \quad @\ \sigma_{yy} = \sigma_{yy}\ (\ r, \theta = 0\ ) \qquad (2.5)$$

For mode II

$$K_{II} = \lim_{r\to 0}(\tau_{xy}\sqrt{2\pi r})\, f_{II}(\theta) = \tau_{xy}\sqrt{2\pi r} \quad @\ \tau_{xy} = \tau_{xy}\ (\ r, \theta = 0\ ) \quad (2.6)$$

For mode III

$$K_{III} = \lim_{r\to 0}(\tau_{yz}\sqrt{2\pi r})\, f_{III}(\theta) = \tau_{yz}\sqrt{2\pi r} \quad @\ \tau_{yz} = \tau_{yz}\ (\ r, \theta = 0\ ) \quad (2.7)$$

Here, $f_I(\theta)$, $f_{II}(\theta)$ and $f_{III}(\theta)$ are trigonometric functions to be derived analytically and was developed by Irwin [24].

Thus, specimens and structural components having flaws or cracks can be loaded to various levels of the applied stress-intensity factor for a particular stress mode shown in Figure 2.3. This is analogous to unflawed components being loaded to various levels of the applied stress σ .In fact, the parameters r and θ are the polar coordinates of a plastic zone that forms ahead of the crack tip. If $\theta = 0$ in Figure 2.3, then the stresses can be evaluated along the crack plane.

The stress intensity factor (s) for a particular crack configuration can be defined as a general function:

$$K_i = f(\text{Stress, Crack Geometry, Specimen Configuration}) \qquad (2.8)$$

Where $i = I, II, III$ which stand for mode 1, mode 2, and mode 3, respectively

The parameter K_i can be used to determine the static or dynamic fracture stress, the fatigue crack growth rate and corrosion crack growth rate. For elastic material, the strain-energy release rate G_i known as the crack driving force, is related to the stress intensity factor and the modulus of elasticity as indicated by the relationship given by

$$G_i = \frac{k_i^2}{E'} \qquad (2.9)$$

Where $E' = E'$ for plane stress (MPa).

$E' = E / (1 - \upsilon^2)$ for plane strain (MPa).

E = Elastic modulus of elasticity (MPa).

υ = Poisson's ratio.

This expression, Equation (2.9), is a fundamental mathematical model in the fracture mechanics field, specifically for mode I.

Various solutions for K can be found in stress intensity handbooks such as Murakami [31]. Generally k for mode I loading K_I , has the form:

$$K_I = Y\sigma_\infty\sqrt{\pi a} \qquad (2.10)$$

Fracture behavior, in the context of LEFM, presumes that a crack would grow unstably to cause catastrophic failure once a critical value of stress,K_C , is reached. Such K_C can be corresponded to a critical load value, P_Q, which can be determined experimentally. When critical load is applied, it causes the formation of finite crack growth. The initiation of such finite crack growth causes release of stored potential elastic – strain energy , which in turn causes formation of additional crack growth with additional release of potential strain energy; in effect causing a positive –feedback loop leading to unstable crack growth . K_C (K_C for mode-I) is therefore regarded as the fracture toughness of the component or structure in question.

2.3.1 Limitation of Linear Elastic Fracture Mechanics:

Most solid materials develop plastic strains when the yield strength is exceeded in the region near a crack tip. Thus, the amount of plastic deformation is restricted by the surrounding material, which remains elastic during loading. Theoretically, linear elastic stress analysis of sharp cracks predicts infinite stresses at the crack tip. In fact, inelastic deformation, such as plasticity in metals and crazing in polymers, leads to relaxation of crack tip stresses caused by the yielding phenomenon at the crack tip. As a result, a plastic zone is formed containing micro structural defects such dislocations and voids. Consequently, the local stresses are limited to the yield strength of the material. This implies that the elastic stress analysis becomes increasingly inaccurate as the inelastic region at the crack tip becomes sufficiently large and linear elastic fracture mechanics (LEFM) is no longer useful for predicting the field Equations.

The size of the plastic zone can be estimated when moderate crack tip yielding occurs. Thus, the introduction of the plastic zone size as a correction parameter that accounts for plasticity effects adjacent to the crack tip is vital in determining the effective stress intensity factor k_e or a corrected stress intensity factor. The plastic zone is also determined for plane conditions; that is, plane strain for maximum constraint on

relatively thick components and plane stress for variable constraint due to thickness effects of thin solid bodies. Moreover, the plastic zone develops in most common in materials subjected to an increase in the tensile stress that causes local yielding at the crack tip [2].

2.4 Elastic – Plastic Fracture Mechanics (EPFM)

Linear elastic fracture mechanics (LEFM) is valid only as long as nonlinear material deformation is confined to a small region surrounding the crack tip, elastic –plastic applies to materials that exhibit time-independent, nonlinear behavior [1].

It is now well-established that the elastic-plastic fracture mechanics (EPFM) provide more realistic measures of fracture behavior of cracked engineering systems when compared with the elastic methods. The use of EPFM becomes almost necessary for structural materials with high toughness and law strength, which generally undergo extensive plastic deformation around a crack tip. Recent analytical ,experimental and computational studies on this subject indicate that the energy release rate (J-integral) and the crack-tip opening displacement (CTOD) are the most viable fracture parameters for characterizing crack initiation ,stable crack growth and subsequent instability in ductile materials [25].

It has been shown that LEFM is applicable only to those situations where crack propagation is accompanied by little or no plastic deformation. Quantitatively this means that the extent of crack tip plasticity should be at least fifty times smaller than the dimensions of the structure including the crack length. Almost all law to medium strength and HSLA structural steels that are used for large complex structures such as bridges, ships, pressure vessels etc. are of insufficient thickness to maintain the plane strain conditions at the temperature and strain rate of the service conditions. Hence in such applications insufficient constraint is available to maintain plane strain conditions and a large plastic zone forms.

For pipe steels, neither the specimen nor the structure (the pipe) is amenable to LEFM analysis. This is shown clearly in Figure 2.4 in which are shown typical schematic load-deflection curves for small specimens of various materials. Figure 2.4a depicts fully linear behavior which is easily handled by LEFM; Figure 2.4b shows a "Pop-in" behavior which

characterizes the initial crack growth, for a given material, regardless of the specimen thickness. LEFM can also be used to calculate K_{IC} by the offset procedure as described in the ASTM standard E-1820; Figure 2.4c shows considerable non-linear behavior in the load-deflection curve prior to sudden failure; while Figure 2.4d shows the behavior of a ductile material where sudden failure never occurs. These non- linearties can arise from two sources, plastic deformation at the crack tip and stable crack extension [26]. Therefore, the test behaviors described in Figure 2.4c and d are the subject matters of Elastic-Plastic Fracture Mechanics (EPFM), a considerable work has been reported on the development of EPFM analysis as an extension of LEFM analysis [26, 27].

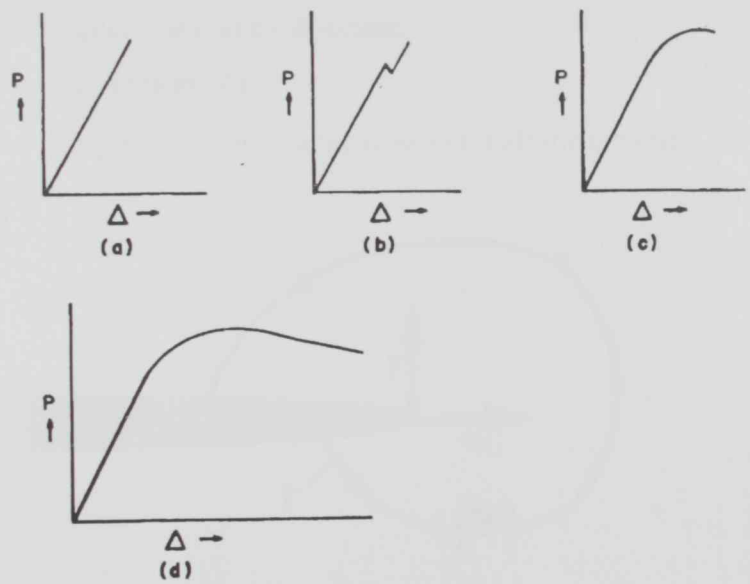

Figure 2.4 Schematic Load (P) vs. Load-point displacement (Δ) curves for:
(a) Perfectly elastic material.
(b) Elastic material with pop-in behavior.
(c) Elastic then plastic behavior.
(d) Ductile material with extensive plasticity prior to failure.

The two most promising and widely accepted techniques for analyzing elastic-plastic fractures are:

1. The J-Integral Method
2. The crack opening Displacement (COD) Method.

2.4.1 The J-Integral Approach

The J-Integral, as shown in Figure 2.5 proposed by Rice, is a way of characterizing the stress-strain field ahead of a crack tip by an integration path:

$$J = \int_{\Gamma} w dy - T_i \left(\frac{\partial u_i}{\partial X}\right) ds \qquad (2.11)$$

$\Gamma = a$; contour travelling counter clock wise around the crack tip.

$T_i =$ The tension vector perpendicular to Γ in an outward direction.

$u_i =$ Displacement in x - direction.

$ds =$ An element of Γ

$w = \int_0^{\epsilon} \sigma_{ij}\, d\varepsilon_{ij}$, strain energy density for elastic materials

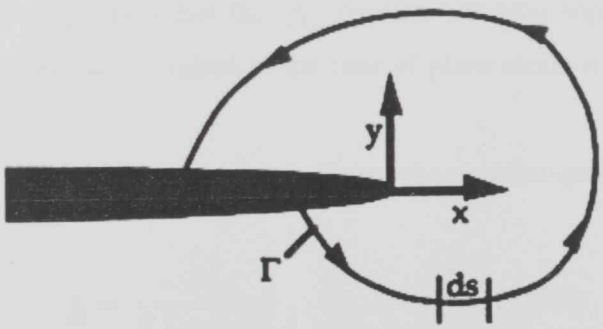

Figure 2.5 Arbitrary contour around the tip of a crack

Therefore, even if considerable yielding occurs near the crack tip, the region away from the crack tip can be analyzed and the condition in the crack tip region can be derived.

Later, Hutchinson and Rice and Rosengren described a stress-strain distribution around a crack tip surrounded by a plastic strain field. They developed a model known as the HRR crack tip model which establishes that J is the amplitude of the near field singularity at the crack tip. McClintock [28] has also shown that by combining J with the HRR crack tip model, the near tip values of stress and strain can be expressed as a function of J. This is

directly analogues to the stress field Equation of LEFM.

Rice [29] has also shown that the J -Integral may be interpreted as the difference in potential energy between two identically loaded bodies with differing crack lengths. This is stated mathematically as

$$J = -\frac{dU}{da} \qquad (2.12)$$

Where $U =$ the potential energy.

$a =$ Crack length.

For the linear elastic behavior and also for small scale yielding, J is therefore equal to G, the strain energy release rate per unit crack extension, i.e. the crack driving force. In cases where the deformation is not reversible that is the general elastic-plastic problem, J loses its physical significance as a crack driving force. Begley and Landes [30] suggest that J is still equal to - $\frac{dU}{da}$ and the physical significance of J for elastic-plastic materials is that J is a measure of the characteristic crack tip elastic-plastic field similar to K in LEFM. They made the additional suggestion that the J_{IC} fracture criterion applies to crack initiation rather than propagation and is limited to the case of plane strain which is denoted by the subscript I in J_{IC}.

Later Rice et al [31] developed a simple, single specimen technique for measuring J_I using the expression:

$$J_I = \frac{2A}{B\,(w-a)} \qquad (2.13)$$

Where A = Area under the load vs. load-point displacement curve

B = Specimen thickness

a = Crack length

w =specimen width

In this technique, a bending load is applied to a bar or compact tension specimen containing a deep notch crack $\frac{a}{w} \geq 0.6$ and J_I is determined as a function of the load-point displacement. The critical value of J_I is then J_{IC} which refers to that value of J_I at which crack initiation takes place.

Once the J value is determined, the corresponding K_{IC} values can be computed from the relationship between the elastic-plastic and the LEFM parameters [30, 31, and 32]

$$J_{IC} = G_{IC} = \frac{1 - v^2}{E} K_{IC}^2 \qquad (2.14)$$

Where v = Poisson's Ratio

E = Young's Modulus

2.4.1.1 Experimental Technique:

Several experimental techniques have been reported [32] for determining the point of crack initiation in a static J-Integral test. These are:

1. J-Resistance curve
2. Compliance
3. Ultrasonic
4. Electrical Potential
5. Resonance Frequency

The J-Resistance curve method is simple and requires less sensitive electronic equipment in comparison with the other test methods. This method is also known as the Resistance curve technique. It has been developed by Landes and Begley [32]. Briefly the testing procedure involves:

a) Loading each specimen to a different displacement value

b) Unload each specimen; mark the crack extension by

c) Pull the specimen apart and measure the crack extension

d) Construct a resistance curve by plotting J for each specimen vs its corresponding crack extension.

In order to find out the J_{IC} value from the resistance curve Landes and Begley suggested the use of a best fit line to the J vs crack size curve. The point of intersection of this curve with the line $J = 2\,\sigma_{flow}\Delta a$ gives the value of J_{IC} ,

Where

$$\sigma_{flow} = \frac{\sigma_{yield\ stress} + \sigma_{UTS}}{2} \qquad (2.15)$$

2.4.1.3 Validity Criteria:

Landes and Begley [32, 36] have proposed a size requirement which must be satisfied by an elastic-plastic fracture toughness test specimen to obtain valid J_{IC}data. This size requirement is stated analytically as

$$a, B, w - a \geq 25 \quad \frac{J_Q}{\sigma_{flow}} \qquad (2.16)$$

If this condition is satisfied, then J_Q becomes J_{IC}.

2.4.2 The Crack – Opening Displacement Method:

For law to medium strength steels extensive plastic flaw takes place before the initiation of the fracture. Under an externally applied load, the two faces of the crack tip move apart without an increase in the length of the crack [33]. The relative movement of the two faces at the crack tip has been termed the Crack-opening Displacement (COD) and has been designated as 'δ' [34].

The consequence of yielding at the crack tip giving rise to physical displacement of the crack surfaces was first applied as a possible fracture criterion by Wells [35].

2.4.2.1 COD as an extension to LEFM:

For a material that exhibits appreciable crack tip plasticity, it is possible to develop a relationship between the stress intensity factor $K$and δ near the tip for the crack tip opening displacement. The size of the plane stress plastic zone may be approximated by the relation:

$$r_y = \frac{1}{2\pi}\left(\frac{K}{\sigma_{ys}}\right)^2 \qquad (2.17)$$

Where r_y = the extent of the plastic zone along the crack plane

σ_{ys} = yield strength of the material in a uni-axial tensile test.

With this corrected crack border model, the y direction displacement, ' η', within the crack at any distance 'r' from its tip may be evaluated using Westergaard's expression [35]

$$\eta = \frac{2K}{E}\sqrt{\frac{2r}{E}} \qquad (2.18)$$

Now the displacement at the elastic-plastic interface corresponds to the displacement at the tip of the crack.

Therefore, the crack opening displacement near the crack tip is:

$$\delta = 2\eta = \frac{4K}{E}\sqrt{\frac{2r_y}{\pi}} \qquad (2.19)$$

Combining the Equation for r_y the plastic zone K2 size and the relationship $G = \frac{K^2}{E}$ [12] gives rise to

$$\delta = \frac{4G}{\pi\sigma_{ys}} \qquad (2.20)$$

This relationship was developed by Wells [46]. He inferred that under local plastic conditions, COD gives a measure of the crack extension force G. Thus the COD can be related to the plane-strain fracture toughness. This also indicates that if the COD is large for a specified value of yield stresses such that $\sigma_{ys}\delta$ exceeds the critical crack extension force G, then fracture follows [37]. Hence the COD measurements in the presence of extensive plastic deformation ahead of the crack tip for elastic-plastic and fully plastic behavior is an index of the fracture toughness and is a direct extension of LEPM into yielding materials.

2.5 Standard Test for Measurements of Fracture

2.5.1 Plane-Strain Fracture Toughness Test [38]:

This test method involves testing of notched specimens that have been precracked in fatigue by loading either in tension or three-point bending, ASTM E1820. Load versus displacement across the notch at the specimen edge is recorded autographically. The load corresponding to a 2 % apparent increment of crack extension is established by a specified deviation from the linear portion of the record. The K_{IC}value is calculated from this load by Equations that have been established on the basis of elastic stress analysis of specimens of the types described in this method. The validity of the determination of the K_{IC}value by this test method depends upon the establishment of a sharp-crack condition at the tip of the fatigue crack, in a specimen of adequate size. To establish a suitable crack-tip condition, the stress intensity level at which the fatigue pre-cracking of the specimen is conducted is limited to a relatively low value. The specimen size required for testing purposes increases as the square of the ratio of toughness to yield strength of the material; therefore a range of proportional specimens is provided. The property K_{IC}determined by this test method characterizes the resistance of a material to fracture in a neutral environment in the presence of a sharp crack under severe tensile constraint, such that the state of stress near the crack front approaches tri-tensile plane strain, and the crack-tip plastic region is small compared with the crack size and specimen dimensions in the constraint direction. A K_{IC} value is believed to represent a lower limiting value of fracture toughness. This value may be used to estimate the relation between failure stress and defect size for a material in service wherein the conditions of high constraint described above would be expected. Plane-strain crack toughness testing is unusual in that there can be no advance assurance that a valid K_{IC}will be determined in a particular test. Therefore it is essential that all of the criteria concerning validity of results be carefully considered as described herein. Clearly it will not be possible to determine K_{IC}if any dimension of the available stock of a material is insufficient to provide a specimen of the required size. In such a case the specimen strength ratio determined by this method will often have useful significance. However, this ratio, unlikeK_{IC}, is not a concept of linear elastic fracture mechanics, but can be a useful comparative measure of the

toughness of materials when the specimens are of the same form and size, and that size is insufficient to provide a valid K_{IC} determination, but sufficient that the maximum load results from pronounced crack propagation rather than plastic instability. In order for a result to be considered valid according to this method it is required that both the specimen thickness, B, and the crack length, a, exceed $2.5(K_{IC}/\sigma_{YS})^2$, where σ_{YS} is the 0.2 % offset yield strength of the material for the temperature and loading rate of the test. The initial selection of a size of specimen from which valid values of K_{IC} will be obtained may be based on an estimated value of K_{IC} for the material. It is recommended that the value of K_{IC} be overestimated, so that a conservatively large specimen will be employed for the initial tests. After a valid K_{IC} result is obtained with the conservative-size initial specimen, the specimen size may be reduced to an appropriate size [a and B > $2.5(K_{IC}/\sigma_{YS})^2$] for subsequent testing. When it has been established that 2.5 $(K_{IC}/\sigma_{YS})^2$ is substantially less than the minimum recommended thickness given in the preceding Table, then a correspondingly smaller specimen can be used. On the other hand, if the form of the available material is such that it is not possible to obtain a specimen with both crack length and thickness greater than $2.5(K_{IC}/\sigma_{YS})^2$, then it is not possible to make a valid K_{IC} measurement according to this method. The configurations of the various specimens are Bend Specimen SE (B), Compact Specimen C (T), Arc-Shaped Tension Specimen A(T), Disk-Shaped Compact Specimen DC(T) and Arc-Shaped Bend Specimen A(B).

The standard bend specimen is a single edge notched and fatigue cracked beam loaded in three-point bending with a support span, S, nominally equal to four times the width, W. The general proportions of this specimen configuration are shown in Figure 2.4. The general principles of the bend test fixture are illustrated in Figure 2.7. This fixture is designed to minimize frictional effects by allowing the support rollers to rotate and move apart slightly as the specimen is loaded, thus permitting rolling contact. Thus, the support rollers are allowed limited motion along plane surfaces parallel to the notched side of the specimen, but are initially positively positioned against stops that set the span length and are held in place by low-tension springs (such as rubber bands).

For the bend specimen shown in Figure 2.6, at a load $P_{(i)}$, K is calculated as follows:

$$K_{(i)} = \left[\frac{P_i S}{(BB_N)^{1/2} W^{3/2}}\right] f\,(a_i/W) \qquad (2.21)$$

where:

$$f\,(a_i/W) = \frac{3(a_i/W)^{1/2}\,[1.99 - (a_i/W)(1 - a_i/W) \times (2.15 - 3.93\,(a_i/W) + 2.7\,(a_i/W}{2\,(1 + 2\,a_i/W)(1 - a_i/W)^{3/2}}$$

and

$$B = specimen\ thickness$$

$$B_N = net\ thickness$$

$$W = specimen\ width$$

$$S = specimen\ span$$

For the compact specimen shown in Figure 2.7 and at a load $P_{(i)}$, K is calculated as follows:

$$K_{(i)} = \left[\frac{P_i}{(BB_N W)^{1/2}}\right] f\,(a_i/W) \qquad (2.22)$$

With

$$f\,(a_i/W) = \frac{[(2 + a_i/W)(0.886 + 4.64(a_i/W) - 13.32\,(a_i/W)^2 + 14.72\,(a_i/W)^3 - 5.6(a_i/W)^4}{(1 - a_i/W)^{3/2}}$$

$$B = specimen\ thickness$$

$$B_N = net\ thickness$$

The standard disk-shaped compact specimen, DC (T), is a single edge-notched and fatigue cracked plate loaded in tension. The specimen geometry which has been used successfully is shown in Figure 2.8 for the DC (T) specimen at a load$P_{(i)}$, K is calculated as follows:

$$K_{(i)} = \left[\frac{P_i}{(BB_N W)^{1/2}}\right] f\,(a_i/W) \qquad (2.23)$$

Where

$$f\,(a_i/W) = \frac{[(2 + a_i/W)(0.76 + 4.8(a_i/W) - 11.58\,(a_i/W)^2 + 11.43\,(a_i/W)^3 - 4.08(a_i/W)^4)]}{(1 - a_i/W)^{3/2}}$$

2.5.2 Crack-Tip Opening Displacement (CTOD) [38]:

This test method covers the determination of critical crack-tip opening displacement (CTOD) values at one or more of several crack extension events. These CTOD values can be used as measures of fracture toughness for metallic materials, and are especially appropriate to materials that exhibit a change from ductile to brittle behavior with decreasing temperature. This test method applies specifically to notched specimens sharpened by fatigue cracking. The recommended specimens are three-point bend [SE(B)] compact [C(T)], or arc-shaped bend [A(B)] specimens. This test method characterizes the fracture toughness of materials through the determination of crack-tip opening displacement (CTOD) at one of three events: (a) onset of unstable crack extension without significant prior stable crack extension, (b) onset of unstable crack extension with significant prior stable crack extension, or (c) achievement of plastic limit load with or without significant stable crack extension. This test method may also be used to characterize the toughness of materials for which the properties and thickness of interest preclude the determination of K_{IC} fracture toughness in accordance with Test Method E 399. The values of CTOD may be affected by specimen dimensions. It has been shown that values of CTOD determined on SE (B) specimens using the square section geometry may not be the same as those using the rectangular section geometry, and may differ from those obtained with either the C (T) or A (B) specimens. The loading rate is slow and influences of environment (other than temperature) are not covered. The specimens are tested under crosshead or clip gage displacement controlled loading. The recommended specimen thickness, B, for the SE (B) and C (T) specimens is that of the material in thicknesses intended for an application. For the A(B) specimen, the recommended depth, W, is the wall thickness of the tube or pipe from which the specimen is obtained. Superficial surface machining may be used when desired. For the recommended three-point bend specimens [SE(B)], width, W, is either equal to, or twice, the specimen thickness, B, depending upon the application of the test. For SE(B) specimens the recommended initial normalized crack size is $0.45 \leq a_o/W \leq 0.70$. The span-to-width ratio (S/W) is specified as 4. For the recommended compact specimen [C(T)] the initial normalized crack size is $0.45 \leq a_o/W \leq 0.70$. The half-height-to-

width ratio (H/W) equals 0.6 and the width to thickness ratio W/B is specified to be 2. For the recommended arc-shaped bend [A (B)] specimen, B is one-half the specimen depth, W. The initial normalized crack size is $0.45 < a_O/W < 0.70$. The span to width ratio, S/W, may be either 3 or 4 depending on the ratio of the inner to outer tube radius. For an inner radius, r_1, to an outer radius r_2, ratio of > 0.6 to 1.0, a span to width ratio, S/W, of 4 may be used. For r_1/r_2 ratios from 0.4 to 0.6, an S/W of 3 may be used.

In CTOD testing, δ_c is the value of CTOD at the onset of unsTable brittle crack extension or pop-in when $\Delta a_p < 0.2$ mm (0.008 in.). The force P_C and the clip gage displacement v_c, for dc δ_c are indicated in Figure 2.10. In CTOD testing, δ_c is the value of CTOD at the onset of unsTable brittle crack extension or pop-in when the event is preceded by $\Delta a_p > 0.2$ mm (0.008 in.). The force P_u and the clip gage displacement v_u, for δ_u are indicated in Figure 2.10 .Also, In CTOD, δ_m is the value of CTOD at the first attainment of a maximum force plateau for fully plastic behavior. The force P_m and the clip gage displacement v_m, for δ_m are indicated in Figure 2.10.

For single edge bend specimen shown in Figure 2.6 the calculations of CTOD for any point on the load-displacement curve are made from the following expression:

$$\delta = \frac{K^2\,(1 - v^2)}{2\sigma_{YS}E} + \frac{r_p(W - a_o)V_{pl}}{[r_p(W - a_o) + a_o + z]} \qquad (2.24)$$

where :

$a_o = original\ crack\ length,$

$K = stress\ intensity\ factor\ with\ a = a_o,$

$v = Poisson's\ ratio,$

$\sigma_{YS} = yield\ or\ 0.2\ \%\ offset\ yield\ strength\ at\ the\ temperature\ of\ interest,$

$E = elastic\ modulus\ at\ the\ test\ temperature,$

$V_{pl} = plastic\ component\ of\ crack\ mouth\ opening\ displacement\ at\ the\ point\ of\ evaluation\ on\ the\ load - displacement\ curve, v_c, v_i, v_u, or\ v_m,$

$z = distance\ of\ knife\ edge\ measurement\ point\ from\ the\ notched\ edge\ on\ the\ single\ edge\ bend\ specimen, and$

$r_p = plastic\ rotation\ factor = 0.44.$

The calculations of CTOD of compact specimen shown in Figure 2.7 for any point on the load-displacement curve are made from the following expression:

$$\delta_{(i)} = \frac{K_{(i)}^2 (1 - v^2)}{2\sigma_{YS}E} + \frac{[r_p(W - a_o)]V_{pl(i)}}{[r_p(W - a_o) + a_o + z]} \qquad (2.25)$$

where :

$a_o = original\ crack\ length,$

$K = stress\ intensity\ factor\ with\ a = a_o,$

$v = Poisson's\ ratio,$

$\sigma_{YS} = yield\ or\ 0.2\ \%\ offset\ yield\ strength\ at\ the\ temperature\ of\ interest,$

$E = elastic\ modulus\ at\ the\ test\ temperature,$

$V_{pl} = plastic\ component\ of\ crack\ mouth\ opening\ displacement\ at\ the\ point\ of\ evaluation\ on\ the\ load - displacement\ curve, v_c, v_i, v_u, or\ v_m,$

$z = distance\ of\ knife\ edge\ measurement\ point\ from\ the\ notched\ edge\ on\ the\ single\ edge\ bend\ specimen, and$

$r_p = plastic\ rotation\ factor = 0.4\,(1 + \alpha).$

where :

$$\alpha = 2\left[\left(\frac{a_o}{b_o}\right)^2 + \frac{a_o}{b_o} + \frac{1}{2}\right]^{1/2} - 2\left(\frac{a_o}{b_0} + \frac{1}{2}\right)$$

For Disk-Shaped compact specimens shown in Figure 2.6 the calculations of CTOD for any point on the load-displacement curve are made from the following expression:

$$\delta_{(i)} = \frac{K_{(i)}^2 (1 - v^2)}{2\sigma_{YS}E} + \frac{[r_p(W - a_o)]V_{pl(i)}}{[r_p(W - a_o) + a_o + z]} \qquad (2.26)$$

where :

$a_o = original\ crack\ length,$

$K = stress\ intensity\ factor\ with\ a = a_o,$

$v = Poisson's\ ratio,$

$\sigma_{YS} =$ *yield or 0.2 % offset yield strength at the temperature of interest,*

$E =$ *elastic modulus at the test temperature,*

$V_{pl} =$ *plastic component of crack mouth opening displacement at the point of evaluation on the load − displacement curve,* $v_c, v_i, v_u,$ *or* v_m,

$z =$ *distance of knife edge measurement point from the notched edge on the single edge bend specimen, and*

$r_p =$ *plastic rotation factor* $= 0.4\,(1 + \alpha)$.

where :

$$\alpha = 2\left[\left(\frac{a_o}{b_o}\right)^2 + \frac{a_o}{b_o} + \frac{1}{2}\right]^{1/2} - 2\left(\frac{a_o}{b_0} + \frac{1}{2}\right)$$

2.5.3 J- Integral [38]**:**

Standard test E1820 covers procedures and guidelines for the determination of fracture toughness of metallic materials using some parameters. One of these parameters is the J-Integral. The recommended specimens are single-edge bend, [SE(B)], compact, [C(T)], and disk-shaped compact, [DC(T)]. All specimens contain notches that are sharpened with fatigue cracks, these types of specimens are shown in Figure 2.6, Figure 2.7 and Figure 2.8.

For the single edge bend specimen, J calculated as follows:

$$J = J_{el} + J_{pl} \qquad (2.27)$$

Where

$J_{el} =$ *elastic component of* J, *and*

$J_{pl} =$ *plastic component of* J.

At a point corresponding to v and P on the specimen load versus load-line displacement, shown in Figure 2.11 J calculated as follows:

$$J = \frac{K^2\,(1 - v^2)}{E} + J_{pl} \qquad (2.28)$$

where:

K is from Equation (2.21) with a = a_o, and

$$J_{pl} = \frac{2\,A_{pl}}{B_N b_o}$$

where:

$A_{pl} = \text{area as shown in figure } 2.11,$

$B_N = \text{net specimen thickness } (B_N = B \text{ if no side grooves are present}),$

$b_o = W - a_o.$

For the compact specimen shown in Figure 2.7 J calculated as follows:

$$J = J_{el} + J_{pl} \qquad (2.29)$$

Where

$$J_{el} = \text{elastic component of } J, \text{and}$$

$$J_{pl} = \text{plastic component of } J.$$

For the compact specimen at a point corresponding to v, P on the specimen load versus load-line displacement record shown in Figure 2.11, calculate as follows:

$$J = \frac{K^2\,(1 - v^2)}{E} + J_{pl} \qquad (2.30)$$

where K is from Equation (2.22) with a = a_o, and

$$J_{pl} = \frac{\eta\,A_{pl}}{B_N b_o}$$

where:

$A_{pl} = \text{area } A \text{ as shown in Figure } 2.11,$

$B_N = \text{net specimen thickness } (B_N = B \text{ if no side grooves are present}),$

$b_o = \text{uncracked ligament }, (W - a_o), \text{and}$

$\eta = 2 + 0.522\ b_o/W.$

For Disk- Shaped Compact specimen, DC (T), shown in Figure 2.8, calculate J as follows:

$$J = J_{el} + J_{pl} \qquad (2.31)$$

where

$$J_{el} = elastic\ component\ of\ J, and$$
$$J_{pl} = plastic\ component\ of\ J.$$

For the compact specimen at a point corresponding to v, P on the specimen load versus load-line displacement record shown in Figure 2.11, calculate as follows:

$$J = \frac{K^2\,(1 - v^2)}{E} + J_{pl} \qquad (2.32)$$

where:

K is from Equation (2.23) with a = a_o, and

$$J_{pl} = \frac{\eta\, A_{pl}}{B_N b_o}$$

where:

$A_{pl} = area\ A\ as\ shown\ in\ Figure$ 2.11,

$B_N = net\ specimen\ thickness\ (B_N = B\ if\ no\ side\ grooves\ are\ present)$,

$b_o = uncracked\ ligament\ , (W - a_o), and$

$\eta = 2 + 0.522\ b_o/W.$

2.5.4 R-curve or J-R curve [38]**:**

As part of ASTM E-1820 procedures for the determination of fracture toughness parameters, Toughness can be measured in the R-curve format or as a point value. In this test method, the J-R curve is a plot of the far-field J-integral versus the physical crack extension, Δa_p. It is recognized that the far-field value of J may not represent the stress-strain field local to a growing crack.

In the Resistance Curve Test Method and at a point corresponding to $a_{(i)}$,$v_{(i)}$, and $P_{(i)}$ on the specimen load versus plastic load-line displacement shown in Figure 2.12. And for

single edge bend $[SE(B)]$ shown in Figure 2.6 the J calculation for the resistance curve as follows:

$$J_{(i)} = \frac{(K_{(i)})^2\,(1 - v^2)}{E} + J_{pl(i)} \qquad (2.33)$$

Where $K_{(i)}$ is from Equation (2.21), and

$$J_{pl(i)} = \left[J_{pl(i-1)} + \left(\frac{2}{b_{(i-1)}}\right)\left(\frac{A_{pl(i)} - A_{pl(i-1)}}{B_N}\right)\right] \cdot \left[1 - \frac{a_{(i)} - a_{(i-1)}}{b_{(i-1)}}\right] \qquad (2.34)$$

In Equation (2.34), the quantity $A_{pl(i)} - A_{pl(i-1)}$ is the increment of plastic area under the load versus load-line displacement record between lines of constant displacement at points $i-1$ and i shown in Figure 2.10. The quantity $J_{pl(i)}$ represents the total crack growth corrected plastic J at point i and is obtained in two steps by first incrementing the existing $J_{pl(i-1)}$ and then by modifying the total accumulated result to account for the crack growth increment. Accurate evaluation of $J_{pl(i)}$ from the Equation (2.34) relationship requires small and uniform crack growth increments. The quantity $A_{pl(i)}$ can be calculated from the following Equation:

$$A_{pl(i)} = A_{pl\,(i-1)} + \frac{[P_{(i)} + P_{(i-1)}][V_{pl(i)} - V_{pl(i-1)}]}{2} \qquad (2.35)$$

where :

$V_{pl(i)} = plastic\ part\ of\ the\ load - line\ displacement = V_{(i)} - P_{(i)}C_{LL\,(i)}$, *and*

$C_{LL\,(i)}$ = slope, $((\Delta V/\Delta P)_{(i)}$, *required to give the current crack length,* a_i.

$C_{LL\,(i)}$ can be determined from knowledge of a_i/W using the follawing Equation:

$$C_{LL\,(i)} = \frac{1}{E\,B_e}\left(\frac{S}{W - a_i}\right)^2 [1.193 - 1.98\,(a_i/W) + 4.478\,(a_i/W)^2 - 4.443\,(a_i/W)^3 + 1.739\,(a_i/W)^4]$$

where:

$B_e = B - (B - B_N)^2/2$

For the C(T) specimen shown in Figure 2.7 at a point corresponding $a_{(i)}$, $V_{(i)}$, and $P_{(i)}$ on the specimen load versus load-line displacement record J Calculation for the Resistance Curve Test as follows:

$$J_{(i)} = \frac{(K_{(i)})^2\,(1 - v^2)}{E} + J_{pl(i)} \qquad (2.36)$$

where $K_{(i)}$ is defined in Equation (2.22), and:

$$J_{pl(i)} = \left[J_{pl(i-1)} + \left(\frac{\eta_{(i-1)}}{b_{(i-1)}}\right)\left(\frac{A_{pl(i)} - A_{pl(i-1)}}{B_N}\right)\right] \cdot \left[1 - \gamma_{(i-1)}\frac{a_{(i)} - a_{(i-1)}}{b_{(i-1)}}\right] \qquad (2.37)$$

where:

$\eta_{(i-1)} = 2.0 + 0.522\, b_{(i-1)}/\, W$, and

$\gamma_{(i-1)} = 1.0 + 0.76\, b_{(i-1)}/\, W$.

In Equation (2.37), the quantity $A_{pl(i)} - A_{pl(i-1)}$ is the increment of plastic area under the load versus plastic load-line displacement record between lines of constant displacement at points $(i-1)$ and (i) shown in Figure 2.12. The quantity $J_{pl(i)}$ represents the total crack growth corrected plastic J at point i and is obtained in two steps by first incrementing the existing $J_{pl(i-1)}$and then by modifying the total accumulated result to account for the crack growth increment. The quantity $J_{pl(i)}$ can be calculated from the following Equation:

$$A_{pl(i)} = A_{pl\,(i-1)} + \frac{[P_{(i)} + P_{(i-1)}][V_{pl(i)} - V_{pl(i-1)}]}{2} \qquad (2.38)$$

where:

$V_{pl(i)} = plastic\ part\ of\ the\ load - line\ displacement = V_{(i)} - (P_{(i)}C_{LL\,(i)})$, *and*

$C_{LL\,(i)}$ = compliance, $((\Delta V/\Delta P)_{(I)}$, *required to give the current crack length,* a_i.

$C_{LL\,(i)}$ Can be determined from knowledge of a_i/W using the following Equation:

$$C_{LL\,(i)} = \frac{1}{E\,B_e}\left(\frac{W + a_i}{W - a_i}\right)^2 [2.163 + 12.219\,(a_i/W) - 20.065\,(a_i/W)^2 - 0.9925\,(a_i/W)^3 + 20.609\,(a_i/W)^4 - 9.9314\,(a_i/W)^5]$$

where:

$B_e = B - ((B - B_N)^2 / B)$

For the disk-shaped compact specimens, DC (T), shown in Figure 2.8 at a point corresponding$a_{(i)}V_{(i)}$, and $P_{(i)}$ on the specimen load versus load-line displacement record J Calculation for the Resistance Curve Test as follows:

$$J_{(i)} = \frac{(K_{(i)})^2\,(1-\nu^2)}{E} + J_{pl(i)} \qquad (2.39)$$

where $K_{(i)}$ is from (2.23), and:

$$J_{pl(i)} = \left[J_{pl(i-1)} + \left(\frac{\eta_{(i-1)}}{b_{(i-1)}}\right)\left(\frac{A_{pl(i)} - A_{pl(i-1)}}{B_N}\right)\right] \cdot \left[1 - \gamma_{(i-1)}\frac{a_{(i)} - a_{(i-1)}}{b_{(i-1)}}\right] \qquad (2.40)$$

where:

$\eta_{(i-1)} = 2.0 + 0.522\, b_{(i-1)}/\,W$, and

$\gamma_{(i-1)} = 1.0 + 0.76\, b_{(i-1)}/\,W$.

In preceding Equation, the quantity $A_{pl(i)} - A_{pl(i-1)}$ is the increment of plastic area under the load versus plastic load-line displacement record between lines of constant displacement at points $(i-1)$ and (i) shown in Figure 2.12. The quantity $J_{pl(i)}$ represents the total crack growth corrected plastic J at point i and is obtained in two steps by first incrementing the existing $J_{pl(i-1)}$and then by modifying the total accumulated result to account for the crack growth increment. The quantity $J_{pl(i)}$ can be calculated from the following Equation:

$$A_{pl(i)} = A_{pl\,(i-1)} + \frac{[P_{(i)} + P_{(i-1)}][V_{pl(i)} - V_{pl(i-1)}]}{2} \qquad (2.41)$$

where :

$V_{pl(i)} = plastic\ part\ of\ the\ load - line\ displacement = V_{(i)} - (P_{(i)}C_{LL\,(i)})$, *and*

$C_{LL\,(i)}$ = compliance, $((\Delta V/\Delta P)_{(I)}$, *required to give the current crack length,* a_i.

$C_{LL\,(i)}$ can be determined from knowledge of a_i/W using the following Equation:

$$C_{LL\,(i)} = \frac{1}{E\,B_e}\left(\frac{W + a_i}{W - a_i}\right)^2 [2.163 + 12.219\,(a_i/W) - 20.065\,(a_i/W)^2 - 0.9925\,(a_i/W)^3 + 20.609\,(a_i/W)^4 - 9.9314\,(a_i/W)^5]$$

where:

$B_e = B - ((B - B_N)^2 / B)$

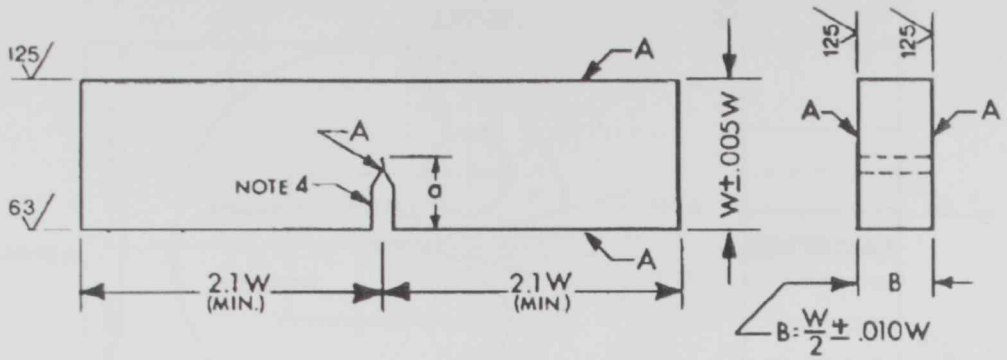

Figure 2.6 Bend specimen SE(B) – Standard Proportions and Tolerances[29].

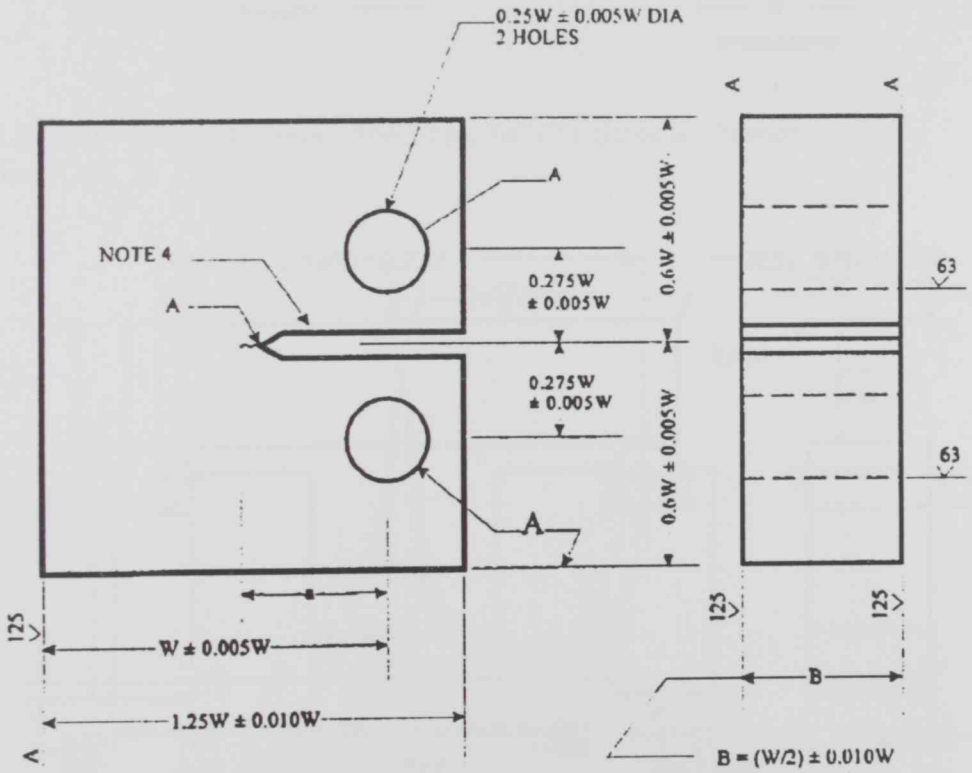

Figure 2.7 Compact specimen for K_{IC} [29].

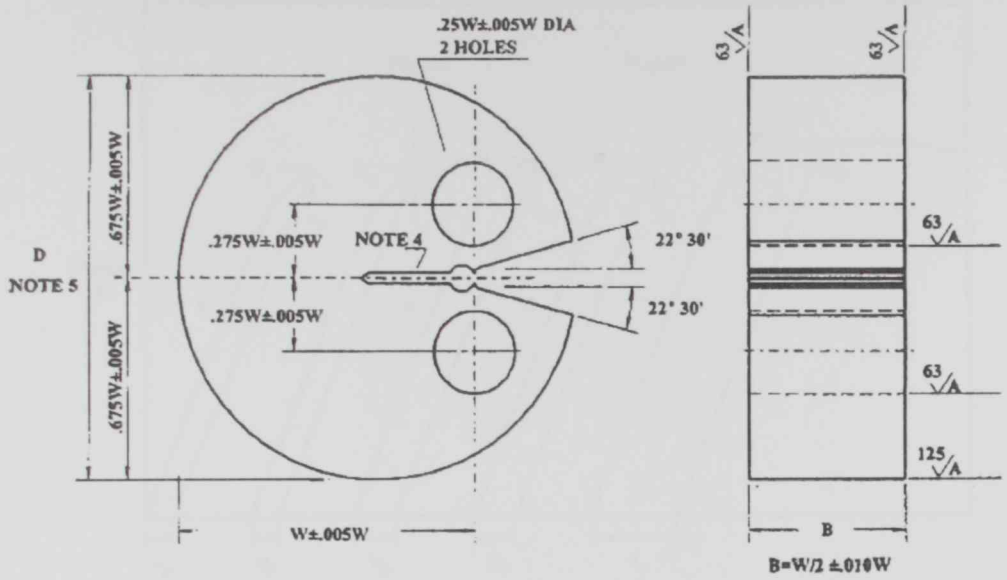

Figure 2.8 Disk – Shaped Compact Specimen, DC (T), Standard Proportion and Dimensions [29].

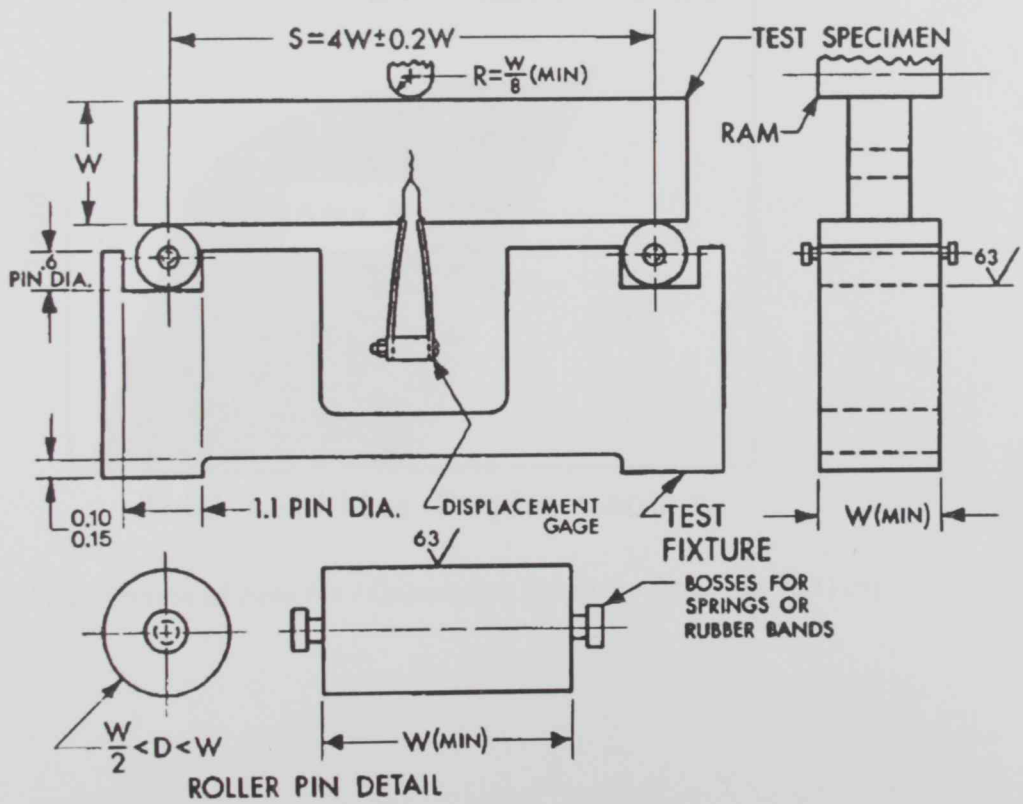

Figure 2.9 Bend fixture design [29].

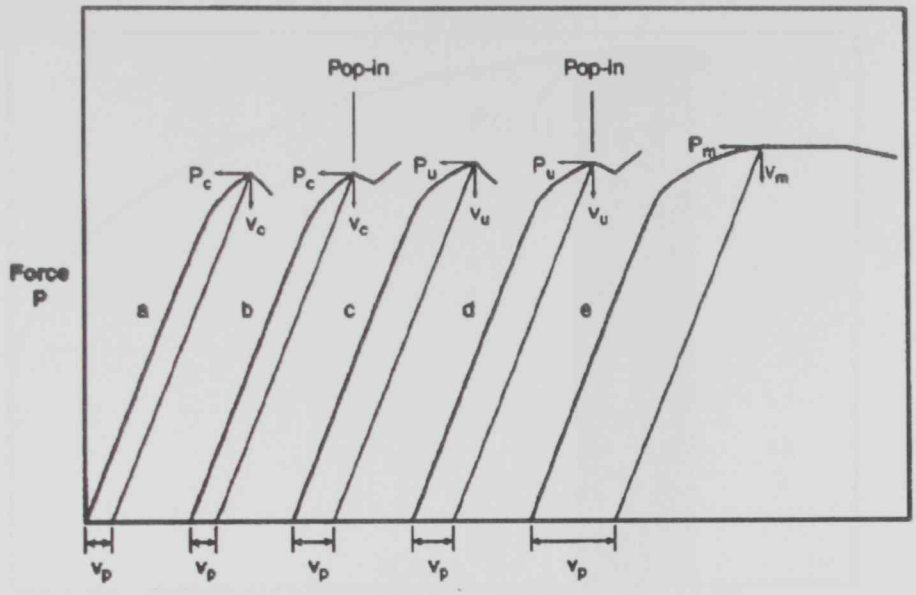

Figure 2.10 Types of Force vs. Clip Gage Displacement Records [29].

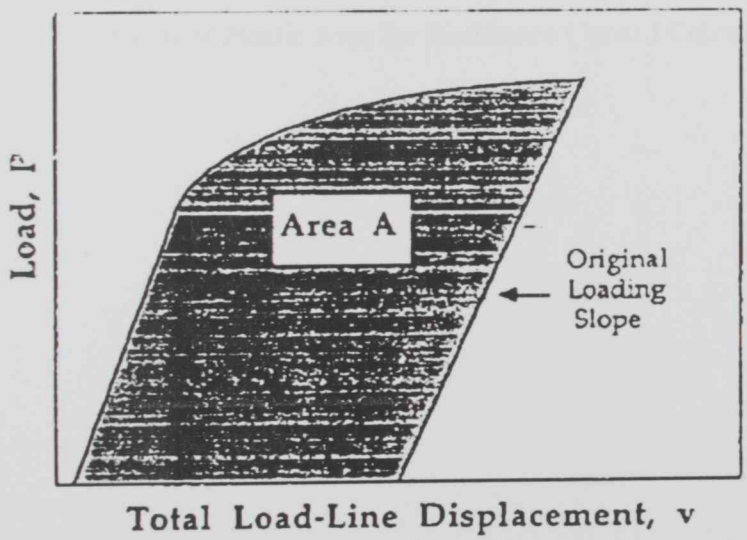

Figure 2.11 Definition of Area for J Calculation Using the Basic Method [29].

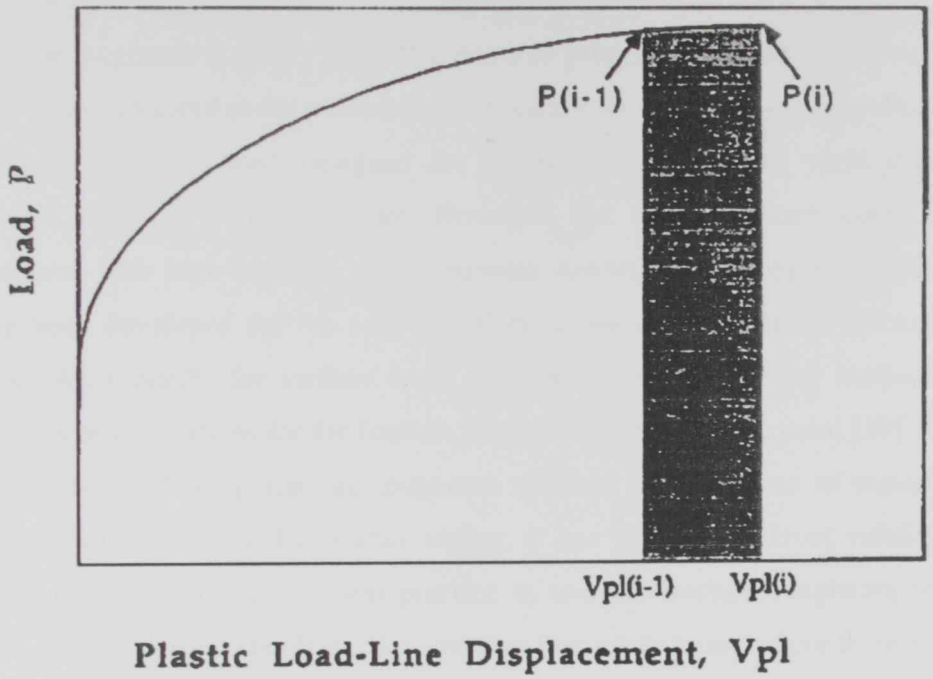

Figure 2.12 Definition of Plastic Area for Resistance Curve J Calculation [29].

2.6 Non Standard Fracture Toughness Evaluation:

Fracture toughness is a very important material property since the occurrence of flaws is not possible to avoid in the processing, fabrication, or service of a material/component. In the past, structures were designed for stresses well below the yield strength of the material to avoid material failure. However, the same approach could not help in structures with high strength under extreme conditions. Consequently, design criteria have been developed for the safe use of materials on the basis of fracture toughness value. As a result, for various crack geometries under different loading conditions, numbers of correlations for the fracture toughness have been proposed [39]. The standard method for evaluating fracture toughness requires large volume of materials and pre cracking of specimens. Even after testing, it has to meet different validity tests [40]. While it is the most convenient practice to test the fracture toughness of a material following the current standards, the situation frequently arises where there is a limitation in the dimension of the material for which the fracture toughness has to be assessed. This necessitates the development of a non-standard method, mainly the design of non-standard specimen geometry. Based on the previous review, there is no standard test to measure the fracture toughness of pipes; therefore one of the main objectives of this work is to develop a new test for the measurement of fracture toughness for full scale pipes.

2.6.1 Fracture Toughness from Notched Bars/Rods:

Testing for the fracture toughness of metallic materials generally requires specimens which are relatively large and expensive to machine. The specimens should be pre-cracked by fatigue, frequently employing servo-hydraulic machines. The pre-cracking is, generally, an expensive and time-consuming process. Moreover, facilities for preparation of standard fracture toughness specimens as outlined in ASTM 399 [41] may frequently be too costly or even unavailable; efforts have been made to overcome the above mentioned difficulties by perfecting a simple, quick and economic technique to estimate the fracture toughness of engineering materials.

The new technique utilizes a small round easy-to-machine specimen with a circumferential notch. This specimen has been employed in the early evaluations of

localized stress fields around notches and is used for plane strain fracture toughness screening tests in order to reduce costs and expedite shipment of the material. Another advantage of this specimen is that it uses normal machine shop tolerances and is easy to test .While fatigue pre-cracking of specimens containing straight notches results in a similar crack, pre-cracking of circumferentially notched round specimens inevitably results in eccentric ligaments. Eccentricity of ligament leads to erroneous values of the fracture toughness when loaded due to the presence of bending stress in addition to tension [42].

M.A.N. SHABARA et al [42] suggested the use of circumferentially blunt-notched round-bar specimens without pre-cracking for evaluating plane strain fracture toughness. He also presented analytical and experimental procedures by using linear elastic fracture mechanics and the principle of stress concentration factors, the elastic stress field in front of a blunt crack with coordinate system as shown in Figure 2.13 is given by Creager and Paris as follows:

$$\sigma_x = \frac{K_I}{\sqrt{2\pi r}}\cos\frac{\theta}{2}\left(1 - \sin\frac{\theta}{2}\sin\frac{3\theta}{2}\right) - \frac{K_I}{\sqrt{2\pi r}}\frac{\rho}{2r}\cos\frac{3\theta}{2r}$$

$$\sigma_y = \frac{K_I}{\sqrt{2\pi r}}\cos\frac{\theta}{2}\left(1 + \sin\frac{\theta}{2}\sin\frac{3\theta}{2}\right) + \frac{K_I}{\sqrt{2\pi r}}\frac{\rho}{2r}\cos\frac{3\theta}{2r} \qquad (2.37)$$

$$\tau_{xy} = \frac{K_I}{\sqrt{2\pi r}}\sin\frac{\theta}{2}\cos\frac{\theta}{2}\cos\frac{3\theta}{2} - \frac{K_I}{\sqrt{2\pi r}}\frac{\rho}{2r}\sin\frac{3\theta}{2}$$

where K_I is the stress intensity factor calculated for the hypothetical case where the notch is collapsed to form a crack of the same major dimension and ρ is the notch tip radius. Alternatively, the stress field can be given in terms of the stress concentration factor, k_t, as follows [42]:

For $k_t \leq 4.5$:

$$\sigma_x = k_t S\left[0.278\left(\frac{x}{\rho}\right)^{1/2} - 0.262\left(\frac{x}{\rho}\right)^{3/2} + 0.093\left(\frac{x}{\rho}\right)^{5/2} - 0.0116\left(\frac{x}{\rho}\right)^{7/2}\right]$$

$$\sigma_y = k_t S \left[1 - 2.330 \left(\frac{x}{\rho}\right) + 2.590 \left(\frac{x}{\rho}\right)^{3/2} - 0.0907 \left(\frac{x}{\rho}\right)^2 + 0.037 \left(\frac{x}{\rho}\right)^3\right] \quad (2.38)$$

For $k_t > 4.5$:

$$\sigma_x = k_t S \left[0.278 \left(\frac{x}{\rho}\right)^{1/2} - 0.168 \left(\frac{x}{\rho}\right)^{3/2} + 0.041 \left(\frac{x}{\rho}\right)^{5/2} - 0.0032 \left(\frac{x}{\rho}\right)^{7/2}\right]$$

$$\sigma_y = k_t S \left[1 - 0.235 \left(\frac{x}{\rho}\right)^{1/2} - 1.33 \left(\frac{x}{\rho}\right) + 1.28 \left(\frac{x}{\rho}\right)^{3/2} - 0.0337 \left(\frac{x}{\rho}\right)^2\right] \quad (2.39)$$

where S is the net stress at the root of the notch and is given by:

$$S = \frac{4P}{\pi d^2}$$

For an element at the tip of a sharp notch where $\theta = 0$, $x = 0$ and $r = \rho/2$, the maximum stress ay may be approximated using Equation (2.37) by:

$$\sigma_y = 2K_I/\sqrt{\pi\rho} \quad (2.40)$$

Another expression for σ_y is determined from Equations (2.38) and (2.39) as:

$$\sigma_y = k_t S \quad (2.41)$$

Assuming that the stress ay given by Equation (2.40) is the same as that given by Equation (2.41), an estimate for the stress concentration factor k_t^- may be written as:

$$k_t^- = \frac{2K_I}{S\sqrt{\pi\rho}} \quad (2.42)$$

The stress concentration factor, k_t^-, given by Equation (2.42) is considered an approximation when compared with the actual stress concentration factor, k_t, found from finite element analysis and theory of elasticity.

Several analytical expressions are available for the stress intensity factor,K_I, for a cylindrical bar under tension ;and containing a circumferential crack emanating from a circumferential notch, as shown in Figure 2.11, Three expressions are summarized as follows:

- *Irwin* (1957) [79],the stress intensity factor is given by:

$$K_I = S\sqrt{d}\sqrt{f_1(\beta)}, \quad (2.43)$$

Where $\beta = d/D = specimen\ geometry\ ratio,$

$$f_1(\beta) = \frac{8\,\pi\,N}{(5+3N)^2}$$

$$N = 1-\beta^2$$

The corresponding stress concentration factor, k_t^-, from Equation (2.42), becomes:

$$k_t^- = \frac{2}{\sqrt{\pi}}\frac{1}{\sqrt{\alpha}}\sqrt{f_1(\beta)} \qquad (2.44)$$

where $\alpha = \rho/d$ = notch bluntness ratio.

- *Benthem and Koiter* (1973) [80], The stress intensity factor is given by:

$$K_I = S\sqrt{\frac{\pi d}{2}}\; f_2(\beta), \qquad (2.45)$$

Where $f_2(\beta)$ is a boundary correction factor which is given by:

$$f_2(\beta) = \frac{1}{2}\left[1+\frac{1}{2}\beta+\frac{3}{8}\beta^2-\;0.363\,\beta^3+\;0.731\,\beta^4\right]\sqrt{1-\beta}\,. \qquad (2.46)$$

The corresponding stress concentration factor k_t^-, becomes:

$$k_t^- = \frac{2}{\sqrt{\pi}}\frac{1}{\sqrt{\alpha}}\sqrt{f_1(\beta)} \qquad (2.47)$$

- *Nisitani and Noda* (1984) [81], the stress intensity factor is given by:

$$K_I = S\beta^2\sqrt{\frac{\pi D}{2}(1-\beta)}\,f_3\,. \qquad (2.48)$$

where f_3 is a correction factor given in ref. [81].

The corresponding stress concentration factor is now given by:

$$k_t^- = \sqrt{2}\frac{\beta^{3/2}}{\sqrt{\alpha}}\sqrt{(1-\beta)f_3} \qquad (2.47)$$

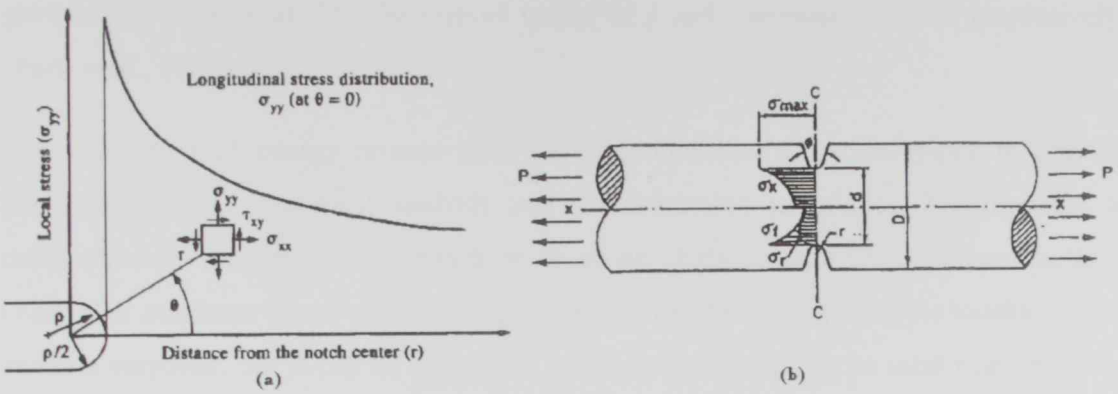

Figure 2.13 (a) Local stress distribution ahead of a notch, (b) Tri-axial state of stress at a blunt notch.

2.6.2 Stable Crack Growth through Pipe:

It is well established that elastic-plastic fracture mechanics (EPFM) provide more realistic measures of the fracture behavior of cracked engineering system. The use of EPFM becomes almost necessary for structural material with high toughness and law strength which generally undergo extensive plastic deformation around a crack tip.

Recent analytical and experimental studies on EPFM indicate that the energy release rate (also known as the J-integral) and crack-tip opening displacement (CTOD) are the most viable fracture parameters for characterizing initiation of crack growth, stable crack growth, and subsequent instability in ductile materials (Rice, 1968; Hutchinson, 1982)[43,44]. This clearly suggests that the fracture parameters like J and/or CTOD can be conveniently used to assess structural integrity for both leak-before-break and in-service flaw acceptance criteria in degraded piping systems [45]. It is, however, noted that the parameter *J* still possesses some theoretical limitations. For example, the Hutchinson–Rice–Rosengren (HRR) singular field (Rice and Rosengren, 1968; Hutchinson, 1968) [43, 44] may not be valid in the case of certain amount of crack extension where *J* ceases to act as amplifier for this singular field. Nevertheless, possible error is considered tolerable if the relative amount of crack extension stays within a certain limit and if elastic unloading and non-proportional plastic loading zones around a crack tip are surrounded by a much larger zone of nearly proportional loading controlled by the HRR field. Under this condition of J-dominance, both the onset and limited amount of crack

growth can be correlated to the critical values of J and J-resistance curve, respectively (Paris et al., 1979) [46].

The evaluation of energy release rates in circumferentially cracked pipes is usually performed by (1) numerical analysis and (2) estimation techniques. Traditionally, a comprehensive numerical study has been based on elastic–plastic finite element method (FEM) for nonlinear stress analysis. In general, the FEM provides accurate results for the fracture response, but it can be expensive and time-consuming to be used routinely. On the other hand, simple mathematical models, often referred to as J-estimation models, can also be used or developed to predict J or other fracture parameters of interest from elastic–plastic fracture theories [45].

However, these models often require simpler representations of the material's stress-strain behavior, flaw shape, orientation, loading, and boundary conditions. If these assumptions are acceptable, then the J-estimation method provides an alternative means for characterizing fracture response with much less computational cost when compared with the FEM . Due to approximations, however, the J-estimation methods, in general, are less accurate than the FEM and hence, often require validation with the latter method.
For circumferentially surface-cracked pipes, perhaps the GE/EPRI (general electric company / electric power research institute) method (Kumar and German, 1988) [47] is the first J-estimation method developed to predict J-integral and other fracture parameters. In this method, Kumar and German (1988)[47] compiled a series of FEM solutions for several crack sizes, pipe geometries, and material properties in a handbook form, this method utilized the non-linear finite element solutions for power-law hardening to estimate plastic components of the J-integral and other relevant deformation parameters [48]
For any arbitrary new problem, the solution is usually achieved from multiple interpolation (and extrapolation, if necessary) of the tabulated results. For surface-cracked pipe, the only functions developed initially were those for 360-degree circumferential cracks under pure tensile loading. For pure bending loads, the functions for finite-length cracks were subsequently determined for a very limited number of cases.

The primary limitation of this method involves the errors introduced in the interpolation and extrapolation of limited tabulated influence functions.

For through wall crack under pure bending, Figure 2.12, closed-form expression developed by S. Rahman [82] for both J_e and J_p, they were described as below :

- Elastic solution for TWC pipe , the elastic component J_e is given by :

$$J_e = \frac{K_I^2}{E} \tag{2.48}$$

Where K_I is the mode-I stress intensity factor in which plane stress condition is assumed, from LEFM theory, K_I can be obtained as

$$K_I = \frac{M}{\pi\, t\, R^2} F\left(\frac{\theta}{\pi}, \frac{R}{t}\right) \sqrt{\pi R\theta} \tag{2.49}$$

Where $F(\theta/\pi, R/t)$ is a dimensionless function that depends on pipe and crack geometry. Hence, the elastic J is

$$J_e = \frac{\theta}{\pi}\, F\left(\frac{\theta}{\pi}, \frac{R}{t}\right)^2 \frac{M^2}{E\, t^2 R^3} \tag{2.50}$$

- Plastic solution for TWC pipe , the plastic component J_p is

$$J_p = \frac{\alpha\, \sigma_0^2}{E}\, R\theta \left(1 - \frac{\theta}{\pi}\right) h_1\left(\frac{\theta}{\pi}, n, \frac{R}{t}\right) \left[\frac{M}{M_O}\right]^{n+1} \tag{2.51}$$

Where h_1(θ/π, n, R/t) is a dimensionless function that depends on pipe geometry, crack geometry, n *and* α are Ramberg- Osgood constants (material constant) and

$$M_0 = 4\, \sigma_0\, R^2\, t \left[\cos\frac{\theta}{2} - \frac{1}{2}\sin\theta\right] \tag{2.52}$$

Is a conventionally defined reference load that represents the limit-load for a TWC pipe under pure bending if σ_0 is the collapse stress.

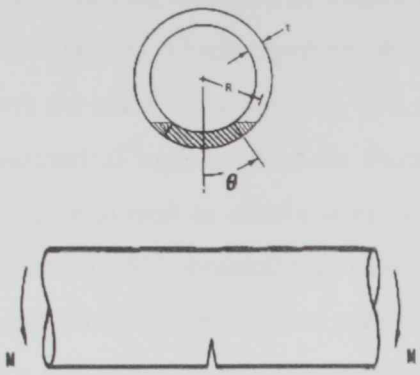

Figure 2.14 a pipe with a circumferential through-wall crack subjected to pure bending [49].

As part of the efforts for developing a flaw assessment Yukio [48] conducted a review of available solutions and evaluation method for a straight pipe with a circumferential through-wall crack, Figure 2.12, based on stress intensity factor , a parameter widely used for the evaluation of cracks in various situations, although this parameter is based on linear-elastic material behavior and cannot be directly applied to situations with large-scale yielding , it has frequently been used as a starting point for J-integral estimation. The stress intensity factor for a circumferential through wall crack in a pipe under axial load and bending moment can be expressed by

$$K_I = (F_t\sigma_t + F_b\sigma_b)\sqrt{\pi R_m\theta} \qquad (2.53)$$

where K_I is the stress intensity factor, while σ_t and σ_b are applied tensile and bending stresses calculated by

$$\sigma_t = \frac{P}{2\,\pi R_m\,t} \qquad (2.54)$$

$$\sigma_b = \frac{M}{2\,\pi R_m^2\,t} \qquad (2.55)$$

From the axial load , P , and the bending moment, M, respectively. F_t and F_b in Equation (2.46) correspond geometrical factors which represent the normalized stress intensity factor. F_t and F_b increase with the crack angle and also with R_m/t.

Because of the absence of numerical tools such as the finite element method in earlier days, analytical methods were employed to obtain stress intensity factor solutions for cracks in cylinders. First, Folias [50, 51] obtained the stress intensity factor solutions for a circumferential crack in a pipe subjected to internal pressure and tensile loading, using classical shell theory (without consideration of transverse shear strain). As the Equations obtained by Folias were valid only for short cracks, Duncan-Fama and Sanders [52] extended the solutions to longer cracks using a numerical technique. Afterwards, a semi-analytical approach based on complete shell theory including transverse strain was developed by Sanders [53, 54] to derive the solutions for a circumferential crack in a pipe subjected to axial load and bending moment. These solutions were employed in the leak-before-break evaluation procedure developed by Paris and Tada [55] as a starting point of evaluation of the elastic– plastic J-integral. They derived expressions for the geometrical factors as a function of the half crack angle. However, their Equations were obtained for a fixed value of R_m/t.; i.e. 10, so that Klecker et al. [56] later extended them to include the effect of R_m/t.for the range between 5 and 15, which covered most of the piping systems, to improve accuracy. Expressions for F_t and F_b were given by Klecker et al. [56] as polynomials of half crack angle with coefficients depending on R_m/t. as shown in Table 1. At about the same time, the same solutions by Sanders were utilized by Zahoor [57] to develop another set of closed form expressions and these are included in the Ductile Fracture Handbook published later by Zahoor [58].

As part of a programme for developing a simplified fracture estimation method now widely called the GE/EPRI method, Kumar et al. [59] also made finite element calculations using thick shell elements for a cylinder with a circumferential crack for selected combinations of R_m/t and the half crack angle. Both the cases of tensile and bending loads were analyzed and the results were summarized in Tables.

More recently, France et al. [60] conducted finite element analysis using three-dimensional solid elements for pipes with an axial and a circumferential crack. Awide range of R_m/t . (From 3 to 100) was employed. Internal pressure, through-wall bending

and global bending moment were considered for a circumferential crack. Their solutions were summarized in tabular format after separation into extensional and bending components as performed by Barsoum et al. Lacire et al. [43] also conducted finite element calculation for pipes with a circumferential through-wall crack for a wide range of R_m/t. (From 1.5 to 80.5) and half crack angle (0–150°). Shell elements were used for thin cylinders ($R_m/t > 10$), but thicker cylinders were analyzed by solid elements. The solutions were given in the form of Tables of the geometrical factors. The solutions by Lacire et al. have been approximated by expressions listed in Table 2 with an error less than a few percent for half crack angles smaller than110°. Figure 2.15 shows a comparison of the geometrical factors calculated by the Equations and tabulated values in for both axial and bending loading. It can be seen that the Equations in Table 2 agree with the tabulated values very well and enable smooth interpolation for R_m/t , Estimates by the Equations developed by Klecker et al. (Table 1) are also plotted in the same Figure. These are in reasonable agreement with other solutions for R_m/t. below 20 but differences begin to increase rapidly at R_m/t.of about 30.

Comparison of the geometrical factors for the bending moment is shown in Figure 2.16 for thicker pipes with R_m/t = 5, 10 and 20, all solutions agree with each other quite well.

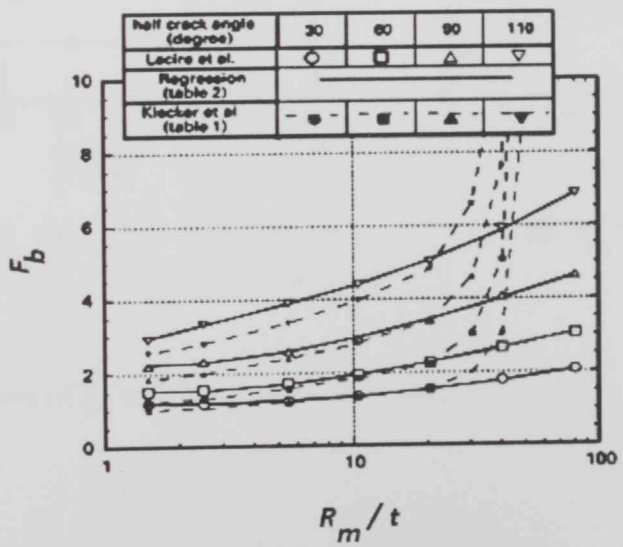

Figure 2.15 Comparison of R_m/t - dependence of geometrical factor for stress intensity factor. [48]

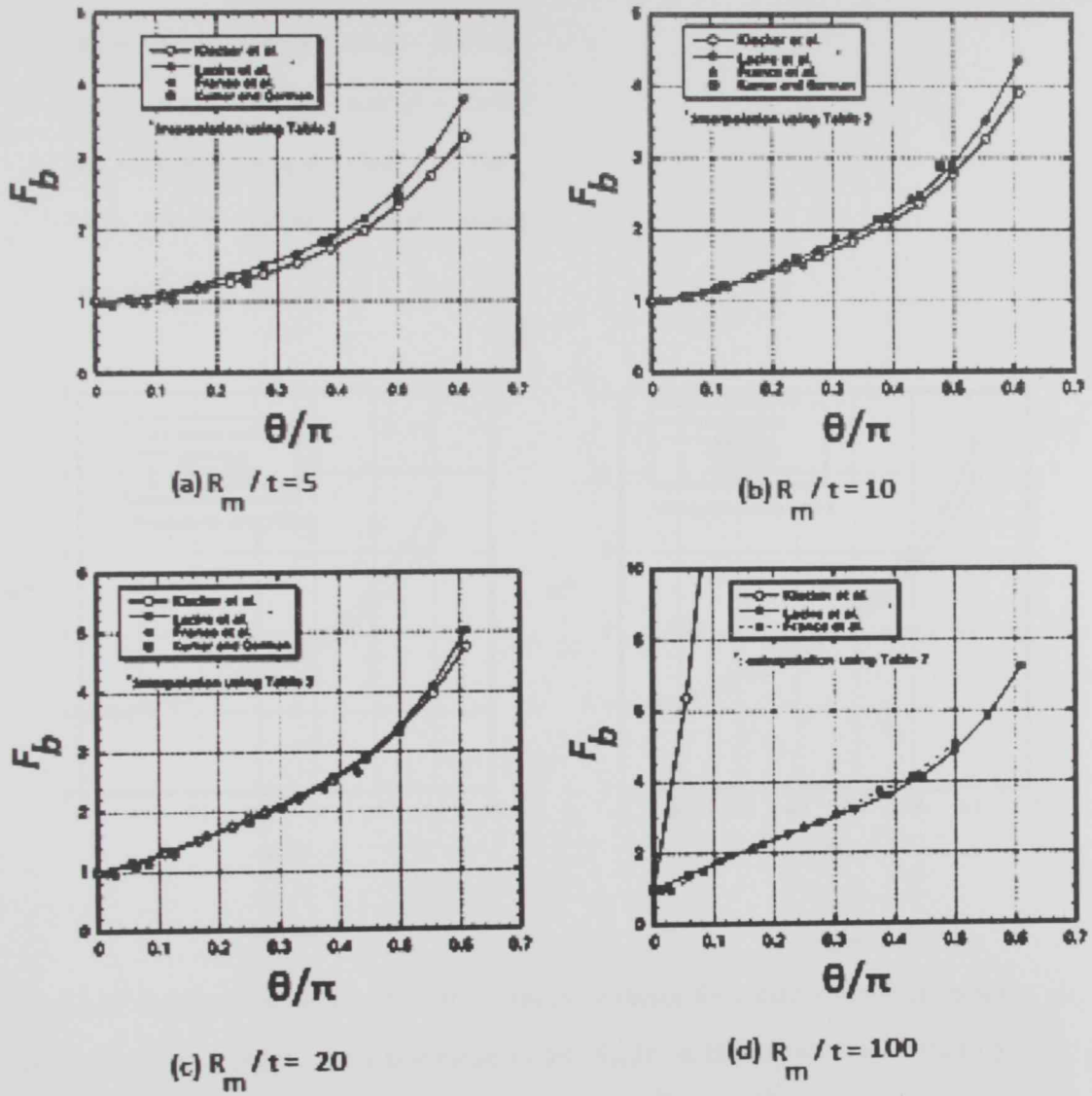

Figure 2.16 Variation of F_b with half crack angle. [48]

$$F_b = \left(1 + \frac{t}{2R_m}\right)\left[A_b + B_b\left(\frac{\theta}{\pi}\right) + C_b\left(\frac{\theta}{\pi}\right)^2 + D_b\left(\frac{\theta}{\pi}\right)^3 + E_b\left(\frac{\theta}{\pi}\right)^4\right]$$

$$A_b = 0.65133 - 0.5774\xi - 0.3427\xi^2 - 0.0681\xi^3$$

$$B_b = 1.879 + 4.795\xi + 2.343\xi^2 - 0.6197\xi^3$$

$$C_b = -9.779 - 38.14\xi - 6.611\xi^2 + 3.972\xi^3$$

$$D_b = 34.56 + 129.9\xi + 50.55\xi^2 + 3.374\xi^3$$

$$E_b = -30.82 - 147.6\xi - 78.38\xi^2 - 15.54\xi^3$$

$$\xi = \log\left(\frac{t}{R_m}\right)$$

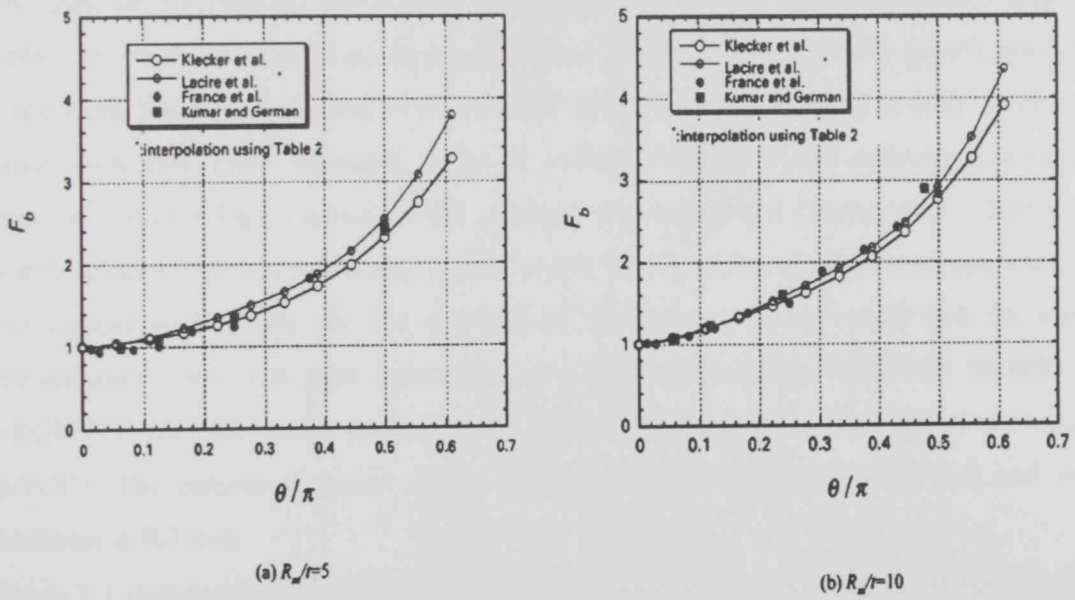

(a) R_m/t=5 (b) R_m/t=10

Figure 2.17 Geometrical factors for stress intensity factor for a circumferential crack (fitted to Lacire et al .[61]: , applicable range: ($1.5< R_m/t < 80.5, 0 < \theta/\pi < 0.611$).

Chapter Three

Experimental Determination of Material Properties

3.1 Introduction

This chapter discusses the selected pipe specification for the present investigation and its properties, and the geometry of the specimen used for tensile test as well as procedures of specimen preparation and the test procedures.

3.2 Material

The material selected for the present investigation is API 5L grade X65 PSL1 (ASTM A694F65) medium strength grade pipeline steel. Pipes furnished to this specification are made from basic-oxygen steel or electric arc furnace steel. The steel is fully killed and made with fine grain structure. Steel is vacuum degassed and calcium treated for inclusion morphology control. Steel is made by continuous casting only. Pipes are seamless construction without any welded seam. The material has numerous applications, and typical applications are for gas and oil industry, pressure vessel and for water transmission lines. The pipe specimens were manufactured by TENARIS SIDERCA, ARGENTENA and were provided by National Petroleum Construction Company (NPCC). The outside diameter of the pipe under investigation is 60.3 mm and wall thickness is 8.7 mm.

Table 3.1 contains the nominal chemical composition of this steel (wt %) as specified by American Petroleum Institute (API).Table 3.2 contains chemical analysis provided by the pipe manufacturer that is supplied to National Petroleum Construction Company (NPCC).Chemical compositions of this material were also measured by Arab center for engineering studies and are listed in Table 3.3

3.3 Metallographic Analysis

All the samples have been prepared for optical microscopy using standard metallographic practice. 2% natal is used as etchant. Etchant is used to reveal the different phases in the micro structure, Figures 3.1 and 3.2 show the microstructure of the prepared samples. A heat treatment was performed to develop the structure that shows the grains and then to calculate their sizes. It was at 750 °C in a chamber furnace for 1 hour then the specimen was furnace cooled. Specimen microstructure shows two phases:

a- Ferrite .(law carbon percent)

b- Pearlite. (Lamellar, one Cementite Fe_3C and one Ferrite).

Standard test method for determining average grain size, mainly planimetric procedure was used to find out the grain size [74] , the grain size number for different samples was calculated and the average number is 12.

Hardness was measured for variety of specimen by Vickers system using a load of 10 Kgf, using Hardness tester AMSLER OTTO WOLPERT- WERKE GMBH .The measured values were ranged between 185 -200 HV. Also micro hardness tests were performed for the phases in the microstructure using micro hardness tester model MHT-1 from MATSUZAWA SEIKI Company , it is worthy to mention here that Macro-hardness testing methods require large sample sizes and many repeated sample tests, requiring a great deal of bulk materials. Therefore, macro-hardness cannot be measured in small samples. Instead, micro-hardness is measured. Micro-hardness is defined as a mechanical parameter related to the structure and composition of the material. This testing gives insight into mechanical properties such as elastic constants, yield strength, plasticity, hardness anisotropy, creep behavior, and fracture behavior. Micro-hardness is more or less constant with load, and is influenced by solid solution effects connected with the chemical nature of atoms, defect aggregates and amorphous regions, and point defects that hinder the motion of dislocations. During micro -hardness testing, the indention made by the indenter is on the micrometer scale, and therefore cannot be seen without the aid of an optical microscope. Micro-hardness testing can be done in accordance with ASTM Standards using either Knoop or Vickers Hardness testing methods. The

procedure is the same for both, but the indenter geometry varies. Therefore, the correlations and error estimations also vary. The results of micro hardness test for the detected phases in the microstructure are:

a- Ferrite phase gives values ranged between 593HV to 441 HV at load of 50g.
b- Pearlite phase gives values ranged between 271HV to 231HV at load 50g.

3.3 Tensile Properties

3.3.1 Tensile Specimen

To measure the tensile properties of the pipeline metal (API 5L grade X65), tensile strip specimens were extracted from a pipe of outer diameter $d_0 = 60.3$mm and wall thickness $t = 8.7$mm (in the longitudinal direction), specimens were not flattened although most standard test methods are based on flat specimens, four specimens were initially rough cut to a rectangular strip using a milling machine and then they were ground ,Figure 3.3 showing a photograph of tensile strip specimen before fracture . Schematic diagram for tensile strip specimen geometry employed in the present work is depicted in Figure 3.4. All specimens were of gripped type. Specimens preparation process was conducted at specialized work shop under professional conditions included and not limited to proper and adequate cooling and feeding rates .The dimensions used for tensile specimen were non-standard. Specimens were ground throughout the gage length in order to ensure that the break will occur in the gage length of the tested specimen.

3.3.2 Test Procedures

Face and grip were selected carefully to avoid and specimen slippage or breakage inside the gripped area, Vertical alignment of the specimen was confirmed to avoid side loading or bending moments created in the specimen by mounting the specimen in the upper grip assembly first and then allowing it to hang freely, then the specimen gripped strongly to the lower grip. Specimen grapping process and the shape of the specimen confirm that the necking will occur within the gage length.

Tests were conducted to measure mechanical properties of the subjected steel including the modulus of elasticity, E, tensile strength,σ_Y , ultimate strength, σ_{UTS} , strain hardening constants α *and* n, also to obtain power law material constants k *and* m. After the tension tests were concluded, the broken specimens were carefully reassembled ,The final gage lengths of the fractured specimens were measured with a caliper having divisions of 0.01 mm. It should be noted that prior to the test, the initial cross section was measured with this same instrument. Figure 3.5 is showing pipe strip specimen after testing.

3.4 Results and Discussion

Tests were performed using universal type test machine, Universal Motion INC. PUNE INDIA, Model MUTE-100 with 1500 kN rated load capacity, Figure 3.6 shows the testing machine at Arab Centre for Engineering studies, tests were conducted under displacement control at a cross-head displacement rate of 0.5 mm/min, and also they were performed at room temperature. The stress – strain curves for the four tests are shown in Figures 3.7 through 3.10, the measured values for all tests, modulus of elasticity, ultimate stress and yielding stress are shown in Table 3.4, the average measured values are also shown in Table 3.4.

True stress and true strain for each test were calculated according to:

$$\sigma_T = \sigma_E \left(1 + \varepsilon_E \right) \qquad (3.1)$$

$$\varepsilon_T = \ln \left(1 + \varepsilon_E \right) \qquad (3.2)$$

A comparison curves for true stress and true strain curves versus engineering stress and engineering strain for all tests were plotted and shown in Figures 3.7 to 3.10.

The constitutive Equations of the material have been obtained using both power law Equation and Ramberg-Osgood Equations. Then the constants of the constitutive Equations were determined from the measured stress – strain curves. The power law Equation 3.3 used to measured material constants,

$$\sigma = k \left(\varepsilon_p \right)^n \qquad (3.3)$$

where: k is the strength coefficient.

n is the strain hardening exponent.

A linear fit was obtained for the four conducted tests as shown in Figures 3.11 through 3.14 and the values of k *and* n were determined and listed in Table 3.5.

True stress- strain curves for each test were plotted against the stress- strain obtained by power Equation as shown Figures 3.15 to 3.18.

According to Ramberg-Osgood relationship:

$$\frac{\varepsilon}{\varepsilon_o} = \frac{\sigma}{\sigma_o} + \alpha \left(\frac{\sigma}{\sigma_o}\right)^m \qquad (3.4)$$

Where α *and* m are constants that depend on the material being considered.

Logarithmic plot of $\left[\frac{\varepsilon}{\varepsilon_o} - \frac{\sigma}{\sigma_o}\right]$ $vs.$ $\left[\frac{\sigma}{\sigma_o}\right]$ beyond yield limit were plotted as shown in Figures 3.19, 3.20, 3.21 and 3.22, also a linear fit was obtained and the plastic constants α *and* m were determined for all test and listed in Table 3.6. then the true stress – strain for each test was plotted against the stress strain obtained by R-O Equation, as shown in Figures 3.23, 3.24, 3.25 and 3.26.Using the obtained average values for power law Equation and Ramberg-Osgood relationship, stress stain curves were plotted together with the curves obtained from experimental work as shown in Figure 3.27, it is clear from the plotted curves that stress strain readings resulting for all experimental works are close to the stress strain curve drawn using power law Equation where average values have been utilized , that is power law represent a better fitness for the experimental data more than R-O Equation. Finally, all mechanical properties obtained from the experimental work and that provided by the manufacturer are presented in Table 3.7 which shows that experimental readings are very close to that provided by the manufacturer and almost cosigned with that presented within API standards.

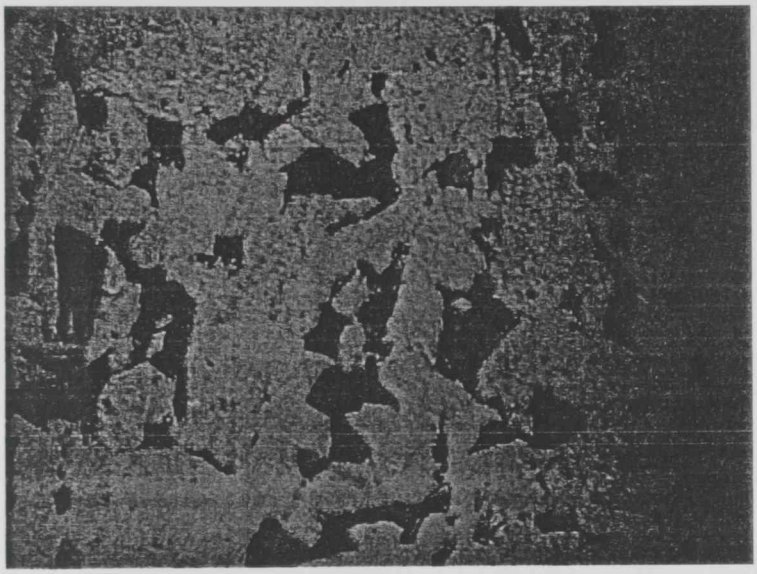

Figure 3.1 Steel X65 Microstructure.

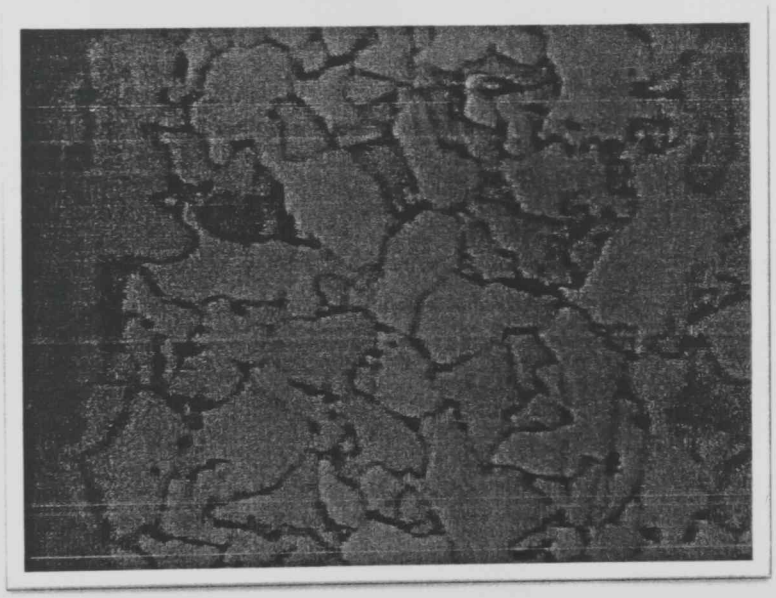

Figure 3.2 Steel X65 Microstructure used to calculate grain size.

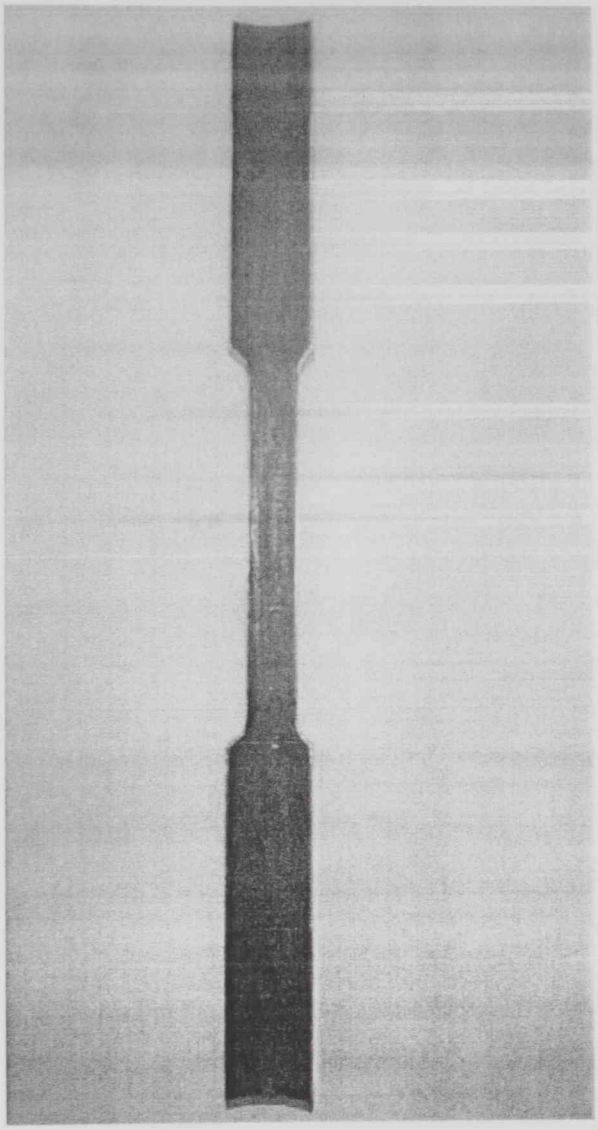

Figure 3.3 photograph showing the tensile strip specimen.

Figure 3.4 Tensile test specimen geometry

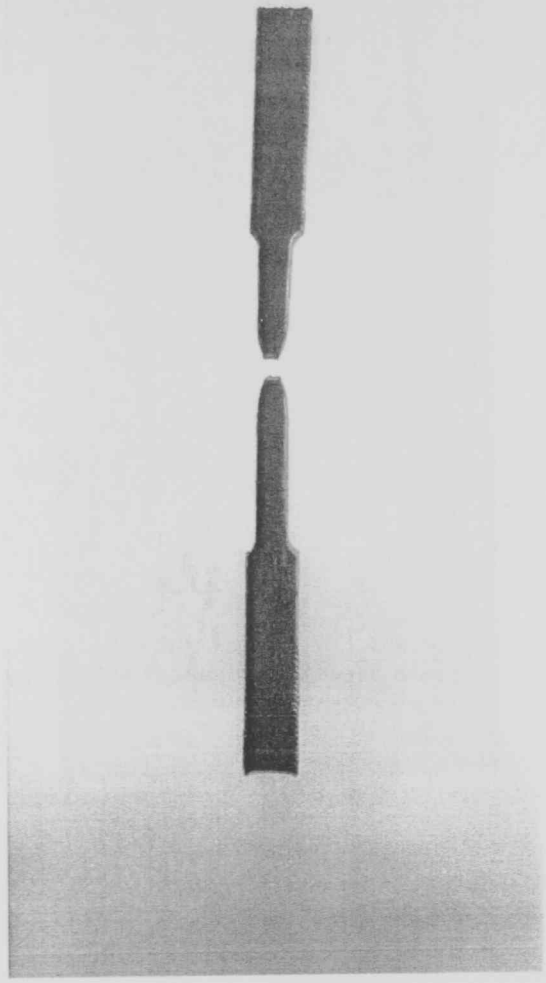

Figure 3.5 sample photograph of tensile specimen after fracture.

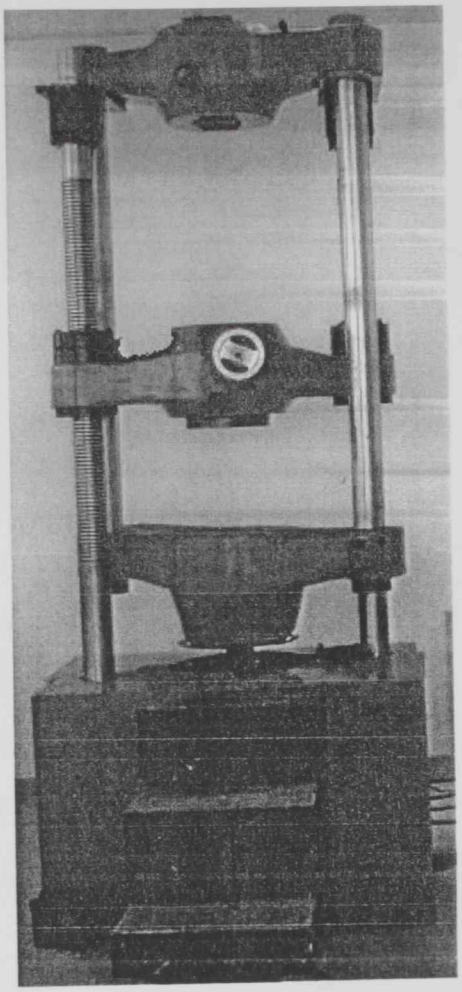

Figure 3.6 Universal Testing Machine at Arab Center for Engineering Studies.

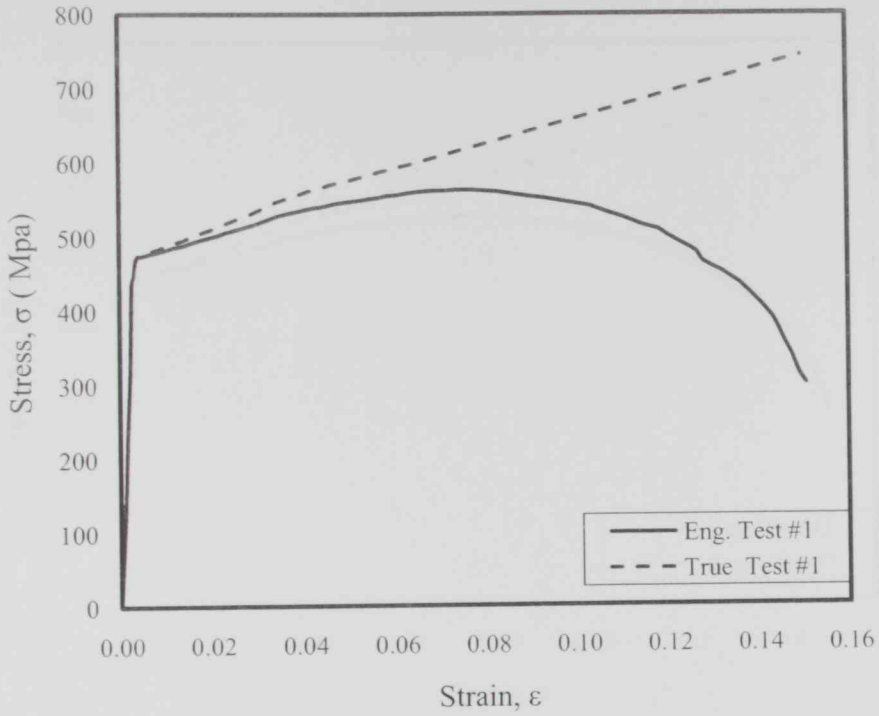

Figure 3.7 Engineering and True Stress-Strain curves for tensile test #1.

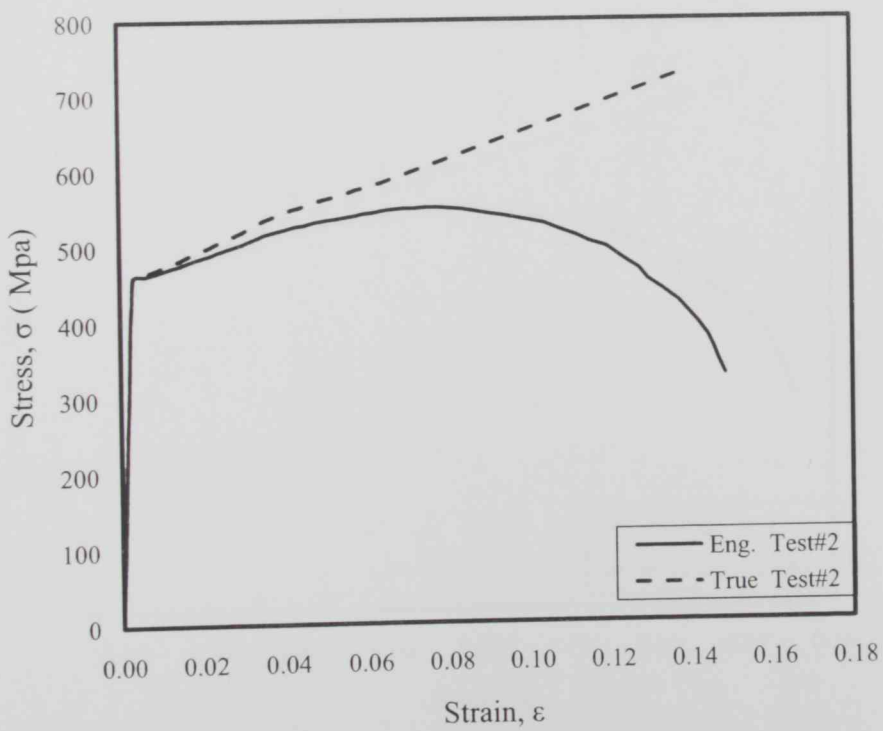

Figure 3.8 Engineering and True Stress-Strain curves for tensile test # 2.

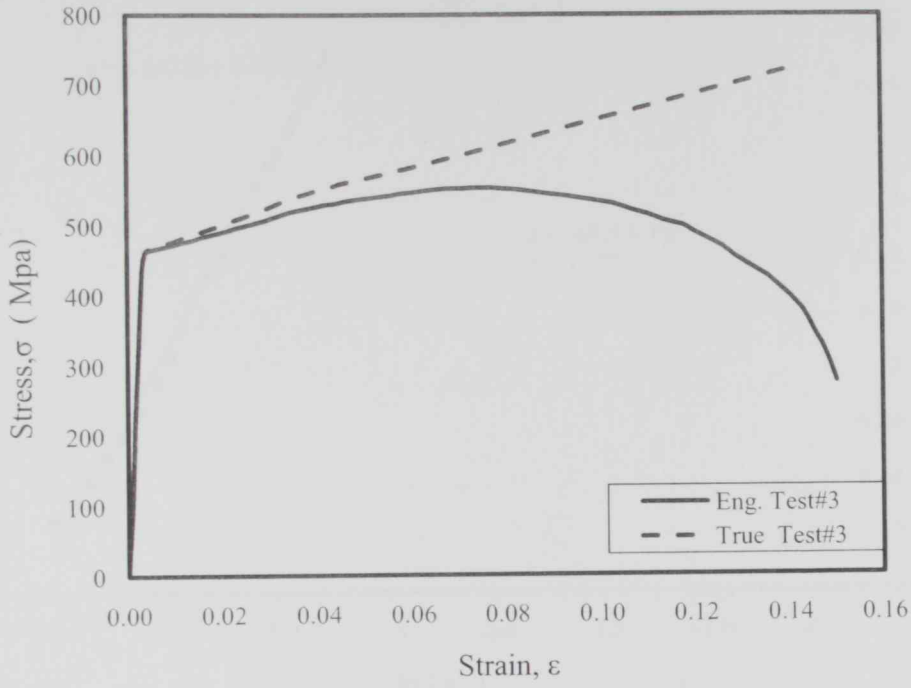

Figure 3.9 Engineering and True Stress-Strain curves for tensile test# 3.

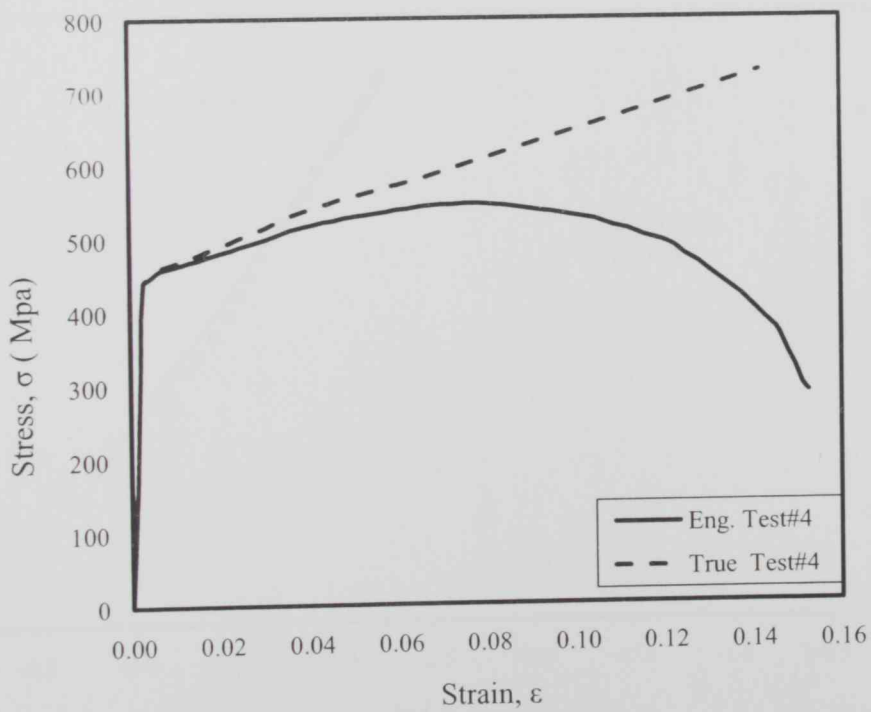

Figure 3.10 Engineering and True Stress-Strain curves or tensile test #4.

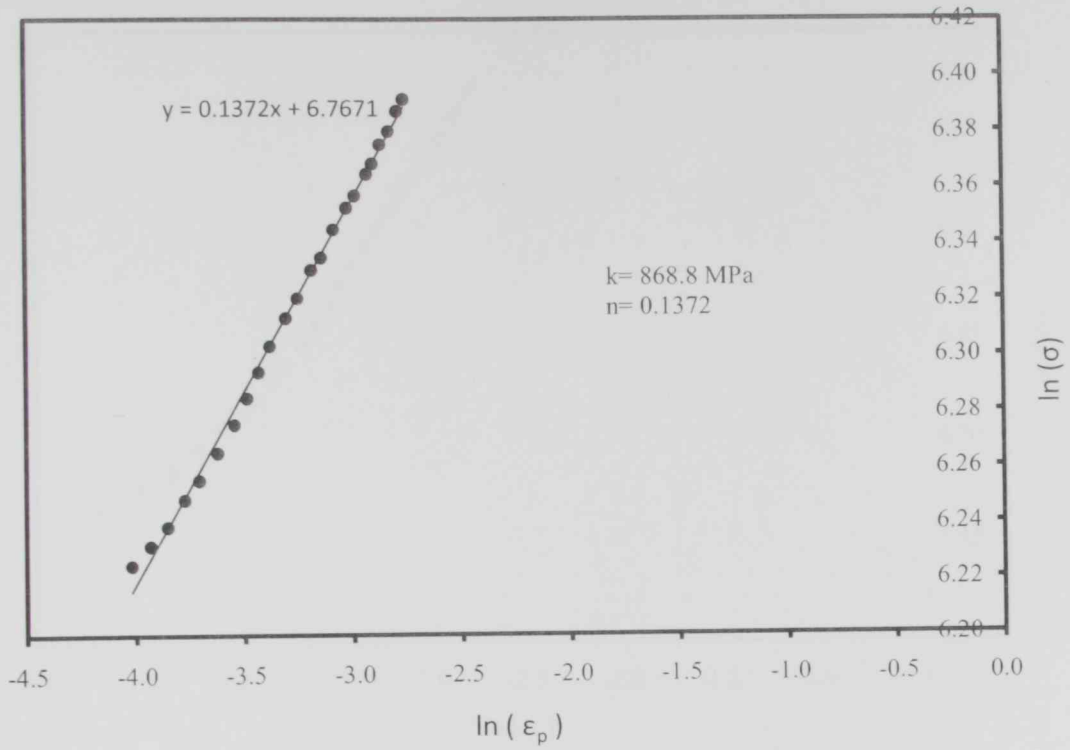

Figure 3.11 Curve fitting plot to obtain plastic power law Equation material constants k and n, test#1.

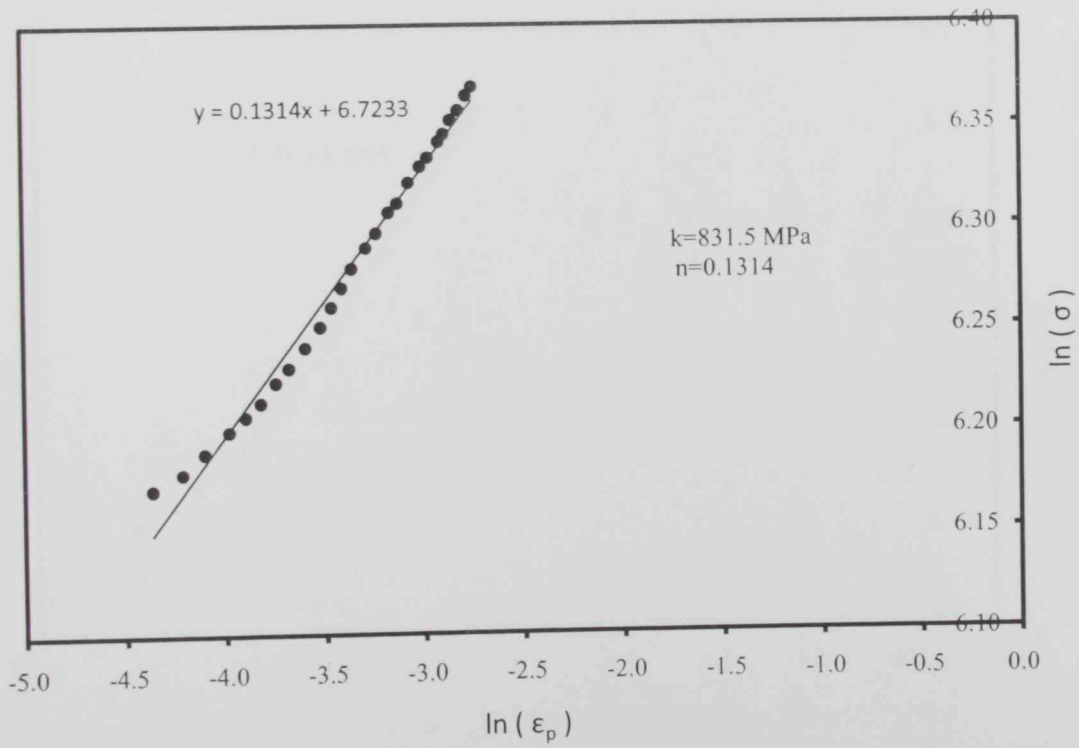

Figure 3.12 Curve fitting plot to obtain plastic power law Equation material constants k and n, test# 2.

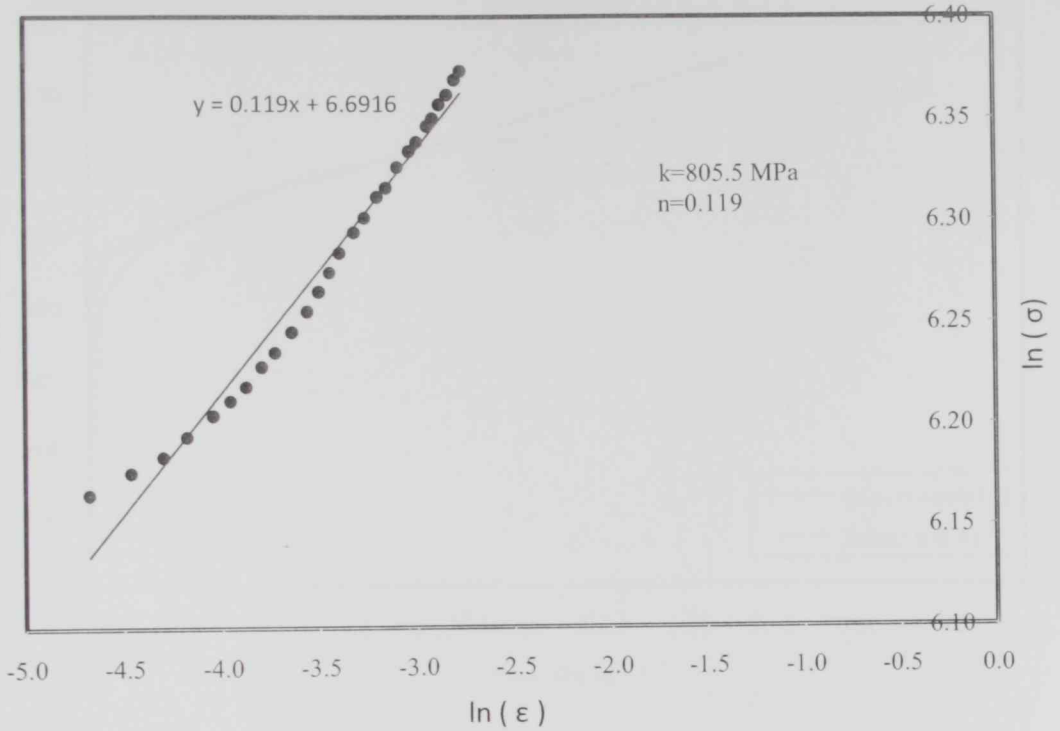

Figure 3.13 Curve fitting plot to obtain plastic power law Equation material constants k and n, test # 3.

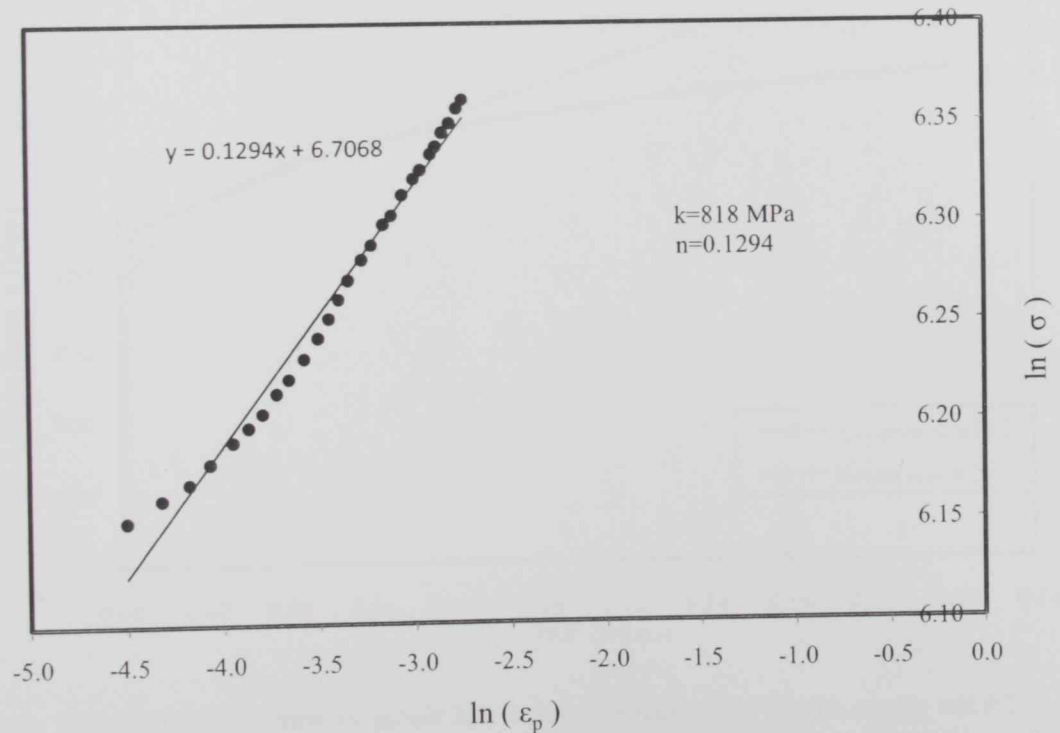

Figure 3.14 Curve fitting plot to obtain plastic power law Equation material constants k and n, test # 4.

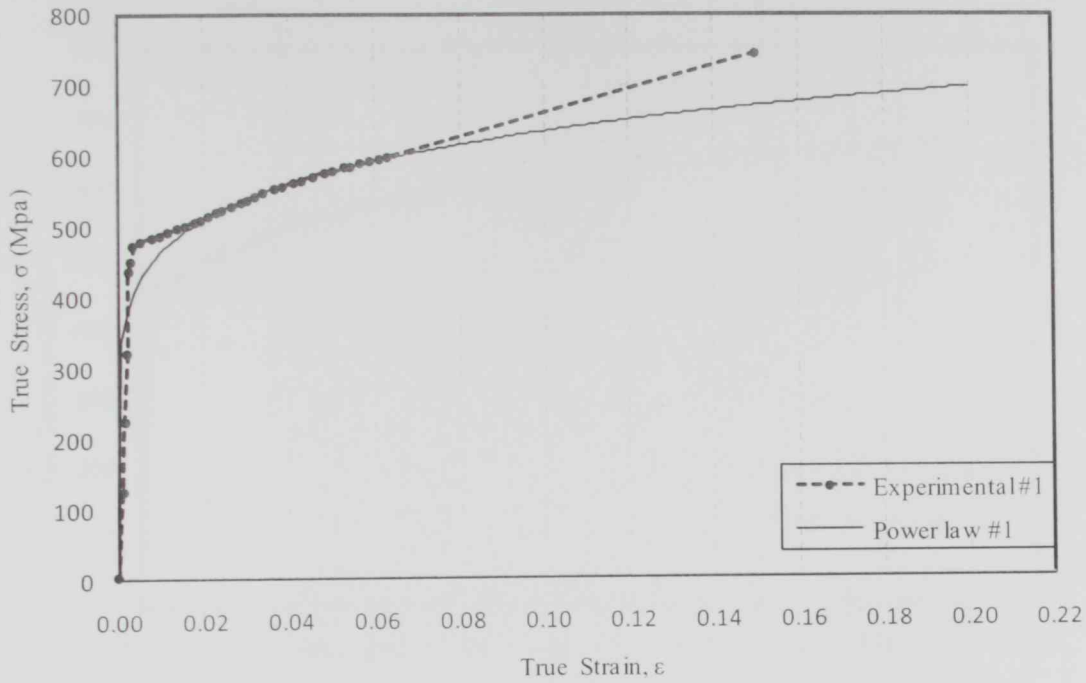

Figure 3.15 True stress- strain vs. power law Equation Stress-Strain Curves, tensile test #1

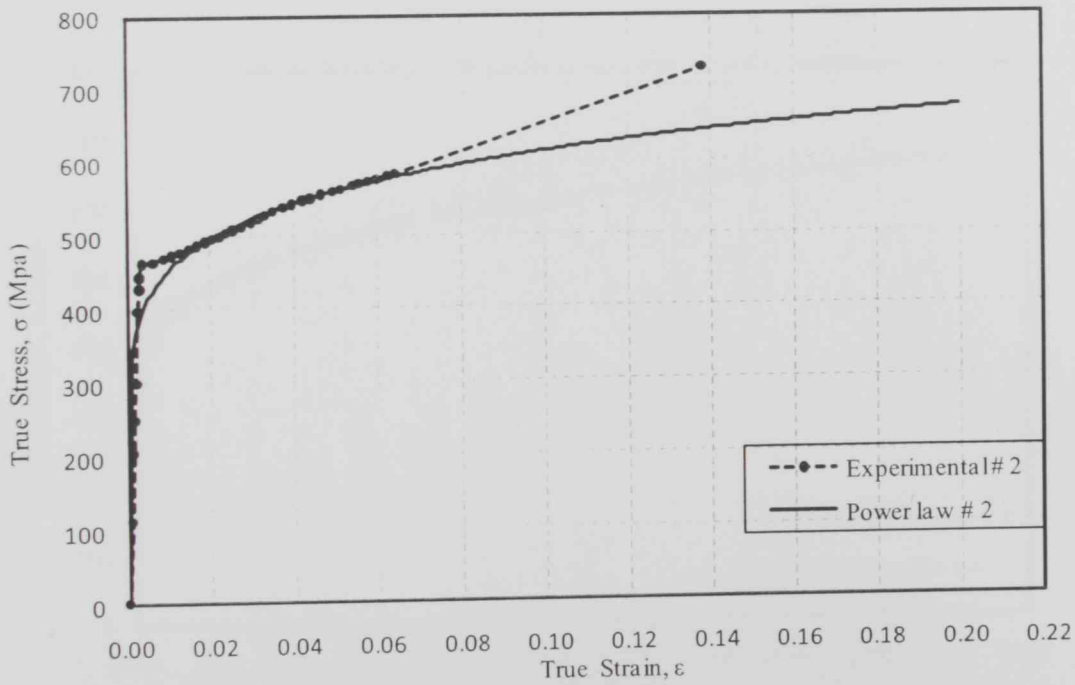

Figure 3.16 True Stress- Strain vs. power law Equation Stress-Strain Curves, tensile test # 2

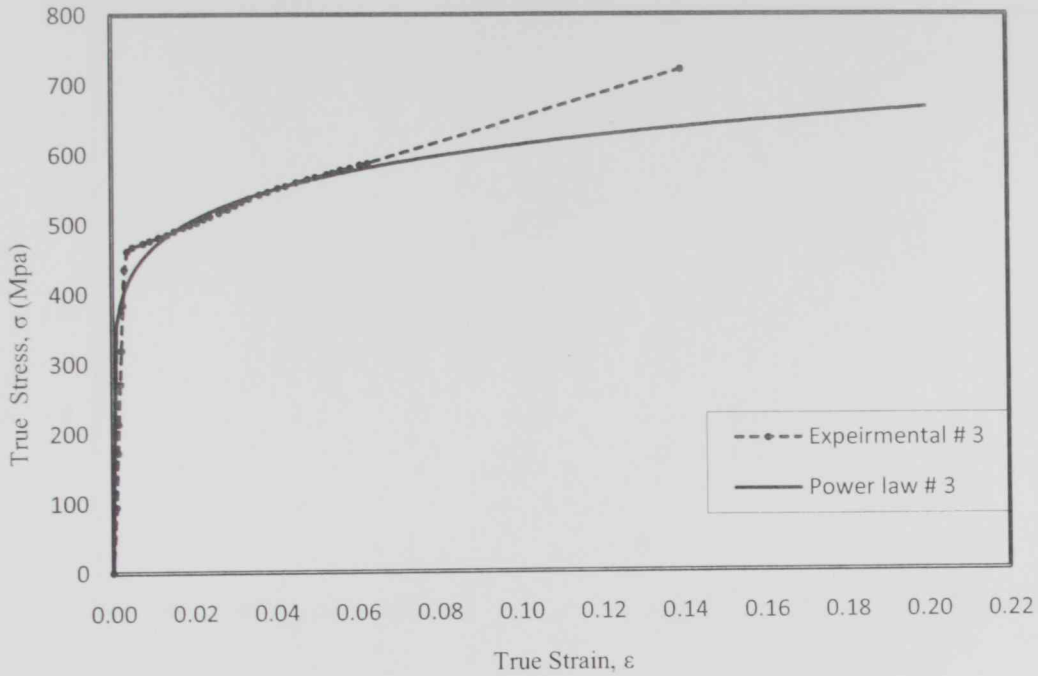

Figure 3.17 True Stress- Strain vs. power law Equation Stress-Strain Curves, tensile test # 3

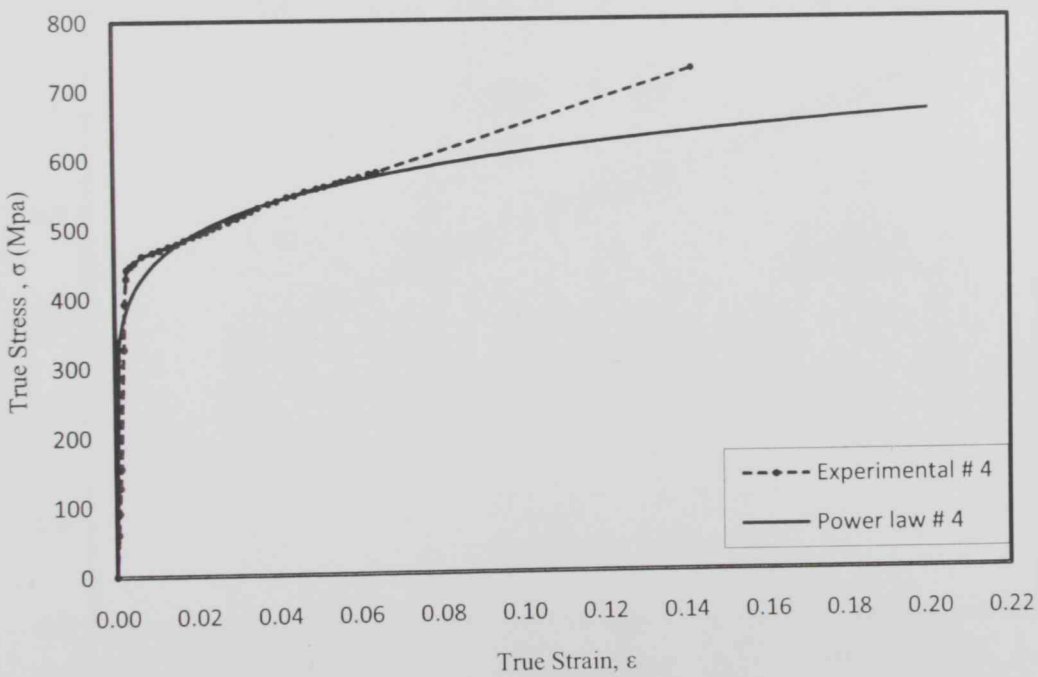

Figure 3.18 True Stress- Strain vs. power law Equation Stress-Strain Curves, tensile test # 4

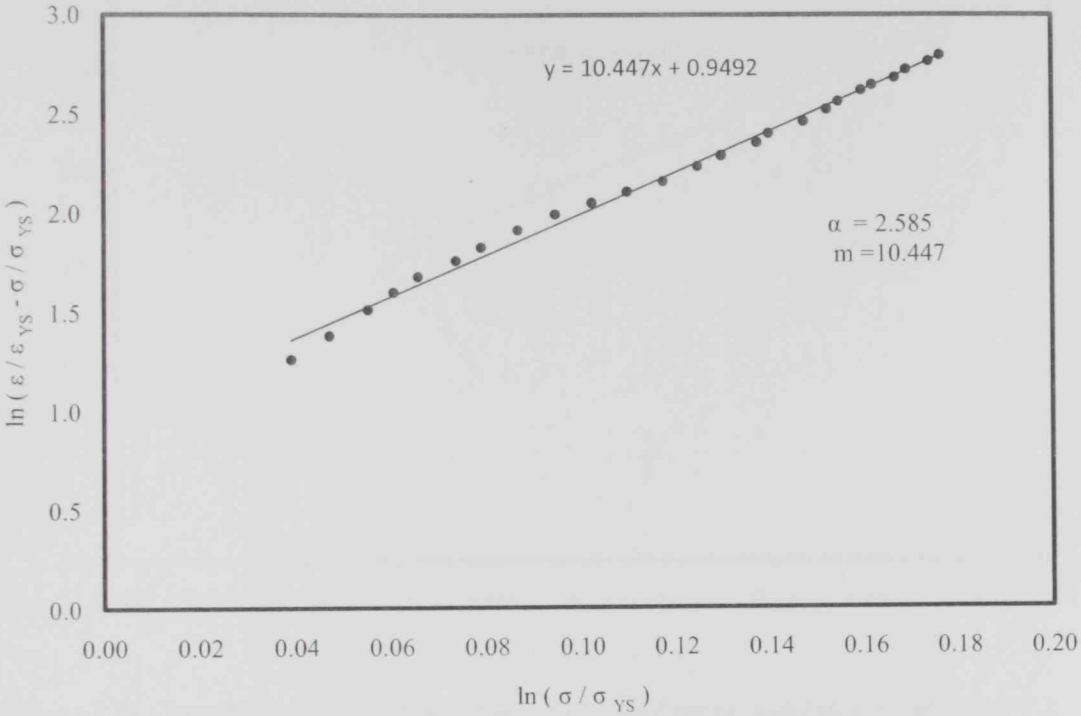

Figure 3.19 Curve fitting plot to obtain plastic Ramberg-Osgood constants m and α, test # 1.

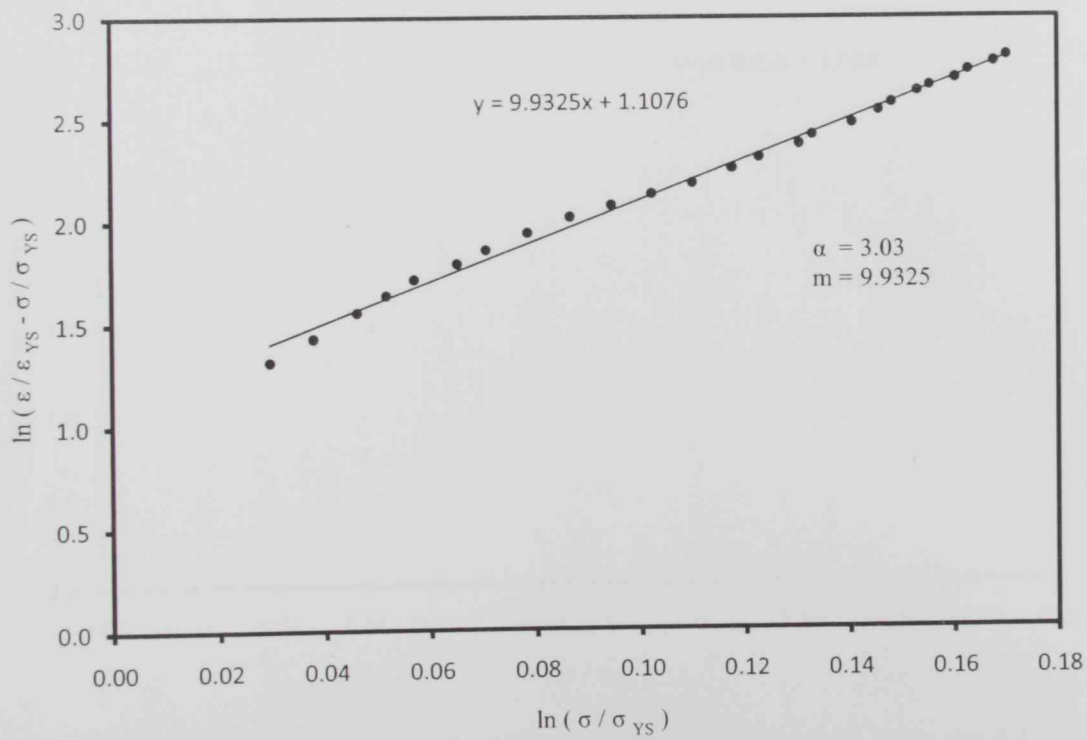

Figure 3.20 Curve fitting plot to obtain plastic Ramberg-Osgood constants m and α, test # 2.

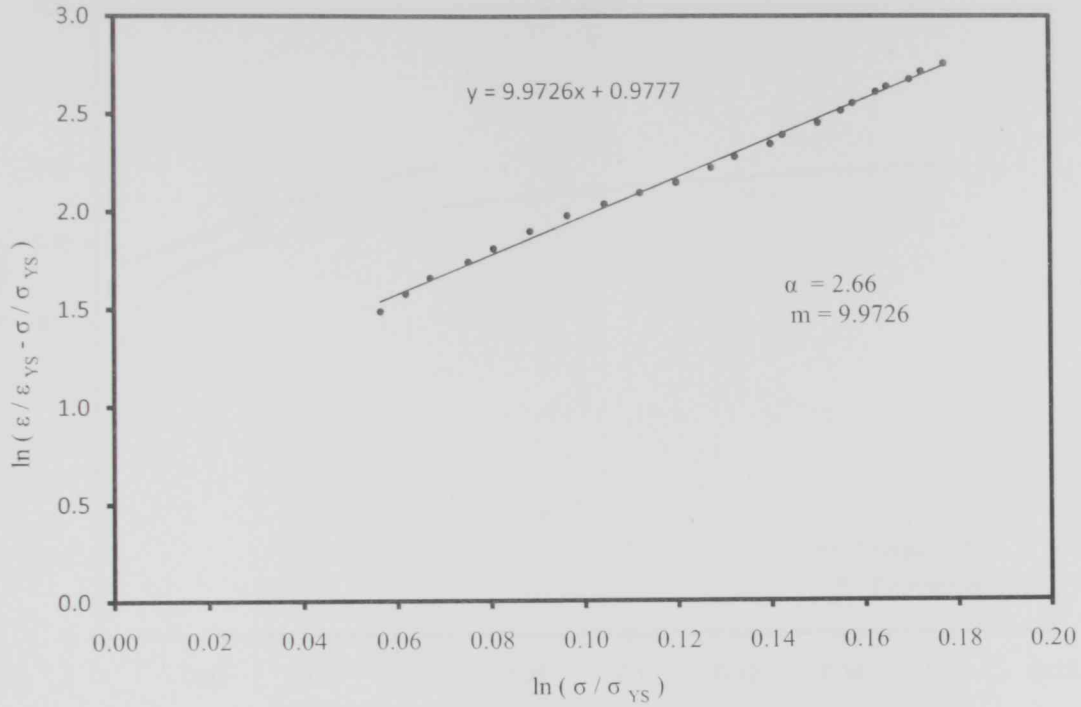

Figure 3.21 Curve fitting plot to obtain plastic Ramberg-Osgood constants m and α, test # 3.

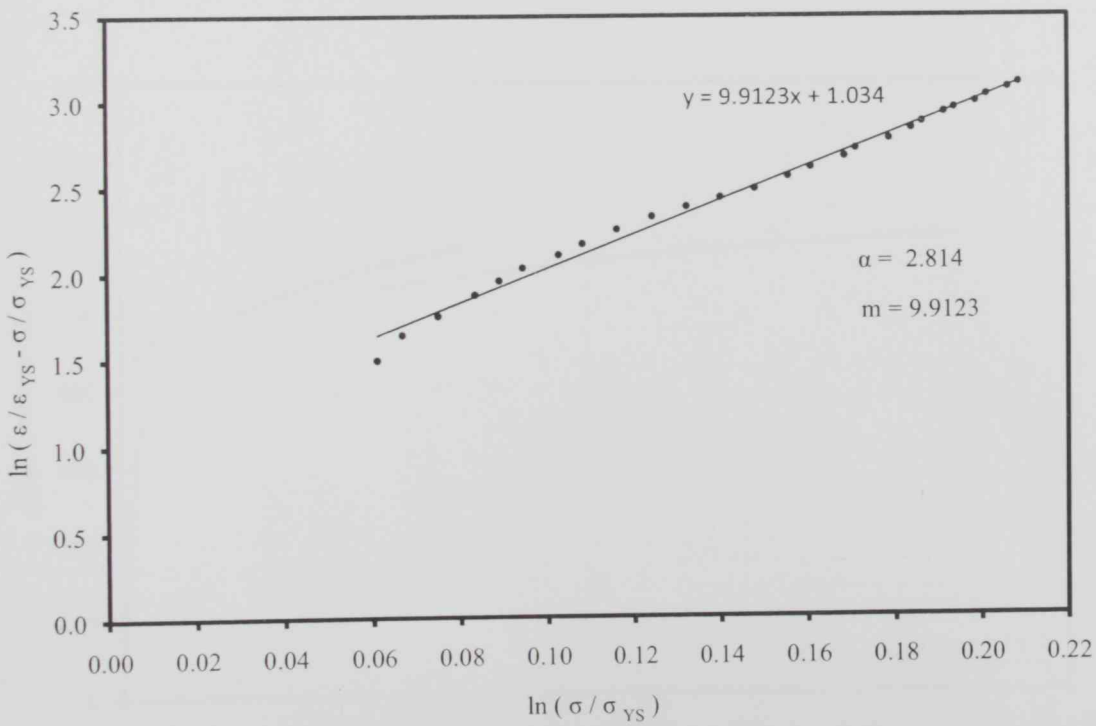

Figure 3.22 Curve fitting plot to obtain plastic Ramberg-Osgood constants m and α, test # 4.

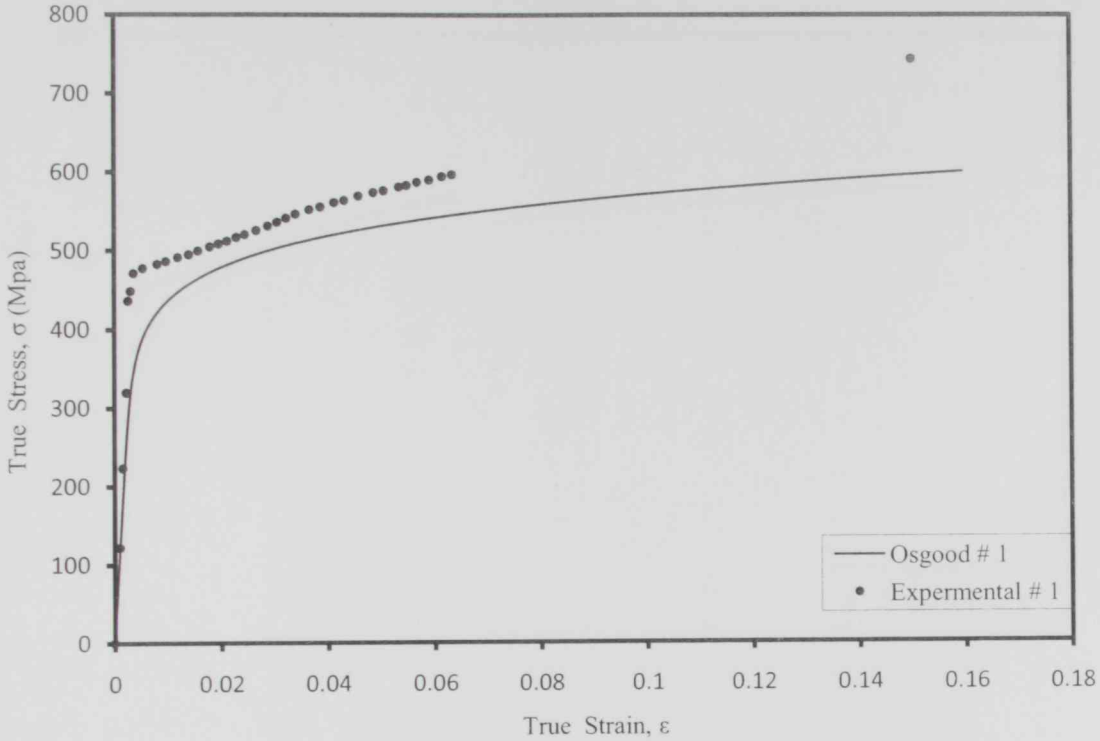

Figure 3.23 True Stress- Strain vs. R-O Equation Stress-Strain Curves, tensile test # 1

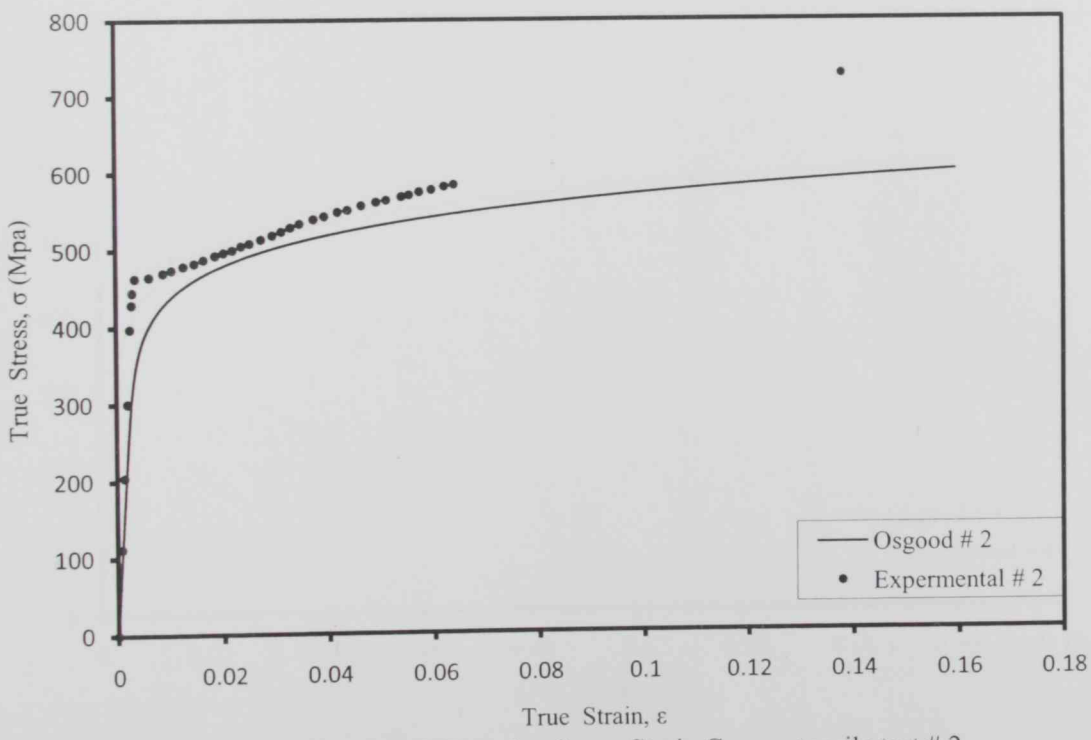

Figure 3.24 True Stress- Strain vs. R-O Equation Stress-Strain Curves, tensile test # 2

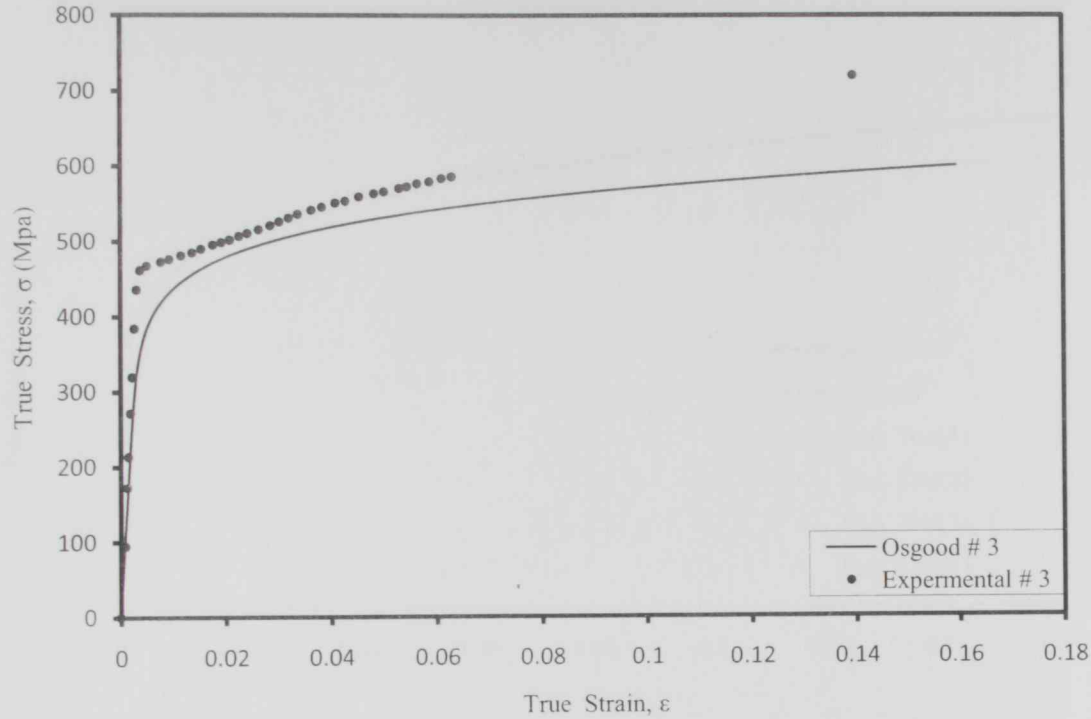

Figure 3.25 True Stress- Strain vs. R-O Equation Stress-Strain Curves, tensile test # 3

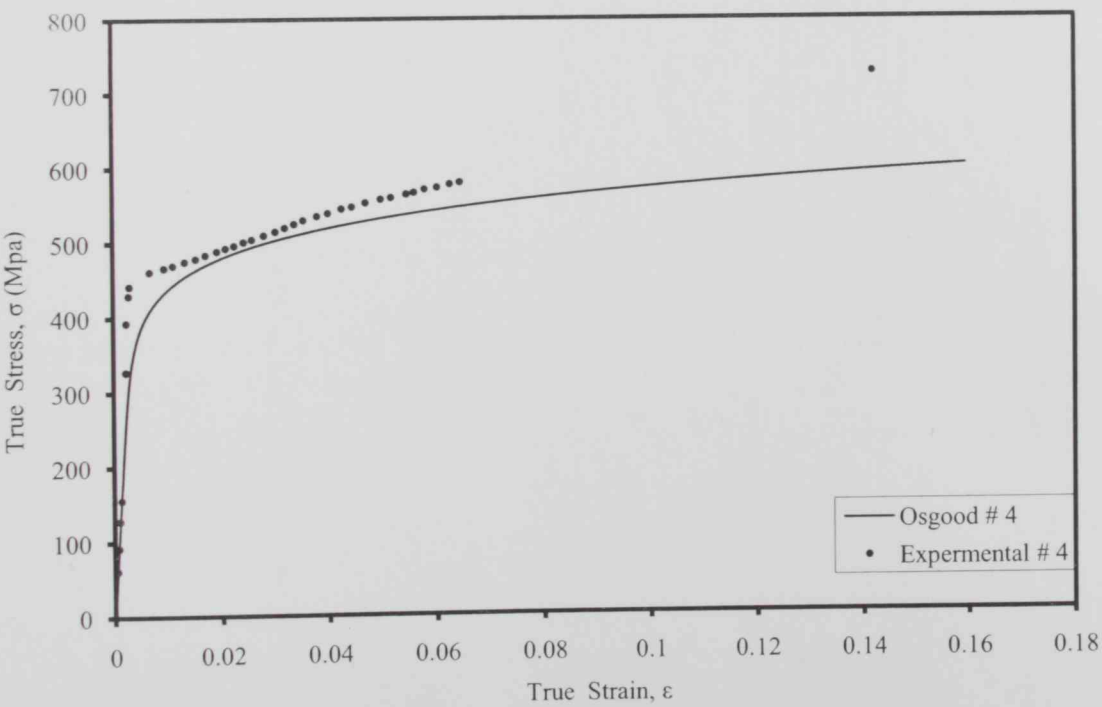

Figure 3.26 True Stress- Strain vs. R-O Equation Stress-Strain Curves, tensile test # 4

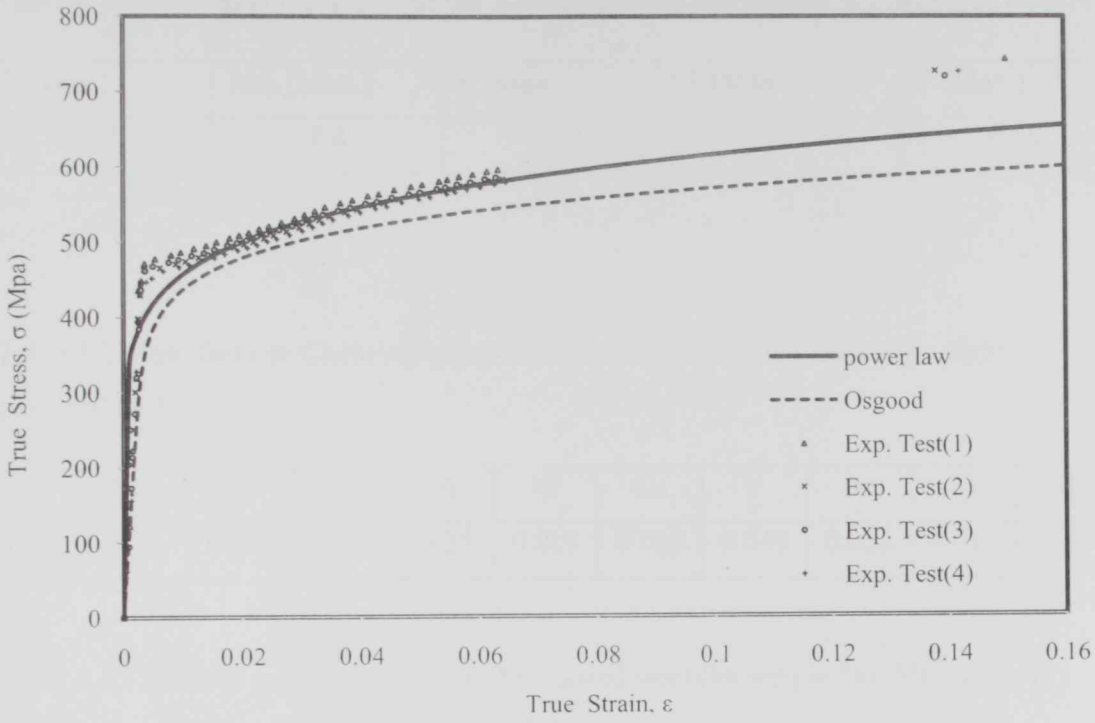

Figure 3.27 Comparison plot of Stress –Strain Curves for all tensile tests with power law and Osgood stress- strain.

Table 3.1 Chemical composition of the X65 tested steel (by weight %), provided by API.

C (Max.)	Mn. (Max.)	P (Max.)	S (Max.)	T (Max.)
0.28	1.4	0.03	0.03	0.06

Table 3.2 Manufacturer Chemical composition of the X65 tested steel (by weight %), provided by NPCC.

C	Mn.	P	S	Si	Ni	Cu	V	Al	Ti	Mo
0.10	1.06	0.007	0.001	0.25	0.019	0.028	0.048	0.022	0.013	0.07

Table 3.3 Chemical composition of the X65 tested steel (by weight %), Measured by Arab Centre for Engineering Studies. (ACES)

C	Mn	P	S	Si	Ni	Cu	Co	Al	Mo	Cr
0.17	0.86	0.017	0.018	0.29	0.06	0.19	0.013	0.036	0.036	0.097

Table 3.4 Mechanical properties of X65 steel pipe obtained from tensile tests.

Test	E (GPa)	σ_Y (MPa)	σ_U (MPa)	σ_Y^- (MPa)	ε^-
1	224	469.64	560.15	471.355	0.004
2	197	461.69	547.44	463.329	0.004
3	221	459.29	550.29	461.490	0.004
4	198	449.19	542.91	451.396	0.005
Average	210	459.95	550.20	461.893	0.004

Table 3.5: Power law Equation material constants (n, K) and their average values obtained from tensile tests.

Test	n	k (MPa)
1	0.14	868.80
2	0.13	831.50
3	0.12	805.50
4	0.13	818.00
average	0.13	830.95

Table 3.6: Ramberg -Osgood constants (m, α) and their average values obtained from tensile tests.

Test	α	m
1	2.59	10.45
2	3.03	9.93
3	2.66	9.97
4	2.81	9.91
average	2.77	10.07

Table 3.7: Mechanical properties of X65 steel pipe provided by steel manufacturer and API standards.

Test	API (Min. Req.)	Manuf. Insp. certificate
Yield strength(Mpa)	448	470.00
Ultimate .T.S (Mpa)	531	558.00
Elongation %	19.1	28.20
Hardness Vickers HV10	240(max)	188.00

Chapter Four

FRACTURE TOUGHNESS TEST

4.1 Introduction

Cracks in piping systems often occur at welding joints. Mostly these are located in circumferential direction. For this reason circumferential cracks play an important role in the safety analysis of pipes. In this study stress intensity factors were measured for complete circumferential surface cracks at the outer wall of a pipe loaded by tensile stress in axial direction. Tensile testing for pipe presents unique challenges. Additionally, operators may inadvertently crush the ends of a specimen while gripping. For the previous mentioned reasons special fixtures were used to conduct the test. A sample pipe was machined with holes at ends and a fork type fixture with extension plugs and suitable pins were prepared to grip the specimens to Universal Testing Machine as shown in Figure 4.1, the fork type fixture was designed and fabricated from steel alloy material, also pins and internal plug fixture were manufactured from AISI 4340, Figure 4.2 shows a photograph for the fork type fixture assembled with the pipe specimen gripped to the universal testing machine. The design of fork based on the rigidity of the fixture, during the trial test pins were failed to withstand the applied load at early stages , several trials were conducted after modifying the size of pins by increasing the pin diameter but unfortunately the extension plugs were deformed badly.

4.2 Specimen Preparation

Since this study is mainly concerned in testing full size cylindrical specimens, several ideas and thoughts were considered to overcome the limitations that obstructing conducting compact tension test. The problem of handling the specimen was solved by machining of two extensions square threaded bars from high strength material as shown in Figure 4.3 and the length of the bar was minimized to overcome any unexpected misalignment of the assembly. Square threaded was selected to maximize the contact area and accordingly increase load bearing capacity of the used fixture. Nine specimens of carbon steel grade X65 pipe with an inner diameter of 42.9 mm and an outer diameter of

60.3 mm were cut from 6 meter standard length pipe by electric saw then fine machined by lathing machine to ensure equal length. Using the same lathing machine and different cutting tool a circumferential surface V notch at mid-section of each pipe specimen was prepared .The pipe geometry and its dimensions after machining are shown in Figure 4.4. The preparation process was done under proper feeding rates and suitable cooling condition to avoid any local changes of the material properties. In other word, high measures were considered during pipe specimens preparation, the angle of V notch is 60^o , special cutting tool was used to confirm that the radius of notch is almost zero , and the depth of the notches were selected randomly to test different thicknesses of remaining materials. The considered depths were 2.55 mm, 3.15 mm, 4.4 mm, 4.65 mm, 4.85 mm, 515 mm and 5.95 mm. The wall thickness of the pipe specimens was kept the same. Figure 4.3 shows pipe specimen after preparation for some notch depths while Figures 4.4 and 4.5 show the pipe specimen geometry and cross sectional drawing respectively. Also as part of preparation procedures; the internal surface of the pipe was machined with square threads up to certain length from both end sides to match with the already prepared threaded extension bars, the threaded bar geometry is shown in Figure 4.6. In order to maintain plane strain conditions ahead the machined notches of each pipe specimen a special high strength insert plug as shown in Figure 4.3 with suitable geometry as shown in Figure 4.7 were machined so fit inside and at the mid of the pipe specimen. That is the main function of the plug is to convert the state of strain into plane strain condition by eliminating the circumferential strain $\varepsilon_{\theta\theta}$ while there are no constraints on the axial ε_{zz} and radial ε_{rr} strains.

4.3 Test Procedure

A 1500 kN rated universal type test machine was used in displacement controlled mode, the head speed of the machine was kept constant and equal to 0.5 $mm\,min^{-1}$ for all tests. After preparation of pipe specimens, the plugs were inserted inside the pipe specimen then the threaded bars were tightened from both sides of the pipe specimen. Figure 4.8 shows a cross sectional drawing of the whole testing assembly showing plug insert, threaded bars fixtures and pipe specimen, then the assembly gripped carefully to the universal testing machine and aligned properly. Figure 4.9 shows a typical

photograph of the pipe specimen under testing. A close-up view of the tensile setup is shown in Figure 4.10.

During the test the load-point displacement were recorded automatically and data were stored in the computer that interfaced with the testing machine. The extension threaded bars at the gripping area as well as the pipe specimen were kept under continuous monitoring against any deformation or any undesired necking, also checked by visual examining after each testing.

After each test, the fractured pipe halves were removed from machine grips and handled carefully and kept inside clean plastic bags separately to avoid any unexpected damage to the fractured surfaces for further investigation as will be shown in the next section. Also the threaded bars were disassembled easily representing a further evidence of deformation free of the assembly. Three pairs of extension threaded bars were used in order to eliminate the effect of any plastic deformation that might occur if the same pair used for all tests .In addition, also seven plugs were used since the removal of plug after the pipe specimen fracture need applying jacking force that might destroy the fractured surfaces. A tight safety measures were considered and followed carefully by the machine operators and due to very loud acoustic emissions that were experienced during the first test it was not allowed to carry out fracture tests while any other nearby testing machine in the lab is on running conditions to avoid damage of expensive tools.

The test repeated for seven different notch depth sizes with plug inserted into the pipe specimen and two selected tests were carried for non plug extreme cases, the biggest and smallest notch depth sizes. Also all nine tests were conducted under room temperature and all fractures occurred at the notch area as expected.

4.4 Results and Discussion

The fracture tests were performed for seven different values of plug type with notch depths (2.55 mm, 3.15 mm, 4.4 mm, 4.65 mm, 4.85 mm, 5.15 mm and 5.95 mm) and two tests without plug of 2.55 mm and 5.95 mm notch depth respectively. All specimens were loaded until the full separation of the specimen into two halves as shown in Figure 4.11. Figures 4.12 through 4.20 show the different load –line displacement diagrams.

Initially the load is varying linearly with the displacement till a certain point at which the curve deviates from its linearity for very small interval after which the pipe specimen separated completely. It is worth to mention that the separation instant is coupled with very loud sound. Figure 4.21 shows a comparison between all tests, the comparison Figure shows that the slope is inversely proportional with the notch depth. Also it is noted that the curve slope of no-plug test is less than of plug type and this might be attributed to the plane strain affect that produced by the presence of inserted plugs. Figures 4.22 and 4.23 show a comparison between plug and no plug for 2.55 mm and 5.95 mm notch depths, respectively. The fracture loads have been recorded for each specimen and the fracture toughness (plane –strain fracture toughness) values were measured using the well known formula:

$$K_{IC} = \sqrt{\frac{J_{IC}\, E}{1-v^2}} \qquad (4.1)$$

Where v is the Poisson's ratio, E is the modulus of elasticity and J is calculated by:

$$J_{IC} = \frac{area\ under\ load-displacement\ curve}{cross\ sectional\ area\ of\ the\ remaining\ material} \qquad (4.2)$$

The cross sectional areas of the remaining material below the circumferential crack for specimens were calculated according to the formula:

$$A_r = \frac{\pi}{4}\,(d_n^2 - d_i^2) \qquad (4.3)$$

Where: d_n is the notch diameter and d_i is the internal diameter of the pipe.

The cross sectional areas, the $J's$ values and the corresponding K_{IC} values are listed in Table 4.1.comparison of the calculated $K_{IC}$with a previous works[73] are shown in Figure 4.25. Figure 4.26 shows the variation of J values and the notch depths. The maximum load (fracture load) and the notch size are presented in Figure 4.24.They are varying mostly in a linear relationship with notch size.

The fracture surfaces of several specimens were examined. Figure 4.27 shows the fracture surface for pipe specimen with plug after fracture, the image was taken with a digital camera of 5X optical zoom. The fracture surfaces show mostly fine and smooth

surfaces, while Figure 4.28 shows a slightly coarse and present of shear lip as an indication of ductile fracture, this specimen of no plug type with notch size equal to 2.55mm.

A further investigation were carried out by Scanning electron microscope (SEM), fractographs of fractured surface of notched pipe specimens using different magnifications are shown in Figures 4.29 through 4.34 . SEM fractographs of fractured surface of plug inserted pipe specimens are shown in Figure 4.35 and Figure 4.36. Fracture mode is almost brittle as cleavages are visible for plugged samples while Fracture mode is ductile as lots of dimples are visible for unplugged samples as shown in Figures 4.37 and 4.38.

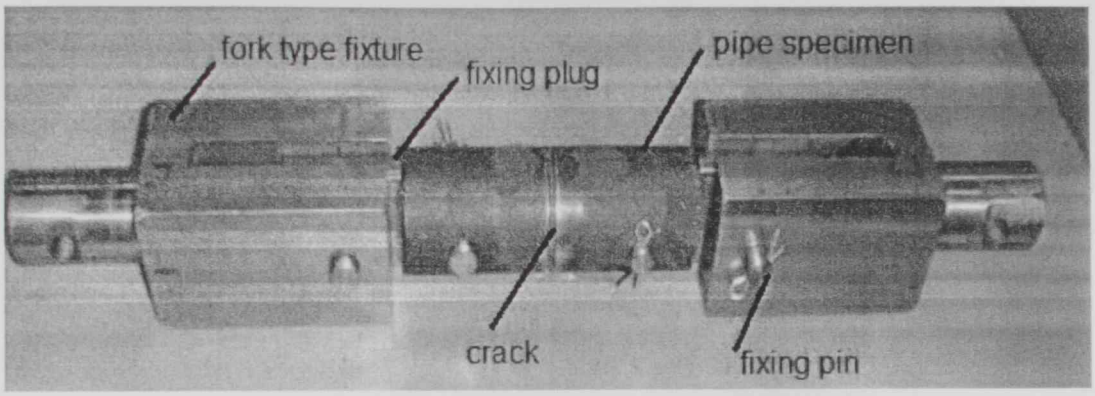

Figure 4.1 Fork type fixtures assembled with pipe specimen using pins.

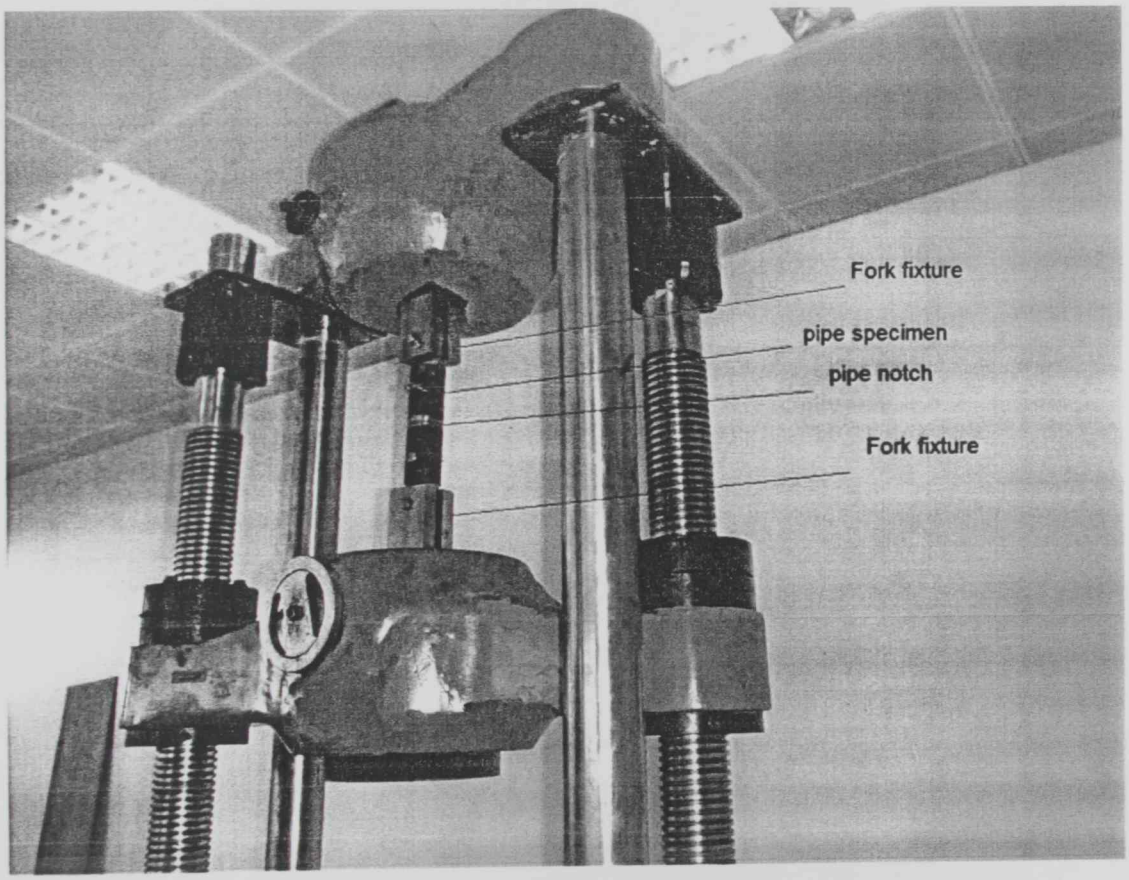

Figure 4.2 Pipe specimen assembled with fork type fixture gripped to Universal Testing Machine

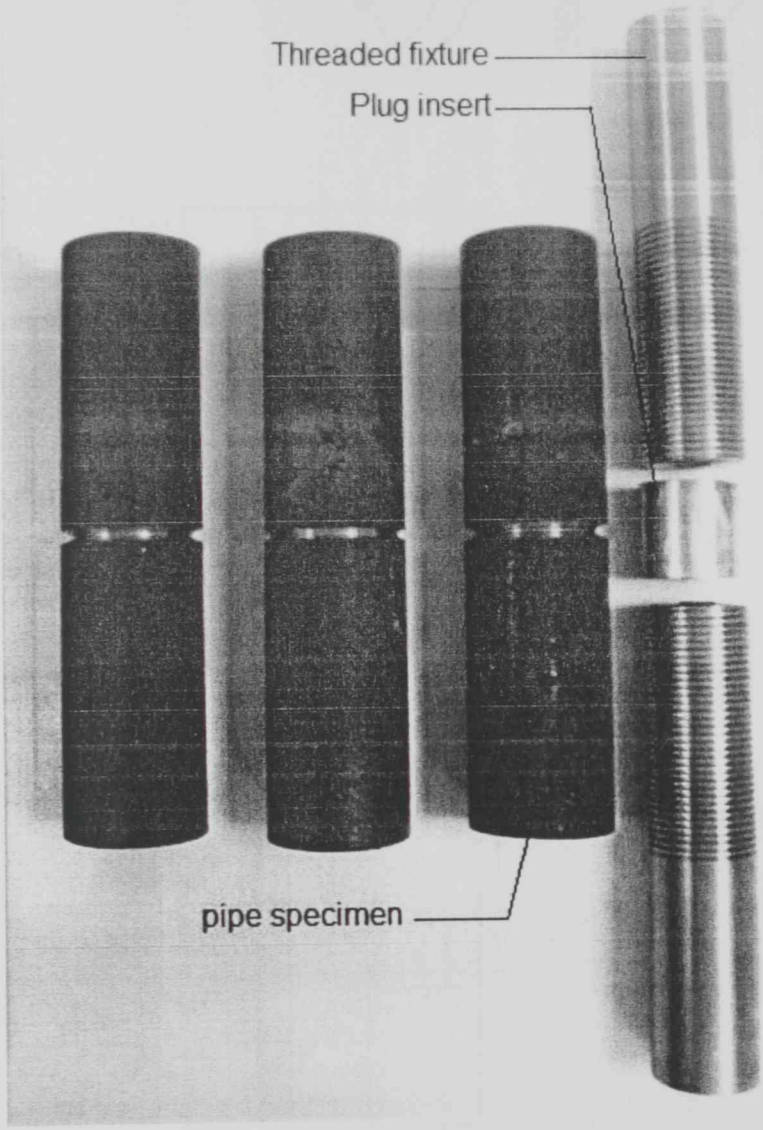

Figure 4.3 Pipe specimens after preparation for selected notch depths

Figure 4.4 Pipe specimen geometry

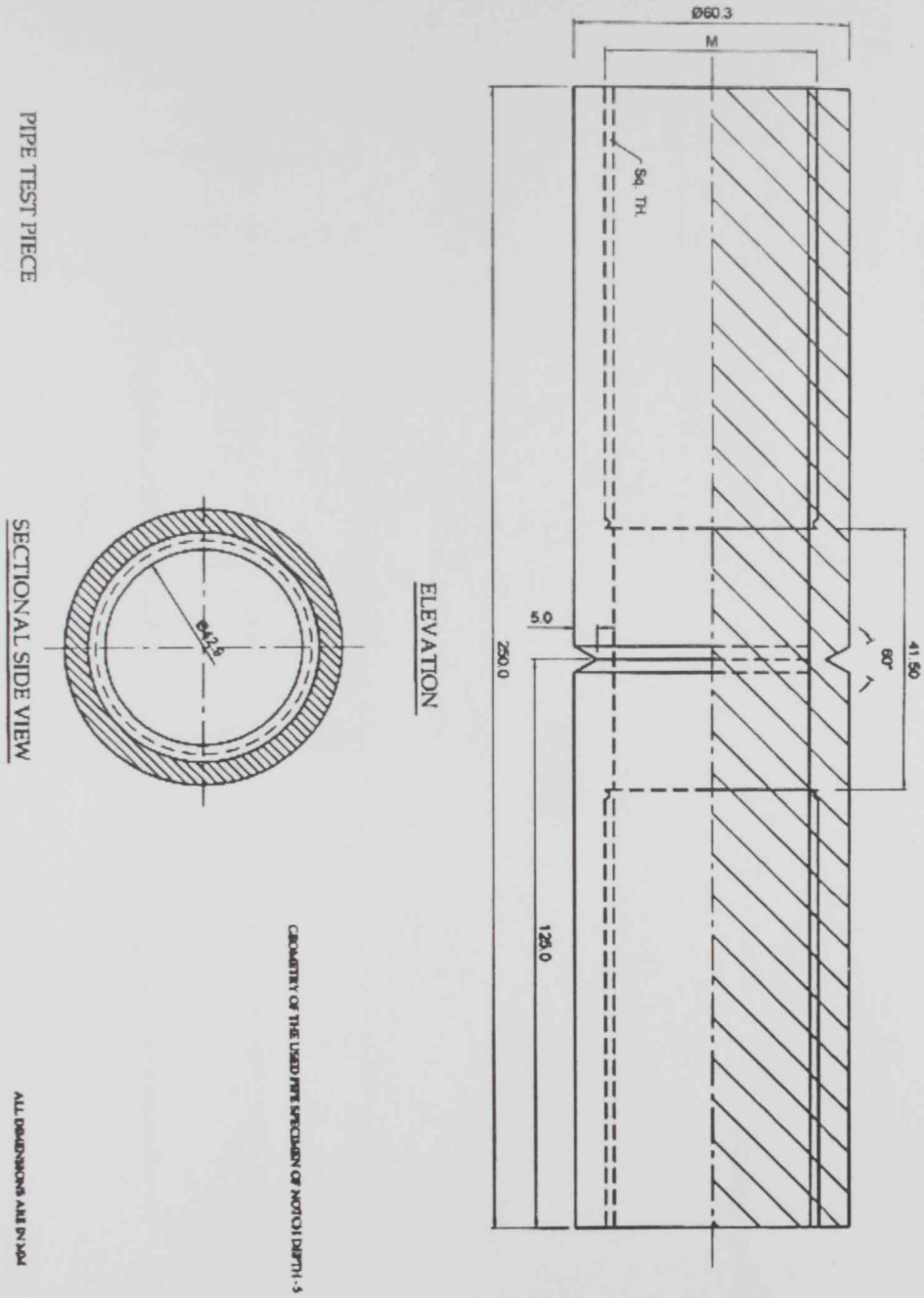

Figure 4.5 Cross sectional view for pipe specimen of notch depth =5mm

Figure 4.6 Threaded bar fixture geometry

Figure 4.7 Plug insert geometry

Figure 4.8 Cross sectional drawing of the assembly

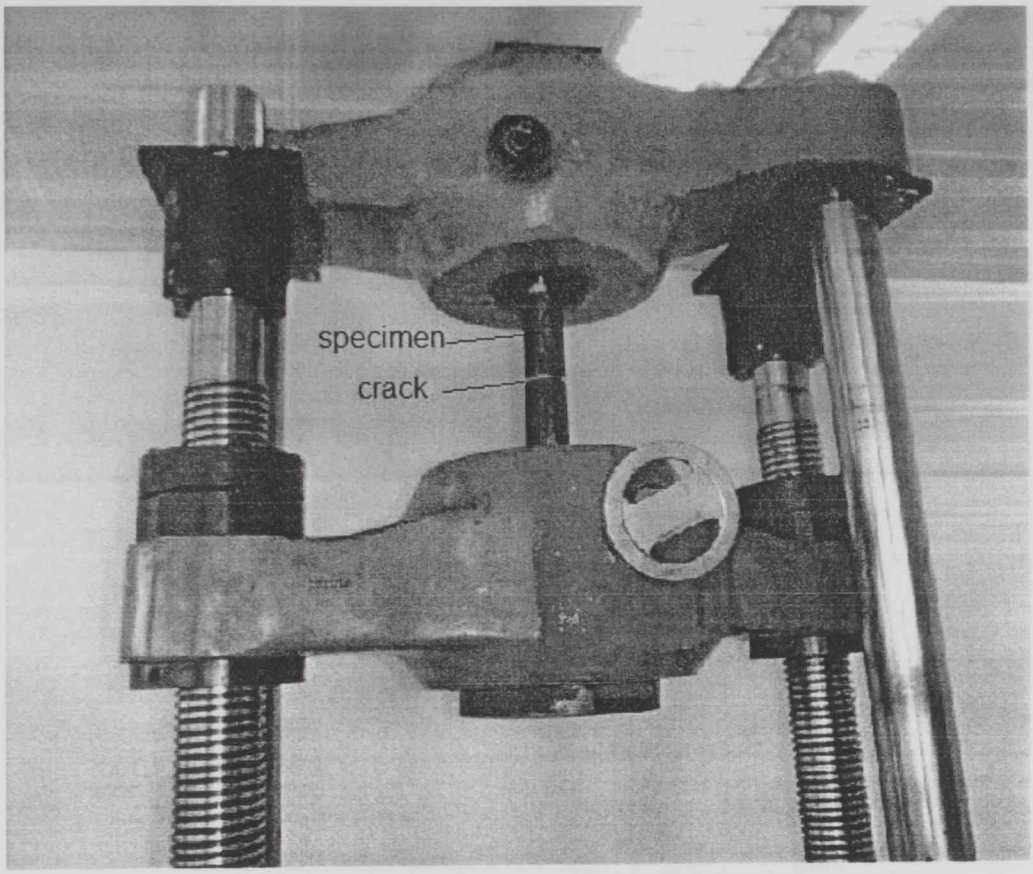

Figure 4.9 Pipe assembly attached to Universal Testing Machine

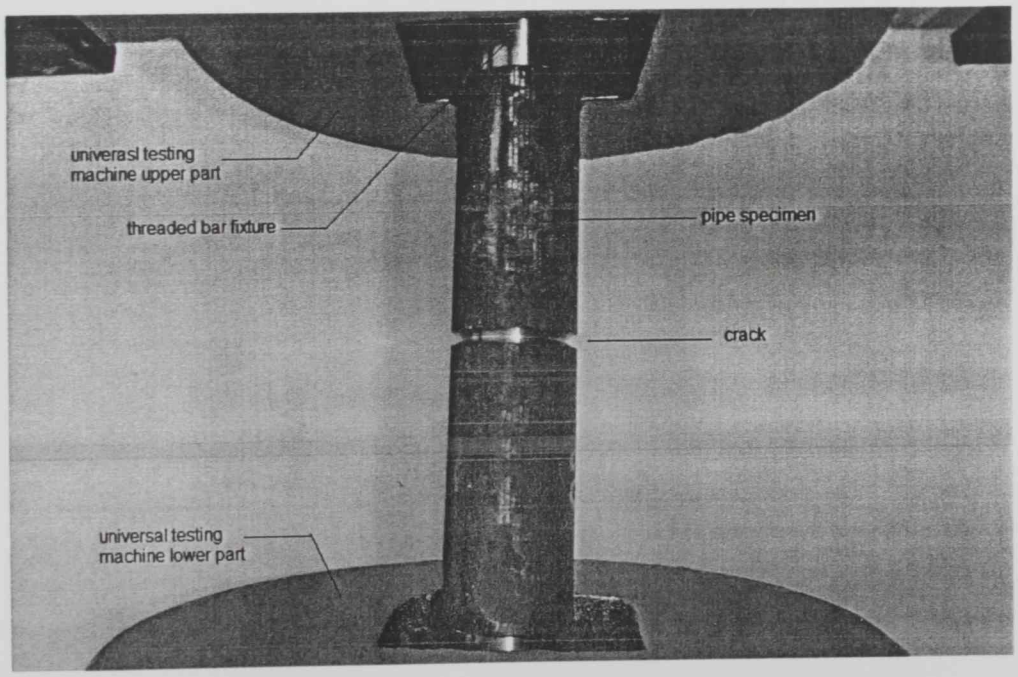

Figure 4.10 Close up view of assembly attached to universal testing machine

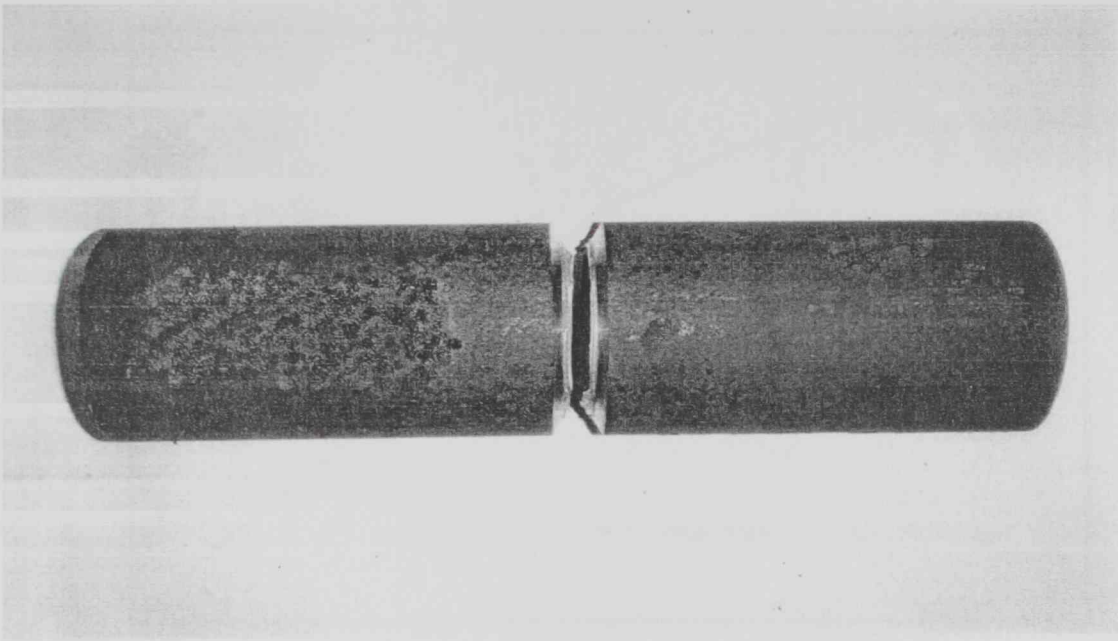

Figure 4.11 Pipe specimen after fracture.

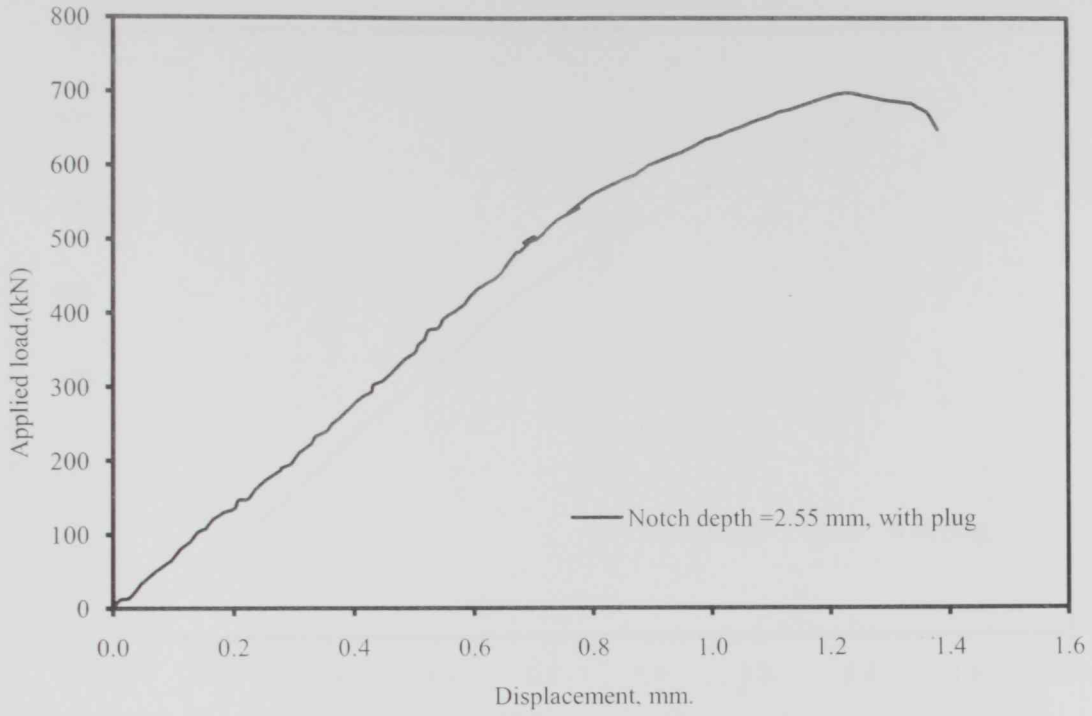

Figure 4.12 Experimental Load-Displacement curve for notch depth 2.55 mm, with plug.

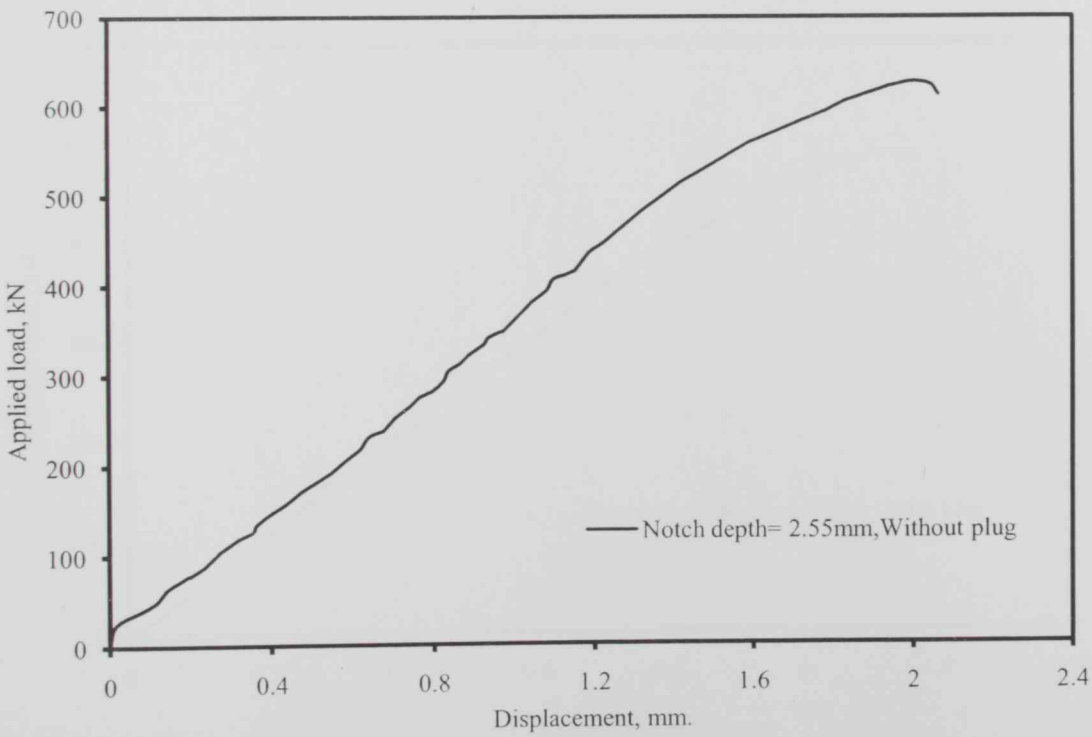

Figure 4.13 Experimental Load-Displacement curve for notch depth 2.55 mm, without plug

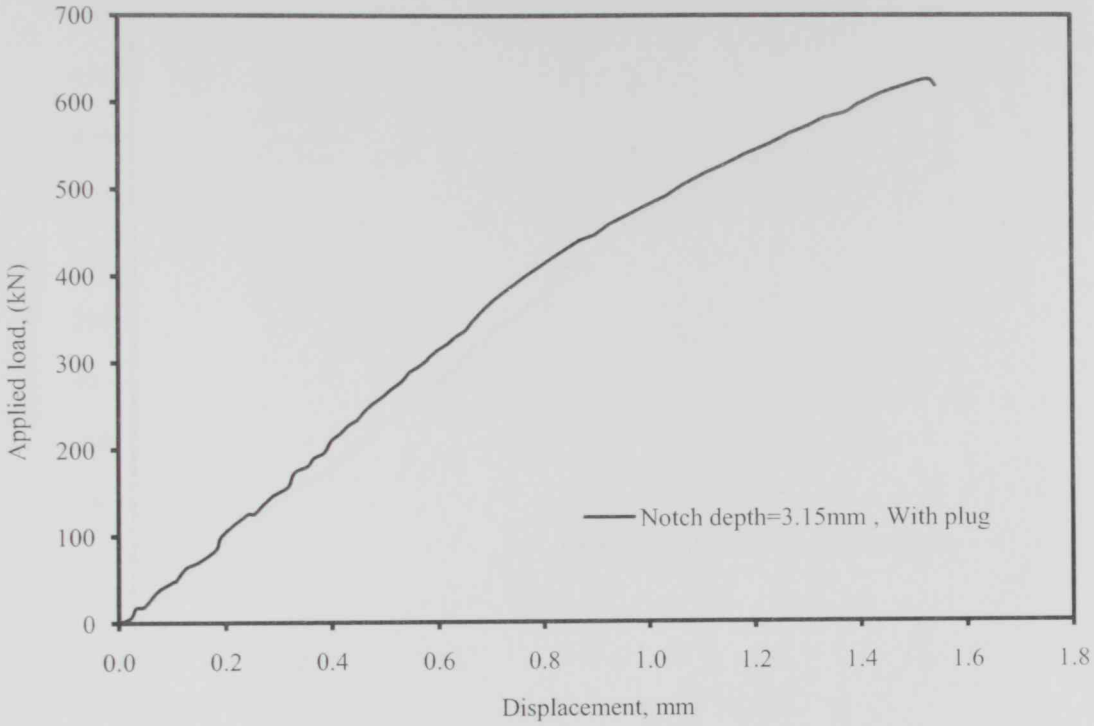

Figure 4.14 Experimental Load-Displacement curve for notch depth 3.15 mm, with plug

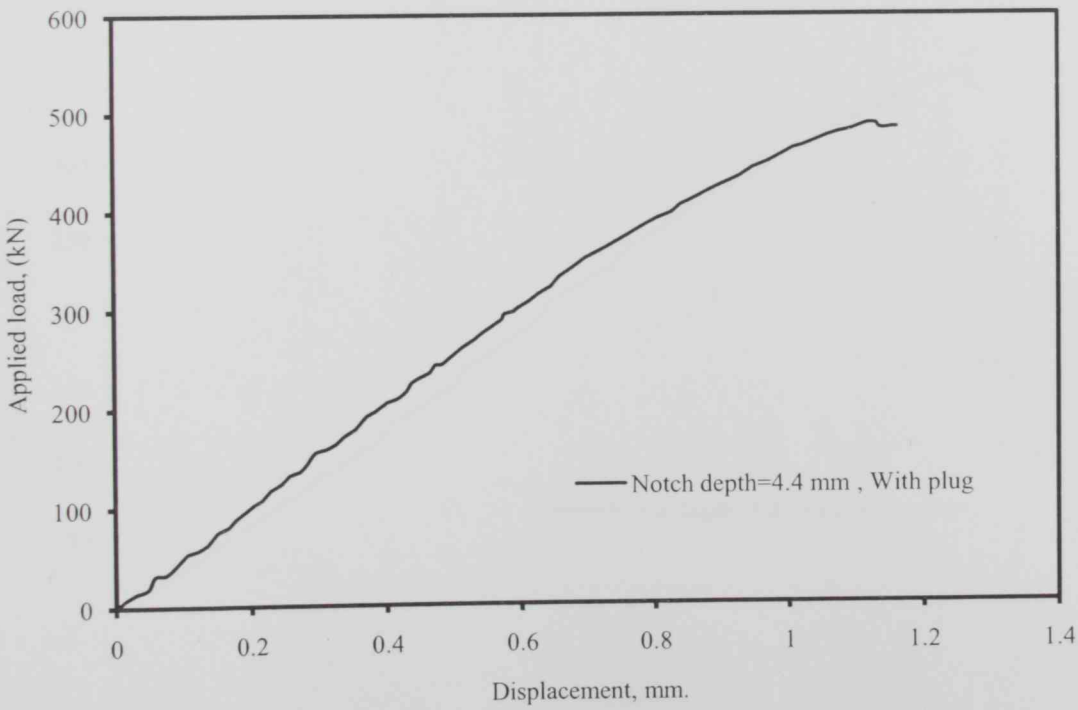

Figure 4.15 Experimental Load-Displacement curve for notch depth 4.4 mm, with plug.

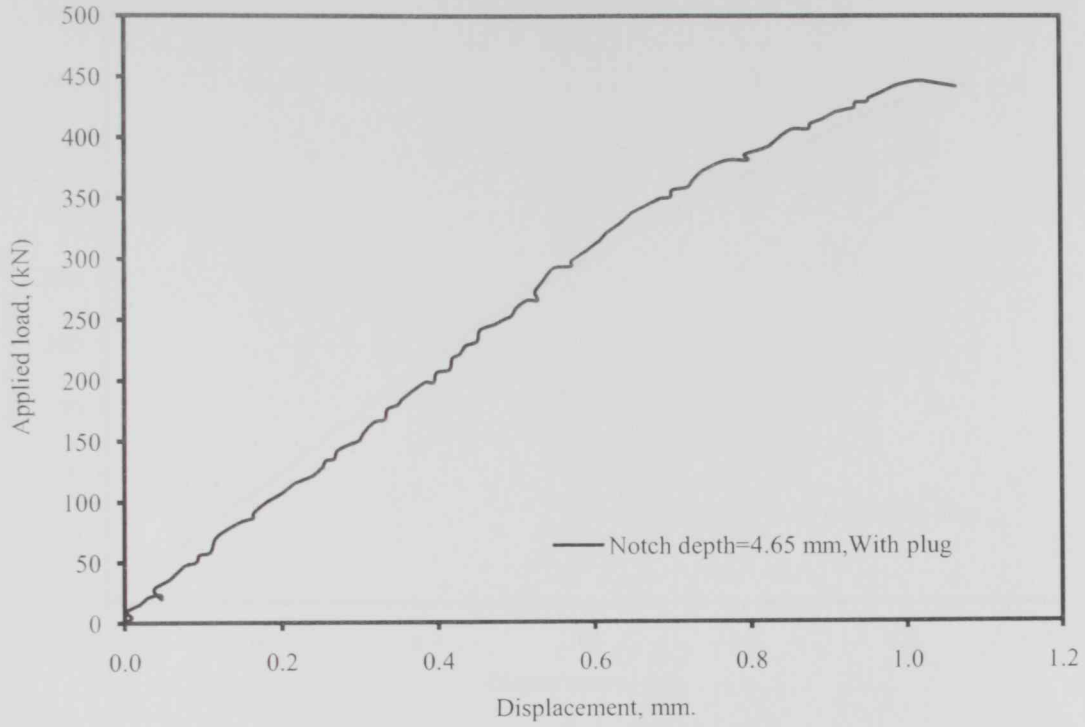

Figure 4.16 Experimental Load-Displacement curve for notch depth 4.65 mm, with plug.

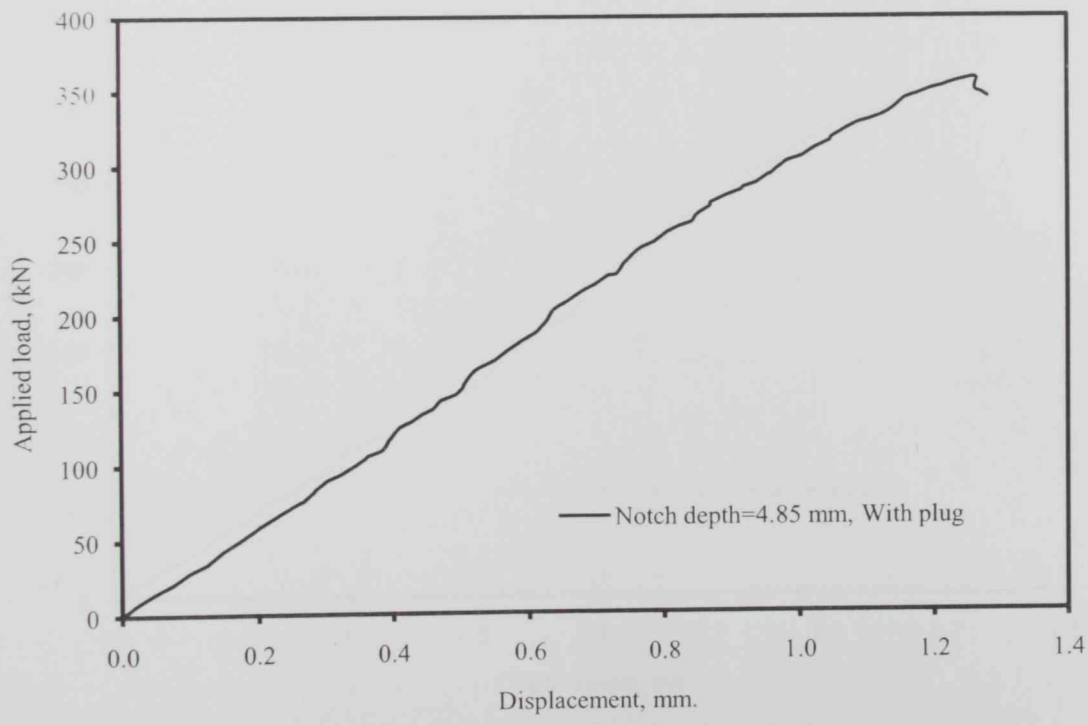

Figure 4.17 Experimental Load-Displacement curve for notch depth 4.85 mm, with plug.

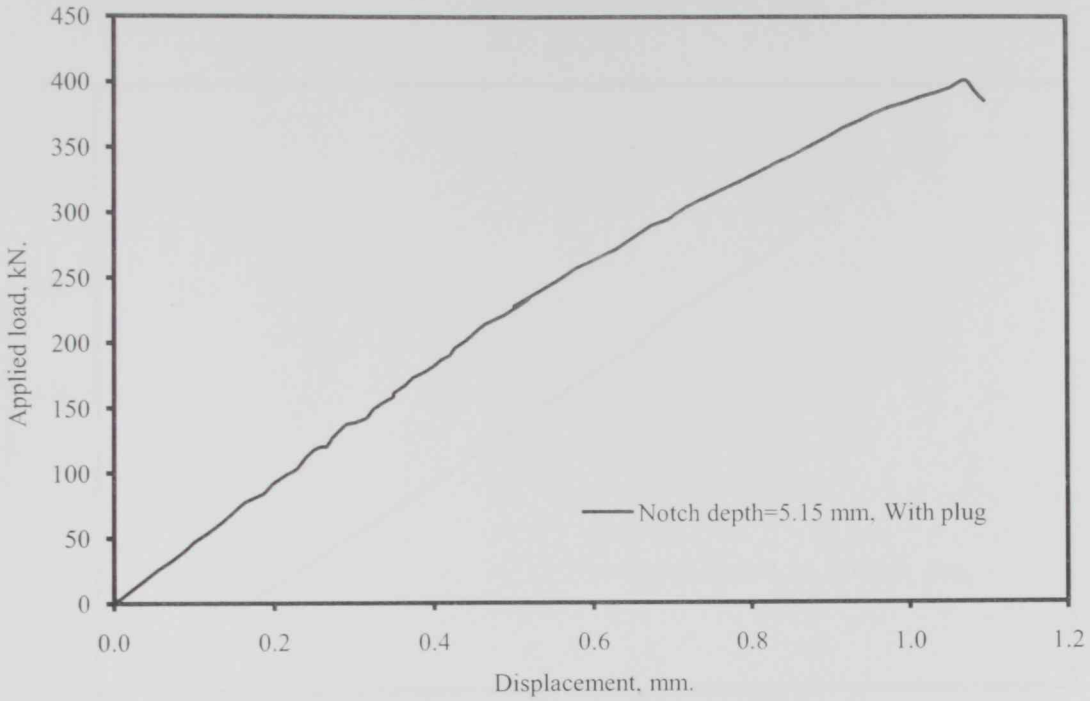

Figure 4.18 Experimental Load-Displacement curve for notch depth 5.15 mm, with plug.

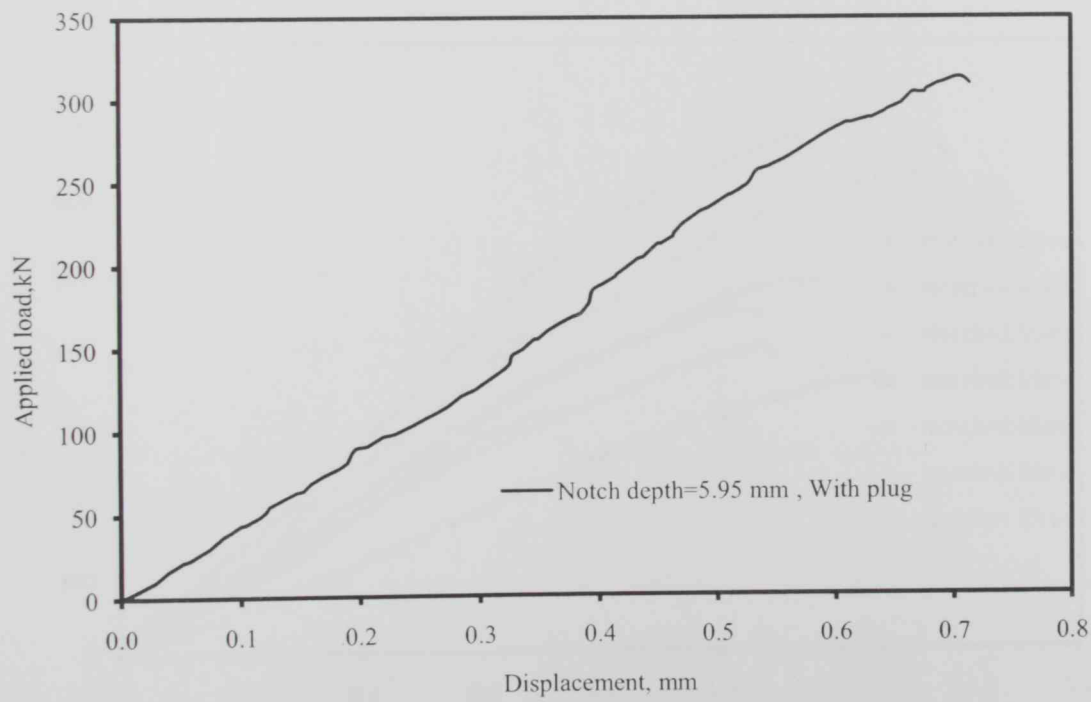

Figure 4.19 Experimental Load-Displacement curve for notch depth 5.95 mm, with plug

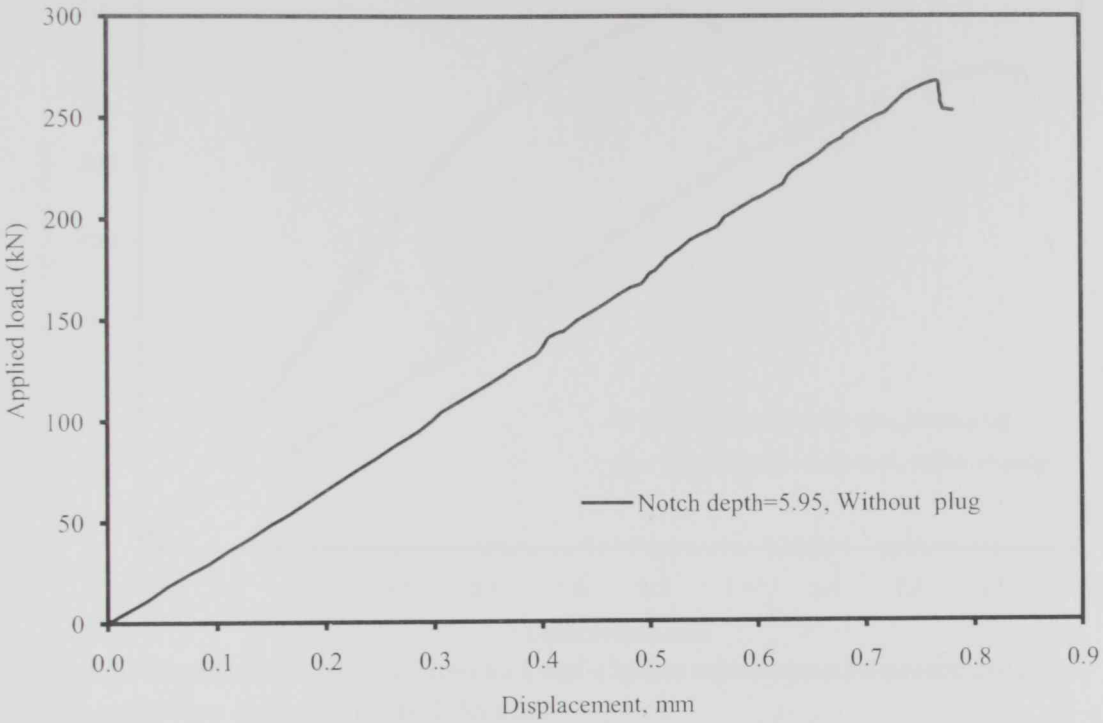

Figure 4.20 Experimental Load-Displacement curve for notch depth 5.95 mm, without plug

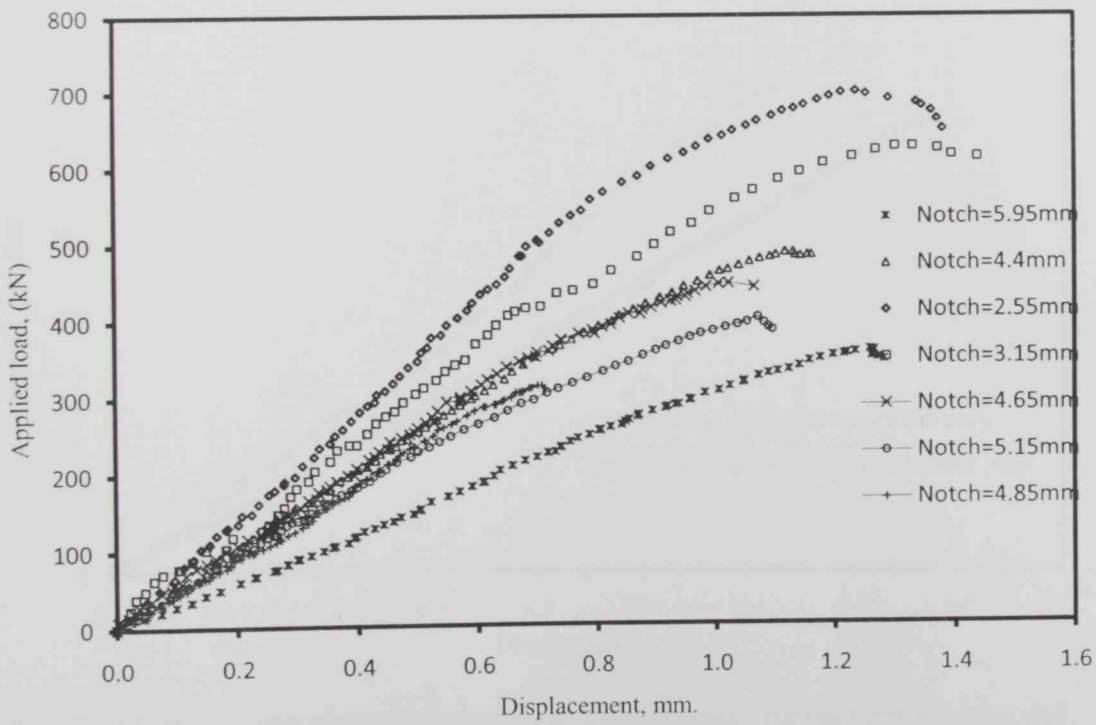

Figure 4.21 comparison Experimental Load-Displacement curves for all notch depths.

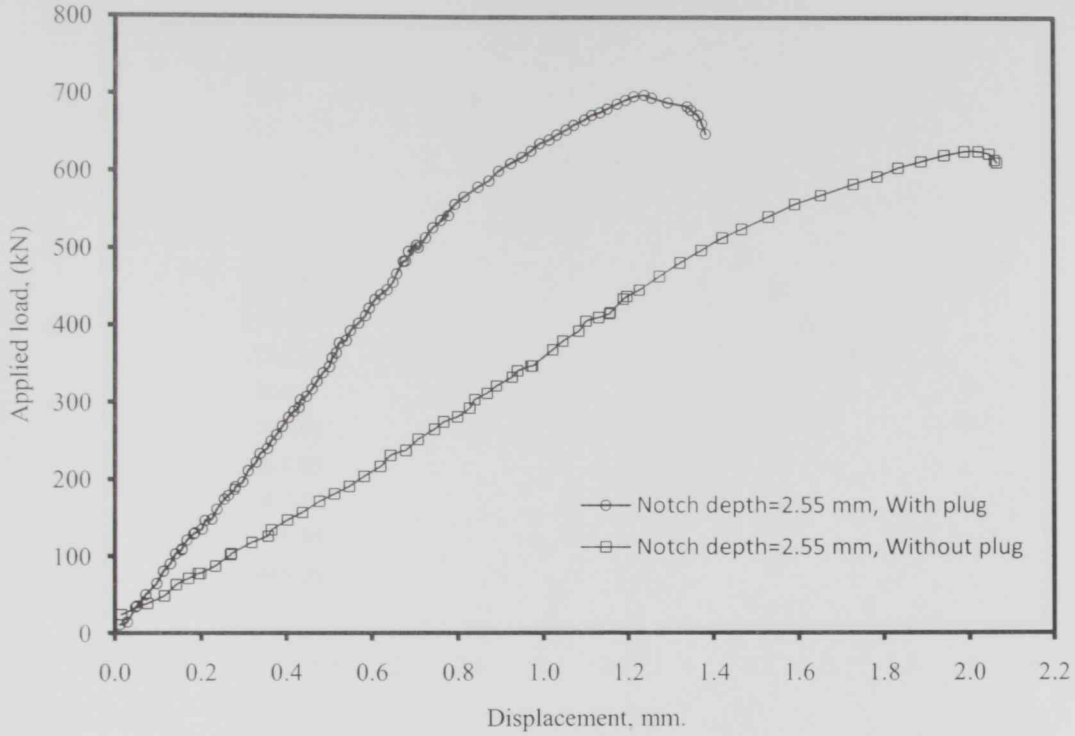

Figure 4.22 Comparisons of experimental Load-Displacement curves between plug and no plug conditions for notch depth 2.55 mm.

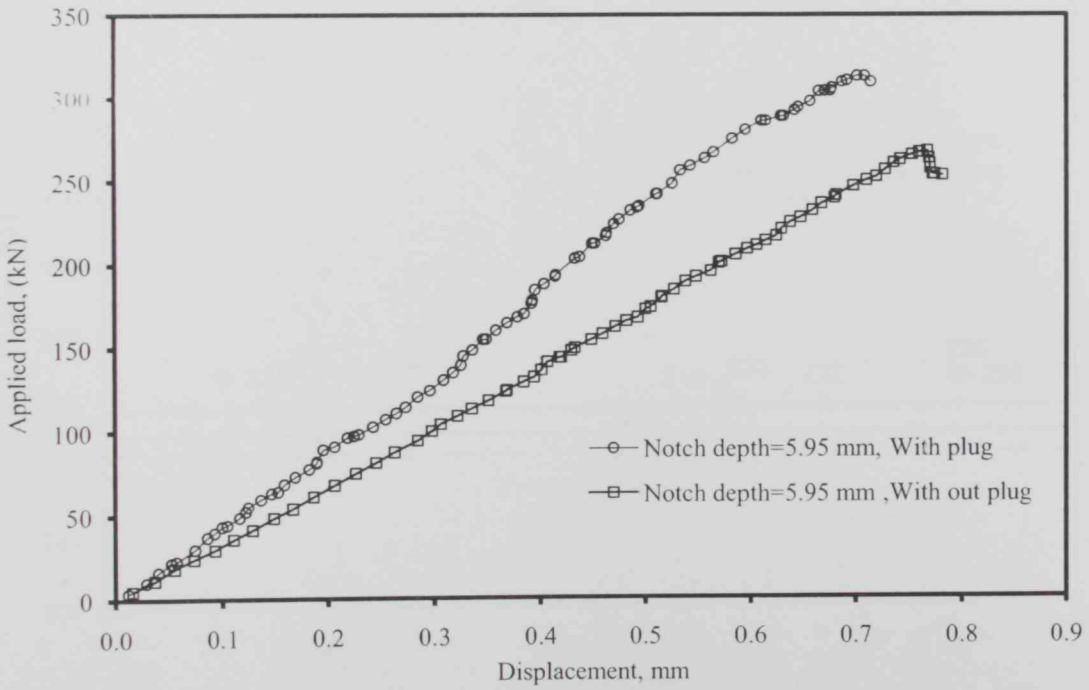

Figure 4.23 Comparisons of experimental Load-Displacement curves between plug and no plug conditions for notch depth 5.95 mm.

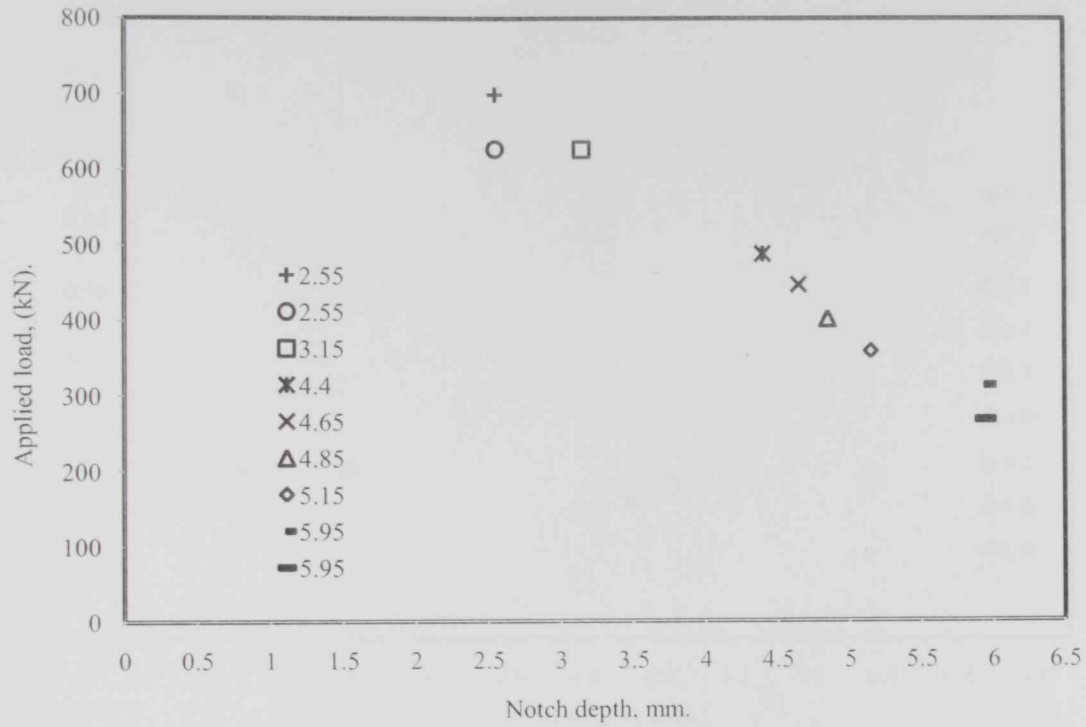

Figure 4.24 Variation of notch depth for all specimens against the maximum load

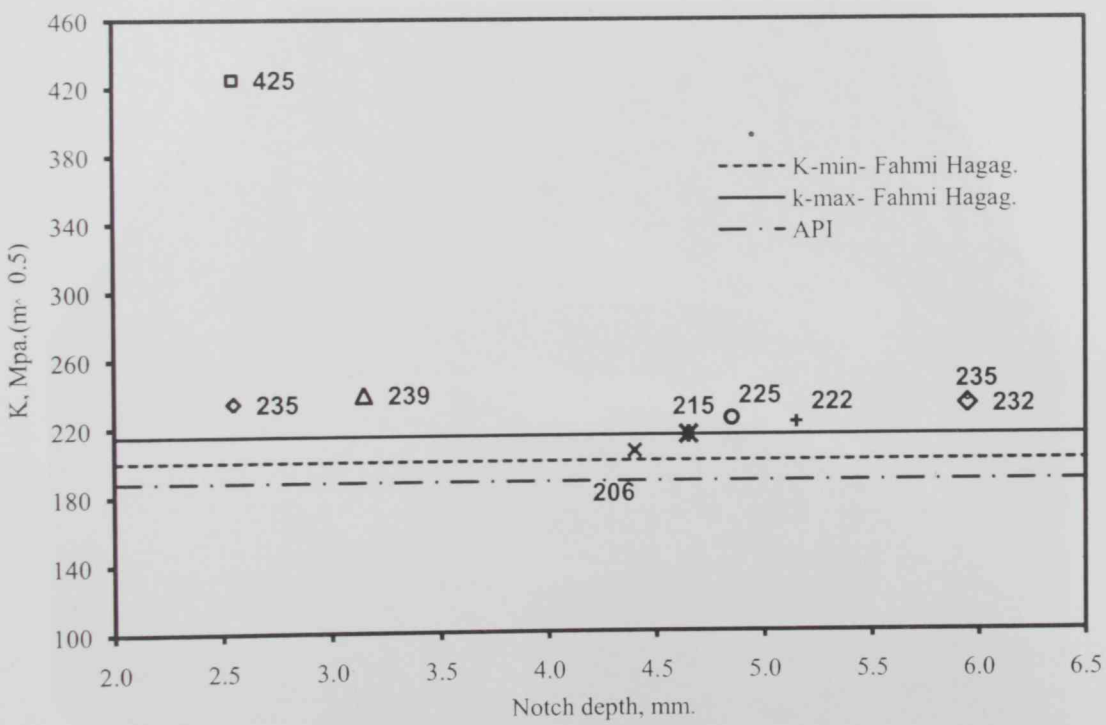

Figure 4.25 Comparison of resulted k_{IC} with previous works [73]

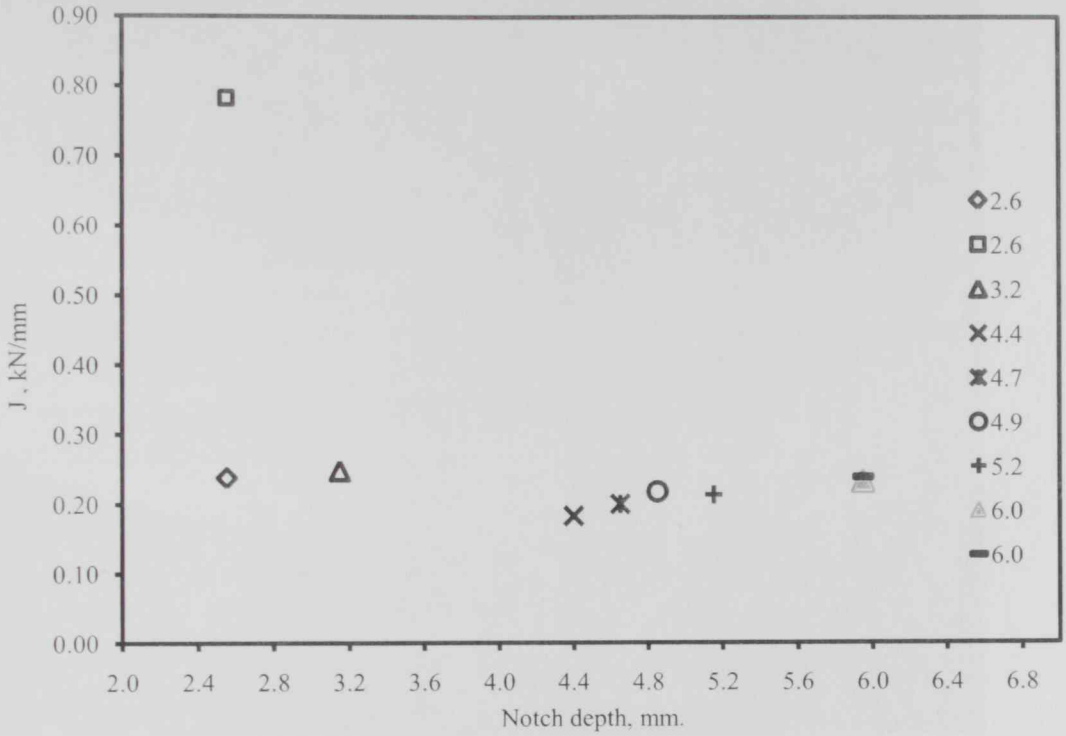

Figure 4.26 Variation of notch depth for all specimens against the J values

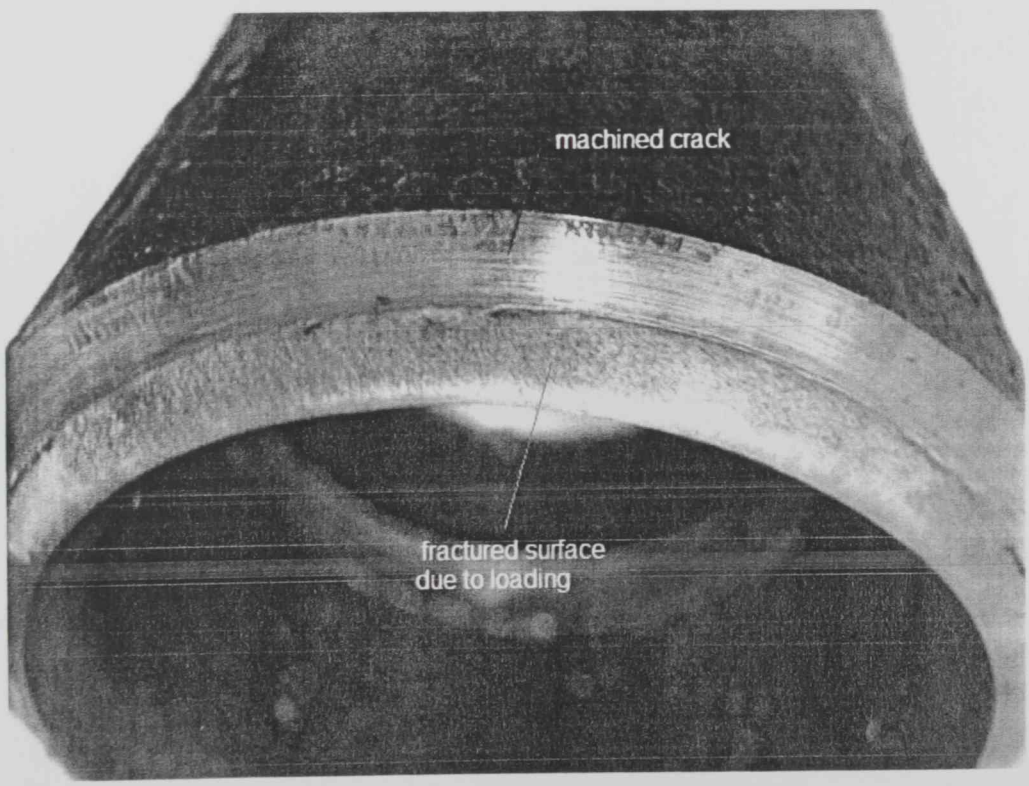

Figure 4.27 Pipe specimen with plug after fracture.

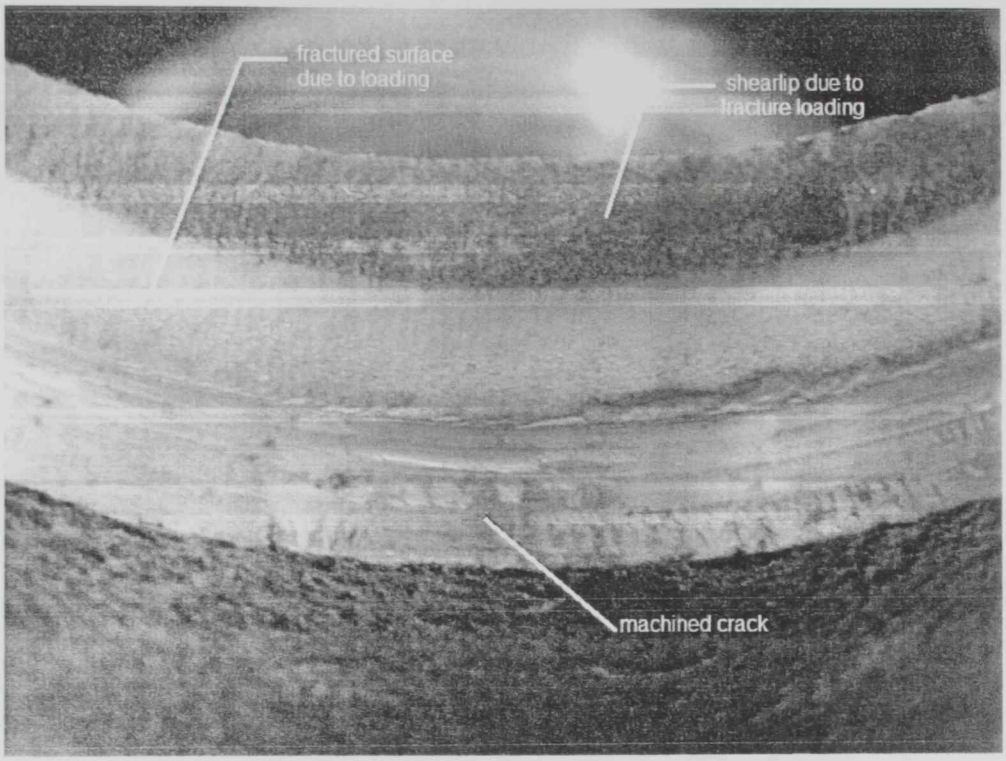

Figure 4.28 Pipe specimen without plug after fracture.

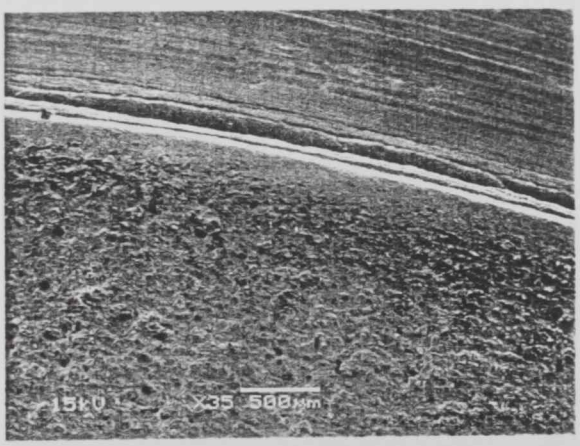

Figure 4.29 Scanning electron micrograph for stable crack growth region (X35)

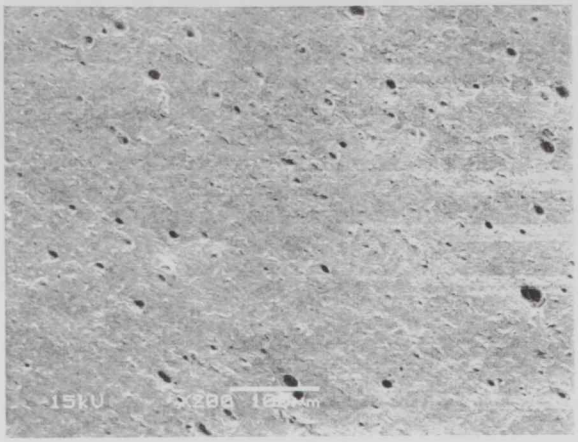

Figure 4.30 Scanning electron micrograph for stable crack growth region (X200)

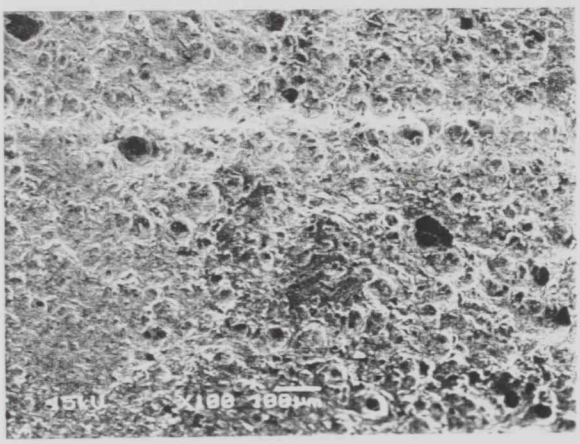

Figure 4.31 Scanning electron micrograph for stable crack growth region (X100)

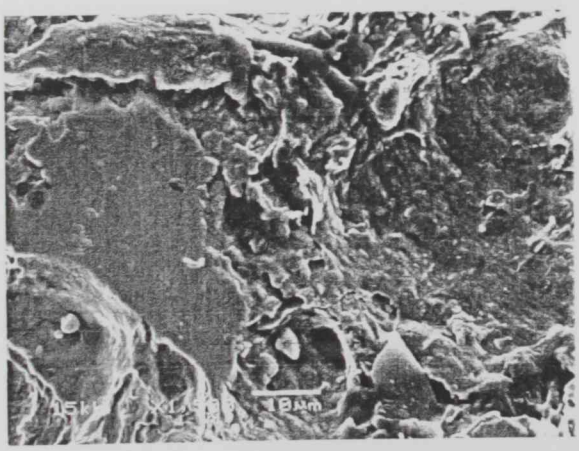

Figure 4.32 Scanning electron micrograph for stable crack growth region (X1500)

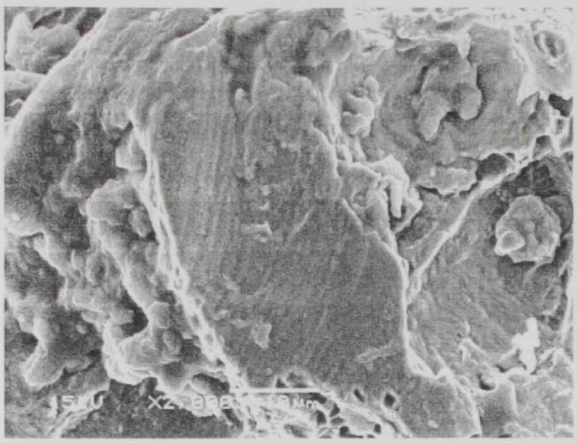

Figure 4.33 Scanning electron micrograph for stable crack growth region (X2000)

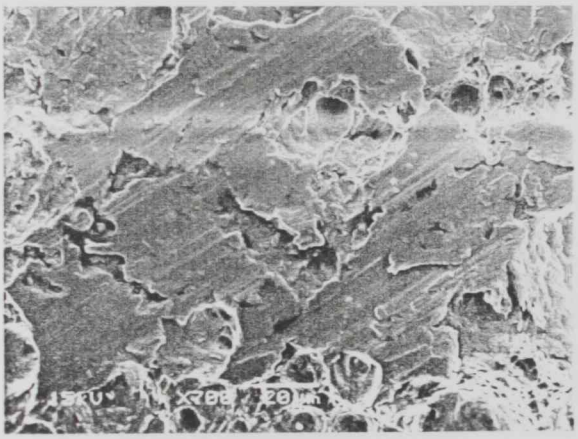

Figure 4.34 Scanning electron micrograph for stable crack growth region (X700)

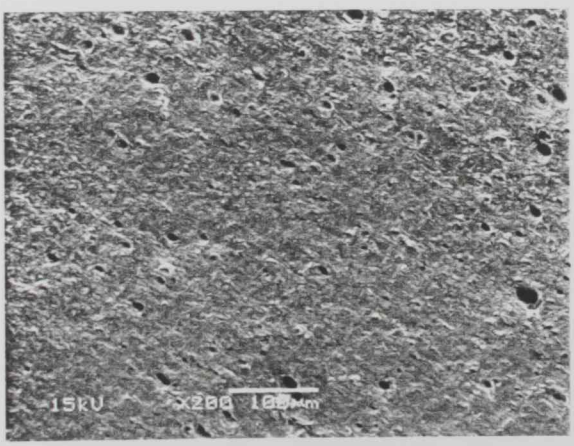

Figure 4.35 Scanning electron micrograph for stable crack growth region (X200)

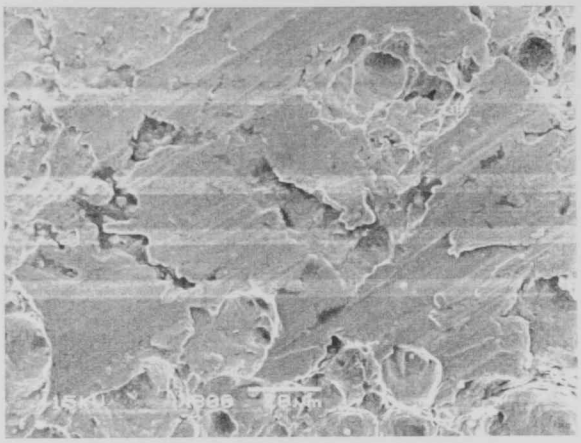

Figure 4.36 Scanning electron micrograph for stable crack growth region (X800)

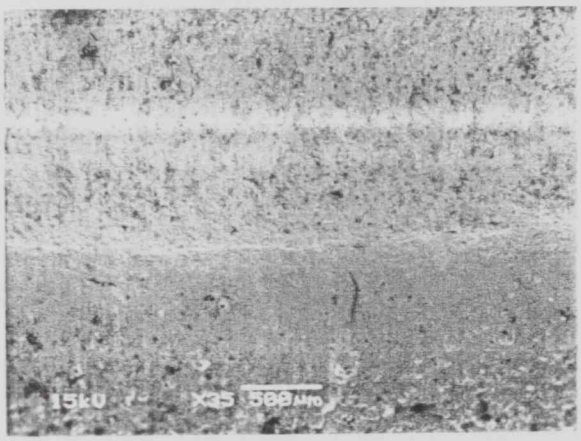

Figure 4.37 Scanning electron micrograph for stable crack growth region (X35)

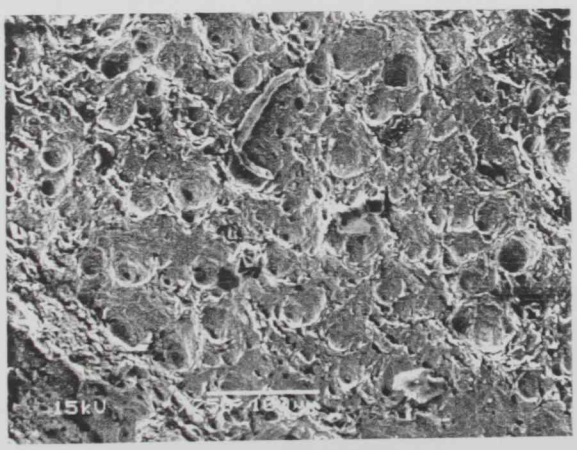

Figure 4.38 Scanning electron micrograph for stable crack growth region (X750)

Table 4.1 summary of the experimental results

Specimen No.	1	2 (no plug)	3	4	5	6	7	8	9(no plug)
Notch Depth (mm)	2.55	2.55	3.15	4.4	4.65	4.85	5.15	5.95	5.95
Remaining thickness(mm) T_f	6.15	6.15	5.55	4.3	4.05	3.85	3.55	2.75	2.75
J-(measured value), kN/mm	0.238	0.783	0.248	0.183	0.200	0.218	0.214	0.234	0.239
K-(measured value), MPa.(m) ^ 0.5	234.5	425.0	239.23	205.58	215.08	224.50	222.08	232.45	235.16
Load max (P) , kN	698.7	626.3	626	487.6	446.4	401.55	358.4	267.6	313

Chapter 5

Stable Crack Growth Test for Cracked Pipes

5.1 Introduction

Analytical methods for elastic-plastic fracture analysis of circumferential through-wall-cracked (TWC) pipes subjected to pure bending are well-developed. Brust et al. (1995a) and Rahman et al. (1995a, 1998a,b) have summarized several methods for predicting the J-integral and crack opening displacement (COD) which are the most viable fracture parameters used to characterize nonlinear fracture behavior of cracked pipes ,evaluation of the crack opening displacement (COD) and the J-integral play a central role in the evaluation of the critical crack length for a detectable leak and unstable fracture of piping systems. Evaluation of the J-integral plays a central part in the calculation of critical crack length. On the other hand, crack opening area and crack opening displacement are the principal parameters in the evaluation of leak rate. In the current work, fracture experiments on carbon steel pipes grade X65 with short circumferential through-wall cracks under pure bending load were conducted. The J-integral values derived from the experimental load-point load–displacement data under pure bending conditions were calculated.

5.2 Specimen Preparation

Seamless carbon steel pipes grade X65 PL5 with an inner diameter of 42.9 mm and an outer diameter of 60.3 mm were used in the present experimental work. This type of pipes is commonly used in piping systems of gas and oil industry. The mechanical properties and chemical compositions of X65 are shown in Tables 3.1 and Table 3.4 respectively. The pipe geometry and its dimensions after machining are shown in Figure 5.1. The wall thickness was reduced by machining to 5 mm along the whole length of specimen. Grounding was done by lathing machine and the process done under suitable feeding rate and adequate cooling rate to avoid any changes of pipe material properties.

Specimen thinning was carried out to meet the load capacity of the available testing machine at UAE University and for the same reason the distance between the two ends of the specimen length of test specimens was maximized. A through-wall sharp crack was machined at the mid-section of each pipe specimen with initial crack length to circumference ratios of 1:5, 1:4, 1:3.5 and 1:3.The crack lengths were prepared by considering the pipe surface as a reference and make the cutting depth accordingly .The cutting depths were 5,7 ,9 and 12 mm. The corresponding angles of the selected depth are $75^o, 86^o, 105^o \; and \; 120^o$. Two specimens were first cut at the mid span using a hand saw with 0.5 mm blade thickness. While the other two specimens were cut using a wire-cutting machine and the crack width was 0.25mm. The fine cutting was done in Cosmoplast Industrial Co.W.L.L., Al-Sharjah by wire cutting machine (FANUC, Japan, and Model (W-2). Figure 5.2 shows a pipe specimen after preparation.

Two plugs were machined and inserted in the ends of each testing specimen to avoid deformation of the pipe ends .Due to limited material availability the test was done once for each specimen geometry.

5.3 Test Procedures

A 100 kN MTS testing machine was used in displacement controlled mode. The experiments were conducted at ambient temperature. The head speed of the machine was kept constant and equal to 0.5 mm min^{-1} for all tests. Figure 5.3 shows a typical photograph of a pipe under four point bending test by the MTS machine. A close-up view of the bending setup is shown in Figure 5.4. The specimen was centered so that the crack is just below the centre of the applied load; free longitudinal motion of the pipe was allowed. Two dial gauges were installed on certain equal distances from the center of crack to measure the corresponding deflections at different locations. A spot light was focused on the instantaneous crack tip to augment visibility through a magnifier of 10 times magnifications. The magnifier was used to detect the onset of crack initiation and the range of stable crack growth, two plugs with diameter equal to pipe specimen internal diameter were inserted at the ends of specimen to avoid ovality occurrence at the supporting pipe. During testing, the bending loads as well as load-point displacement were recorded automatically and the data were stored in a computer that was interfaced

with the MTS testing machine. A monotonic bending load was applied to the specimens by four-point loading. The specimens were loaded to the maximum load and beyond. The crack length was measured optically during the test without unloading except for the first specimen; Figure 5.5 shows the pipe specimen under testing. The unloading technique was used to measure the crack length for one pipe specimen. The unloading was carried out after reaching the maximum load and it was done six times to determine the crack length on the outer surface of the pipe. Dial gauges with suitable stands, filler gauge, a high precision caliper and soft clay were used to measure the required parameters. Figure 5.6 shows tools used for the experimental setup. The pipe ovalization were eliminated by inserting suitable plugs in specimen pipe ends, also it was checked and confirmed by examining the pipes after testing. A typical fractured pipe is shown in Figure 5.7.

5.4 Results and Discussion

Elastic–plastic fracture experiments under pure bending loading have been carried out on short circumferential through-wall cracked X65 carbon steel pipes. The fracture behavior was determined using the J-integral estimation method which can predict the whole fracture behavior from initiation to stable ductile crack growth to unstable fracture.

During all tests, the bending loads as well as load-point displacement were recorded automatically. In addition, to automatic recording, a manual recording was also done. The manual recording included the applied load with the corresponding deflection at the crack area and for two locations at the mid spans between the crack and the supporting ends; crack tip open displacement and crack extension on the surface of pipe were also recorded manually. Initially the load is varying linearly with the displacement till a certain point at which the curves deviates from linearity. There was a change in the slope of the load-load line displacement record around the commencement of the crack extension corresponding to the initiation load. As the crack proceeds the slope of the curve decreases till it reaches the maximum load, crack blunting was observed around the point at which the curve deviates from its linearity, then the crack was observed to initiate an extended stably up to the instability point. The load-point load–displacement curves for the cracked pipes are shown in Figures 5.8 through 5.11 for pure bending with different initial crack depths, and crack depths of 12 mm, 9mm, 5mm and 7mm. A

comparison of load displacement curves for all tests is shown in Figure 5.12. From the comparison graph it can be seen that the maximum load for specimen No. 3 is much higher than that of specimen No. 2 because the initial crack size of specimen No. 1 was 1.5 times the initial crack size of specimen No. 3. Generally the maximum load is inversely proportional to the crack depth. It was noticed during the test that the maximum load point is the point of crack instability or the point at which the crack starts to propagate. It can be seen from the applied load versus load-point displacement curves shown in Figures 5.8 through 5.11 for bending that the load starts to decrease once the crack starts to propagate. Crack extension data bending Figures 5.13 through 16 show that crack length increases monotonically with applied load. Initially, the crack length remains almost unchanged and a blunting of the machined crack took place up to the maximum load point. The increase in crack length with loading was better defined after initiation of crack from the blunted machined crack and, particularly, after reaching the maximum load. Since extensive crack-tip blunting occurred before stable tearing was clearly visible, it was not possible to identify the exact point of crack initiation due to the limited magnification of the magnifier. This issue needs more investigation in order to adequately identify the onset of crack extension and in turns the corresponding points of initial load on load-line load displacement curves. Therefore, initiation loads were defined as the maximum loads. So that the initiation load was defined as the load during which a crack growth increment of 0.5 mm was recorded. It was observed from Figures 5.12 through 5.15 that the crack length increases while the load is decreasing. Figure 5.17 shows a comparison curves of all tests, crack opening displacement (COD) for all tests was measured by using filler gauge and replica method in which soft clay was applied on crack area, it was observed that the COD starts to increase slightly below the maximum load and once reached the maximum load the COD value starts to increase significantly as shown in Figures 5.18 through 21. Figure 5.22 shows a comparison curves for all tests.

The J-estimation methods in this study can be best described with the aid of Figures 5.23a and b. As shown in Figure 5.23a, a circumferential constant-depth, internal, surface crack is assumed to exist in the pipe that has mean radius, R_m, and wall thickness, t. The depth and total angle of the surface crack are denoted by a and 2θ, respectively. The crack is symmetrically placed with respect to the bending plane of the pipe. The crack is

located sufficiently far from the pipe ends such that the end effects on crack-driving force are inconsequential. In Figure 5.23.b, the pipe is subjected to a pure bending moment, M, applied at the remote ends. In the development of a J-estimation scheme, it is generally assumed that the crack driving force J, can be split into elastic and plastic components

$$J = J_e + J_P \qquad (5.1)$$

where the subscripts 'e' and 'p' refer to elastic and plastic contributions, respectively.

The elastic energy release rate J_e, at the point of maximum depth can be defined as

$$J_e = \frac{\partial U^T}{\partial A} = \frac{\partial}{\partial A}\left(U^c + U^{nc}\right) = \frac{\partial U^c}{\partial A} \qquad (5.2)$$

where U^T is the total internal strain energy, U^{nc} is the strain energy which would exist if there were no crack present, $U^c = U^T - U^{nc}$ is the additional strain energy in the pipe due to the presence of a crack, and $A = 2a\theta(R_m - t/2 + a/2)$ is the cracked area. For thin-walled pipe with mode-I crack growth; Je at the point of maximum depth can be obtained as

$$J_e = \frac{K_I^2}{E'} \qquad (5.3)$$

where $E' = E/(1-v^2)$ for plane strain condition with E and v representing elastic modulus and Poisson's ratio of the material, respectively. The term K_I is the mode-I stress intensity factor. From the LEFM theory, K_I at the deepest point of the crack is given by

$$K_I = \frac{M}{\pi R_m^2 t} F_B\left(R_m/t\ , \theta/\pi\right)\sqrt{\pi R_m \theta} \qquad (5.4)$$

in which F_B (R_m/t , θ/π) is a geometry function relating K_I of a cracked pipe to that for the same size (depth) of a through-wall crack in an infinite plate. In general, F_B should be a function of R_m/t and θ/π.

Therefore the elastic J_e can be calculated by substituting stress intensity factor Equation (5.4) into Equation (5.3) ,accordingly the elastic J is

$$J_e = \frac{\theta}{\pi} F \left(\frac{\theta}{\pi}, \frac{R_m}{t}\right)^2 \frac{M^2}{E R^3 t^2} \qquad (5.5)$$

The geometry factor (F) was calculated using several solutions available in the literature, they involved analytical solutions by Sander's energy release rate (elastic) formula [62,63], analytical solutions by Klecker et al [64] and Zahoor [65] and extensive finite-element calculations by Kumar et al [66,67] and Brust et al [68,69] .Figure 5.24 shows the comparisons of Rahman proposed F with these solutions as a function of crack size θ/π for R/t = 5,10 and 20. More recently, France et al [70] conducted finite element analysis using three-dimensional solid elements for pipes with an axial and a circumferential crack. A wide range of R_m/t (from 3 to 100) was employed, global bending moment was considered for circumferential crack. Their solutions were summarized in tabular format after separation into extensional and bending components as performed by Barsom et al.

Lacire et al. [61] also conducted finite element calculation for pipes with a circumferential through-wall crack for a wide range of R_m/t (from 1.5 to 80.5) and half crack angle (0–150°). Shell elements were used for thin cylinders($R_m/t > 10$); but thicker cylinders were analyzed by solid elements. The solutions were given in the form of Tables of the geometrical factors. The solutions by Lacire et al. have been approximated by expressions listed in Figure 5.34 with an error less than a few percent for half crack angles smaller than110°. Figure 5.25 shows a comparison of the geometrical factors calculated by the Equations and tabulated values in Ref. [61] for bending loading. It can be seen that the Equations in Figure 5.34agree with the tabulated values very well and enable smooth interpolation for R_m/t .Estimates by the Equations developed by Klecker et al. (Table 5.1) are also plotted below Table. These are in

reasonable agreement with other solutions for R_m/t below 20 but differences begin to increase rapidly at R_m/t of about 30. Comparisons of the geometrical factors for the bending moment are shown in Figure 5.26 for three values of R_m/t ranging from 5 to 20. The extensional components were used for the solutions of Barsom et al. and France et al. In spite of the variations in derivation methods and finite element models, available solutions agree relatively well with each other for R_m/t = 10 and 20. For the pipe with R_m/t= 5; the difference between the solutions increases. Although the reason is not clear, the solution by France et al. does not converge to 1.0 as the half crack angle approaches zero and gives larger values than the others. For the thinnest pipe with R_m/t = 100; the Equations by Klecker et al. gave excessively larger values than other solutions. This condition is outside the stated applicable range ($5 < R_m < 15$) of the Equations and application to such a thin-walled pipe appears to be inappropriate. The Equations developed using the solutions by Lacire et al, considering the good agreement with other solutions in most cases and the range of applicability with regard to geometrical parameters, use of the Equations given in Figure 5.34 is recommended for general use within the range of R_m/t between 1.5 and 100 and the half crack angle less than 110°.Depending on the previous discussion the geometry factor F was calculated based on different mentioned approaches.

The plastic solution of J_p, for the pipe crack problem can be expressed as [68,69]

$$J_P = \frac{\alpha\sigma_o^2}{E} R\,\theta \left(1 - \frac{\theta}{\pi}\right) h_1 \left(\frac{\theta}{\pi}, n, \frac{R}{t}\right) \left[\frac{M}{M_O}\right]^{n+1} \qquad (5.6)$$

In which $h_1\,(\theta/\pi\,, n\,, R/t\,)$ is another dimensionless function that depends on the pipe geometry, and material constant, and

$$M_O \quad = 4\,\sigma_O\,R^2\,t\,\left[\cos\frac{\theta}{2} - \frac{1}{2}\sin\theta\right] \qquad (5.7)$$

is a conveniently defined reference load that represent the limit load for through wall cracked(TWC) pipe under pure bending if σ_O is the collapse stress .Figure 5.26 shows plots of h_1 as a function of material constant n for several cases of crack size θ/π =

$1/16, 1/8, 1/4$ *and* R/t = 5,10 and 20 by various methods. In addition the values of h_1 function were calculated utilizing different above mentioned approaches.

Thus, for the cases under study the J resistance curves were determined using the load – displacement data and the J- integral solution method described above given by Equations 5.5 and 5.6 and plotted against crack area, moment, crack length and pipe deflection as shown in Figures 5.27 through Figure 5.30 for the tests.

The radius of the pipe deflection (ρ) shown in schematic drawing of the pipe specimen under deflection (see Figure 5.31) was calculated using two different approaches. The average value was then considered, Equation 5.8 represents the first way and Equation 5.9 used for the second approach, the results values were plotted in Figures 5.32 and 5.33 against the pipe deflection and applied moment.

$$\rho_1 = (s_1^2 + V_m^2)/2V_m \qquad (5.8)$$

$$\rho_2 = \frac{s_2^2 - V_m^2 + 2V_m V + V^2}{2V_m} \qquad (5.9)$$

$$\rho = \frac{s_2^2 + s_1^2 + 2V_m V + 2V^2}{2V_m} \qquad (5.10)$$

where s_1, V_m, s_2, V *and* ρ are shown in Figure 5.31

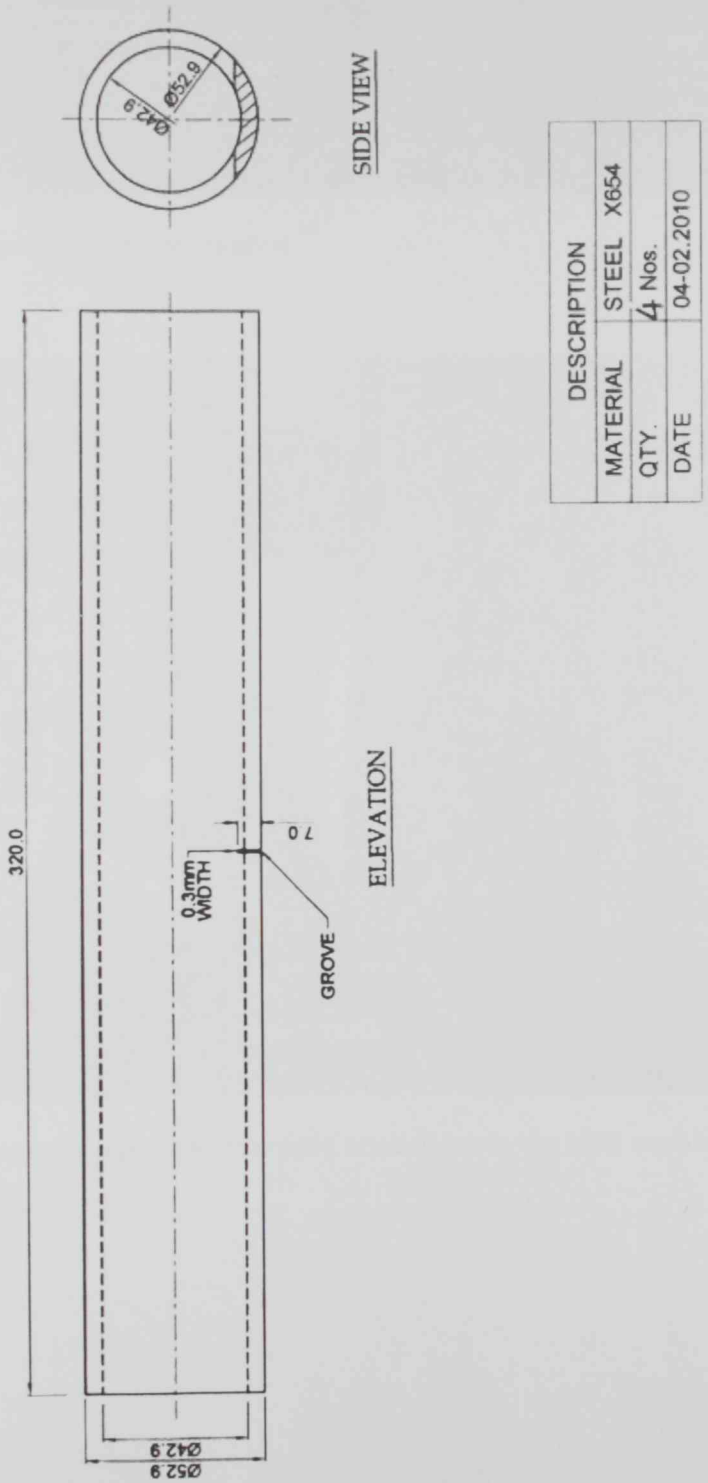

Figure 5.1 Geometry of bending pipe specimen

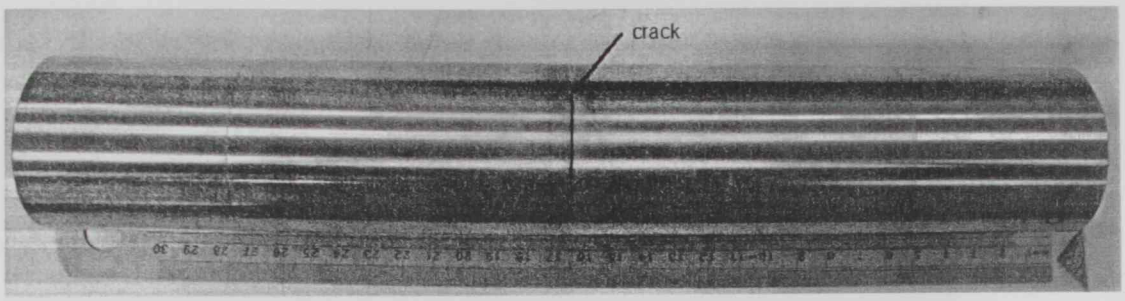

Figure 5.2 X65 pipe specimen after preparation

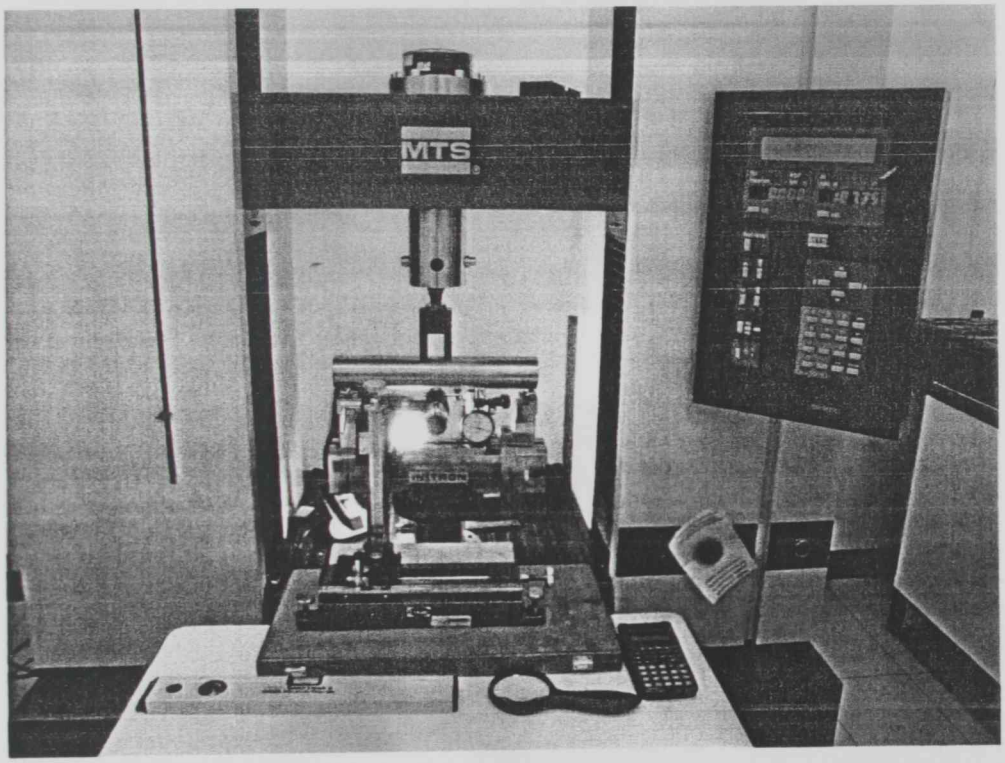

Figure 5.3 A photograph of a pipe under four point bending test by the MTS machine

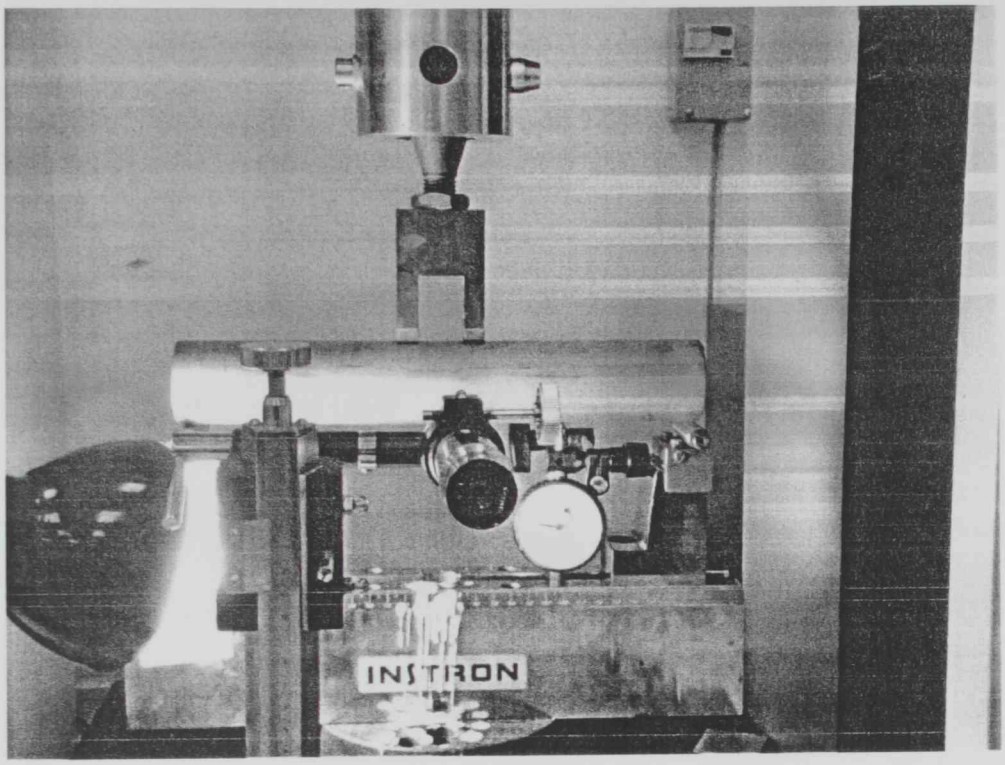

Figure 5.4 A close-up view of the bending setup.

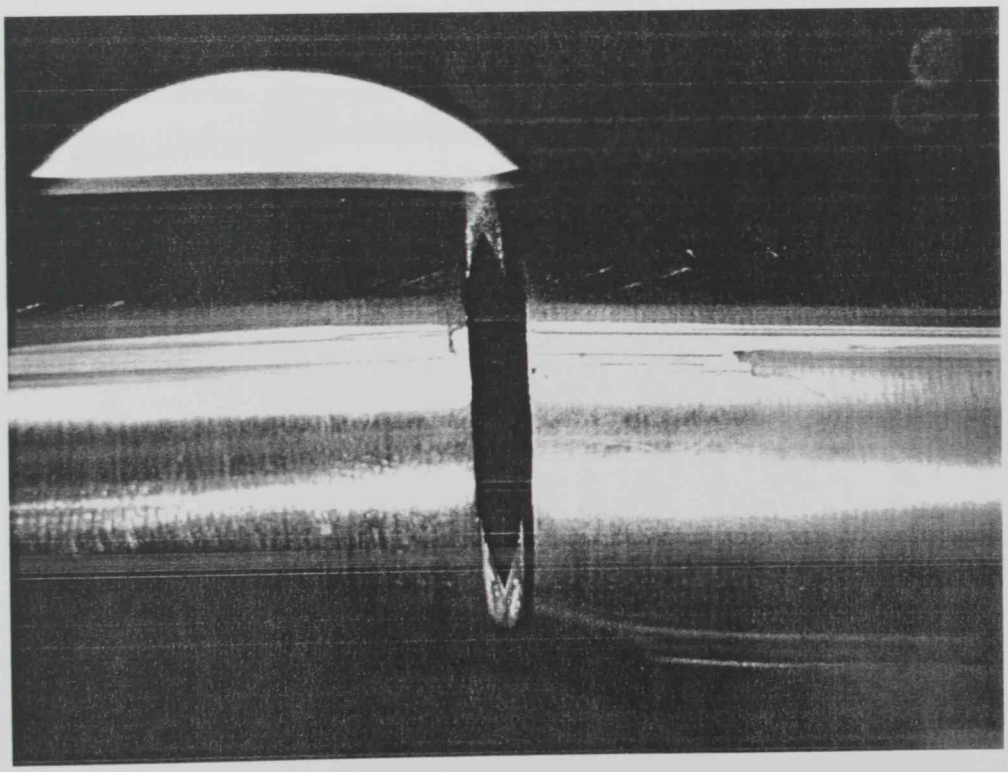

Figure 5.5 Pipe specimen while conducting the bending experiment.

Figure 5.6 Tools used for the experimental setup

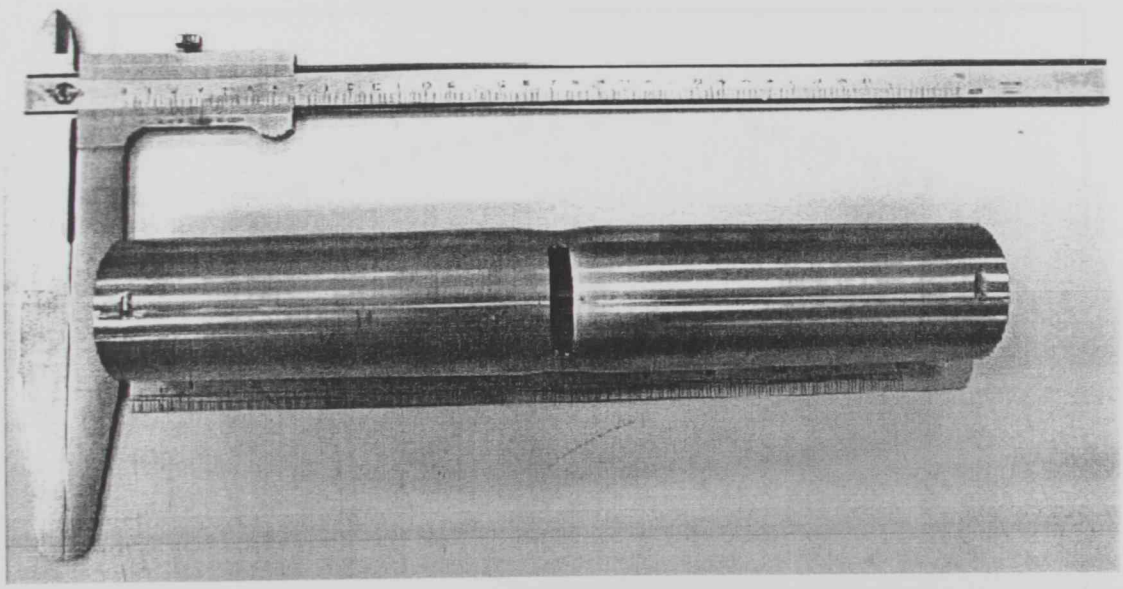

Figure 5.7 A fractured pipe specimen.

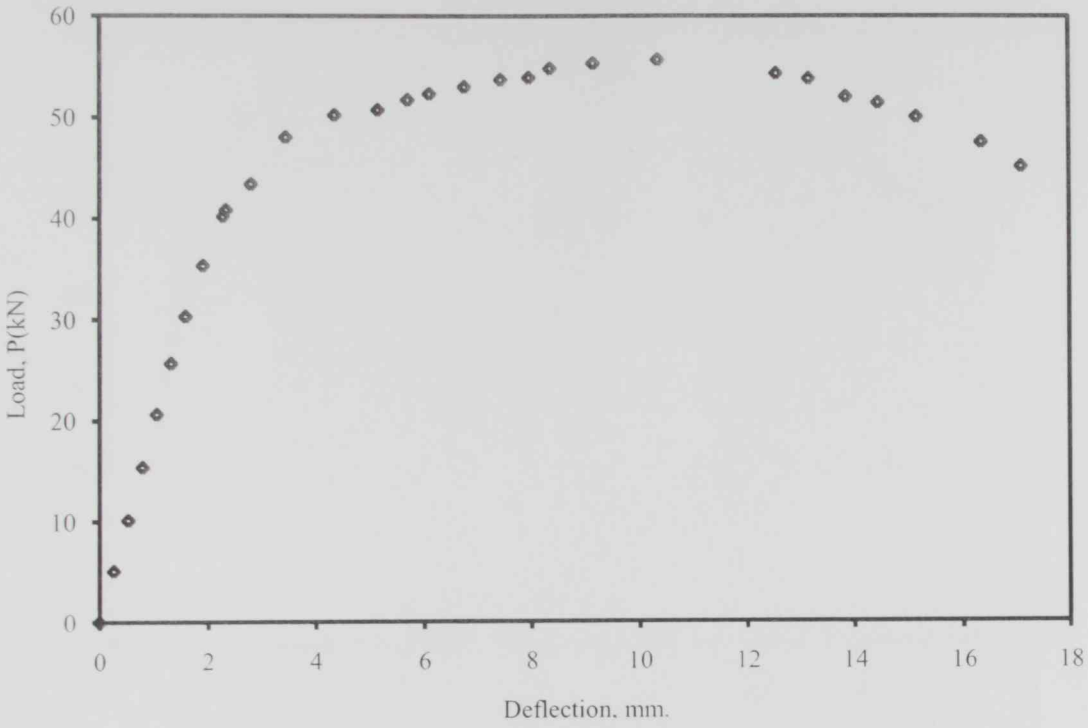

Figure 5.8 Experimental load – displacement curve for bending test (crack depth = 12mm)

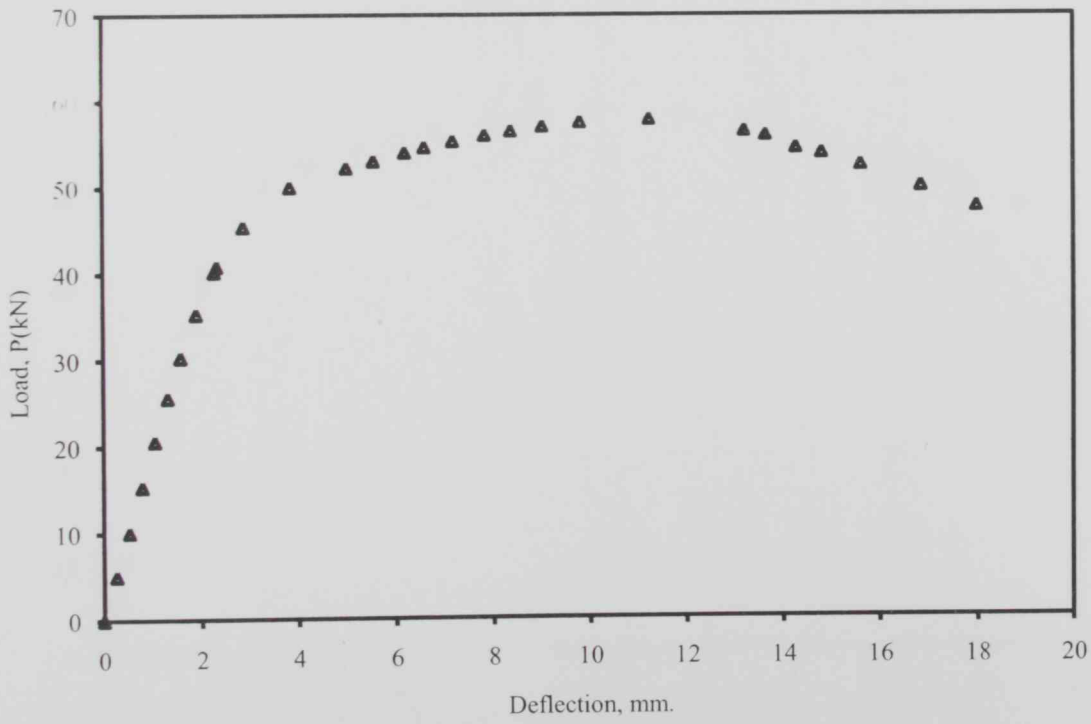

Figure 5.9 Experimental load – displacement curve for bending test (crack depth = 9mm)

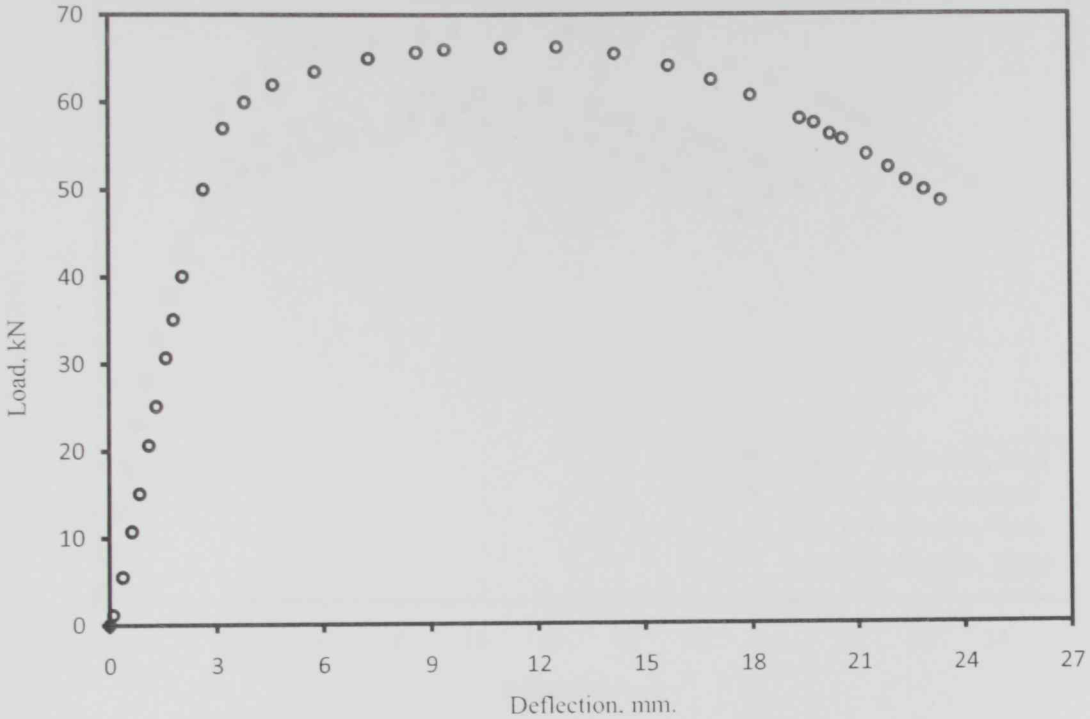

Figure 5.10 Experimental load – displacement curve for bending test (crack depth = 5mm)

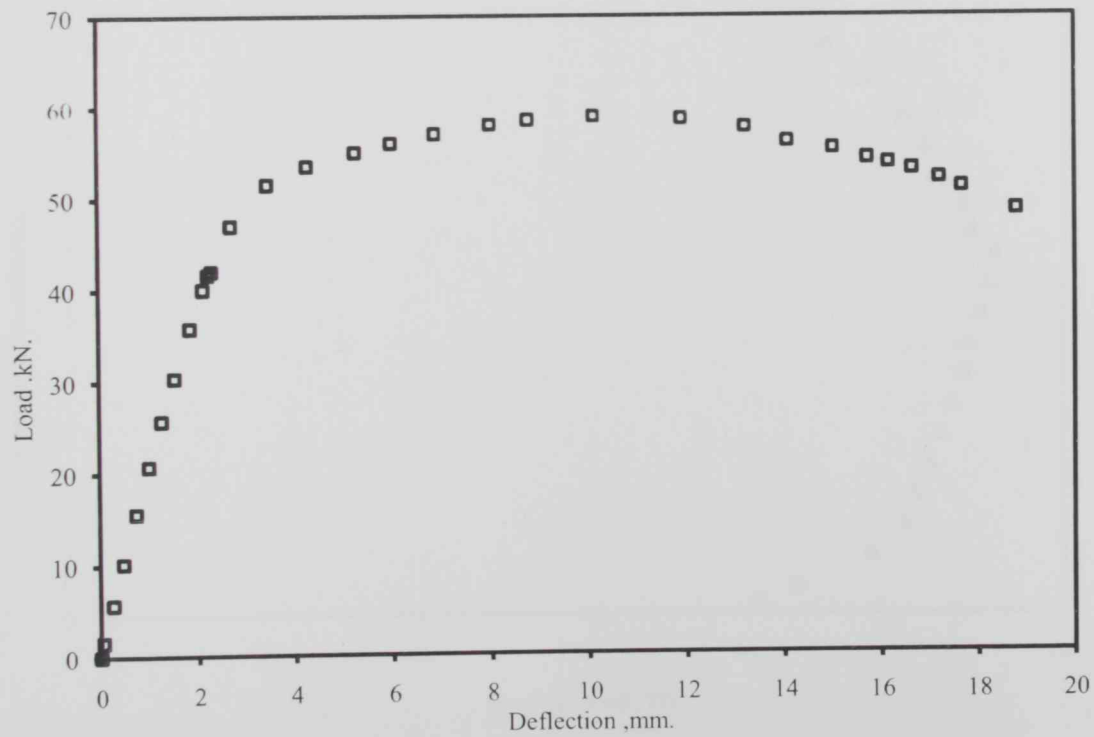

Figure 5.11 Experimental load – displacement curve for bending test (crack depth = 7mm)

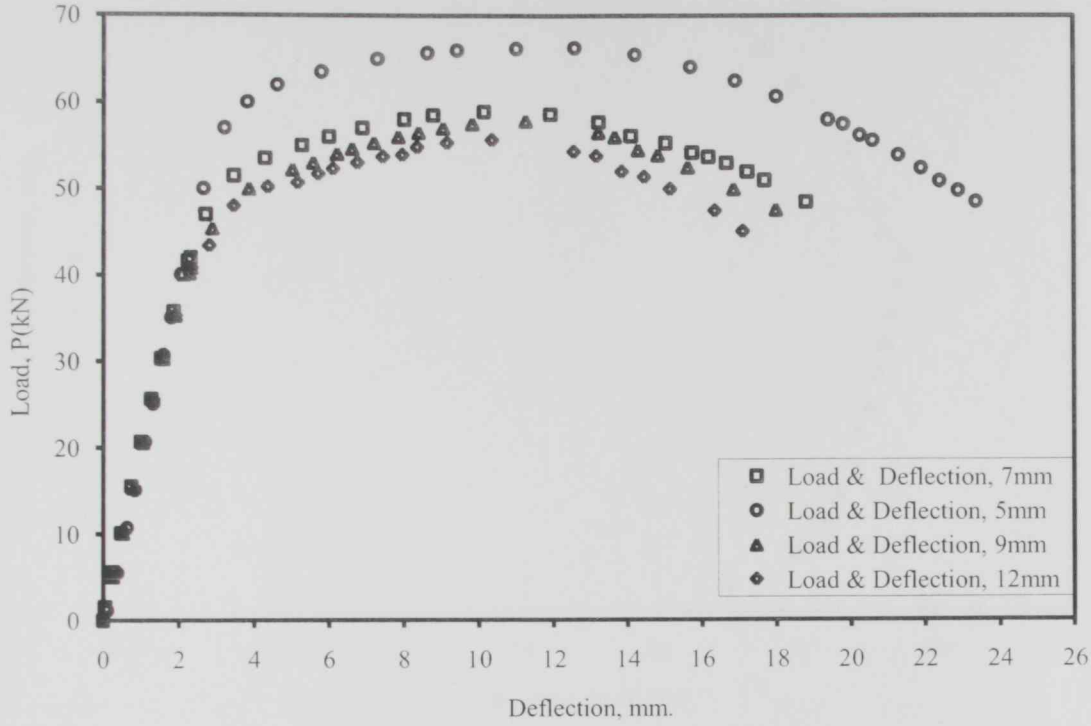

Figure 5.12 Experimental Load – Displacement curves for bending tests.

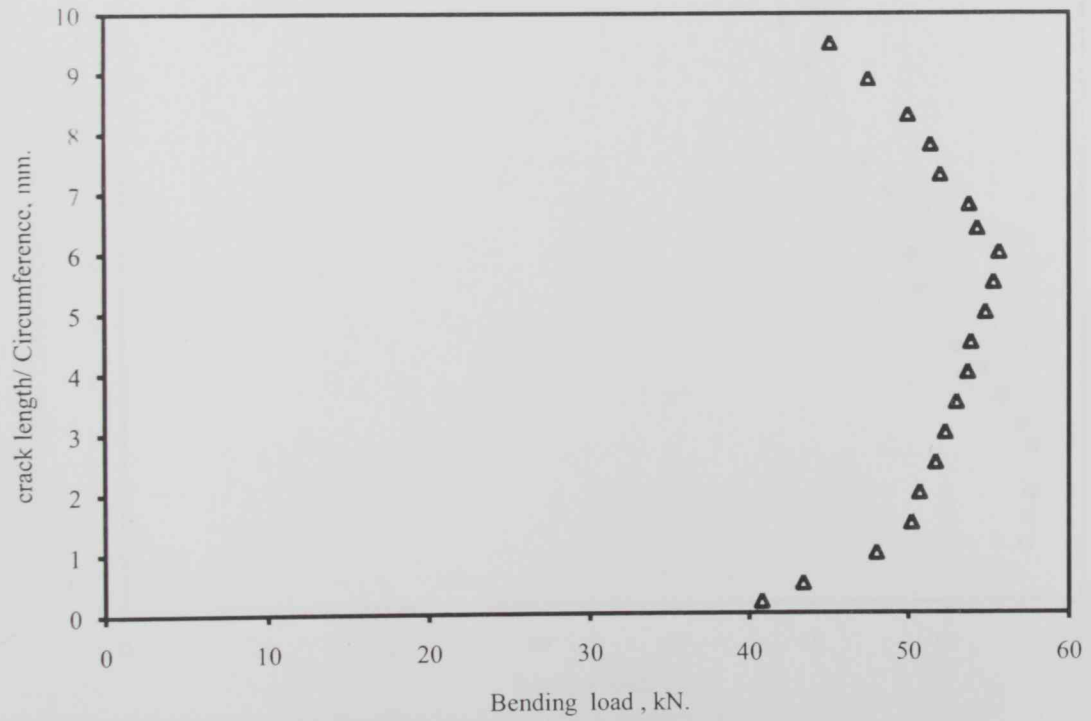

Figure 5.13 Crack length vs. bending load test (crack depth= 12)

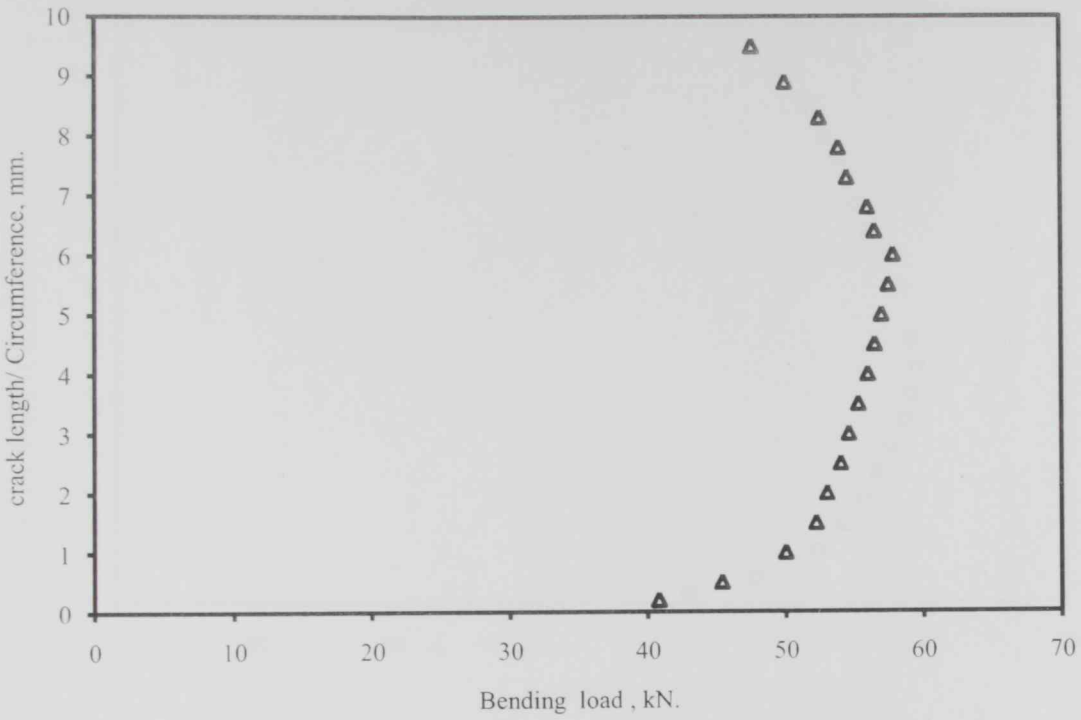

Figure 5.14 Crack length vs. bending load test (crack depth= 9)

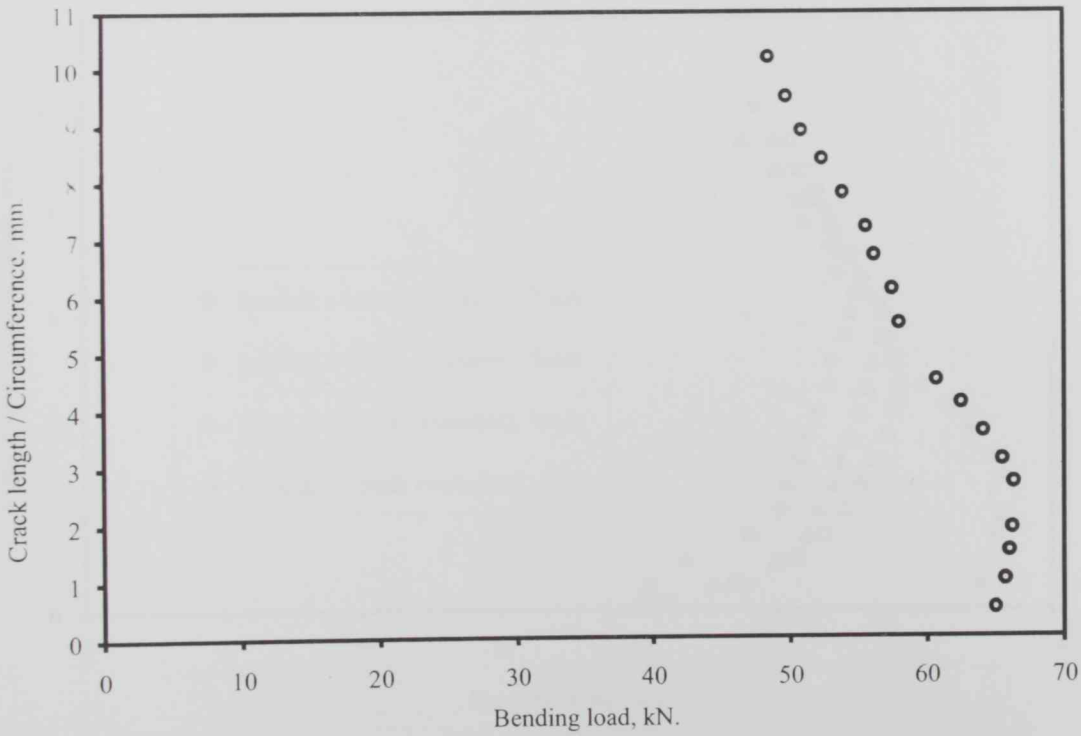

Figure 5.15 Crack length vs. bending load test (crack depth= 5)

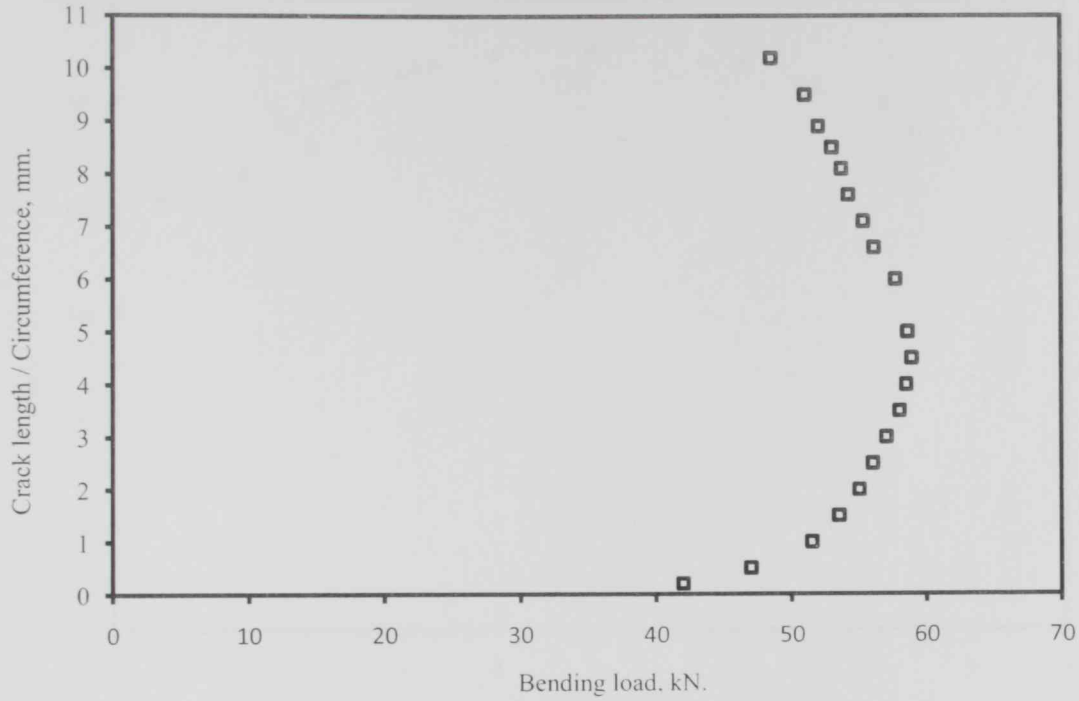

Figure 5.16 Crack length vs. bending load test (crack depth= 7)

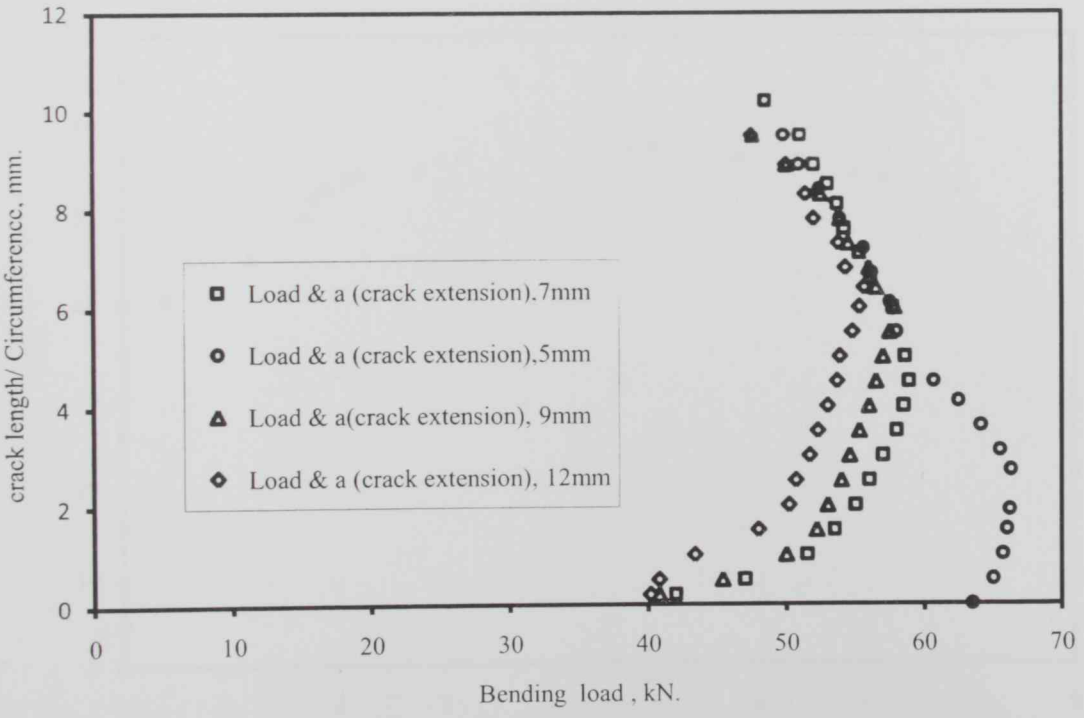

Figure 5.17 Comparison of the crack length vs. bending load for all tests

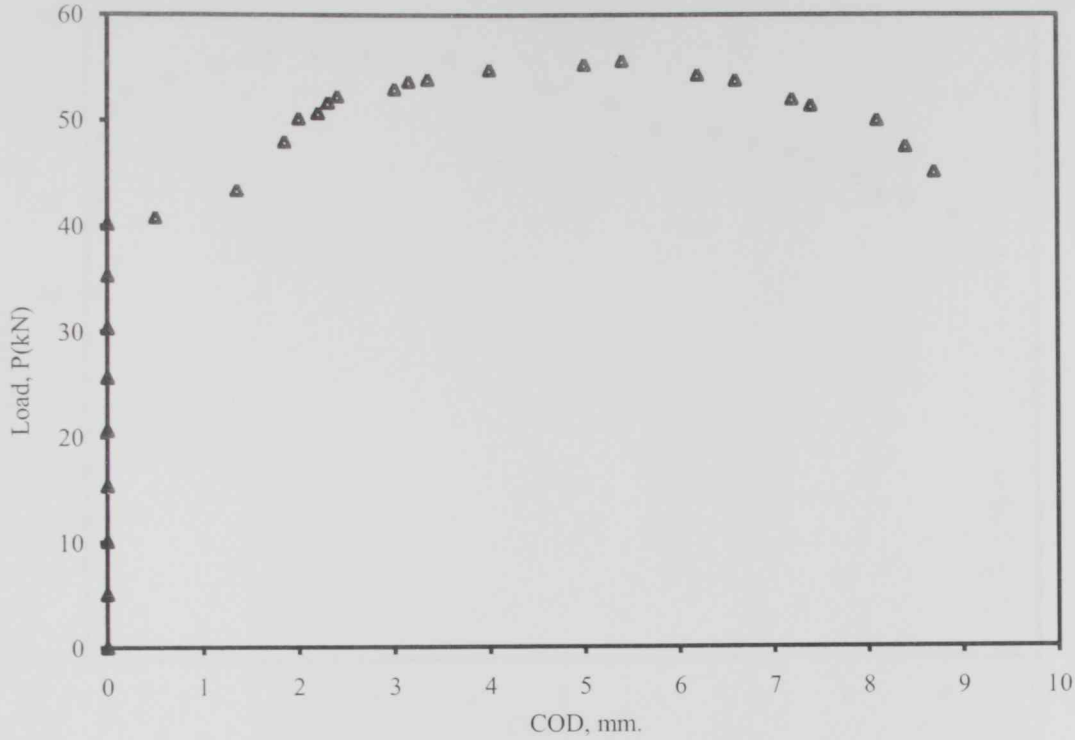

Figure 5.18 Bending load vs. crack opening displacement (crack depth= 12mm)

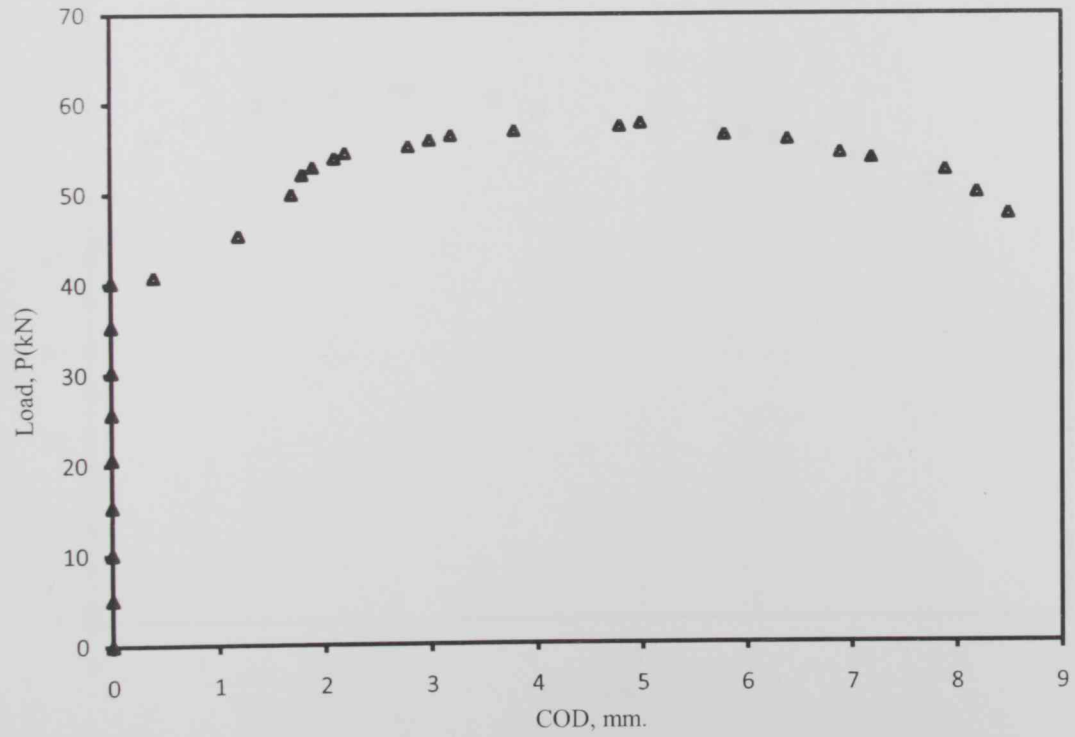

Figure 5.19 Bending load vs. crack opening displacement (crack depth= 9mm)

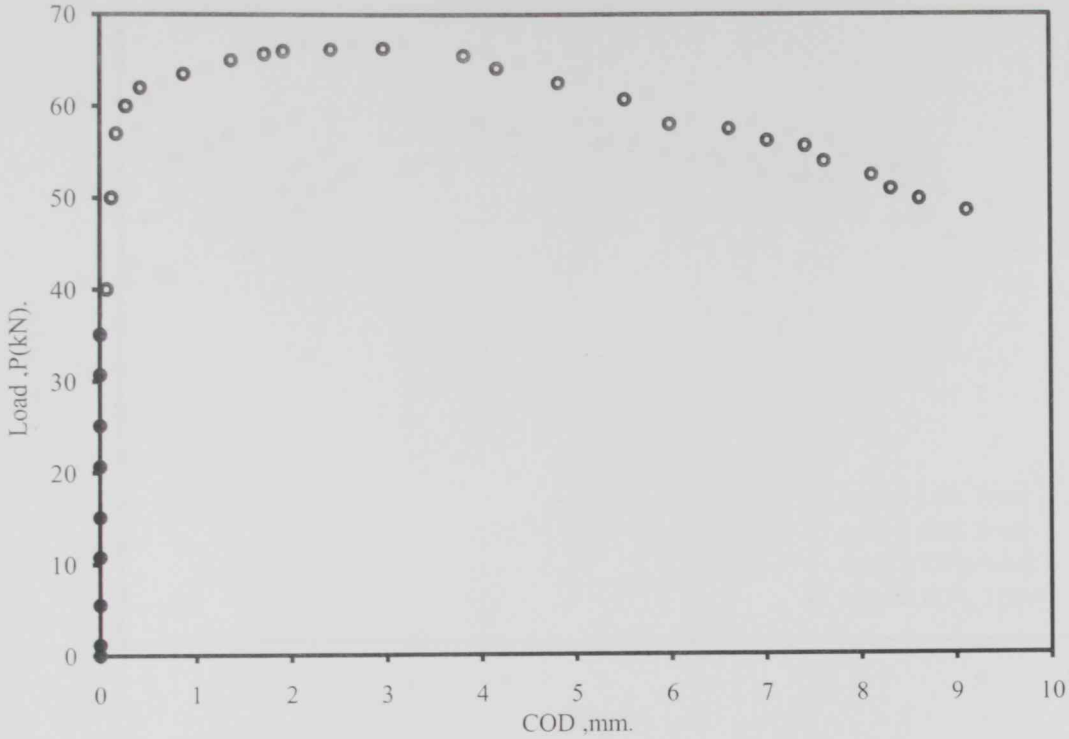

Figure 5.20 Bending load vs. crack opening displacement (crack depth= 5mm)

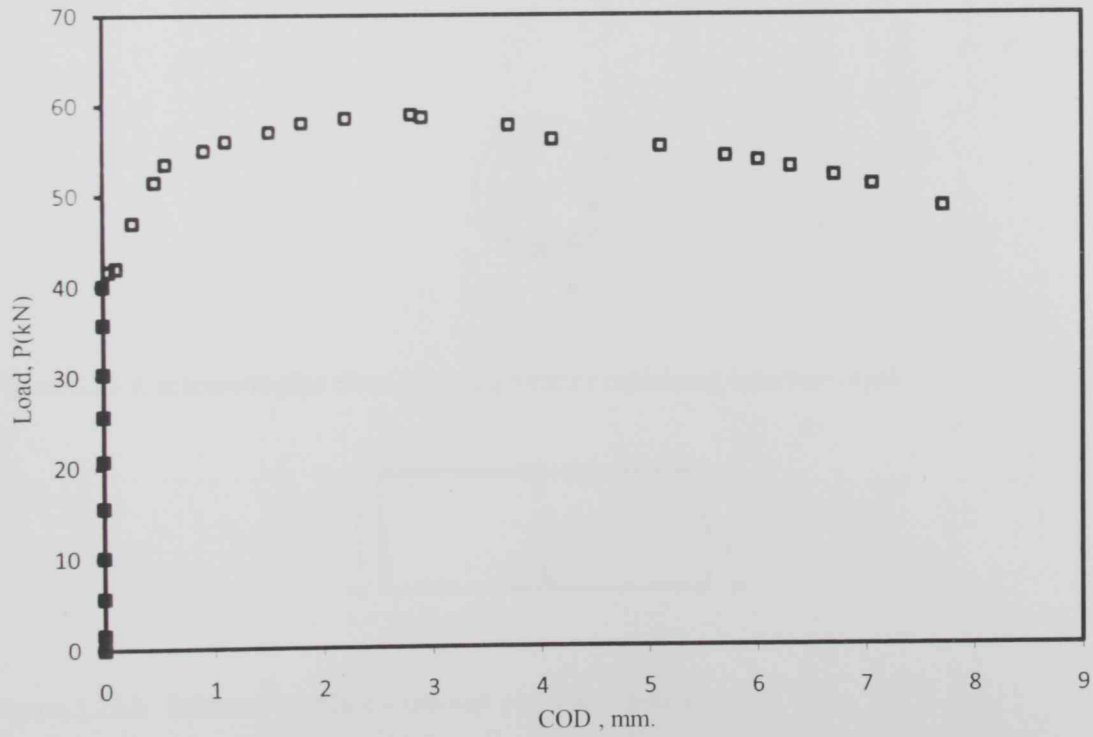

Figure 5.21 Bending load vs. crack opening displacement (crack depth= 7mm)

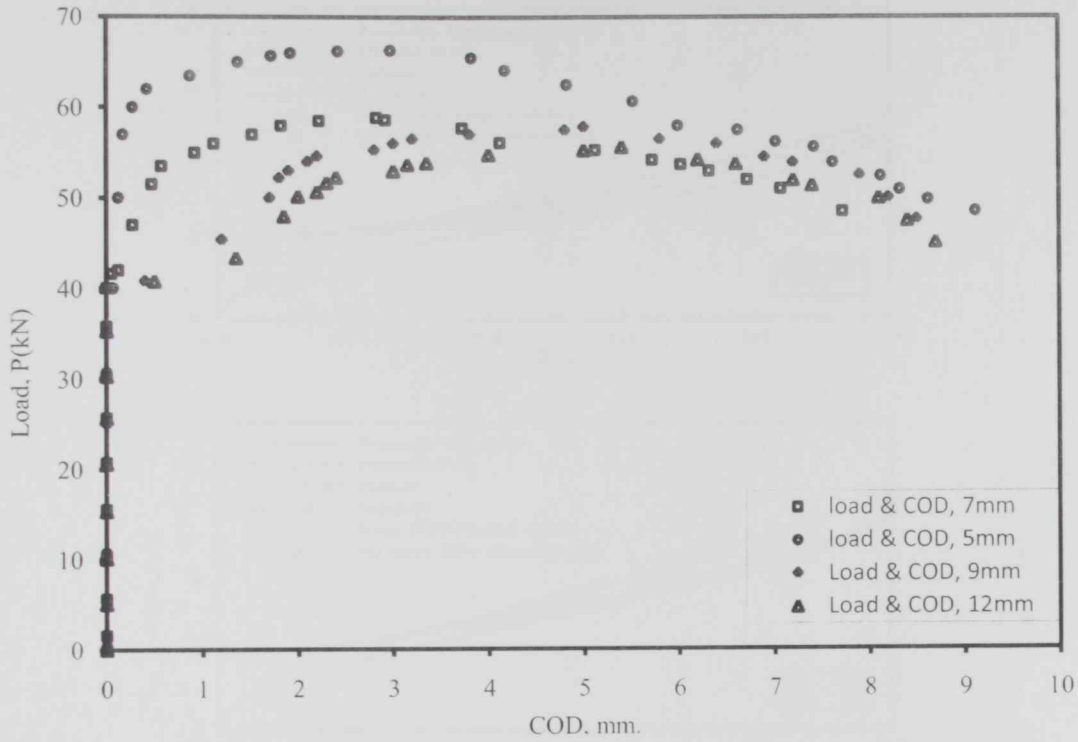

Figure 5.22 Bending load vs. crack opening displacement curves for all tests.

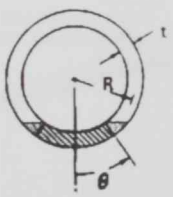

Figure 5.23 A schematic pipe cross-section geometry containing a surface crack.

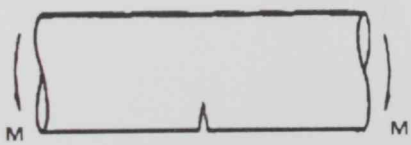

Figure 5.23.b Schematic surface – cracked pipe under pure bending.

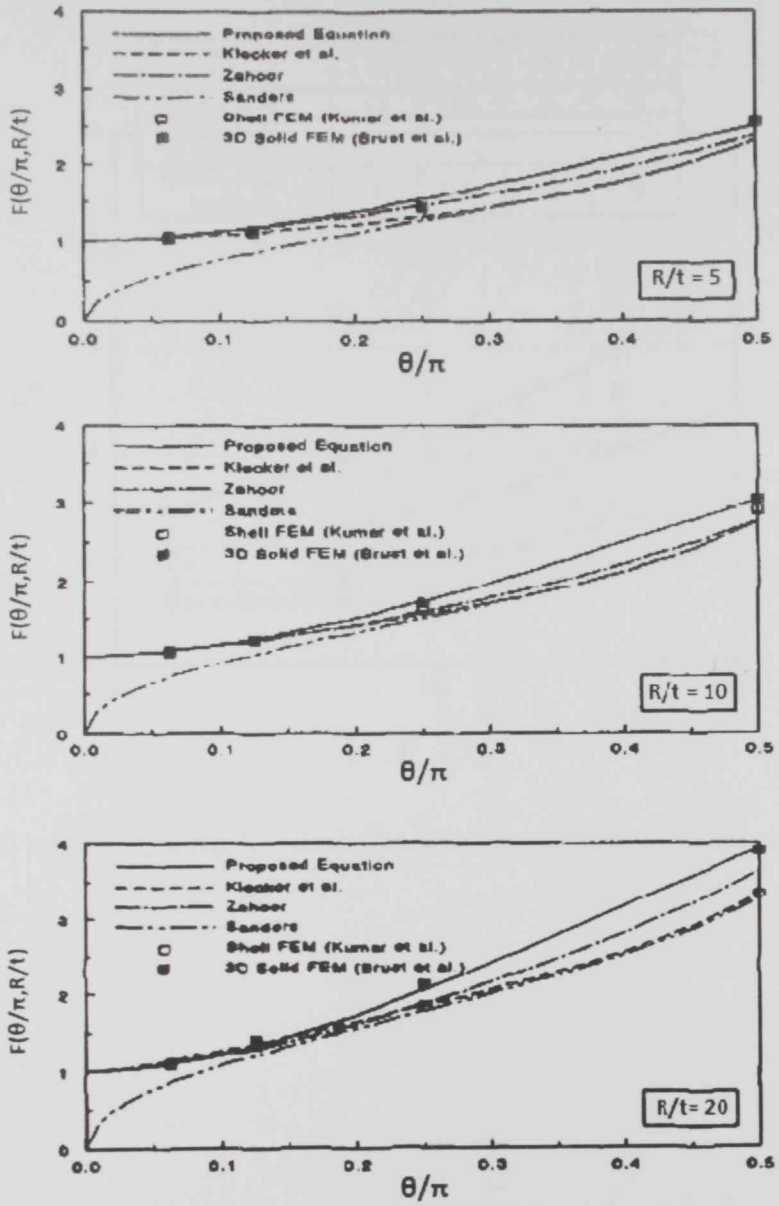

Figure 5.24 Comparisons of F- functions by various methods [71]

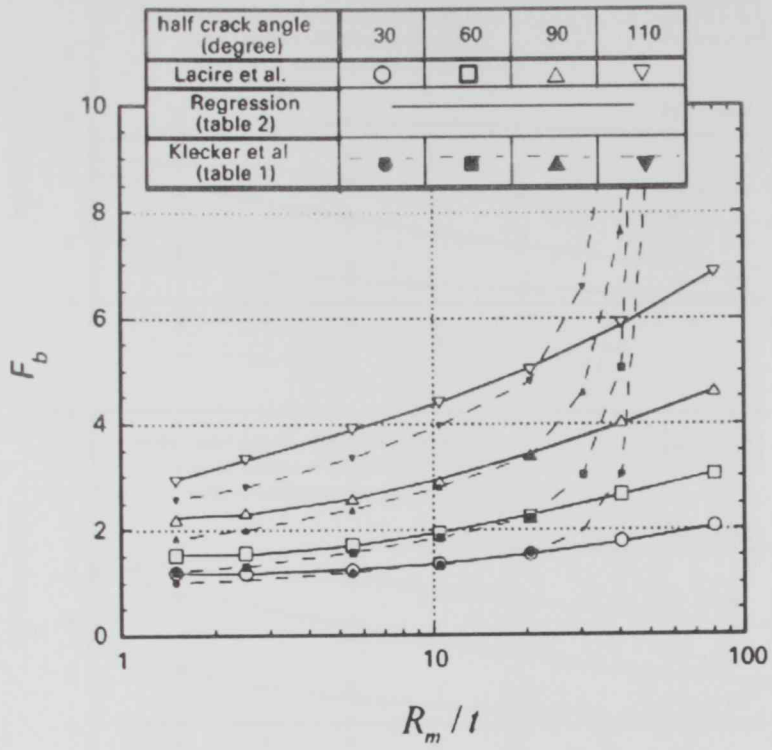

Figure 5.25 Comparison of R_m/t - dependence of geometrical factor for stress intensity factor.

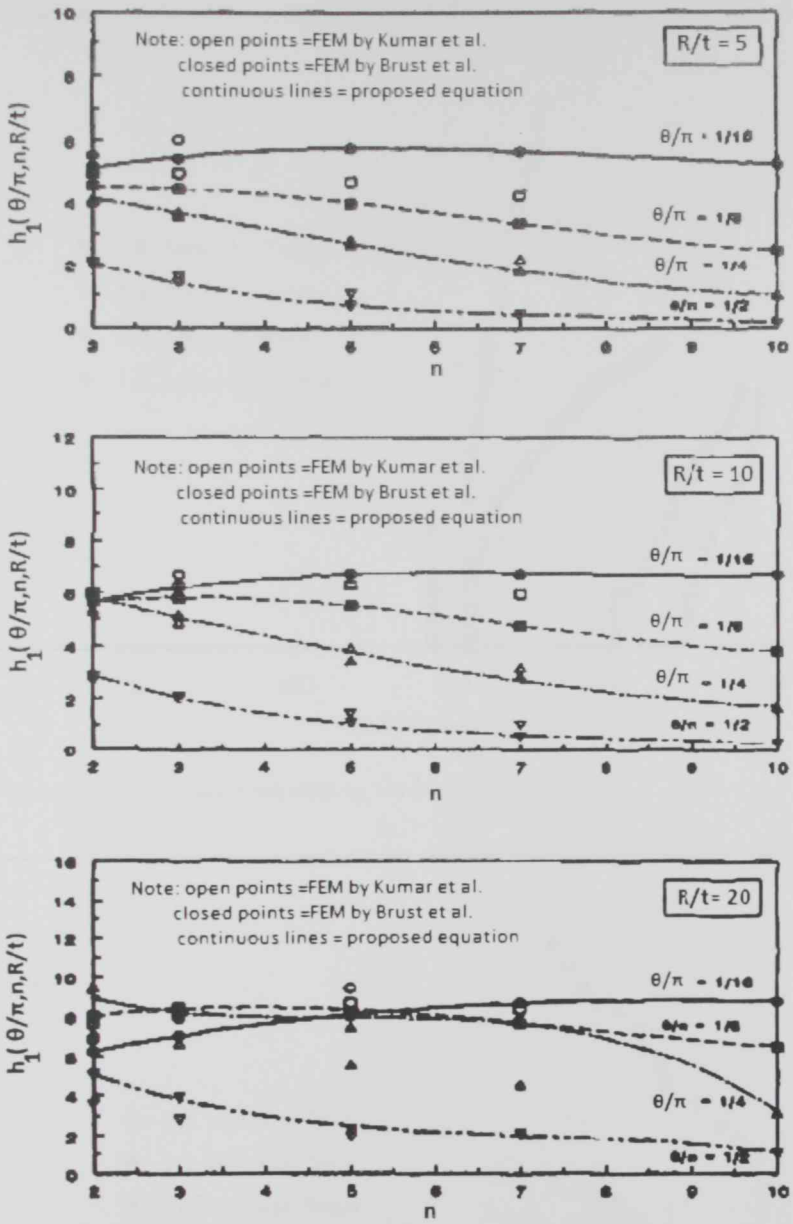

Figure 5.26 Comparisons of h_1-functions by various methods.[71]

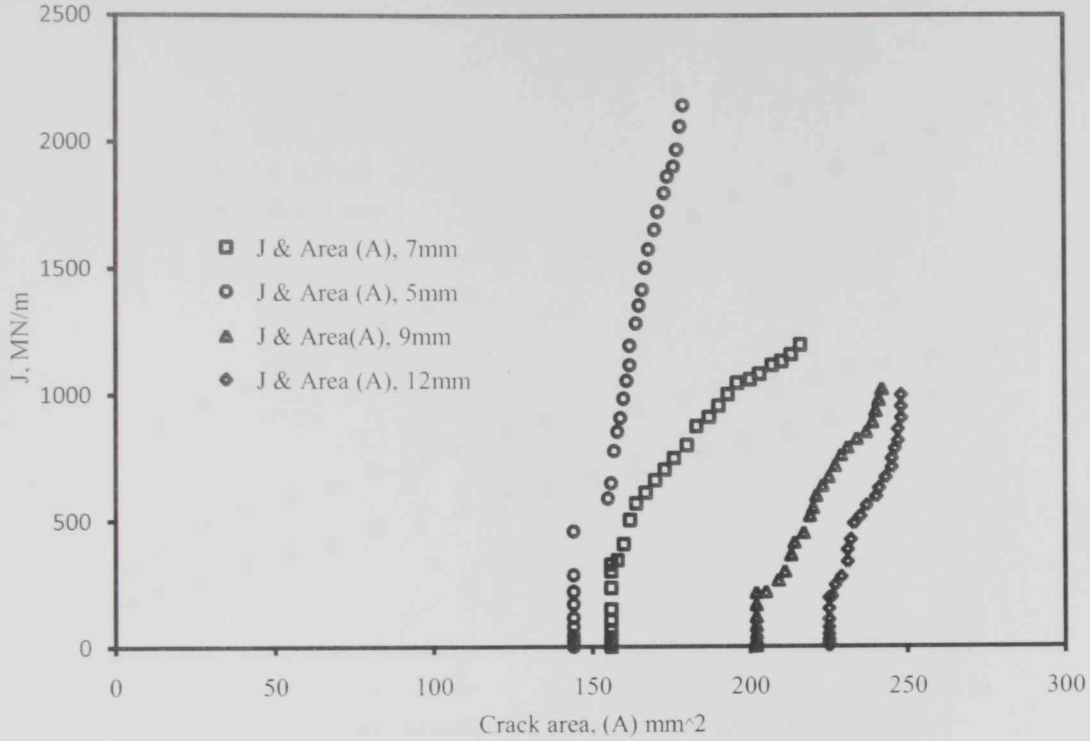

Figure 5.27 J-resistance vs. crack area curves for bending tests.

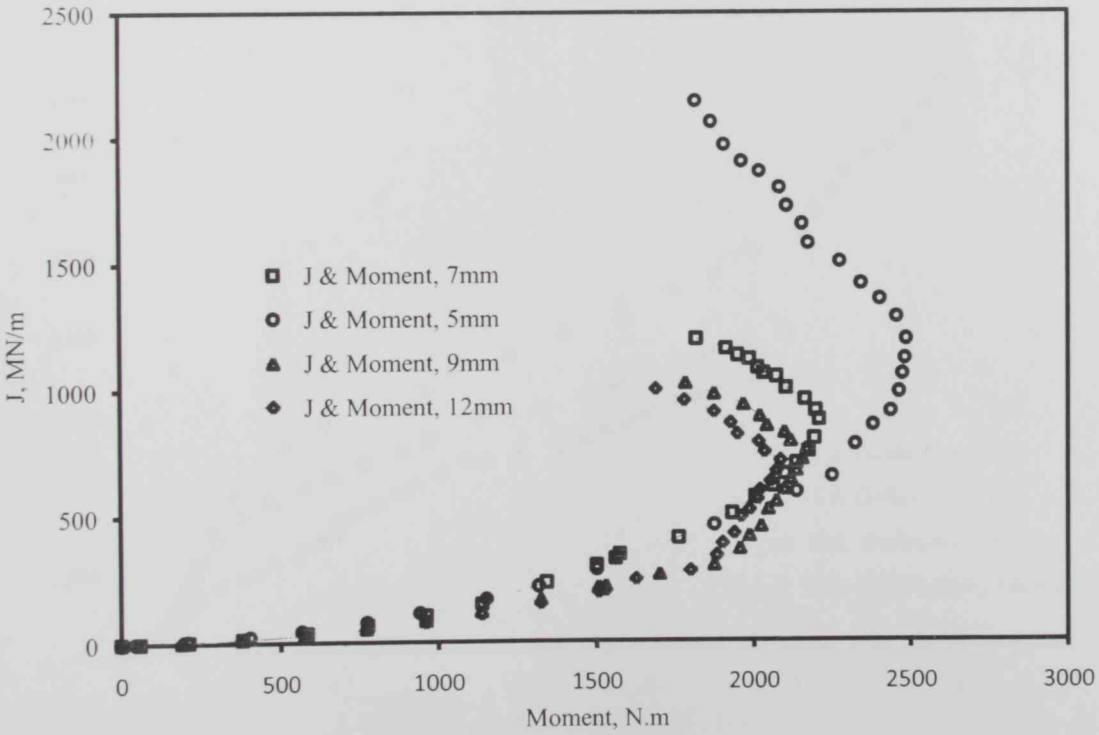

Figure 5.28 J-resistance vs. moment curves for bending tests.

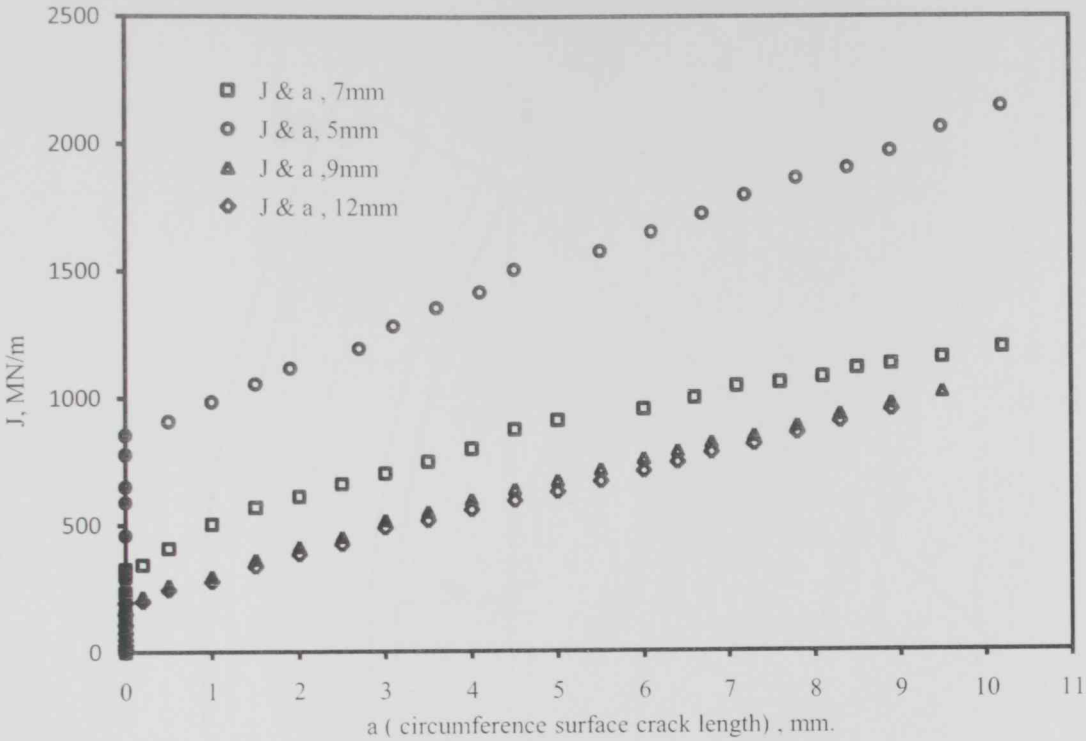

Figure 5.29 J-resistance vs. a (circumference surface crack length) curves for bending tests.

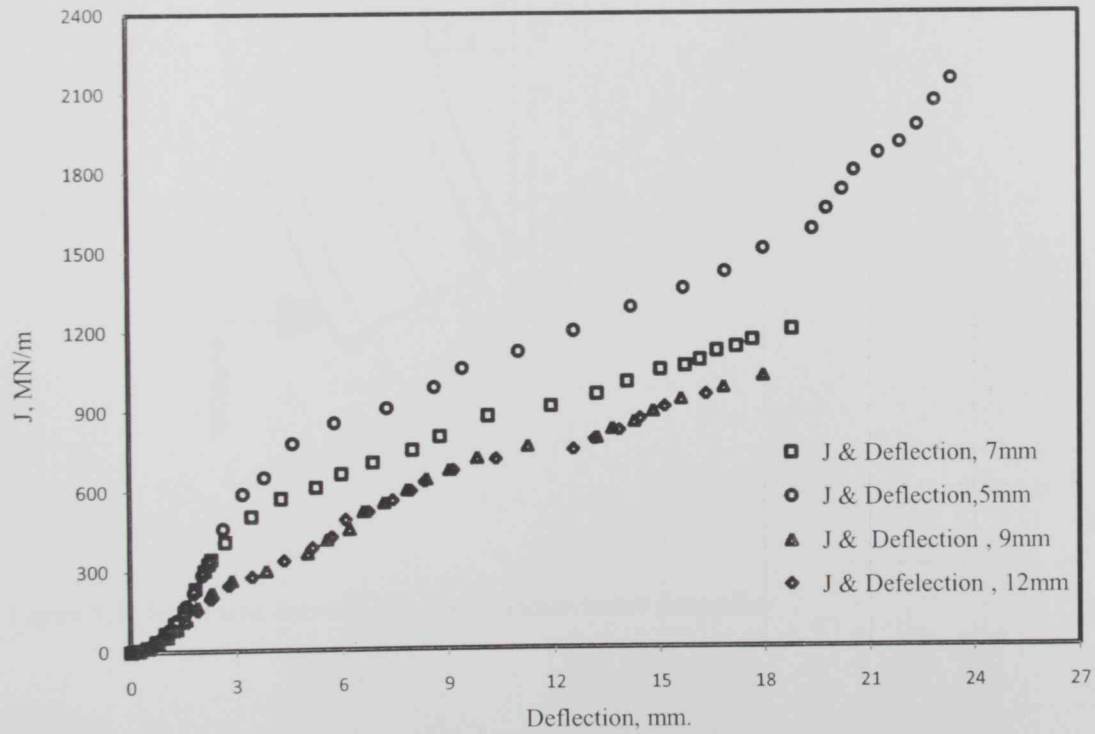

Figure 5.30 J-resistance vs. deflection curves for bending tests.

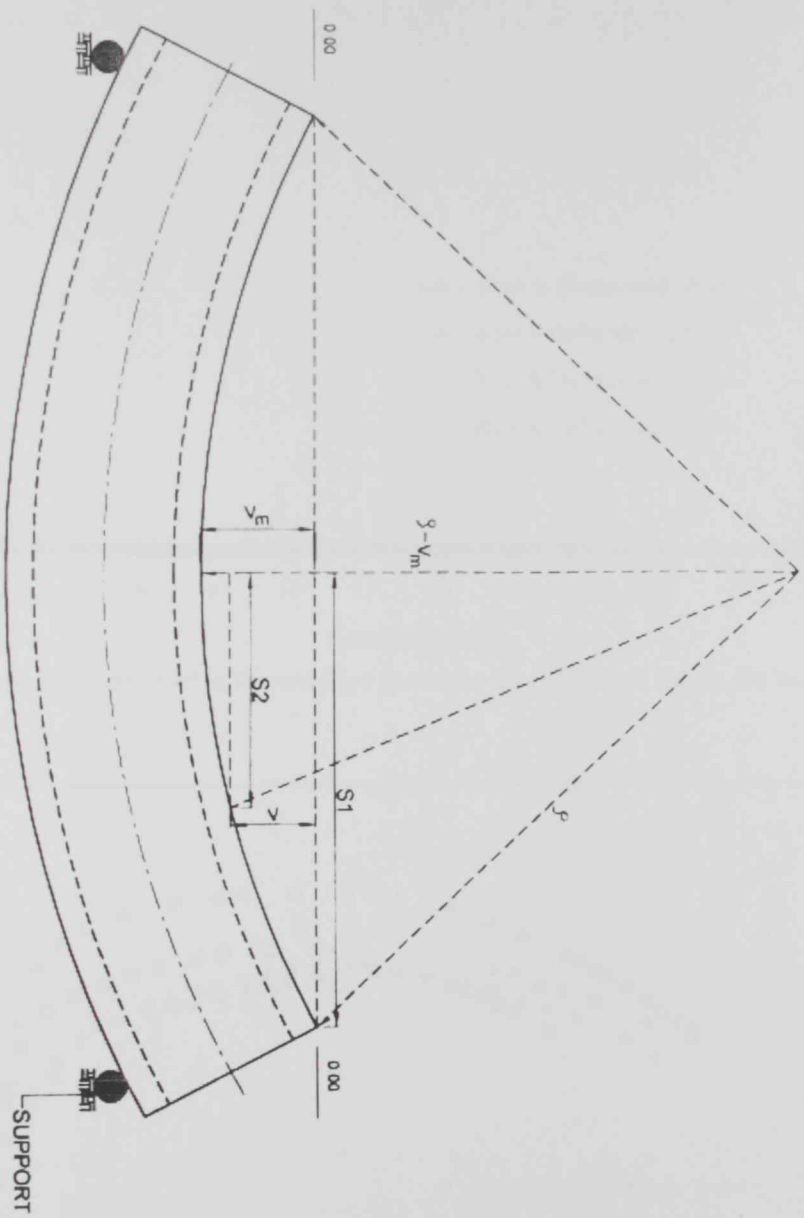

Figure 5.31 Schematic drawing for pipe specimen under deflection

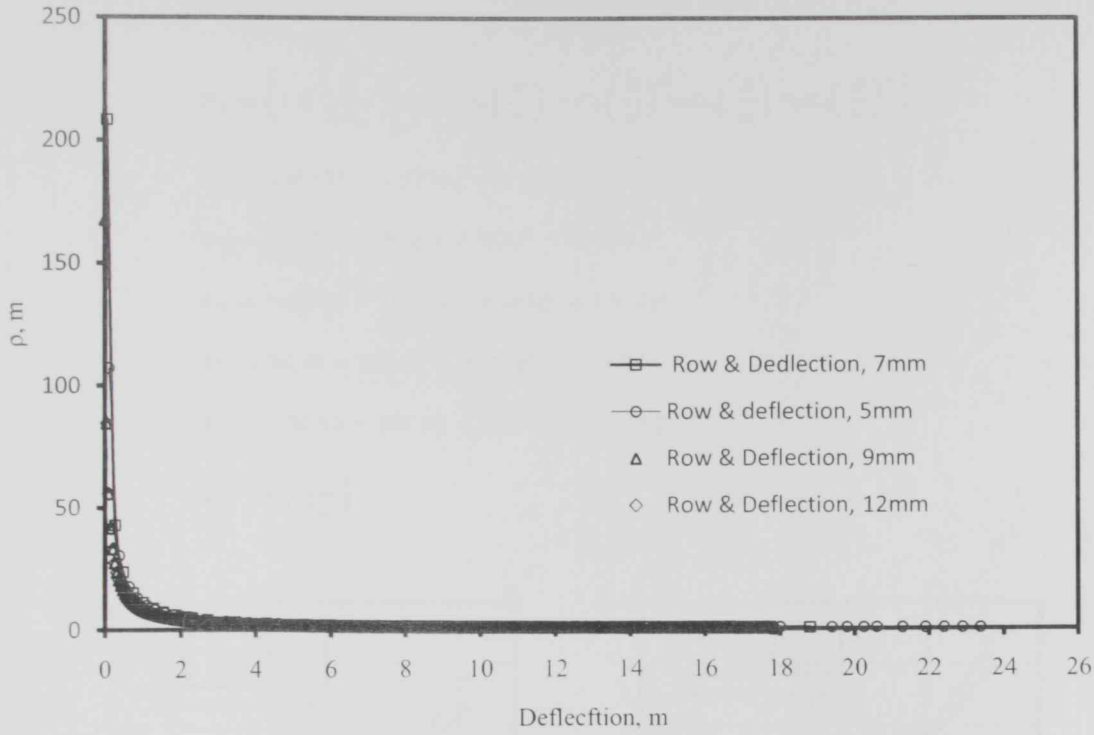

Figure 5.32 Radius of curvature of deformed pipe specimen vs. deflection curves for bending tests.

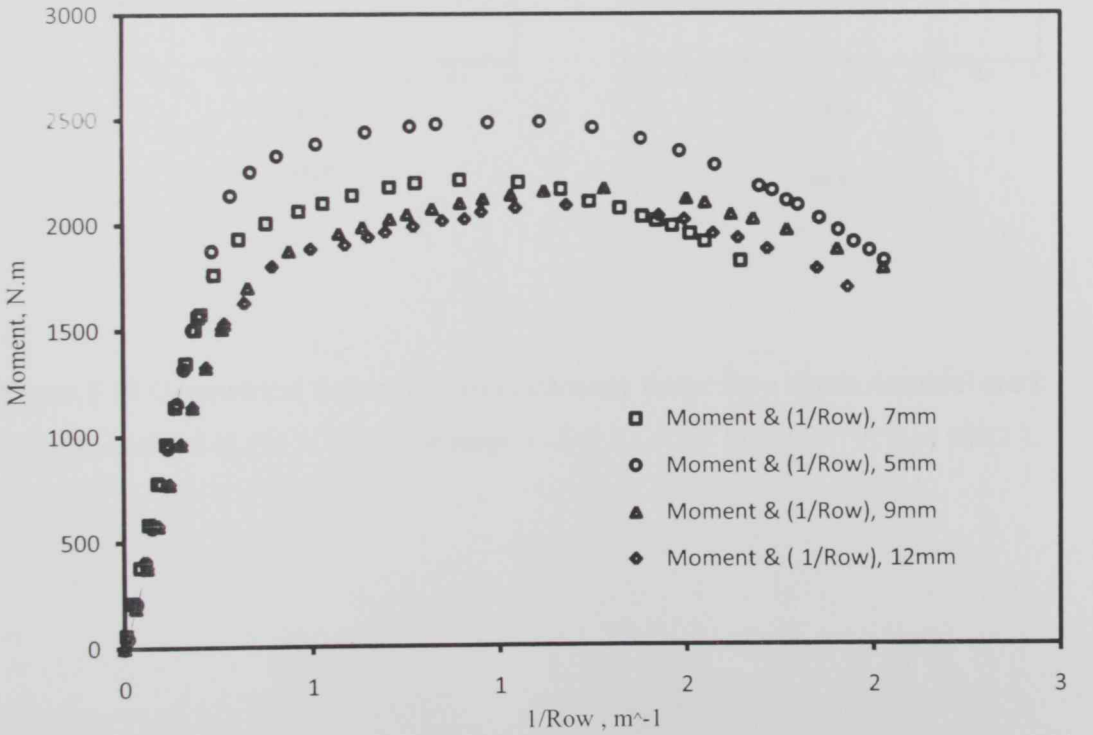

Figure 5.33 Moment vs. the reciprocal the radius of curvature of deformed pipe specimen curves for bending tests.

$$F_b = \left(1 + \frac{t}{2R_m}\right)\left[A_b + B_b\left(\frac{\theta}{\pi}\right) + C_b\left(\frac{\theta}{\pi}\right)^2 + D_b\left(\frac{\theta}{\pi}\right)^3 + E_b\left(\frac{\theta}{\pi}\right)^4\right]$$

$$A_b = 0.65133 - 0.5774\xi - 0.3427\xi^2 - 0.0681\xi^3$$

$$B_b = 1.879 + 4.795\xi + 2.343\xi^2 - 0.6197\xi^3$$

$$C_b = -9.779 - 38.14\xi - 6.611\xi^2 + 3.972\xi^3$$

$$D_b = 34.56 + 129.9\xi + 50.55\xi^2 + 3.374\xi^3$$

$$E_b = -30.82 - 147.6\xi - 78.38\xi^2 - 15.54\xi^3$$

$$\xi = \log\left(\frac{t}{R_m}\right)$$

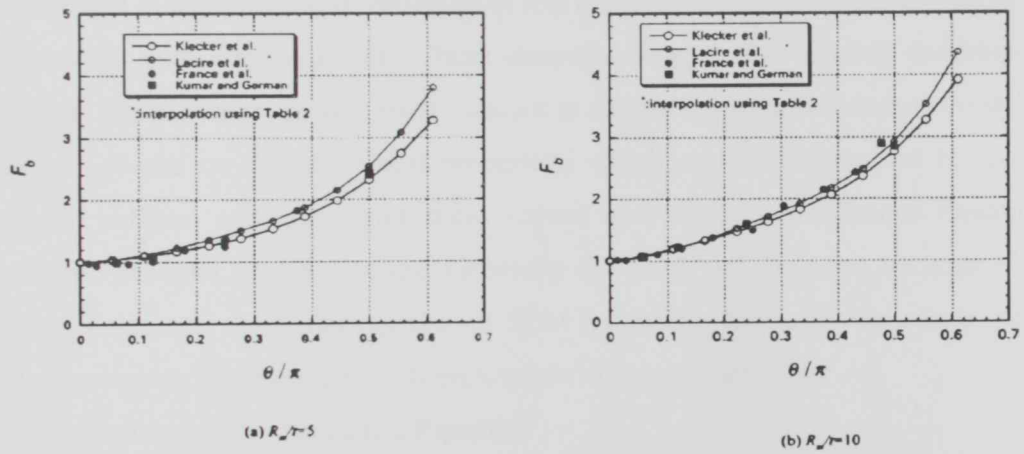

Figure 5.34 Geometrical factors for stress intensity factor for a circumferential crack (fitted to Lacire et al .(61) , applicable range: ($1.5< R_m/t < 80.5, 0 < \theta/\pi < 0.611$).

Chapter 6

FINITE ELEMENT ANALYSIS

6.1 Introduction to Finite Element Method

Finite Element Method is a numerical method which provides solutions of problems that would otherwise be difficult to obtain analytically. Finite element method is an efficient and powerful tool to numerically solve mathematical problems. FEM has various aspects. On a computational point of view, efficiency should be sought in solving actual problems which results in large degree of freedom. Sophisticated algorithms need to be implemented in applying FEM. Basically in this method the object is divided into smaller elements for more precise results. These elements along with boundary conditions are termed as finite element model. Each element is assigned a set of characteristic stiffness Equations (based on its mechanical properties) which are then assembled to form the structural stiffness equation which then solved as a set of simultaneous Equation to predict the behavior of the structure. Generally the result will be more accurate if large number of elements of smaller size is used. FEM follows the following three basic steps:

1. Pre-processing of input data, to discretize functions and Equations.
2. Computation to solve the matrix Equation.
3. Post –Processing of output results, to retrieve the solution from discretization.

6.2 ABAQUS Model

It was decided that the simulation part would be done in the commercial software ABAQUS/CAE version 6.8-2 by using 3-D modeling. Due to the symmetry only one half of the specimen was modeled with symmetry boundary conditions.

To recognize the effect of element size on the stresses, mesh size sensitivity analyses were carried out. These analyses were performed iteratively at different element sizes until the stresses around the crack zone converge to the required appropriate accuracy. The geometrical symmetry in the longitudinal direction was exploited to reduce the computational effort.

A 160 mm long and 42.9 mm diameter pipe with 5mm thickness and four different angles of circumferential through wall crack have been meshed. These different angles are resulted from different crack depths measured from the top surface of pipe. The depths are 5mm, 7mm, 9mm and 12mm. pipe geometry and different sizes of circumferential depths are shown in Figures 6.1 a, b, c and d. Views of the mesh are presented in Figure 6.2 a, b, c and d. The crack meshes for the four different cases under investigation have been refined as they can be seen in Figure 6.3 a, b, c and d. Four different meshes/models have been constructed in order to be able to model pipes with deferent crack geometries. The number of nodes of meshed pipes is around 58000, and the mesh elements are of tetrahedral type.

6.3 Input and Boundary conditions

Since finite element analysis gives an approximate solution for the high and low stress concentration distributions, Von Misses or σ_{33} stresses which can be used to allocate the location of the zones of high stress concentration.

The boundary conditions (BC's) are one of the main parameters that affect severely the results of any finite element model. In the considered model, the BC's are not compatible with the experimental setup but it will not affect the crack start. The right end of the tube was simply supported in the x-y plane but not z-direction as shown in Figure 6.4.The force was applied in the Y-direction. The four samples under testing had been given the same boundary conditions.

The material was modeled as homogenous, isotropic and elastic-plastic, it is assumed to follow the widely used and the well-known Ramberg-Osgood constitutive law describing material's post yield stress-strain ($\sigma - \varepsilon$) relation, Equation constants and material properties are shown in tables 3.6 and 3.7.

A saddle part was constructed with specific dimensions and attached to the opposite top upper surface of the induced crack. Distributed load as pressure was applied on the upper surface of the saddle.

6.4 Results and Discussions

The load versus displacement for different crack sizes and depths were obtained and plotted as shown in Figures 6.5 through 6.8.In the same Figure the result from experimental works are also presented. The Figures show that the load readings resulted from finite element are higher than experimental loads corresponding to the same displacement. This might be attributed to the fact that input boundary conditions were not mimic the experimental conditions. Also, it is might attributed to the way the load was applied on the surface of saddle and not directly onto the surface of pipe.

It has been noticed while conducting the experimental work that, in all studied cases, the crack starts propagation at the inner side of the initiated crack.

Therefore the purpose of the FEA conducted in this study is to predict the location (not magnitude) of the maximum opening stress due to which the crack extends.

Figures 6.9 through 6.16 show von missies and σ_{33} stress distributions for the four cases resulted from finite element modeling's, it is obvious that stress values are highest at the inner face and gradually decreasing towards the outer surface.

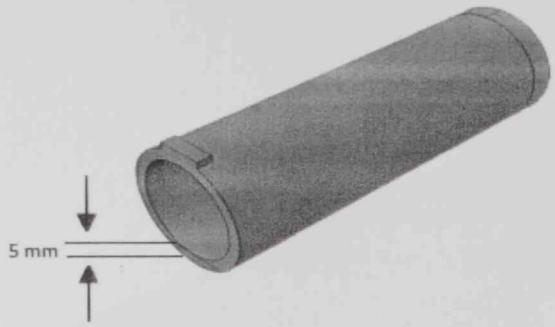

Figure 6.1.a Model geometry – crack depth 5mm.

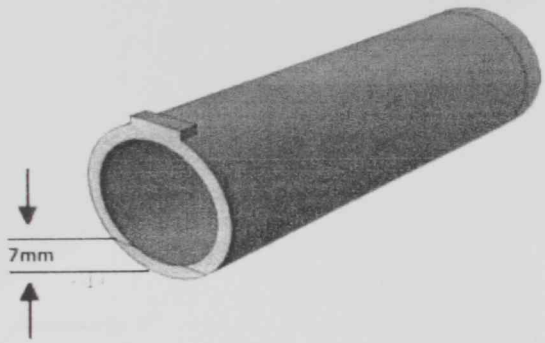

Figure 6.1.b Model geometry – crack depth 7mm.

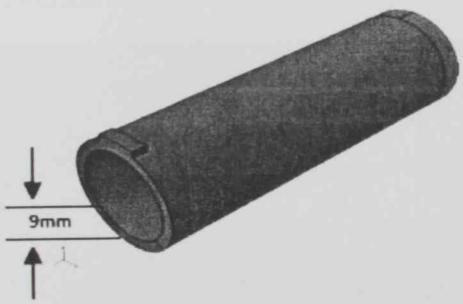

Figure 6.1.c Model geometry – crack depth 9mm.

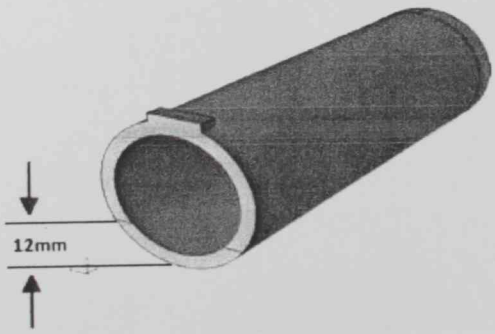

Figure 6.1.d Model geometry – crack depth 12mm.

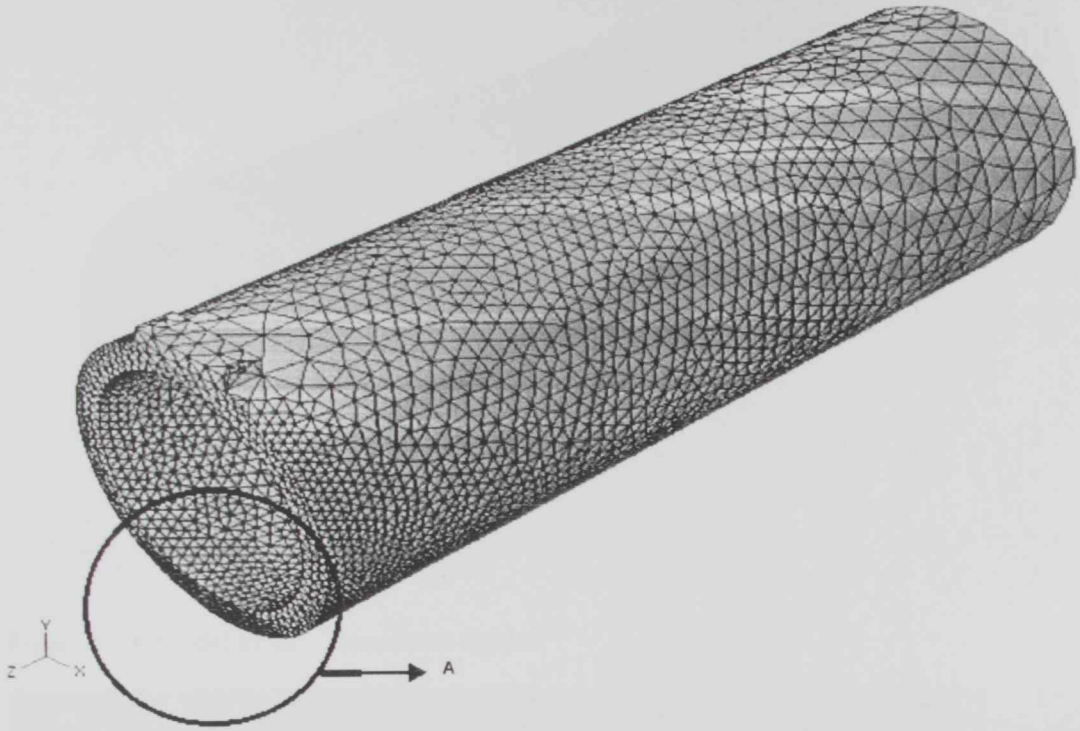

Figure 6.2.a Model mesh – 5mm crack depth.

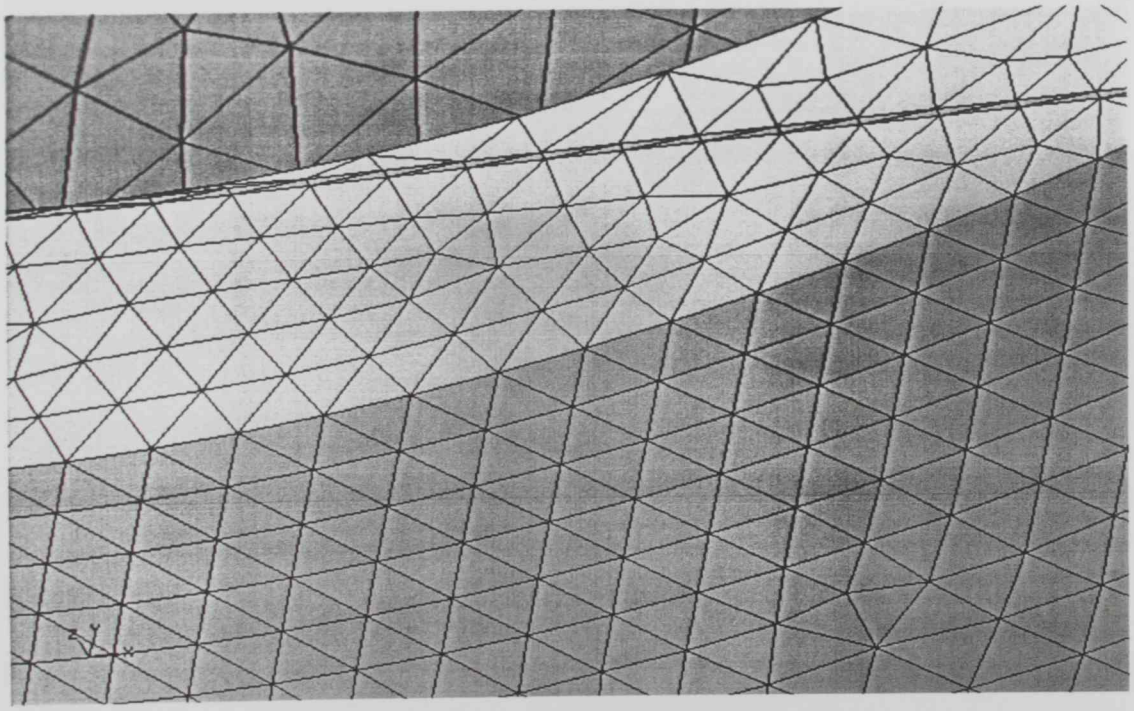

Figure 6.3.a Detailed A: Model mesh –5mm crack depth.

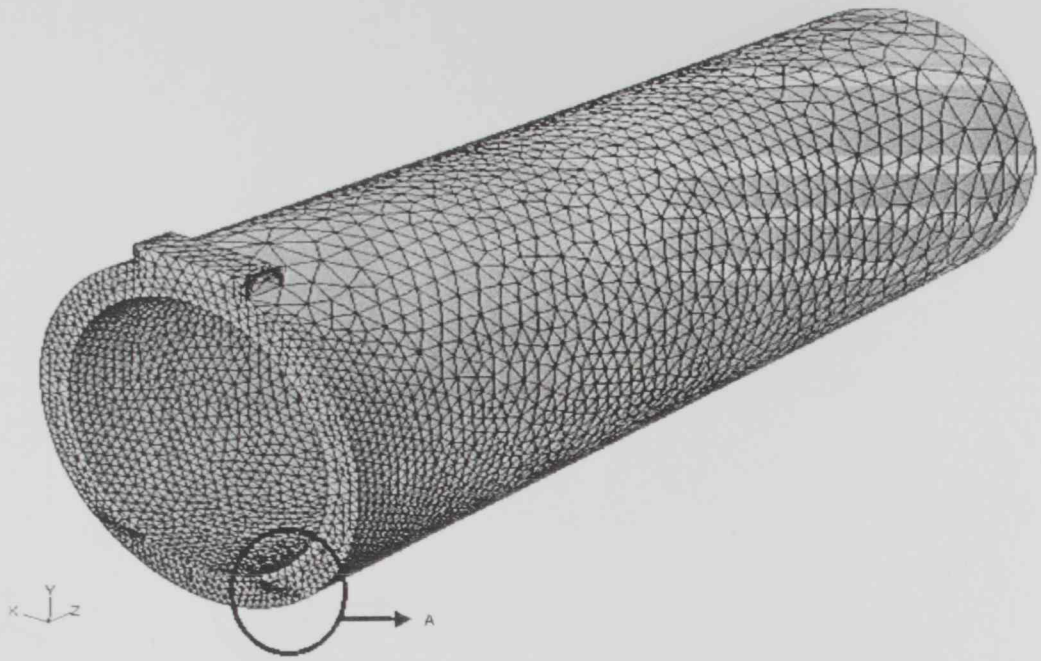

Figure 6.2.b Model mesh – 7mm crack depth.

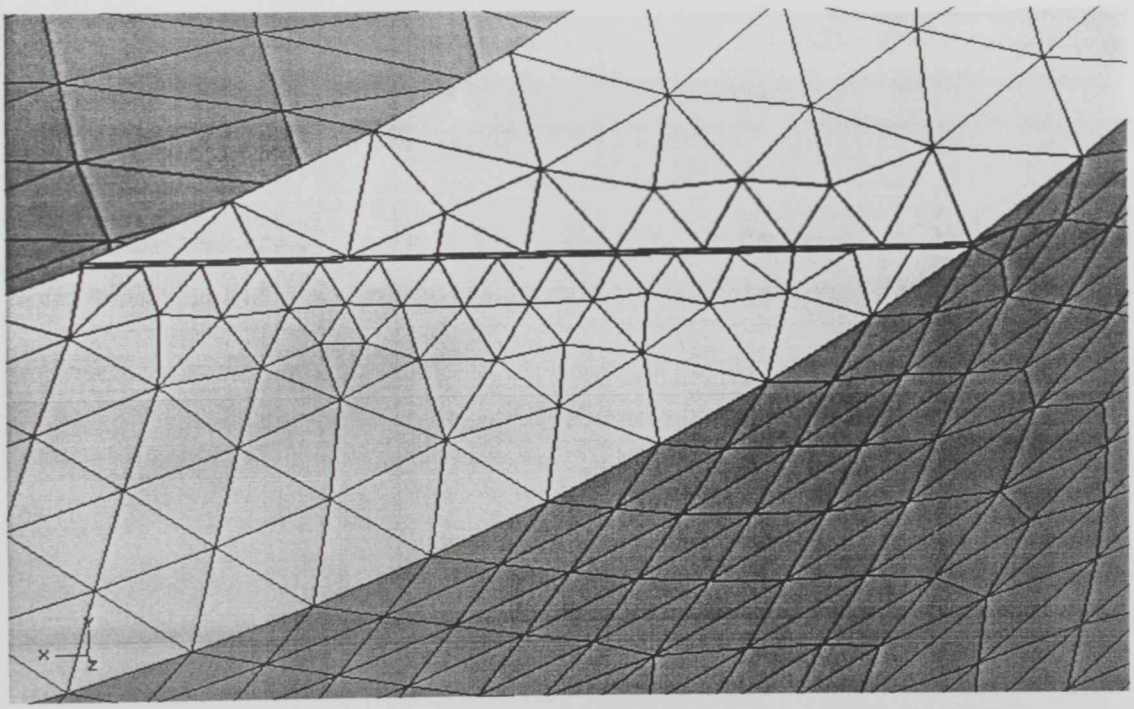

Figure 6.3.b Detailed A: Model mesh –7mm.

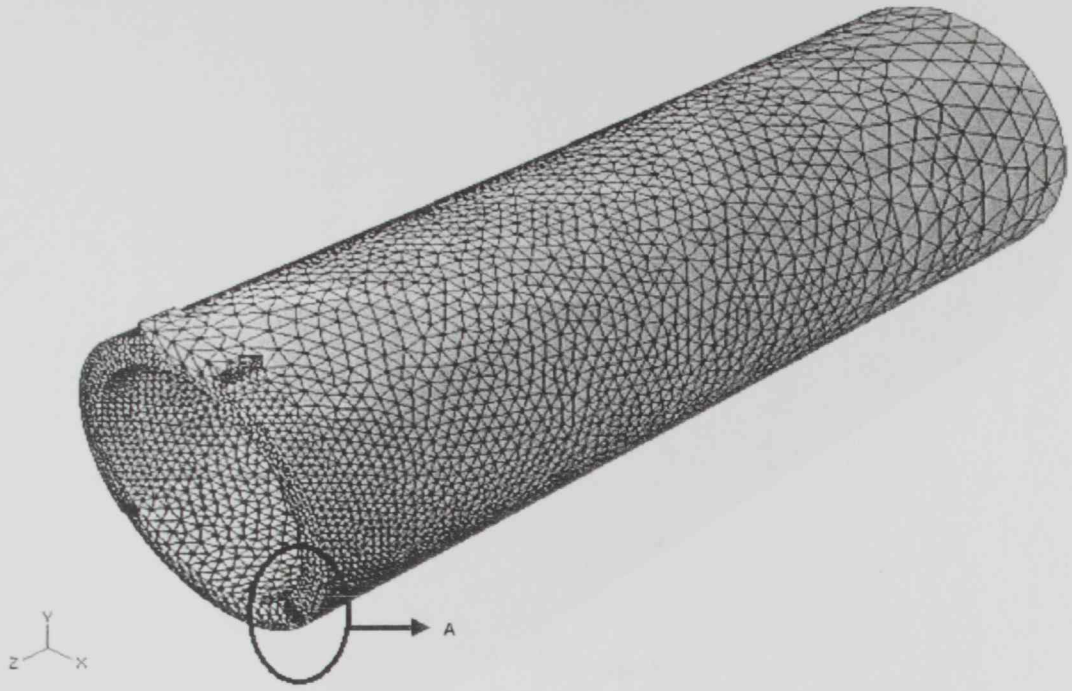

Figure 6.2.c Model mesh – 9mm crack depth.

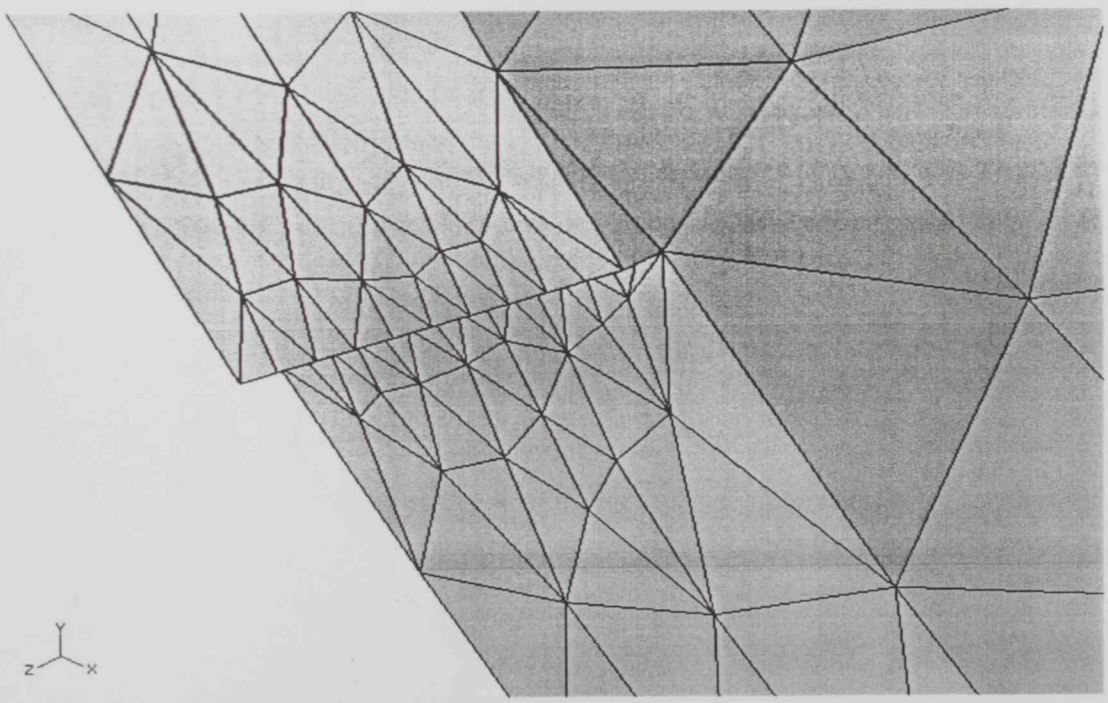

Figure 6.3.c Detailed A: Model mesh –9mm.

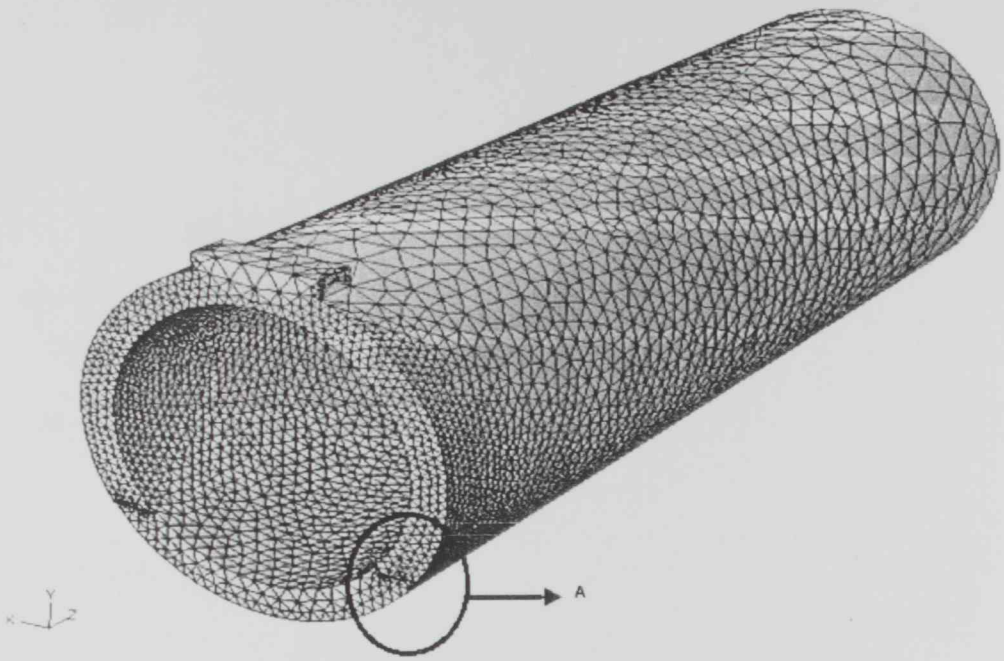

Figure 6.2.d Model mesh – 12mm crack depth.

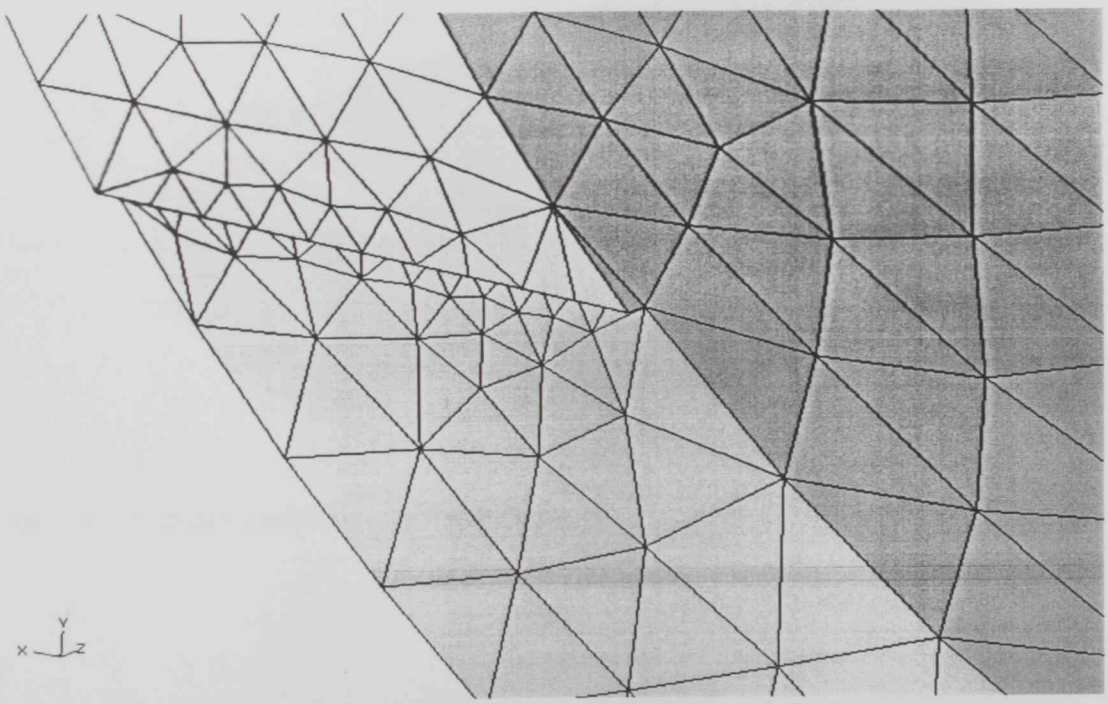

Figure 6.3.d Detailed A: Model mesh –12mm.

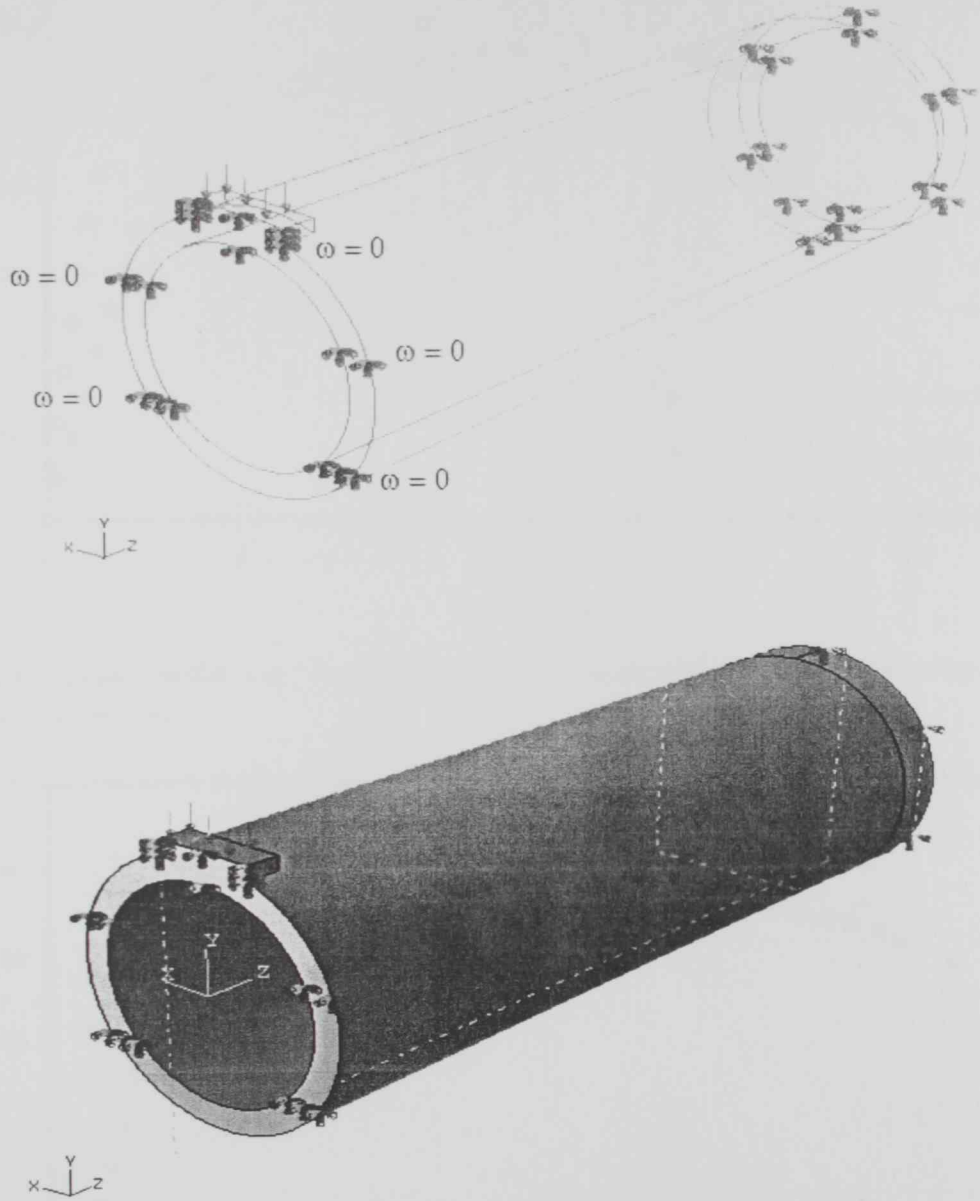

Figure 6.4 Boundary conditions used for modeling.

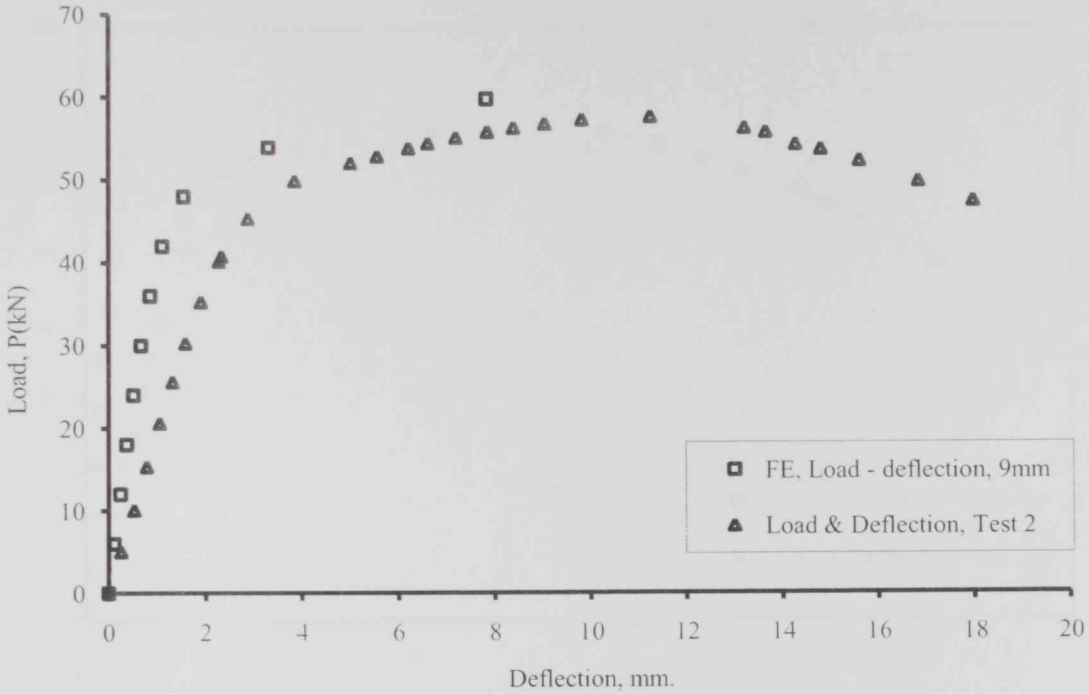

Figure 6.6 Load – deflection curves comparison of experimental work with finite element method results– 9mm.

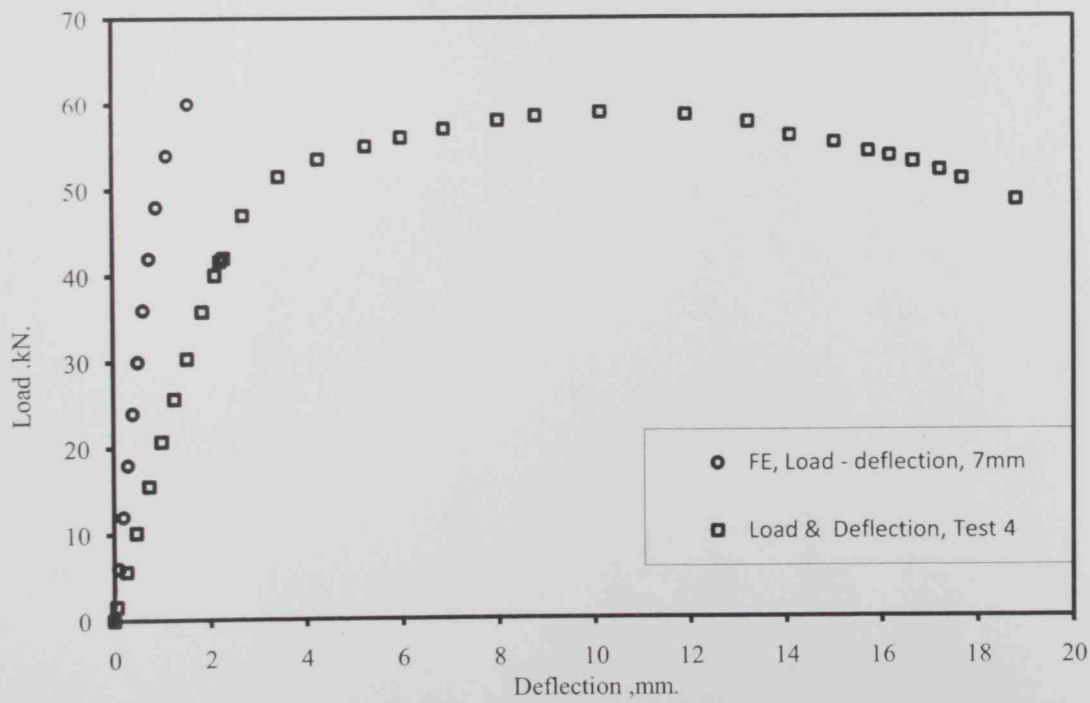

Figure 6.7 Load – deflection curves comparison of experimental work with finite element method results– 7mm.

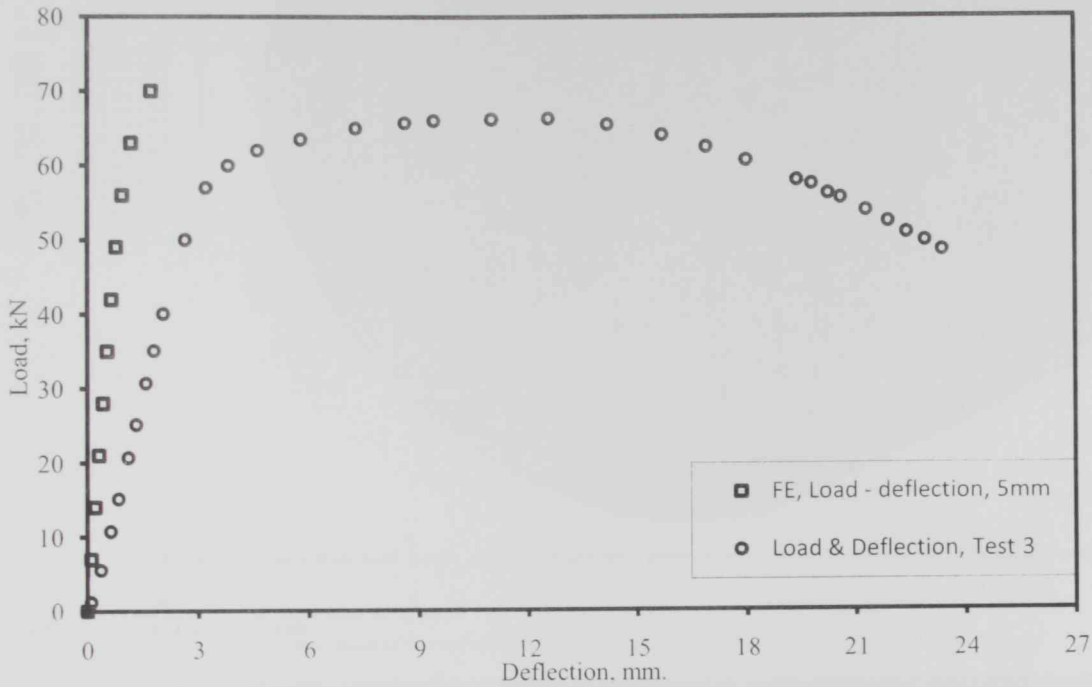

Figure 6.8 Load – deflection curves comparison of experimental work with finite element method results– 5mm.

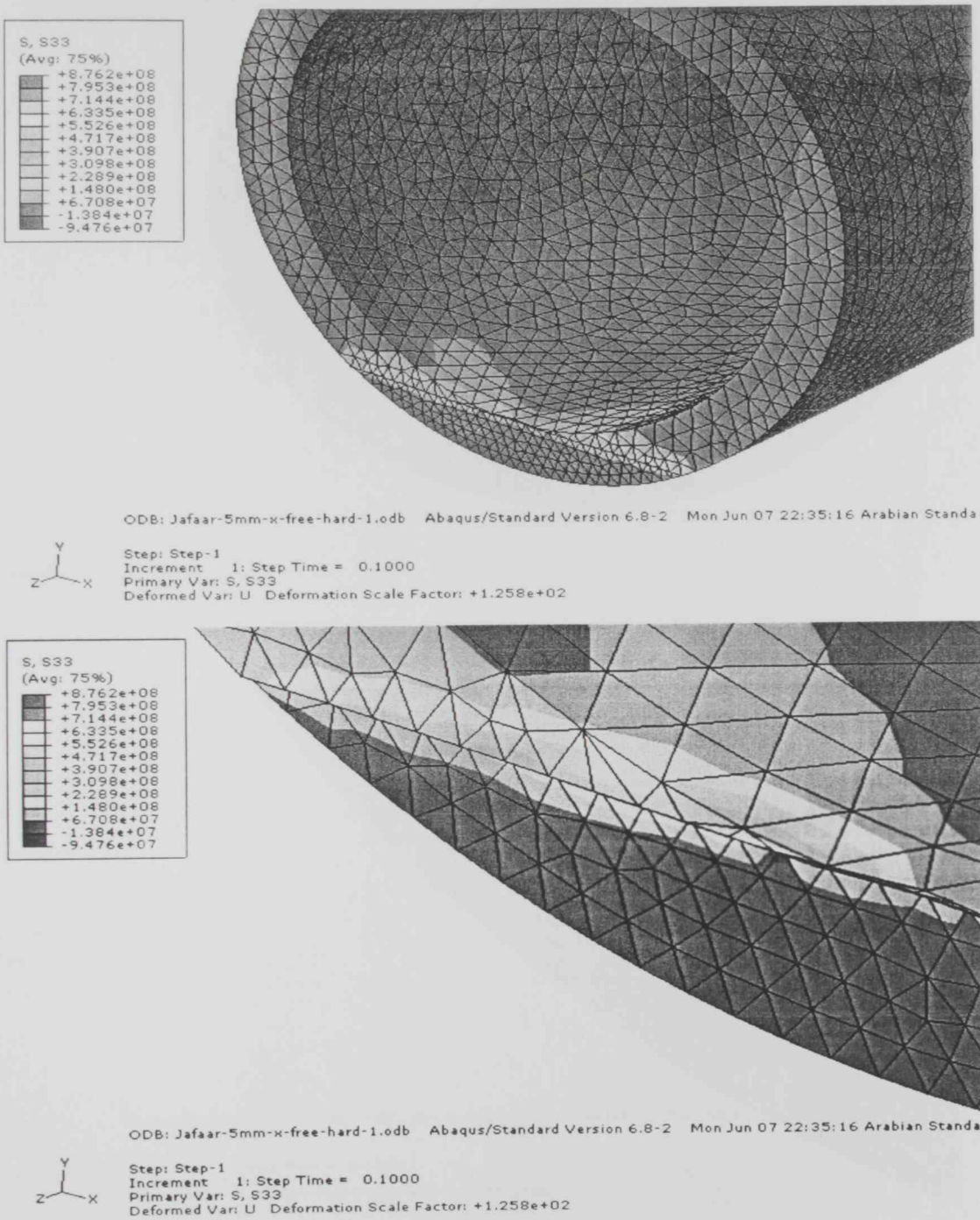

Figure 6.9 Stress distribution - σ_{33} – 5mm

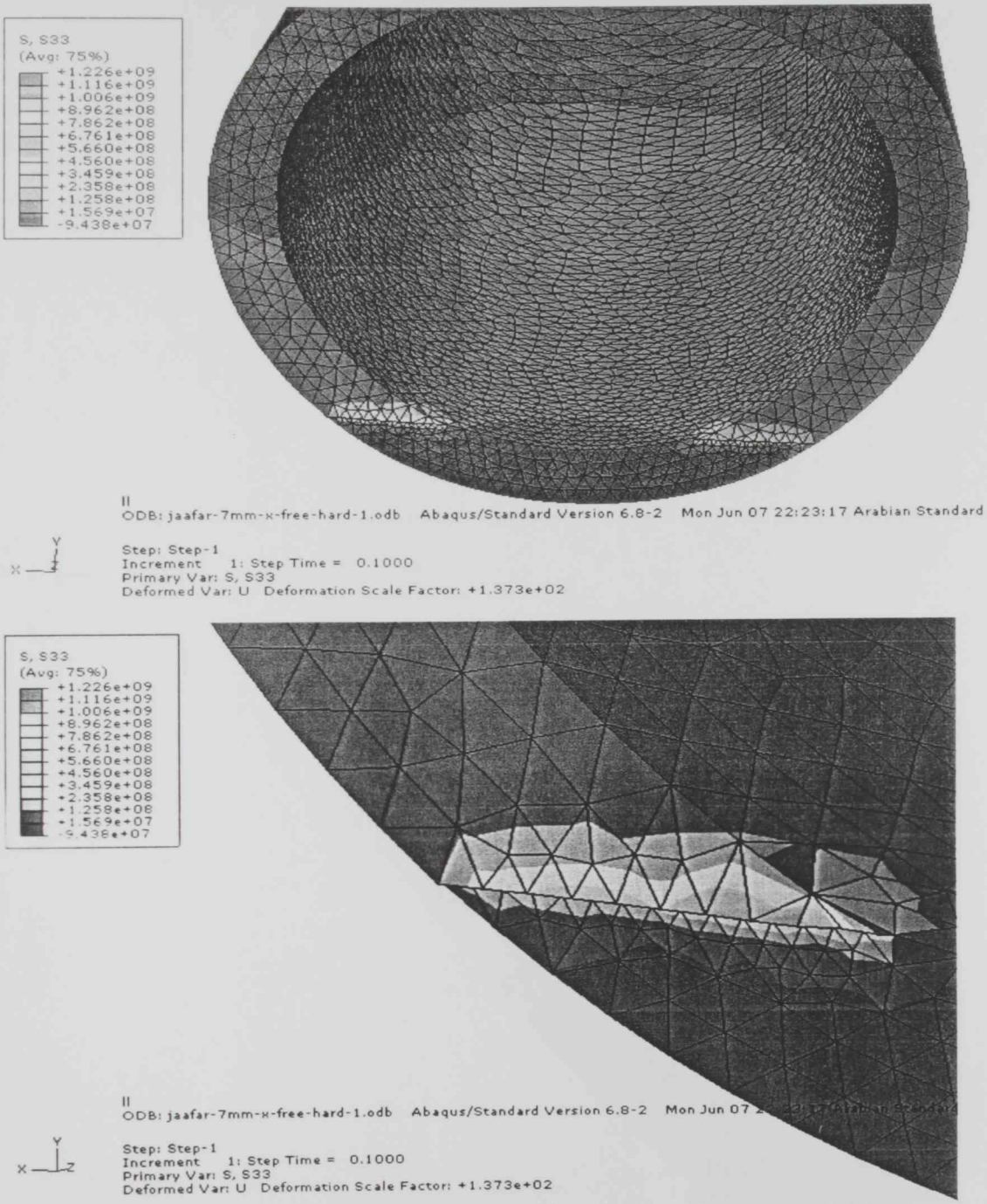

Figure 6.10 Stress distribution - σ_{33} – 7mm

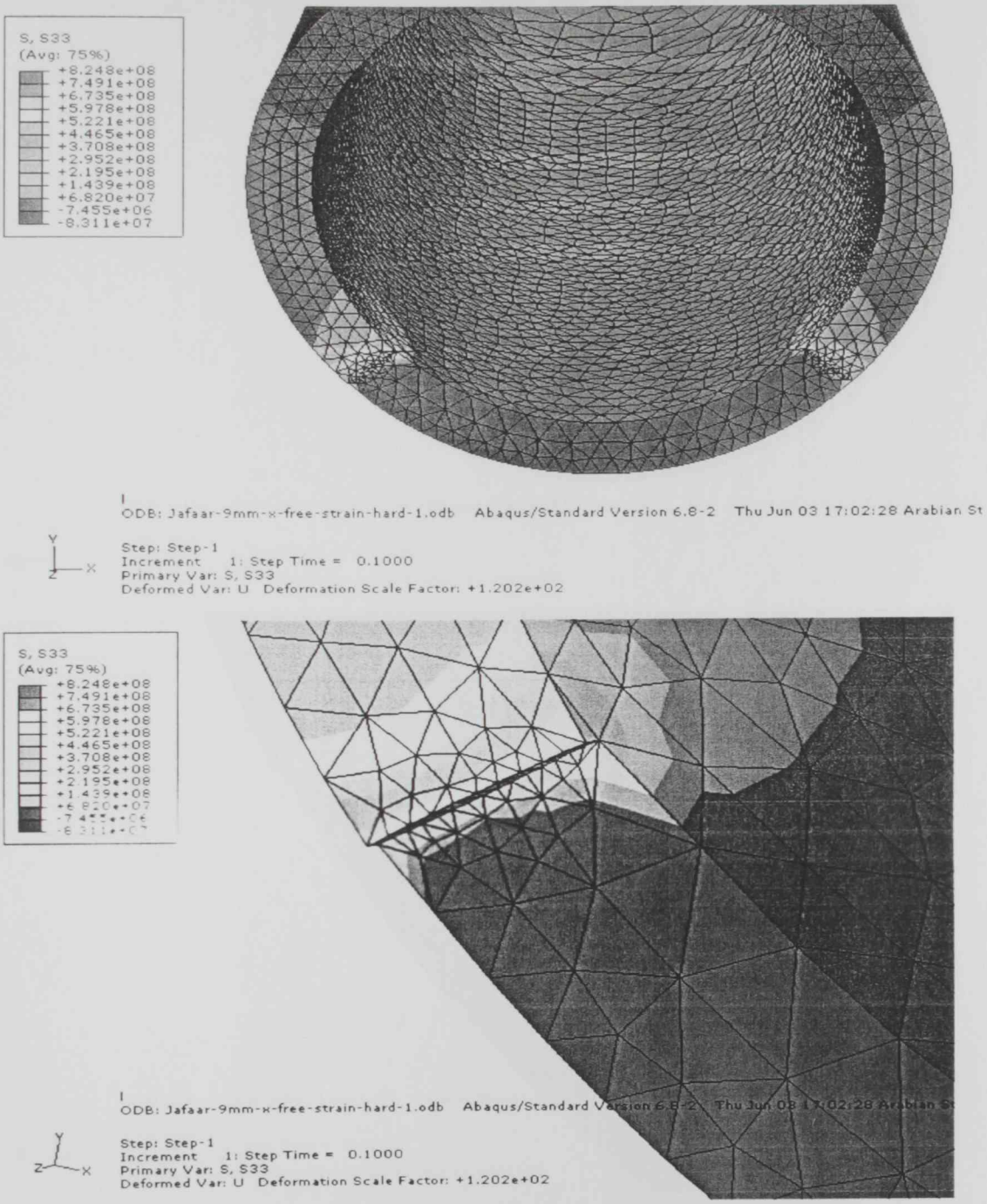

Figure 6.11 Stress distribution - σ_{33} – 9mm

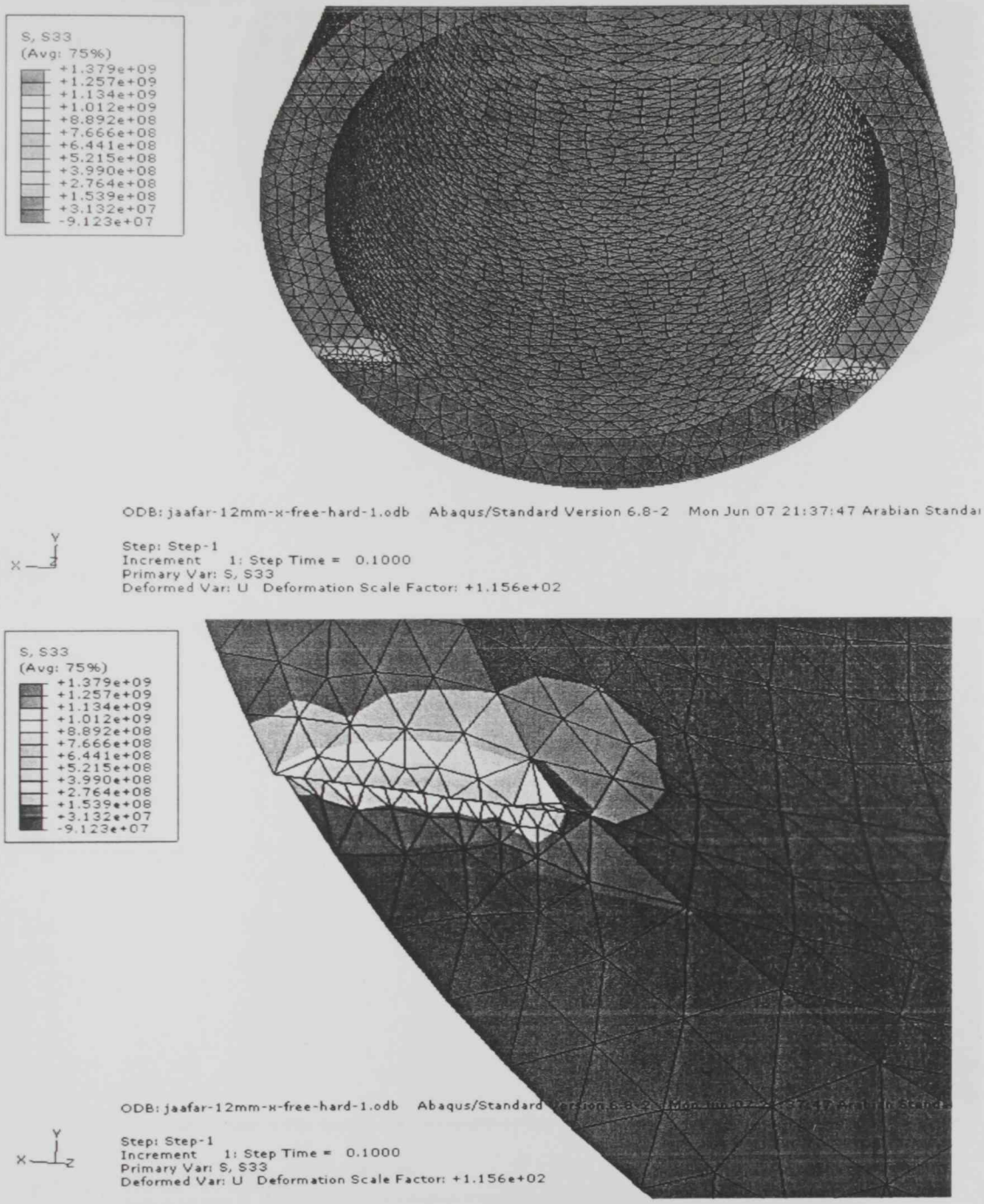

Figure 6.12 Stress distribution - σ_{33} – 12mm

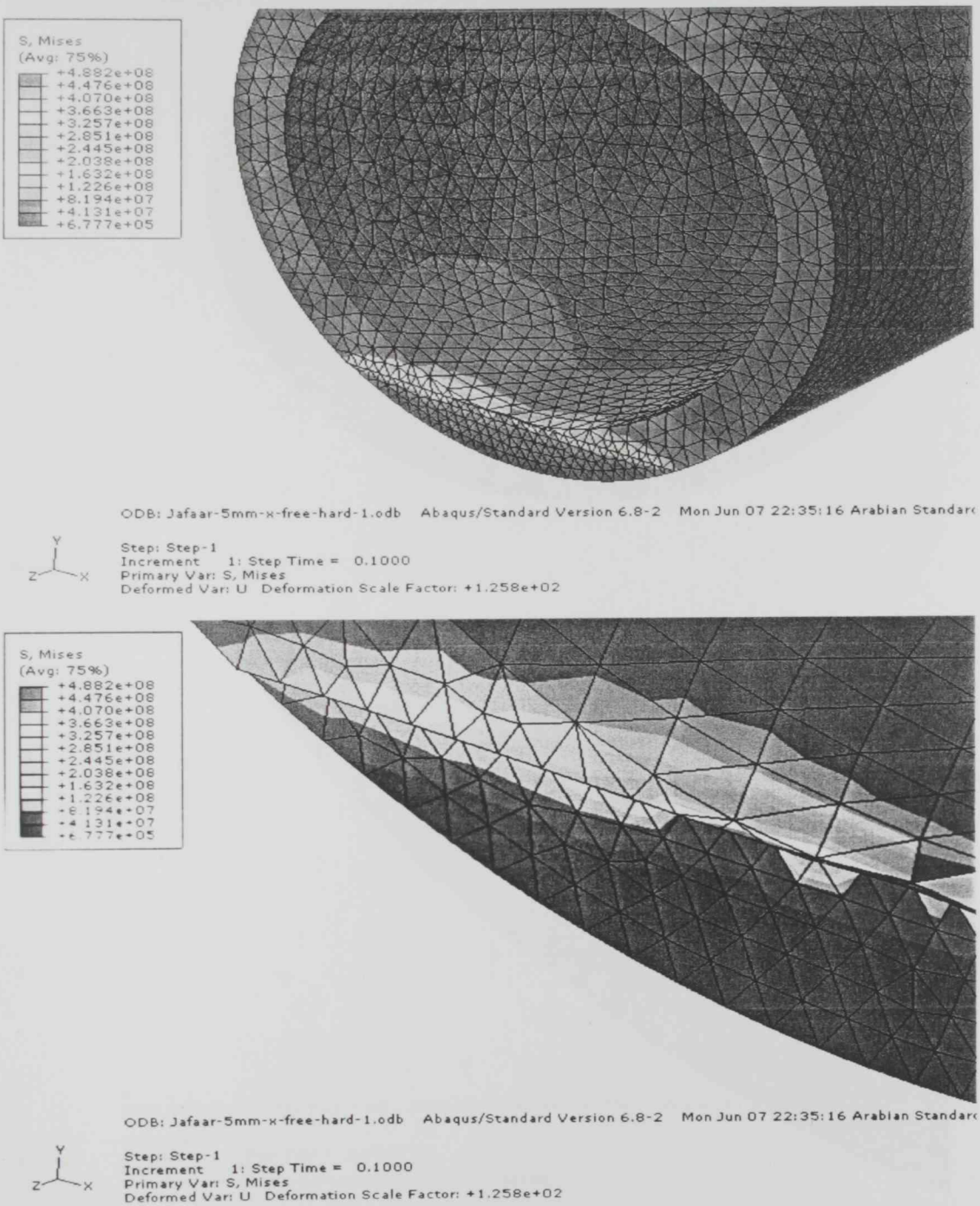

Figure 6.13 Stress distribution – von misses – 5mm.

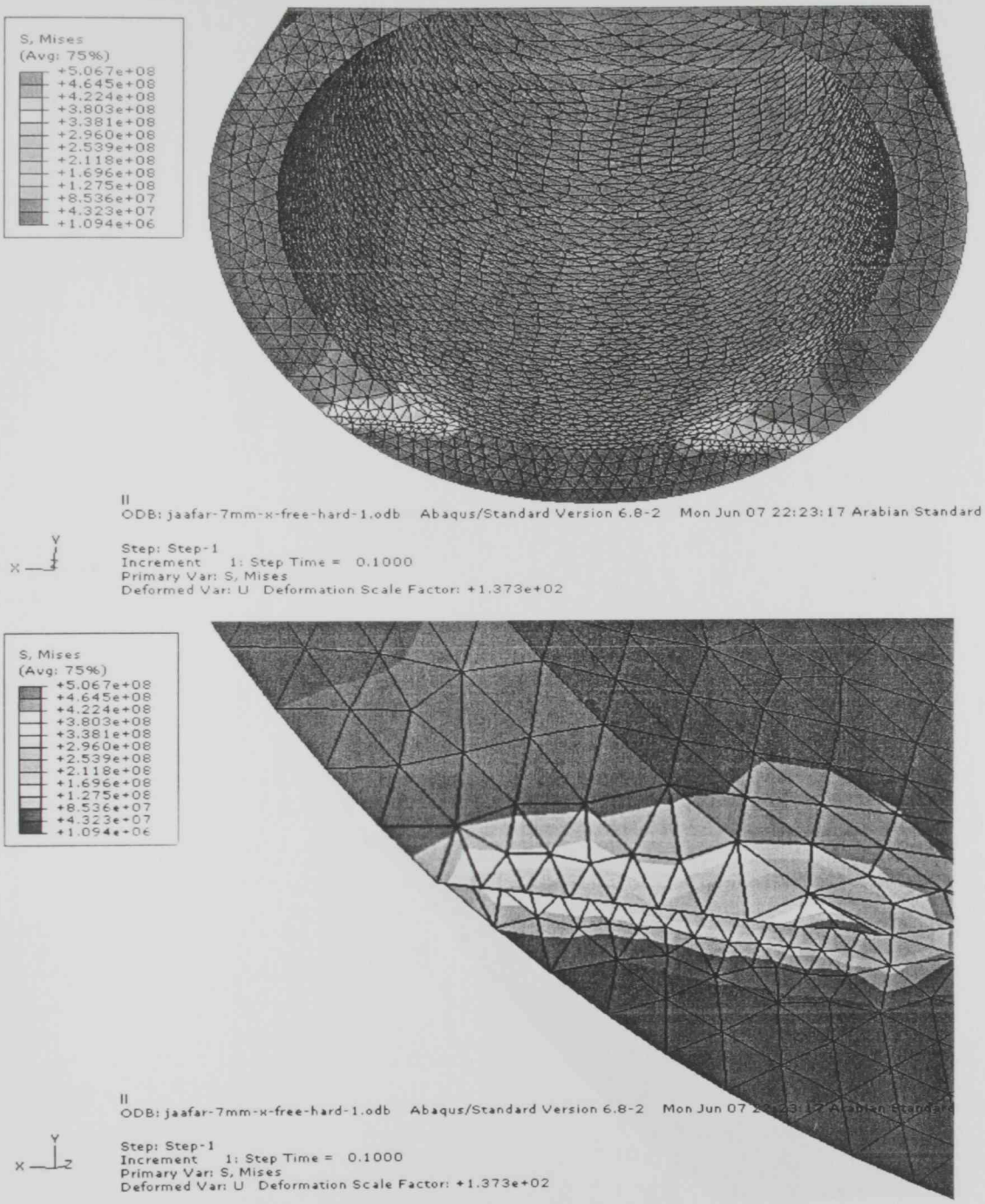

Figure 6.14 Stress distribution – von misses – 7mm.

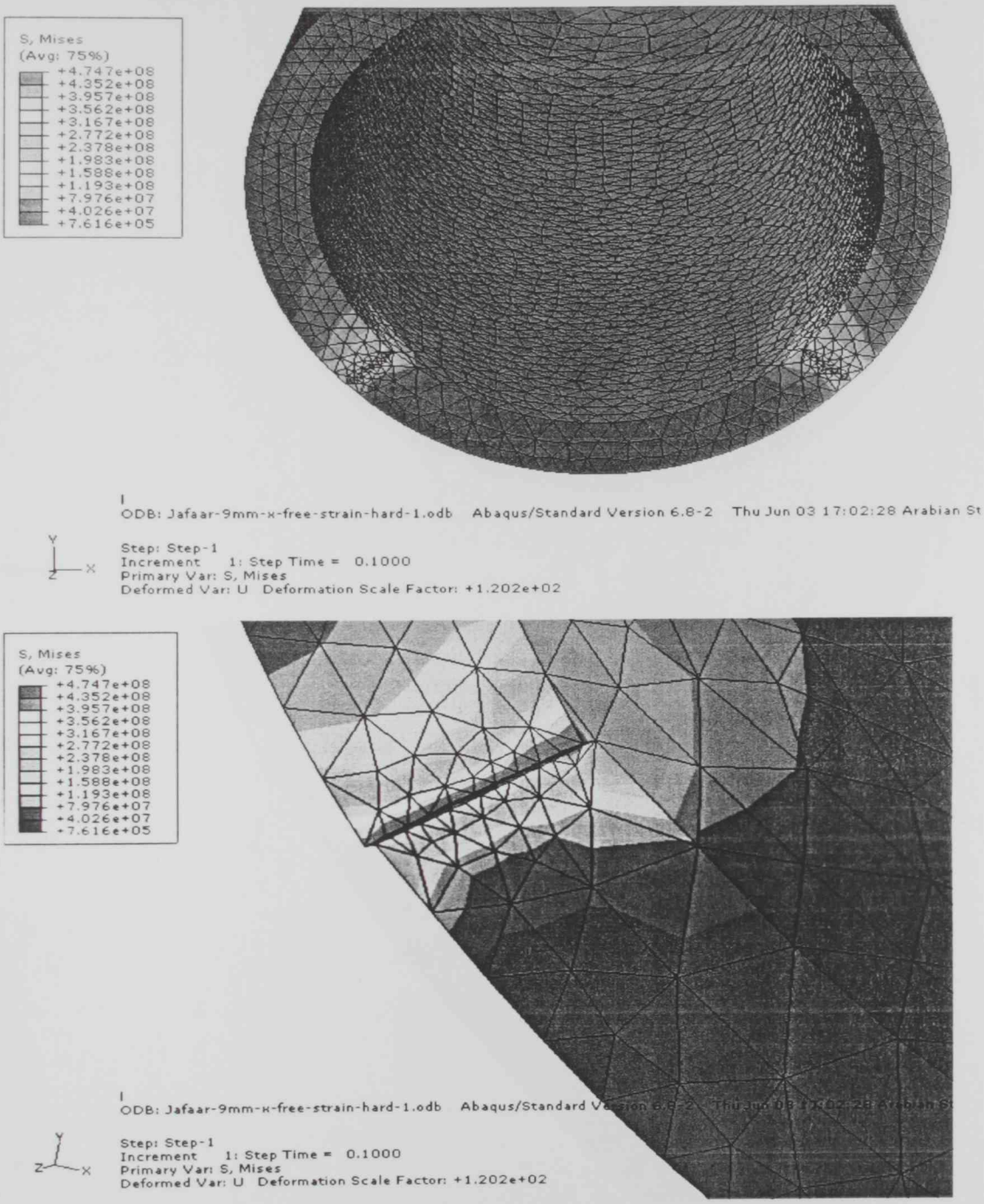

Figure 6.15 Stress distribution – von misses – 9mm.

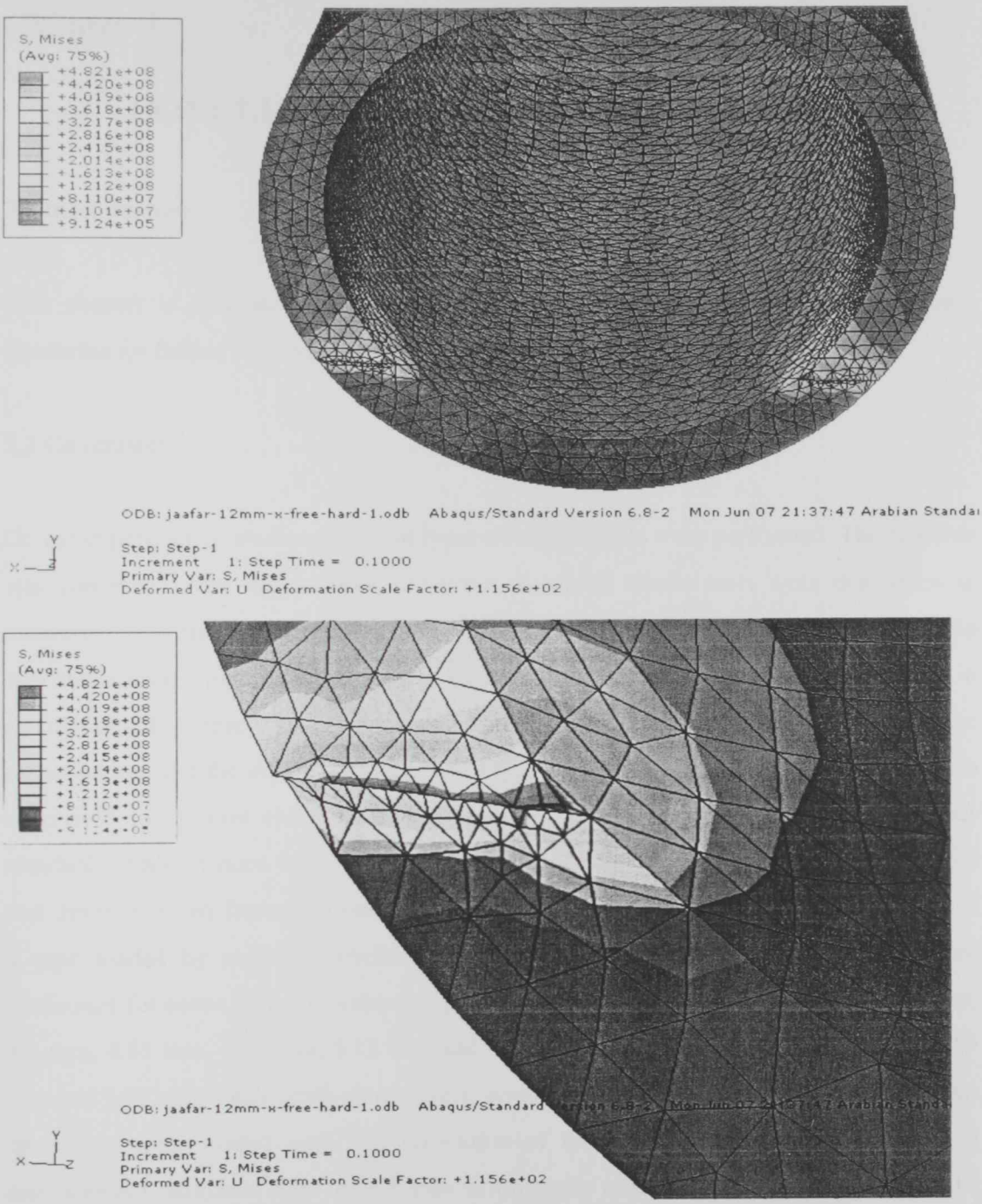

Figure 6.16 Stress distribution – von misses – 12mm.

Chapter 7

CONCLUSION AND RECOMMENDATIONS

7.1 Introduction

This chapter is dedicated for the general discussion of results, suggestions of some directions for further investigations, and summary of the main conclusions.

7.2 Conclusion

On the experimental studies, different types of experiments were performed. The first one was concerned with the material properties at which tensile tests were conducted to measure the tensile properties of the pipeline metal (grade X65) by extracting strip specimens from a pipe. Four samples were extracted and the average values were used in calculation. The results of tensile test were compared with that given by the pipe manufacturer and the API standards and used in further calculations. Another test was conducted to confirm that the chemical composition of the pipe material is as per standards. Another main test conducted to measure fracture toughness of the pipe material and stress intensity factors for complete circumferential surface cracks at the outer wall of a pipe loaded by constant tensile stress in axial direction, The fracture tests were performed for seven different values of plug type with notch depths (2.55 mm, 3.15 mm, 4.4 mm, 4.65 mm, 4.85 mm, 5.15 mm and 5.95 mm) and two tests without plug of 2.55 mm and 5.95 mm notch depth respectively, and the notch of V type with angle of 60. All specimens were loaded until full separation of the specimen into two halves. Load displacement diagrams show that P max is inversely related to the depth of notch. The fracture toughness values of the pipe material were calculated and the values are almost the same and they are independent of the pipe geometry.

The fracture surfaces of several represented specimens were examined. The fracture surfaces show mostly flat surfaces, one specimen shows a slightly coarse and a presence of shear lip as an indication of ductile fracture (this specimen of no plug type). A further

investigation was carried out by Scanning electron microscope (SEM). SEM fractographs of fractured surface of plug inserted pipe specimens show almost brittle features.

Elastic–plastic fracture experiments under pure bending loading have been carried out on short circumferential through-wall cracked X65 carbon steel pipes. the crack lengths were prepared by considering the pipe surface as a reference and make the cutting depth accordingly. The cutting depths were 5, 7, 9 and 12 mm. The corresponding angles of the selected depth are $75^o, 86^o, 105^o$ *and* 120^o .The fracture behavior was determined using the J-integral estimation method which can predict the whole fracture behavior from initiation to stable ductile crack growth to unstable fracture. It was noticed during the test that the maximum load point is the point of crack instability or the point at which the crack starts to propagate. The J value was calculated and plotted against crack area, moment, and crack length and pipe deflection.

A finite element analysis was carried out on four models to represent fracture experimental works .The finite element results agree reasonably with the experimental results, although the load readings resulted from finite elements are slightly higher than that resulted from experimental work for the same displacement .In addition, finite element analysis emphasises the fact that the crack will start from the internal surface by showing that the stress distribution is maximum at the internal side of the crack and it is decreasing toward the pipe outside surface.

7.3 Recommendations:

Some of the recommendations which can be made are as follows:

- The number of samples for all tests was minimized due to the limited material availability, future works are recommended to maximize the number of samples to achieve the proper and the desired repeatability of results.
- More precise tools would have a positive impact on the obtained results; fracture toughness tests were carried outside university lab due to the limited capacity of UAE university MTS machine, the availability of machine with high capacity at university lab would implement more academic measures.

- In this study it was not possible to identify the exact point of crack initiation due to the limited magnification of the magnifier. This issue needs more investigation in order to adequately identify the onset of crack extension and in turns the corresponding points of initial load on load-line load displacement curves.
- A more accurate FEA should be conducted to consider the exact geometry, loading and boundary conditions. This will enhance the predictability of FEM and allow for more realistic quantitative predictions. More FE mesh may be considered for more accurate results.
- Machining and preparation of samples were carried out in conditions that avoid any side effect, further measures to be implemented to make sure the limitation of any unexpected changes that might disturb the results.
- In finite element analysis and modeling, crack growth was not considered, in any further future works, fracture parameters to be considered so that the achieved results from fracture toughness tests and fracture tests would be compared with that resulted from finite element modeling.
- Investigate the effect of loading rate on the load – deflection curves and crack growth.
- Helmets, goggles, and all safety precautions are recommended while performing all tests.

References

[1] Anderson, T. L. (1995) Fracture Mechanics Fundamentals and Applications-2nd Edition, CRC Press (Florida).

[2] Fracture mechanics ,Nestor Perez, Kluwer academic publisher.

[3] Barsom, J.M.; Rolfe, S.T. Fracture and Fatigue Control in Structures, 2nd Ed.; Prentice-Hall: Englewood Cliffs, NJ, 1987.

[4]Griffith, A.A. The phenomena of rupture and flaw in solids. Phil. Trans. Royal Society 1920, 221, 163–198.

[5] Irwin, G.R. Fracture dynamics. In Fracturing of Metals; American Society of Metals: Cleveland, 1948.

[6] Orowan, E. Fracture strength of solids. In Report on Progress in Physics; Physical Society of London: London, 1949; Vol. 12, 185–232.

[7] Practical Fracture Mechanics in Design. Second Edition. Arun Shukla

[8]Irwin, G.R.; Kies, J.A. Fracturing and fracture dynamics. Welding Journal 1952, 31 (Research Supplement), 95s–100s.

[9]Irwin, G.R.; Kies, J.A. Critical energy rate analysis of fracture strength of large welded structures. Welding Journal 1954, 33, 193s–198s.

[10] Irwin, G.R. Onset of fast crack propogation in high strength steel and aluminum alloys. Sagamore Research Conference Proceedings 1956, 2, 298–305.

[11]Wells, A.A. The condition of fast fracture in aluminum alloys with particular reference to comet failures. British Welding Research Association Report, April 1955.6, 49–53.

[12]Williams, M.L. On the stress distribution at the base of a stationary crack. J. Appl. Mech. 1957, 24, 109–114.

[13] Wells, A.A.; Post, D. The dynamic stress distribution surrounding a running crack—A photoelastic analysis. Proceedings of the Society of Experimental Stress Analysis 1958, 16, 69–92.

[14] Irwin, G.R. Discussion of: The dynamic stress distribution surrounding a running crack — A photoelastic analysis. Proceedings of the Society of Experimental Stress Analysis 1958, 16, 93–96.

[15] Paris, P.C.; Gomez, M.P.; Anderson, W.P. A rational analytic theory of fatigue. Trend Engng 1961, 13, 9–14.

[16] Dugdale, D.S. Yielding of steel sheets containing slits. J. Mech. Phys. Solids 1960, 8, 100–104.

[17] Barenblatt, G.I. The mathematical theory of equilibrium cracks in brittle fracture. Adv. Appl. Mech. 1962, VII, 55–129.

[18] Rice, J.R. A path independent integral and the approximate analysis of strain concentration by notches and cracks. J. Appl. Mech. 1968, 35, 379–386.

[19] Rice, J.R.Mathematical Aspects of Fracture;Academic Press:NewYork, 1968; Vol. 2.

[20] Begley, J.A.; Landes, J.D. The J integral as a fracture criterion. In Stress Analysis and Growth of Cracks. ASTM STP 514; American Society for Testing and Materials: Philadelphia, 1972; 1–20.

[21] E813-81. Standard test method for JIC , a measure of fracture toughness. American Society for Testing and Materials: Philadelphia, 1981.

[22] Sih, G.C. Handbook of Stress Intensity Factors; Institute of Fracture and Solid Mechanics: Lehigh University, Bethlehem, PA, 1973.

[23] J. W. Dally and W.F. Riley, "Experimental Stress Analysis", 3rd ed., McGraw-Hill, Inc. New York, (1991).

[24] G.R. Irwin, "Fracture I," S. Flugge editor, Handbuch der physik VI, Springer-Verlag, New York, (1958) 558-590.

[25]A stochastic model for elastic-plastic fracture analysis of circumferential through wall-cracked pipes subjected to bending.

[26] L.A. Simpson : Elastic-Plastic Fracture Mechanics – TR AECL -5991,Pinawa, Mainttoba.

[27] S.T Rolfe and J.M. Barsom- Fracture and Fatigue controlin structures, Prentice Hall Inc. , Englewood Cliffs, New Jersey.

[28]F.A. McClinntock,Fracture – Ed.H.Liebowitz, v-3, academic press, New York, 1971,P.47.

[29] J.R. Rice – Fracture ,Ed.H. v-2, academic press, New York, 1968,P191.

[30] J.A.Begly and J.D. Landes: Fracture Toughness,ASTM, STP-1972,P.1.

[31] J.R. Rice and Pris, J.G. Merkle – " Progress in Flaw Growth and Fracture Toughness Testing ",ASTM,Stp – 536,ASTM, 1973, P.231.

[32] J.D. Landes and J.A.Begly :"Fracture Analysis", astm,stp – 560,1974, P.170.

[33] G. Frederick: Centre De Recherches Metallurgignes, Metallurgical Reports - 31, June, 1972, PP 27-37.

[34] F.M. Burdekin and D.E. Stone: J. of Strain Analysis, Vol. 1, No. 2, 1966, P. 145.

[35] A.A. Wells - "Crack Propagation in Metals" -Cleavage and Fast Fracture", M Cranfield crack propagation symposium, V.I, Sept. 1961, P.210.

[36]J.D. Landes and J.A. Begley: "Fracture Toughness", ASTM - STP - 514, 1972, P. 24.

[37] G.R. Egan: Engg. Fracture Mechanics, vol. 5, 1973, P. 167.

[38] E1820 .ASTM

[39] G.R. Irwin, in: Structural Mechanics, Springer, New York, 1960, pp. 557–592.

[40] E399-06

[42] M. A. N. Shabara, A. A. EL-Domiaty and M. D. AL-Ansary,I Estimation of plane strain fracture toughness from circumferentially bluntly notched round bar specimen, Engineering Fracture Mechanics Vol. 54, No. 4, pp. 533-541, 1996,

[43] Rice, J.R. (1968). A path-independent integral and the approximate analysis of strain concentration by notches and cracks. Journal of Applied Mechanics 35, 376–386.

[44] Hutchinson, J.W. (1968). Singular behavior at the end of a tensile crack in a hardening material. Journal of Mechanics and the Physics of Solids 16, 13–31.

[45] S. RAHMAN1 and F.W. BRUST2, Approximate methods for predicting J-integral of a circumferentially surface-cracked pipe subject to bending, International Journal of Fracture 85: 111–130, 1997.

[46] Paris, P.C., Tada, H., Zahoor, A. and Ernst, H. (1979). The theory of instability of the tearingmode of elastic–plastic crack growth. ASTM STP 668, Elastic–Plastic Fracture, 5–36.

[47] Kumar,V. andGerman, M.D. (1988). Elastic–plastic fracture analysis of through-wall and surface flaws in cylinders, EPRI NP-5596, Electric Power Research Institute, Palo Alto, CA.

[48] Yukio Takahashi, Evaluation of leak-before-break assessment methodology for pipes with a circumferential through-wall crack. Part II: J-integral estimation, International Journal of Pressure Vessels and Piping 79 (2002) 393–402.

[49]S. Rahman , a stochastic model for elastic-plastic fracture analysis of circumferential through –wall – cracked pipes subjected to bending, engineering fracture mechanics , Vol.52,No.2,pp.265-288,1995.

[50] Folias ES. An axial crack in a pressurized cylindrical shell under tension. Int J Fract Mech 1965;1:104–13.

[51] Folias ES. A circumferential crack in a pressurized cylindrical shell. Int J Fract Mech 1967;3:1–11.

[52] Duncan-Fama ME, Sanders Jr. JL. A circumferential crack in a cylindrical shell under tension. Int J Fract Mech 1972;8:15–20.

[53] Sanders Jr. JL. Circumferential through-wall cracks in cylindrical shells under tension. J Engng Mater Technol 1982;49:103–7.

[54] Sanders Jr. JL. Circumferential through-wall cracks in cylindrical shells under combined bending and tension. J Engng Mater Technol 1983;50:221.

[55] Paris PC, Tada H. The application of fracture-proof design methods using tearing-instability theory to nuclear piping postulating circumferential through-wall cracks. NUREG/CR-3464; 1983.

[56] Klecker R, Brust F, Wilkowski GM. NRC leak-before-break (LBB-NRC) analysis method for circumferentially through-wall cracked pipes under axial plus bending loads. NUREG/CR-4572; 1986.

[57] Zahoor A. Closed form expressions for fracture mechanics analysis of cracked pipes. ASME J Pressure Vessel Technol 1981;107:203–5.

[58] Zahoor A. Ductile fracture handbook. EPRI NP-6301; 1989.

[59] Kumar V, German MD, Wilkening WW, Andrews WR, deLorenzi HG, Mowbray DF. Advances in elastic–plastic fracture analysis. EPRI NP-3607; 1984.

[60] France CC, Green D, Sharples JK, Chivers TC. New stress intensity factor and crack opening area solutions for through-wall

[61] Lacire MH, Chapuliot S, Marie S. Stress intensity factors of through wall cracks in plates and tubes with circumferential cracks. ASME PVP 1999;388:13–21.

[62] Sanders, J.L. Jr , Circumferential through-crack in cylindrical shells under tension .Journal of Applied Mechanics, 1982, 49,103-107.

[63] Sanders, J.L. Jr , Circumferential through-crack in cylindrical shells under combined bending and tension .Journal of Applied Mechanics ,1983,50,221.

[64] Klecker, R.,Brust ,F. W. & Wilkowski ,G. M., NRC Leak –Before-Break (LBB.NRC) analysis method for Circumferentially Through – Wall Cracked Pipes Under Axial Plus Bending Loads.NUREG/CR-4572, U.S.Nuclear Regularaty Commission , Washington , D.C.,1986.

[65] Zahoor , A., Closed form expression for fracture mechanics analysis of cracked pipes. Journal of Pressure Vessel Technology,1985,107.

[66] Kumar ,V., German , M. D. & Shih, C. F., An Engineering Approach for Elastic – Plastic Fracture Analysis.EPRI/NP-1931,Electric Power Research Institute ,Palo Alto,CA,1981.

[67] Kumar ,V., German ,M.,Wilkening ,W., Andrews,W.,deLorenzi,W., & Mowbray, D.,Advances in Elastic –Plastic Fracture Analysis. EPRI/NP-3607, Electric Power Research Institute , Palo Alto,CA,1984.

[68] Brust, F ., Rahman, S. & Ghalidi, N., Elastic – Plastic analysis of small cracks in tubes.Journal of Offshore Mechanics and Arctic Engineering, 1985, 117(1) 57-62;also available in the Proceedings of the Offshore Mechanics and Arctic Engineering, Calgray,Canada,June 1992.

[69] Brust ,F. W., Scott, P.,Rahman, S., Ghadiali,N., Kilinski ,T. ,Francini ,B. , Marschall ,C.W.,Mura,N.,Krishnaswamy,P. & Wilkowski,G. M., Assessment of Short Through –

مقدمه

في هذا البحث تم تحري الانهيار بالكسر للأنابيب المستخدمة في صناعة الغاز و النفط و المصنوعة من الصلب بالاستفادة من نظرية الكسر الخطي المرن و التحليلات الخاصة به, و في السياق نفسه تم فحص قساوة الكسر باستخدام أسلوب جديد يختلف عن الطريقة المتبعة في المواصفات القياسية, حيث تتميز الجديدة باستخدام عينات كاملة من الأنابيب دون إجراء أي تعديلات على إبعادها على عكس الطرق القياسية والتي تستخدم عينات بمواصفات خاصة من حيث الأبعاد و الشروط الواجبة.

و استكمالا لنفس البحث تم دراسة سلوك النمو المستقر للصدع باستخدام نظرية الكسر المرن واللدن الخطيين .

فمن اجل قياس قساوة الكسر للأنابيب المستخدمة في صناعة الغاز و النفط تم تحضير عدد كاف من العينات التي تتمثل في وصلات كاملة من الأنابيب بدون إجراء تعديلات على السماكة و الأقطار الداخلية و الخارجية , بعد ذلك تم تجهيز العينات بعمل شرخ سطح على كامل محيط الأنابيب و بأعماق مختلفة . ومن اجل إيجاد طريقة مثلى لمسك العينات بجهاز الفحص تم تصنيع تثبيه خاصة بتصميم و أبعاد مناسبة, و لتحقيق و توفير شرط الجهاد المستوي تم تثبيت سده مناسبة داخل كل عينه و تحت منطقة الشرخ مباشره .

إما التحليلات الخاصة بالكسر المرن و اللدن الخطيين فقد تم تجهيز عينات من نفس النوع من الأنابيب و تم تحضير هذه العينات بعمل قطع نافذ بعمق و زوايا معينه في الوسط وعلى المحيط الدائري بالتحديد , مع العلم إن عملية القطع تمت باستخدام تقنية السلك القاطع. بعد التحضير تم إجراء اختبارات الثني الصافي و مراقبة سلوك الكسر عند منطقة الشرخ.

استكمالا للبحث تم إجراء بعض الاختبارات لتحديد الخواص ألفيزيائيه و ألكيميائيه للصلب المستخدم في صناعة الأنابيب .

وفي نهاية البحث تم استخدام إحدى برامج تحليل العنصر المحدود من اجل المقارنة مع النتائج المعملية.

جامعة الإمارات العربية المتحدة

عمادة الدراسات العليا

سلوك الانهيار بالكسر للأنابيب المصنوعة من الصلب و المستخدمة في صناعات الغاز و البترول

رسالة مقدمه من

جعفر يوسف الطراونه

إشراف:

د. عبد الحميد إسماعيل مراد
قسم الهندسة الميكانيكية
جامعة الإمارات العربية المتحدة

رسالة مقدمة إلى عمادة الدراسات العليا في جامعة الإمارات العربية المتحدة
لاستكمال متطلبات الحصول على درجة الماجستير في الهندسة الميكانيكية

نوفمبر 2010

Shrieen

Digitally signed by Shrieen
DN: cn=Shrieen, o=UAE University, ou=UAEU Libraries Deanship, email=shrieen@uaeu.ac.ae, c=US
Date: 2016.09.04 12:57:19 +02'00'